



The University of  
**Nottingham**

UNITED KINGDOM · CHINA · MALAYSIA

# **Mechanisms of Reactive Gliosis in Cortical and Spinal Cord Astrocytes at Different Developmental Stages**

Rawan Hassan Hareeri

*Thesis submitted for the degree of Doctor of Philosophy*

*University of Nottingham*

2019

## **Abstract**

Astrocytes represent a major class of glial cells responsible for maintaining the microenvironment of the central nervous system. They are thought to play an important role in the development of many diseases, such as stroke, neurodegenerative disease and pain. It is apparent that astrocytes become reactive during the onset of these diseases to form foci of reactive gliosis; however, the mechanisms of reactive gliosis are poorly characterised. This thesis therefore aims to investigate the mechanisms underlying reactive gliosis astrocytes in different CNS regions and during development in vitro.

To investigate the mechanisms of gliosis, we compared the responses of primary cultures of spinal cord astrocytes and cortical astrocytes as a model. We then, compared the response of cortical astrocytes at two developmental stages, before and after birth (E18 and P2, respectively), as a second model to further elucidate the mechanisms of gliosis relative to astrocyte phenotype during development. To induce gliosis, astrocytes were treated with pharmacological stimuli (forskolin, LPS, TNF $\alpha$ , noradrenaline, histamine and substance P). The reactive astrogliosis was quantified by calculating the percentage of stellate cells, quantifying the sensitivity of cells to the P2Y<sub>14</sub> receptor agonist UDP-glucose, as this receptor is up-regulated in reactive astrocytes, and measuring the distribution of p-STAT3 between cytoplasm and nucleus.

It was found that neonatal cortical astrocytes demonstrated time-dependent stellation in response to forskolin and noradrenaline. In contrast, primary cultures of other astrocytes exhibited a less reliable and more heterogeneous response to the stimuli, suggesting there are significant differences in the sensitivity of astrocytes to these stimuli or their ability to undergo stellation, depending on the site and age. Further investigation showed that cAMP levels were higher in neonatal cortical cultures compared to the neonatal spinal and embryonic cortical cultures. In addition, the intensity of p-STAT3 (considered a master regulator of

reactive gliosis) was different in the different region and during development, both of which were consistent with the changing of astrocyte morphology.

To investigate the role of STAT3 in stellation, it was found that inhibition of p-STAT3 can prevent astrocytes from undergoing stellation in the presence of forskolin or noradrenaline and decrease the tonic level of STAT3, suggesting the involvement of p-STAT3 in stellation. IL-6 STAT3 activator cannot induce stellation; the inhibitors significantly block stellation in the presence of a cAMP analog, and forskolin or noradrenaline are unable to activate STAT3, implying a cooperative effect of STAT3 and cAMP to cause stellation. None of the stimuli induced STAT3 translocation to the nucleus, thus the transcription role of STAT3 was not enabled. This indicates that cytoplasmic STAT3 induces stellation through a non-genomic role.

Together, these data provide evidence of age- and region-related differences in astrocytes stellation, which are correlated with cAMP and STAT3 expression and their activities. These findings help elucidate the mechanisms of stellation and may explain the actions of STAT3 on morphology that are independent of its nuclear transcriptional activity.

## **Acknowledgement**

I would like to thank my supervisors, Dr. Tomas Bellamy and Dr. Gareth Hathway, for all their help, guidance and constructive comments throughout my PhD journey. They have always encouraged me to pursue my ideas and enlightened me with their valuable academic advice.

I also would like to thank my all lab colleagues for a great time and friendly working atmosphere: Zoe, Laura and Jessica. My special thanks for excellent technical support, ordering and administration go to Alex Rathbone and Marleen Groenen.

My thanks also go to Dr. Federico Dajas-Bailador and Dr. Andrew Bennett for their comments and allowing me to work in their lab.

My sincere thanks go to Rawan Edan for her support and help throughout my PhD journey, especially during the tissue dissection.

I would also like to express my gratitude towards the King Abdulaziz University for funding my PhD study. Without its support, this PhD thesis would not have been completed.

Finally, I would like to thank my family, especially my dad, my mom, my husband Mohammed, my friend Shimaa and my son Yazan for their unquestioning love, without which I would not have lasted the course.

## **Publications and poster participation**

Hareeri, R., Hathway, G., Bellamy, T. (2017) 'Differences between cortical and spinal cord astrocytes in the induction of reactive gliosis' *GLIA* 65:E103–E578

Hareeri, R., Hathway, G., Bellamy, T. Differences between cortical and spinal cord astrocytes in the induction of reactive gliosis. *Pharmacology 2017- British Pharmacological Society, London; 2017*

Hareeri, R., Hathway, G., Bellamy, T. Role of p-STAT3 in astrocytes stellation. *Physiology, Pharmacology and Neuroscience Science Day, Nottingham;2019*

Hareeri, R., Hathway, G., Bellamy, T. Role of p-STAT3 in astrocytes stellation. *School away day, Nottingham;2019*

<b>Abstract</b> .....	<b>II</b>
<b>Acknowledgement</b> .....	<b>V</b>
<b>Publications and poster participation</b> .....	<b>V</b>
<b>Chapter 1 General introduction</b> .....	<b>1</b>
<b>1.1 Astrocyte overview</b> .....	<b>2</b>
<b>1.1.1 Astrocyte heterogeneity</b> .....	<b>2</b>
<b>1.1.2 Astrogliogenesis</b> .....	<b>5</b>
<b>1.1.3 Physiological function of mature astrocyte</b> .....	<b>9</b>
<b>1.1.4 Role of astrocytes at different developmental stages</b> .....	<b>12</b>
<b>1.2 Reactive gliosis</b> .....	<b>15</b>
<b>1.2.1 Features of reactive gliosis</b> .....	<b>15</b>
<b>1.2.1.1 Morphology change</b> .....	<b>15</b>
<b>1.2.1.2 Change in the gene expression profile</b> .....	<b>17</b>
<b>1.2.1.3 Molecular regulators of astrogliosis</b> .....	<b>17</b>
<b>1.2.2 Heterogeneity of reactive astrocytes</b> .....	<b>25</b>
<b>1.3 Astrocyte stellation signalling pathway</b> .....	<b>27</b>
<b>1.3.1 cAMP-induced stellation</b> .....	<b>28</b>
<b>1.3.2 Role of RhoA and ROCK in stellation</b> .....	<b>30</b>
<b>1.3.3 p-STAT3 and reactive gliosis</b> .....	<b>30</b>
<b>1.4 Aim and objective</b> .....	<b>34</b>
<b>Chapter 2 Materials and methods</b> .....	<b>35</b>
<b>2.1 Animals</b> .....	<b>36</b>
<b>2.2 Pharmacology</b> .....	<b>36</b>
<b>2.3 Antibodies</b> .....	<b>37</b>
<b>2.4 Primary astrocyte isolation and culturing</b> .....	<b>38</b>
<b>2.5 Subculture and treatment of primary astrocyte</b> .....	<b>38</b>
<b>2.6 Epifluorescence live cell Ca<sup>2+</sup> imaging</b> .....	<b>40</b>
<b>2.7 Real-time morphology imaging</b> .....	<b>41</b>
<b>2.8 Immunocytochemistry</b> .....	<b>41</b>
<b>2.9 Protein preparation and Western blotting</b> .....	<b>42</b>
<b>2.9.1 Protein preparation from astrocytes</b> .....	<b>42</b>
<b>2.9.2 Western Blots</b> .....	<b>43</b>
<b>2.10 Cell lysis and Hit-Hunter cAMP assay</b> .....	<b>44</b>
<b>2.10.1 Cell lysis</b> .....	<b>44</b>
<b>2.10.2 Hit-Hunter cAMP assay</b> .....	<b>44</b>
<b>2.11 Accell siRNA transfection of STAT3</b> .....	<b>45</b>
<b>2.12 Image analysis</b> .....	<b>47</b>
<b>2.13 Statistical analysis</b> .....	<b>49</b>

<b>Chapter 3 Optimising astrocyte culture and characterisation of different assays of reactive gliosis. ....</b>	<b>50</b>
<b>3.1 Introduction .....</b>	<b>51</b>
<b>3.2 Results.....</b>	<b>54</b>
<b>3.2.1 Optimising spinal astrocyte culture .....</b>	<b>54</b>
<b>3.2.1.1 Purity of spinal astrocyte culturing .....</b>	<b>54</b>
<b>3.2.1.2 Establish the functional response in astrocytes by measuring Ca<sup>2+</sup> responses .....</b>	<b>57</b>
<b>3.2.2 Characterisation of different assays of reactive gliosis in cortical neonatal astrocyte .....</b>	<b>60</b>
<b>3.2.2.1 Assess the morphological change (stellation) with GFAP immunocytochemistry .....</b>	<b>60</b>
<b>3.2.2.2 Assess the morphological change (stellation) with calcein-AM real-time imaging.....</b>	<b>65</b>
<b>3.2.2.3 Release of Ca<sup>2+</sup> after stimulation of the P2Y<sub>14</sub> receptor .....</b>	<b>71</b>
<b>3.2.2.4 Measure intensity of p-STAT3 in the nucleus with confocal microscopy .....</b>	<b>73</b>
<b>3.3 Discussion .....</b>	<b>80</b>
<b>Chapter 4 Characterisation of stellation in different CNS regions and at various developmental stages .....</b>	<b>86</b>
<b>4.1 Introduction .....</b>	<b>87</b>
<b>4.2 Results.....</b>	<b>89</b>
<b>4.2.1 Neonatal spinal vs Neonatal cortical astrocytes.....</b>	<b>89</b>
<b>4.2.1.1 Assess the morphological change (stellation) with GFAP immunocytochemistry .....</b>	<b>89</b>
<b>4.2.1.2 Assessing morphological change (stellation) with calcein-AM real-time imaging.....</b>	<b>93</b>
<b>4.2.1.3 Release of Ca<sup>2+</sup> after stimulation of the P2Y<sub>14</sub> receptor .....</b>	<b>96</b>
<b>4.2.2 Neonatal cortical vs Embryonic cortical astrocytes .....</b>	<b>99</b>
<b>4.2.2.1 Assess the morphological change (stellation) with GFAP immunocytochemistry .....</b>	<b>99</b>
<b>4.2.2.2 Assessing the morphological change (stellation) with calcein-AM real-time imaging .....</b>	<b>103</b>
<b>4.2.2.3 Release of Ca<sup>2+</sup> after stimulation of the P2Y<sub>14</sub> receptor .....</b>	<b>106</b>
<b>4.2.3 Cyclic AMP involvement in stellation difference according to site and age .....</b>	<b>109</b>
<b>4.2.3.1 Assess the stellation with GFAP immunocytochemistry in response to a cAMP analog .....</b>	<b>109</b>
<b>4.2.3.2 Measuring cAMP accumulation.....</b>	<b>113</b>
<b>4.2.3.2.1 Optimising the cAMP level measurement in neonatal cortical astrocytes .....</b>	<b>113</b>
<b>4.2.3.2.2 cAMP level measurement in all groups.....</b>	<b>115</b>

<b>4.3 Discussion</b> .....	<b>118</b>
<b>Chapter 5 Role p-STAT3 in astrocytes stellation</b> .....	<b>123</b>
<b>5.1 Introduction</b> .....	<b>124</b>
<b>5.2 Results</b> .....	<b>127</b>
<b>5.2.1 Effect of p-STAT3 and JAK inhibitors on astrocyte stellation</b>	<b>127</b>
5.2.1.1 Neonatal cortical astrocytes .....	127
5.2.1.2 Neonatal spinal astrocytes .....	127
<b>5.2.2 Effect of different inhibitors on neonatal cortical astrocyte stellation</b> .....	<b>130</b>
5.2.2.1 Kinase inhibitors.....	130
5.2.2.2 Adrenergic receptors blockers .....	130
<b>5.2.3 Measuring Ca<sup>2+</sup> release in astrocytes treated with static (p-STAT3 inhibitor)</b> .....	<b>133</b>
<b>5.2.4 Measuring cAMP accumulation</b> .....	<b>135</b>
5.2.4.1 Effect of p-STAT3 and JAK inhibitors in cAMP level .....	135
5.2.4.2 Effect of adrenergic receptor blockers in cAMP level .....	135
<b>5.2.5 Stellation assay of neonatal cortical astrocytes treated with cAMP analog in the presence of p-STAT3 and JAK inhibitors</b> .....	<b>138</b>
<b>5.2.6 Effect of IL-6 in astrocytes stellation</b> .....	<b>140</b>
5.2.6.1 Neonatal cortical astrocytes .....	140
5.2.6.2 Neonatal spinal astrocytes .....	140
5.2.6.3 Embryonic cortical astrocytes .....	140
<b>5.2.7 Measuring intensity of p-STAT3 in the nucleus with confocal microscopy</b> .....	<b>143</b>
5.2.7.1 Neonatal spinal astrocytes .....	143
5.2.7.2 Embryonic cortical astrocytes .....	150
<b>5.2.8 Measuring protein expression of p-STAT3 with western blots</b> .....	<b>155</b>
5.2.8.1 Optimising the p-STAT3 protein detection .....	155
5.2.8.2 Tyrosine p-STAT3 activation in different types of astrocytes ....	158
5.2.8.3 Tyrosine p-STAT3 protein levels in the presence of p-STAT3 and JAK inhibitors .....	160
<b>5.2.9 Effect of Accell siRNA STAT3 transfection in astrocytes stellation</b> .....	<b>164</b>
5.2.9.1 Accell siRNA STAT3 in 2% serum medium.....	164
5.2.9.2 Accell siRNA STAT3 in serum-free medium.....	169
<b>5.3 Discussion</b> .....	<b>174</b>
<b>Chapter 6 General discussion</b> .....	<b>179</b>
<b>6.1 Summary of findings</b> .....	<b>180</b>
<b>6.2 Overall significance of findings</b> .....	<b>180</b>

<b>6.2.1 Quantitative assays of reactive gliosis.....</b>	<b>180</b>
<b>6.2.2 Developmental variation in stellation .....</b>	<b>184</b>
<b>6.2.3 Implications for the role of astrocytes in chronic pain.....</b>	<b>187</b>
<b>6.2.4 STAT3 controlling astrocyte stellation .....</b>	<b>187</b>
<b>6.3 Future work .....</b>	<b>187</b>
<b>List of References .....</b>	<b>191</b>

## List of figures

<b>Figure 1.1</b> Developmental origins of astrocytes .....	7
<b>Figure 1.2</b> A cross-sectional view of the neural tube .....	9
<b>Figure 1.3</b> The tripartite synapse.....	12
<b>Figure 1.4</b> Schematic diagram showing the interaction of an astrocyte with microglia and neurons under pathological conditions .....	24
<b>Figure 1.5</b> Schematic diagram showing the proposed signalling pathways stimulated with forskolin that controls the stellation of astrocyte morphology.....	28
<b>Figure 1.6</b> Schematic diagram showing the extracellular signals that activate STAT3 signalling pathway.....	33
<b>Figure 2.1</b> Experimental workflow for Accell siRNA-mediated gene knockdown. ....	47
<b>Figure 3.1</b> Cell identity of astrocytes in culture from neonatal rats.....	55
<b>Figure 3.2</b> Cell identity of astrocytes in culture from neonatal rats.....	56
<b>Figure 3.3</b> Ca <sup>2+</sup> response of neonatal astrocyte without shaking by adding glutamate and ATP.. ..	58
<b>Figure 3.4</b> Ca <sup>2+</sup> response of neonatal astrocyte with shaking by adding glutamate and ATP.....	59
<b>Figure 3.5</b> Identify morphology change in astrocytes, staining with GFAP. ....	61
<b>Figure 3.6</b> Stellation response of neonatal cortical astrocytes.....	63
<b>Figure 3.7</b> Stellation model on neonatal cortical .....	64
<b>Figure 3.8</b> Stellation assays of neonatal cortical astrocytes.....	66
<b>Figure 3.9</b> Stellation assays of neonatal cortical astrocytes.....	67
<b>Figure 3.10</b> Stellation assays of neonatal cortical astrocytes .....	68
<b>Figure 3.11</b> Stellation assays of neonatal cortical astrocytes.....	69
<b>Figure 3.12</b> Stellation assays of neonatal cortical astrocytes.....	70
<b>Figure 3.13</b> Ca <sup>2+</sup> response of neonatal cortical by adding UDP-glucose. ....	72
<b>Figure 3.14</b> Intensity of S727 p-STAT3 on neonatal cortical astrocytes with confocal microscopy .....	74
<b>Figure 3.15</b> Intensity of S727 p-STAT3 on neonatal cortical astrocytes with confocal microscopy .....	75
<b>Figure 3.16</b> Intensity of S727 p-STAT3 on neonatal cortical astrocytes with confocal microscopy .....	76
<b>Figure 3.17</b> Intensity of Y705 p-STAT3 on neonatal cortical astrocytes with confocal microscopy .....	77

<b>Figure 3.18</b> Intensity of Y705 p-STAT3 on neonatal cortical astrocytes with confocal microscopy .....	78
<b>Figure 3.19</b> Intensity of Y705 p-STAT3 on neonatal cortical astrocytes with confocal microscopy .....	79
<b>Figure 4.1</b> Stellation response of neonatal spinal astrocytes .....	91
<b>Figure 4.2</b> Comparison between neonatal cortical and spinal astrocytes in stellation .....	92
<b>Figure 4.3</b> Stellation assays of neonatal spinal astrocytes.....	94
<b>Figure 4.4</b> Comparison between neonatal cortical and spinal astrocytes in stellation .....	95
<b>Figure 4.5</b> Ca <sup>2+</sup> response of neonatal spinal by adding UDP-glucose .....	97
<b>Figure 4.6</b> Ca <sup>2+</sup> response of neonatal cortical and spinal astrocytes by adding UDP-glucose .....	98
<b>Figure 4.7</b> Stellation response of embryonic cortical astrocytes .....	101
<b>Figure 4.8</b> Comparison between neonatal and embryonic cortical astrocytes in stellation .....	102
<b>Figure 4.9</b> Stellation assays of embryonic cortical astrocytes .....	104
<b>Figure 4.10</b> Comparison between neonatal and embryonic cortical astrocytes in stellation .....	105
<b>Figure 4.11</b> Ca <sup>2+</sup> response of embryonic cortical astrocytes by adding UDP-glucose.....	107
<b>Figure 4.12</b> Ca <sup>2+</sup> response of neonatal and embryonic cortical astrocytes by adding UDP-glucose .....	108
<b>Figure 4.13</b> Stellation assay on neonatal cortical, neonatal spinal and embryonic cortical astrocytes.....	111
<b>Figure 4.14</b> Comparison between neonatal cortical and spinal or embryonic cortical astrocytes in stellation. ....	112
<b>Figure 4.15</b> Time course of cAMP response to forskolin and noradrenaline in astrocytes.....	114
<b>Figure 4.16</b> Effect of forskolin and noradrenaline 10µM on the cAMP accumulation in neonatal cortical, spinal and embryonic cortical astrocytes .....	116
<b>Figure 4.17</b> Comparison of cAMP concentration between neonatal cortical and spinal astrocytes or between neonatal and embryonic cortical astrocytes.....	117
<b>Figure 5.1</b> Effect of p-STAT3 and JAK inhibitors on stellation of neonatal cortical astrocytes.....	128
<b>Figure 5.2</b> Effect of p-STAT3 and JAK inhibitors on stellation of neonatal spinal astrocytes .....	129

<b>Figure 5.3</b> Effect of different kinase inhibitors on the stellation of neonatal cortical astrocytes .....	131
<b>Figure 5.4</b> Effect of adrenergic receptor blockers on the stellation of neonatal cortical astrocytes .....	132
<b>Figure 5.5</b> Ca <sup>2+</sup> response of neonatal cortical to ATP and noradrenaline in the presence and absence of static incubation for 1 hour before imaging. ....	134
<b>Figure 5.6</b> Measuring the level of cAMP of neonatal cortical astrocytes treated with inhibitors for 1 hour and forskolin or noradrenaline for 10 minutes .....	136
<b>Figure 5.7</b> Measuring the level of cAMP of neonatal cortical astrocytes treated with inhibitors for 1 hour and noradrenaline for 10 minutes .....	137
<b>Figure 5.8</b> Effect of p-STAT3 and JAK inhibitors on stellation of neonatal cortical astrocytes .....	139
<b>Figure 5.9</b> Stellation assay of neonatal cortical astrocytes .....	141
<b>Figure 5.10</b> Stellation assay of neonatal spinal astrocytes .....	141
<b>Figure 5.11</b> Stellation assay of embryonic cortical astrocytes .....	142
<b>Figure 5.12</b> Intensity of S727 p-STAT3 on neonatal spinal astrocytes with confocal microscopy .....	144
<b>Figure 5.13</b> Intensity of S727 p-STAT3 on neonatal spinal astrocytes with confocal microscopy .....	145
<b>Figure 5.14</b> Intensity of S727 p-STAT3 on neonatal spinal astrocytes with confocal microscopy .....	146
<b>Figure 5.15</b> Intensity of Y705 p-STAT3 on neonatal spinal astrocytes with confocal microscopy .....	147
<b>Figure 5.16</b> Intensity of Y705 p-STAT3 on neonatal spinal astrocytes with confocal microscopy .....	148
<b>Figure 5.17</b> Intensity of Y705 p-STAT3 on neonatal spinal astrocytes with confocal microscopy .....	149
<b>Figure 5.18</b> Intensity of S727 p-STAT3 on embryonic cortical astrocytes with confocal microscopy .....	151
<b>Figure 5.19</b> Intensity of S727 p-STAT3 on embryonic cortical astrocytes with confocal microscopy .....	152
<b>Figure 5.20</b> Intensity of S727 p-STAT3 on embryonic cortical astrocytes with confocal microscopy .....	153
<b>Figure 5.21</b> Western blot of S727 p-STAT3 and Y705 p-STAT3 protein in neonatal cortical astrocytes after 10µM forskolin treatment.....	156
<b>Figure 5.22</b> Western blot of Y705 p-STAT3 protein in neonatal cortical astrocytes after 10µM noradrenaline treatment.....	157

<b>Figure 5.23</b> Western blot of Y705 p-STAT3 protein in neonatal cortical, spinal and embryonic cortical astrocytes after 30 minutes of 10µM forskolin and 10 minutes of 100ng/ml IL-6 treatment .....	159
<b>Figure 5.24</b> Western blot of Y705 p-STAT3 protein in neonatal cortical astrocytes after treated with p-STAT3 and JAK inhibitors for 1 hour and 10µM forskolin for 30 minutes.....	161
<b>Figure 5.25</b> Western blot of Y705 p-STAT3 protein in neonatal cortical astrocytes after treated with p-STAT3 and JAK inhibitors for 1 hour and 10µM noradrenaline for 10 minutes. ....	162
<b>Figure 5.26</b> Western blot of Y705 p-STAT3 protein in neonatal cortical astrocytes after treated with p-STAT3 and JAK inhibitors for 1 hour and 100ng/ml IL-6 for 10 minutes.....	163
<b>Figure 5.27</b> Stellation assay of astrocytes transfected with siRNA knockdown of STAT3 for 72 hours in 2% serum medium.....	166
<b>Figure 5.28</b> Stellation assay of astrocytes transfected with siRNA knockdown of STAT3 for 96 hours in 2% serum medium.....	168
<b>Figure 5.29</b> Stellation assay of astrocytes transfected with siRNA knockdown of STAT3 for 72 hours in serum-free medium.....	171
<b>Figure 5.30</b> Stellation assay of astrocytes transfected with siRNA knockdown of STAT3 for 96 hours in serum-free medium.....	173
<b>Figure 5.31</b> Known pathways for potential crosstalk between cAMP and STAT3 signalling .....	177

## List of tables

<b>Table 1.1</b> Molecular regulators of reactive gliosis.....	22
<b>Table 1.2</b> Role of different molecules in reactive gliosis.....	23
<b>Table 2.1</b> Overview of the primary and secondary antibodies used.....	37
<b>Table 2.2</b> Buffers used in Western Blots .....	44
<b>Table 3.1</b> The mean±SEM (total number of cells counted) percentage of positive staining of three antibodies.....	54
<b>Table 3.2</b> The mean±SEM (total number of cells counted) percentage of positive staining of three antibodies.....	54
<b>Table 3.3</b> Summary table of Ca <sup>2+</sup> responses .....	57
<b>Table 5.1</b> Summary of the intensity of p-STAT3 in nucleus.....	154

## List of abbreviations

<b>A1 receptor</b>	adenosine receptor
<b>A20</b>	Alpha-induced protein 3
<b>Acan</b>	Aggrecan
<b>Act1</b>	Alpha-actinin-1
<b>Adra2a</b>	Adrenoceptor Alpha 2A
<b>Akt</b>	Serine/threonine-specific protein kinase
<b>Aldh1L1</b>	Aldehyde dehydrogenase 1 family member L1
<b>AMPA</b>	$\alpha$ -amino-3-hydroxy-5-methyl-4-isoxazolepropionic acid
<b>AMPK</b>	AMP-activated protein kinase
<b>ANLSH</b>	Astrocyte-neuronal lactate shuttle hypothesis
<b>Arf</b>	Small ADP ribosylation factor
<b>Arp2/3</b>	Actin related protein 2/actin related protein 3 complex
<b>ATP</b>	Adenosine triphosphate
<b>AUC</b>	Area Under the curve
<b>Axin2</b>	Axin-related protein
<b>A<math>\beta</math></b>	Amyloid beta
<b>BBB</b>	Blood-brain barrier
<b>BCA</b>	Bicinchoninic acid protein assay
<b>BDNF</b>	Brain-derived neurotrophic factor
<b>Bmpr1a</b>	Bone morphogenetic protein receptor, type IA
<b>Bmpr1b</b>	Bone morphogenetic protein receptor, type IB
<b>Bmpr2</b>	Bone Morphogenetic Protein Receptor Type 2
<b>BMPs</b>	Bone morphogenetic proteins
<b>BSA</b>	Bovine serum albumin
<b>BSU</b>	Biological Services Unit
<b>C1q</b>	Complement component c1q
<b>C3</b>	Complement component
<b>CFB</b>	Complement factor B
<b>C4B</b>	Complement Component 4B
<b>Ca<sup>2+</sup></b>	Calcium
<b>CaCl<sub>2</sub></b>	Calcium chloride
<b>cAMP</b>	Cyclic adenosine monophosphate
<b>Caspases</b>	Cysteine-aspartic proteases
<b>CCL</b>	C-C Motif Chemokine
<b>Ccnb1,Ccnb2</b>	Cyclins b1 and b2 ( )
<b>Ccr12</b>	C-C Motif Chemokine receptor type 2
<b>Cdc42</b>	Cell division control protein 42 homolog
<b>Cdh2</b>	Cadherin 2
<b>Cdk1</b>	Cyclin Dependent Kinase 1
<b>Chst11</b>	Carbohydrate sulfotransferase 11
<b>Cl<sup>-</sup></b>	Chloride
<b>CNS</b>	Central nervous system
<b>CNTF</b>	Ciliary neurotrophic factor

<b>CO<sub>2</sub></b>	Carbon dioxide
<b>COMT</b>	Catechol-O-methyl transferase
<b>COX2</b>	Prostaglandin-endoperoxide synthase 2
<b>CRF</b>	Corticotropin-releasing factor
<b>Csgalnact1</b>	Chondroitin Sulfate N-Acetylgalactosaminyltransferase 1
<b>CSPG</b>	chondroitin sulfate proteoglycans
<b>Ctnnb1</b>	Catenin beta-1
<b>CTR</b>	Calcitonin receptor
<b>CX3CR1</b>	CX3C chemokine receptor 1 (Fractalkine receptor)
<b>CX43</b>	Gap junction alpha-1 protein (also called connexin43)
<b>CXCL-</b>	C-X-C motif chemokine-
<b>Cxcr4</b>	C-X-C chemokine receptor type 4
<b>DAMPs</b>	Danger-associated molecular patterns
<b>DAPI</b>	4',6-diamidino-2-phenylindole
<b>DAT</b>	Dopamine transporter
<b>dbcAMP</b>	dibutyryl cAMP
<b>DMEM</b>	Dulbecco's Modified Eagle Medium
<b>DMSO</b>	Dimethyl sulfoxide
<b>DNase</b>	Deoxyribonuclease
<b>DTT</b>	Dithiothreitol
<b>EAAT1</b>	Excitatory amino acid transporter 1
<b>EAAT2</b>	Excitatory amino acid transporter 2
<b>Ednra</b>	Endothelin Receptor Type A
<b>EDTA</b>	Ethylenediaminetetraacetic acid
<b>EGF</b>	Epidermal growth factor
<b>EPAC</b>	Exchange factor directly activated by cAMP
<b>ER</b>	Endoplasmic reticulum
<b>ERK</b>	Extracellular signal-regulated kinases
<b>ERK</b>	extracellular signal-regulated kinases
<b>ERM</b>	Ezrin / radixin/ moesin
<b>F/FO</b>	Ratio of fluorescence at time t divided by mean intensity for 0-120 seconds before the addition of agonist.
<b>FBS</b>	Fetal bovine serum
<b>FGF</b>	Fibroblast growth factor
<b>g</b>	Gravitational force
<b>GABA</b>	γ-aminobutyric acid
<b>GAP43</b>	Growth Associated Protein 43
<b>GAPDH</b>	Glyceraldehyde 3-phosphate dehydrogenase
<b>GAT3</b>	GABA transporter type 3
<b>G-CSF</b>	Granulocyte-colony stimulating factor
<b>GDNF</b>	Glial cell line-derived neurotrophic factor
<b>GDP</b>	Guanine nucleotide-binding proteins
<b>GFAP</b>	Glial fibrillary acidic protein
<b>Gi</b>	Heterotrimeric G protein-coupled to Gi protein

<b>GLAST</b>	Glutamate Aspartate Transporter
<b>GLT1</b>	Glutamate transporter 1
<b>Glu</b>	Glutamate
<b>Gnao1</b>	Guanine nucleotide-binding protein Go subunit alpha
<b>Gnb4</b>	Guanine nucleotide-binding proteins beta 4
<b>Gng7</b>	Guanine nucleotide-binding proteins gama 7
<b>GPCRs</b>	G-protein-coupled receptors
<b>GS</b>	Glutamine synthetase
<b>GTP</b>	Guanosine triphosphate
<b>G<sub>αq</sub></b>	Heterotrimeric G protein-coupled to G <sub>αq</sub> protein
<b>G<sub>αs</sub></b>	Heterotrimeric G protein-coupled to G <sub>αs</sub> protein
<b>H</b>	Hour
<b>H<sup>+</sup></b>	hydrogen
<b>H2-D1</b>	Histocompatibility 2, D region locus 1
<b>H2-K1</b>	Histocompatibility 2, K region locus 1
<b>HCl</b>	Hydrochloric Acid
<b>HCO<sub>3</sub><sup>-</sup></b>	Bicarbonate ion
<b>HEK 293</b>	Human embryonic kidney 293 cells
<b>HEPES</b>	4-(2-hydroxyethyl)-1-piperazineethanesulfonic acid
<b>Hes1</b>	Hairy and enhancer of split-1
<b>HMG</b>	High mobility group box
<b>IBA1</b>	Ionized Calcium-binding adapter molecule 1
<b>IFN-δ</b>	Interferon-δ
<b>IL-</b>	Interleukin-
<b>IP<sub>3</sub></b>	Inositol (1,4,5) trisphosphate
<b>JAK</b>	Janus kinase
<b>JNK</b>	c-Jun N-terminal kinase
<b>K<sup>+</sup></b>	Potassium
<b>KCl</b>	Potassium chloride
<b>Kir4.1</b>	Potassium channel
<b>Klf6</b>	Kruppel like factor 6
<b>Lcn2</b>	Lipocalin 2
<b>Lgals-1 -3</b>	Galectin-1 -3
<b>LIF</b>	Leukemia inhibitory factor
<b>LPS</b>	Lipopolysaccharide
<b>MAO</b>	Monoamine oxidase
<b>MAPK</b>	Mitogen-activated protein kinase
<b>MCM</b>	Modified chemically defined medium
<b>mGluRs</b>	Metabotropic glutamate receptors
<b>MgSO<sub>4</sub></b>	Magnesium sulfite
<b>Min</b>	Minute
<b>MLC</b>	Light chain of myosin
<b>Mmp-</b>	Matrix metalloproteinase-
<b>Mob</b>	Monopolar spindle-one-binder
<b>MPTP</b>	1-methyl-4-phenyl-1,2,3,6-tetrahydropyridine

<b>MX1S</b>	Interferon-induced GTP-binding protein
<b>NA</b>	Noradrenaline
<b>Na<sup>+</sup></b>	Sodium
<b>Na<sub>3</sub>VO<sub>4</sub></b>	Sodium orthovanadate
<b>NaCl</b>	Sodium chloride
<b>NaF</b>	Sodium fluoride
<b>NaOH</b>	Sodium hydroxide
<b>Nes</b>	Nestin
<b>NET</b>	Norepinephrine transporter
<b>NFIA</b>	Nuclear Factor I A
<b>NF-κB</b>	Necrosis factor-kappa B
<b>NGF</b>	Nerve growth factor
<b>NMDA</b>	N-methyl-D-aspartate
<b>NO</b>	Nitric oxide
<b>NP-40</b>	Nonidet P-40
<b>Nurr1</b>	Nuclear receptor related 1
<b>OCT</b>	Organic cation transporter
<b>Olig2</b>	Oligodendrocyte transcription factor
<b>OPC</b>	Oligodendrocyte precursor cells
<b>Osmr</b>	Oncostatin M receptor
<b>p2ry14</b>	Purinergic receptor P2Y, G-protein coupled,14
<b>P2X</b>	purinergic cation channel receptor
<b>P2Y</b>	purinergic G protein-coupled receptor
<b>P38</b>	P38 mitogen-activated protein kinases
<b>PACAP</b>	Pituitary adenylyl cyclase-activating polypeptide
<b>PAMPs</b>	Pathogen-associated molecular patterns
<b>PBS</b>	Phosphate-buffered saline
<b>Pcan</b>	Phenol hydroxylase subunit
<b>PFN1</b>	Actin-binding protein profilin 1
<b>PI3K</b>	Phosphatidylinositide 3-kinases
<b>PIP2</b>	Phosphatidylinositol bisphosphate
<b>PIP3</b>	Phosphatidylinositol (3,4,5)-trisphosphate
<b>PKA</b>	Protein kinase A
<b>PKC</b>	Protein kinase C
<b>Plaur</b>	Urokinase plasminogen activator surface receptor
<b>PLC</b>	Phospholipase C
<b>PLL</b>	Poly-L-lysine
<b>PMAT</b>	Plasma membrane monoamine transporter
<b>p-STAT3</b>	Phosphorylated signal transducer and activator of transcription 3
<b>PTEN</b>	Phosphatase and tensin homolog
<b>PTEN</b>	Phosphatase and tensin homolog
<b>Ptx3</b>	Pentraxin-related protein
<b>Rab</b>	Small GTPase

<b>Rac 1</b>	Ras-related C3 botulinum toxin substrate 1
<b>Ran</b>	RAs-related Nuclear protein
<b>Rap</b>	GTP-binding protein (Ras-related proteins)
<b>Ras</b>	Small GTPase
<b>RGK</b>	Small GTP-binding proteins
<b>RhoA</b>	Ras homolog family member A
<b>RIPA</b>	Radioimmunoprecipitation assay buffer
<b>ROCK</b>	Rho-associated protein kinase
<b>ROI</b>	Regions of interest
<b>Rpm</b>	Revolutions per minute
<b>S100A10</b>	S100 Calcium Binding Protein A10
<b>S100<math>\beta</math></b>	S100 calcium-binding protein $\beta$
<b>S1pr3</b>	Sphingosine-1-phosphate receptor 3
<b>S727 p-STAT3</b>	Serine p-STAT3
<b>SDS</b>	Sodium dodecyl sulfate
<b>SEM</b>	Standard error of mean
<b>Serpina3n</b>	Serine protease Inhibitor
<b>Shh</b>	Sonic hedgehog
<b>sIL-6R</b>	Soluble IL-6 receptor
<b>siRNA</b>	Small interfering RNA
<b>Slit2</b>	Slit Guidance Ligand 2
<b>Smad</b>	Mothers against decapentaplegic
<b>SOCS3</b>	Suppressor of cytokine signalling 3
<b>SOX2</b>	SRY-Box Transcription Factor 2
<b>SOX9</b>	SRY-Box Transcription Factor 9
<b>Spp1</b>	Osteopontin
<b>Src</b>	Protooncogene tyrosine-protein kinase (non-receptor tyrosine kinase)
<b>STAT3</b>	Signal transducer and activator of transcription 3
<b>TBS</b>	Tris-buffered saline
<b>TBST</b>	Tris-buffered saline-tween 20
<b>TG</b>	Tris-glycine blotting buffer
<b>TGF-<math>\beta</math></b>	Tumour growth factor beta
<b>TGS</b>	Tris-glycine-SDS running buffer
<b>Thbs1</b>	Thrombospondin-1
<b>Thbs4</b>	Thrombospondin-4
<b>TKT</b>	Transketolase
<b>TLR-4</b>	Toll-like receptor-4
<b>Tnfrsf12a</b>	TNF Receptor Superfamily Member 12A
<b>TNF-<math>\alpha</math></b>	Tumour necrosis factor-alpha
<b>Top2a</b>	DNA Topoisomerase II Alpha
<b>UDP-glucose</b>	Uridine diphosphate glucose
<b>V</b>	Volt
<b>VEGF</b>	Vascular endothelial growth factor

<b>VIP</b>	Vasoactive intestinal peptide
<b>Xylt1</b>	Xylosyltransferase 1
<b>Y705 p-STAT3</b>	Tyrosine p-STAT3

## **Chapter 1 General introduction**

## **1.1 Astrocyte overview**

Astrocytes among of the largest glial cell populations in the central nervous system (CNS), where they represent 30% of the cells (Liddelow and Barres, 2017). They are a heterogeneous group of non-neuronal cells that play a crucial function in several aspects of CNS development and function. They can modulate synaptic transmission and plasticity (Paixão and Klein, 2010), control potassium buffering (Chiang, Sessle and Dostrovsky, 2012) and play a role in regulating metabolic partitioning (Chiang, Sessle and Dostrovsky, 2012; Kimelberg, 2010).

### **1.1.1 Astrocyte heterogeneity**

Several lines of evidence show that astrocytes are a heterogeneous cell type within and between brain regions. They are diverse in their morphology, gene expression profile, physiological properties, electrophysiological properties, function and response to injury and disease (Matyash and Kettenmann, 2010; Zhang and Barres, 2010).

Morphologically, Emsley and Macklis (2006) found many types of astrocyte by using GFAP and S100 $\beta$  immunostaining including Bergmann glia, ependymal glia, fibrous astrocytes, marginal glia, perivascular glia, protoplasmic astrocytes, tanycytes and velate glia within many brain regions. Another study found that striatal and hippocampal astrocytes have the same somatic volumes and number of primary branches, but the branching of striatal astrocytes was significantly more extensive than hippocampal astrocytes (Chai et al., 2017). Glial fibrillary acidic protein (GFAP), an intermediate filament protein that forms part of the astrocyte cytoskeleton, is the standard marker used to identify astrocytes (Oberheim, Goldman, and Nedergaard, 2012). GFAP levels differ between brain regions (Taft, Vertes and Perry, 2005); hippocampal astrocytes express readily detectable GFAP, whereas thalamus astrocytes express less. GFAP expression also differs in many layers of cerebral cortex astrocytes (Khakh and Sofroniew, 2015); GFAP expression is high in white matter astrocytes (fibrous astrocytes) and low in grey

matter astrocytes (protoplasmic astrocytes) (Cahoy et al., 2008). Additionally, it has been found that many astrocytes do not express GFAP but could be identified by other astrocytes markers such as S100 $\beta$  (Gonçalves, Concli Leite and Nardin, 2008) and Aldh1L1 (Sofroniew and Vinters, 2010) which are also used for recognising astrocyte morphology. Conversely, GFAP can be expressed by other cells in the CNS which are not astrocytes (Oberheim, Goldman, and Nedergaard, 2012), such as radial glial cells, the main alternative cell type in the CNS responsible for generating neurons and glia (Malatesta, Appolloni and Calzolari, 2008). Therefore, GFAP expression for the purpose of identifying mature astrocytes is still not sufficient for defining cell type. Furthermore, it has been found that GFAP is an essential marker of reactive astrogliosis and glial scar formation (Sofroniew and Vinters, 2010). Thus, reactive astrocytes lead to an increase in the presence of GFAP-labelled cells (Pekny and Pekna, 2004).

In addition to morphological differences, heterogeneity in astrocyte gene expression profiles has led to diversity in their functions. Compared with cortex and cerebellum populations, spinal cord astrocytes highly expressed *Hes1* gene, which is the main target of Notch signalling, and can affect neuronal reprogramming activity (Hu et al., 2019). Molofsky et al. (2014) discovered that astrocyte in the spinal cord could express the *sema3a* gene, which is required for proper motor neuron and sensory neuron circuit organisation. Moreover, many studies recognised several genes that are differentially expressed by astrocytes in vivo and in vitro. These genes include: surface glycoproteins (Barbin et al., 1988), which suggests differences in astrocyte-neuron interactions or astrocyte-astrocyte interactions (Zhang and Barres, 2010); neuropeptides (Klein and Fricker, 1992) which lead to differences in peptidergic signalling activity (Zhang and Barres, 2010); sodium channels (Black, Sontheimer and Waxman, 1993); potassium channels (Hibino et al., 2004; Tang, Taniguchi and Kofuji, 2009); glutamate receptors (Cai, Schools and Kimelberg, 2000); NMDA receptors (Karavanova et

al., 2007); and glutamate transporters (Regan et al., 2007), which suggests variation in ion homeostasis and neurotransmitter recycling. For example, the glutamate transporter GLT1 is mainly expressed in the hippocampus, cortex and striatum in both protoplasmic and fibrous astrocytes, while GLAST is primarily expressed in the cerebellum and cortical astrocytes (Lehre et al., 1995; Tanaka et al., 2016). Also, GLT1 expression is higher in brain astrocyte than in spinal cord astrocytes (Regan et al., 2007). It was found that glutamate uptake in a group of astrocytes from the hypothalamus is absent (Israel et al., 2003). With respect to glutamate receptors, NMDA receptor can be expressed in cortical and spinal cord astrocyte but not in hippocampal astrocytes (Matyash and Kettenmann, 2010). Moreover, regarding the purinergic receptor, it has been established that only a subpopulation of astrocytes in the rat hippocampus co-express P2Y<sub>1</sub>, P2Y<sub>2</sub> or P2Y<sub>4</sub> (Zhu and Kimelberg, 2004). While cortical astrocytes express functional P2X receptors (Lalo et al., 2008), hippocampal astrocytes do not express any (Jabs et al., 2007). Buosi et al. (2017) demonstrated that cerebellar astrocytes have a higher synaptogenic effect than other brain regions. These differences may be due to distinct gene expression profiles and different expression levels of known synaptogenic factors (Bosworth and Allen, 2017).

Furthermore, astrocytes have different membrane currents activity. Connexin-43 is expressed by grey but not white matter astrocytes (Haas et al., 2006; Nagy et al., 1999). The astrocytes can also express high levels of potassium channel Kir4.1 in the hippocampus and cerebellum (Seifert et al., 2009), low levels in white matter astrocytes, and at variable levels in grey matter astrocytes (Poopalasundaram et al., 2000). While expression is region-specific in the spinal cord, Kir4.1 channel expression is generally expressed higher in the ventral horn than the dorsal horn (Olsen, Campbell and Sontheimer, 2007; Matyash and Kettenmann, 2010).

In the case of intercellular calcium signalling, a difference was found between grey and white matter astrocytes (Matyash and Kettenmann, 2010). As a result of diverse mechanisms, seven types of  $\text{Ca}^{2+}$  signals can exist in astrocytes and occur in distinct CNS locations (Khakh and Sofroniew, 2015). Cortical layer 1 astrocytes show distinct features of spontaneous  $\text{Ca}^{2+}$  activity compared to layer 2/3 astrocytes (Takata and Hirase, 2008). Also,  $\text{Ca}^{2+}$  activity in cerebellar Bergman glia exhibits patterns which differ from those of neocortical protoplasmic astrocytes (Nimmerjahn, Mukamel and Schnitzer, 2010), and  $\text{Ca}^{2+}$  signal frequency is shown to be higher in the hippocampus than the striatum (Chai et al., 2017). In cortical astrocytes, calcium can be released in response to glutamate and norepinephrine (Bekar, He and Nedergaard, 2008), while hippocampal astrocytes exhibit responses to ATP, GABA, glutamate, acetylcholine, prostaglandins and endocannabinoids to increase calcium signalling (Araque et al., 2002; Porter and McCarthy, 1996).

Overall, astrocytes are highly heterogeneous in their phenotype, which is reflected in their morphology and gene expression and can affect cell identity and function. There is still uncertainty in the definition of what an astrocyte is; it is unclear whether there is one class of cells or many classes because astrocytes have different functions and many roles. Thus, the origin of this heterogeneity is important to investigate.

### **1.1.2 Astrogliogenesis**

Studying the formation of astrocytes during development could reveal the main source of astrocyte heterogeneity. In this section, we will review the source and steps of astrogliogenesis as well as the factors that are controlling these steps and regulating the diversity of astrocytes in their morphology and function during development.

There are four distinct sources of astrocytes in CNS: radial glia in the ventricular zone, intermediate progenitors in the subventricular zone,  $\text{NG2}^+$  glial progenitor

cells and local proliferation of differentiated astrocytes (Ge et al., 2012; Sloan and Barres, 2015; Sohn et al., 2015). During neurogenesis, neuroepithelial cells that generate from the neural tube transform into radial glial cells and produce neurons in the early stage. Following the cessation of neurogenesis during mid-gestation, radial glia become gliogenic and form astrocytes (Holst et al., 2019; Molofsky et al., 2012; Martini et al., 2013; Rowitch and Kriegstein, 2010); however, the direct involvement of radial cells in the formation of astrocytes is small because the population of astrocytes in the adult is much larger than the population of radial cells (Ge and Jia, 2016). Another study found that each radial cell generates intermediate progenitor cells and many astrocyte cells (Magavi et al., 2012). Both radial cells and intermediate progenitor cells start to disappear in the late embryonic stages, and few continue after postnatal week 2, at which point they play a role in migrating neurons and astrocytes to their final location in the CNS (Tabata, 2015). After birth, local proliferation is the main source of astrocytes. There are two peaks of proliferation: the first is at P3–7, and the second is at P16 (Ge and Jia, 2016). The proliferation of spinal cord astrocytes is earlier than brain astrocytes (Molofsky and Deneen, 2015) (Figure 1.1).

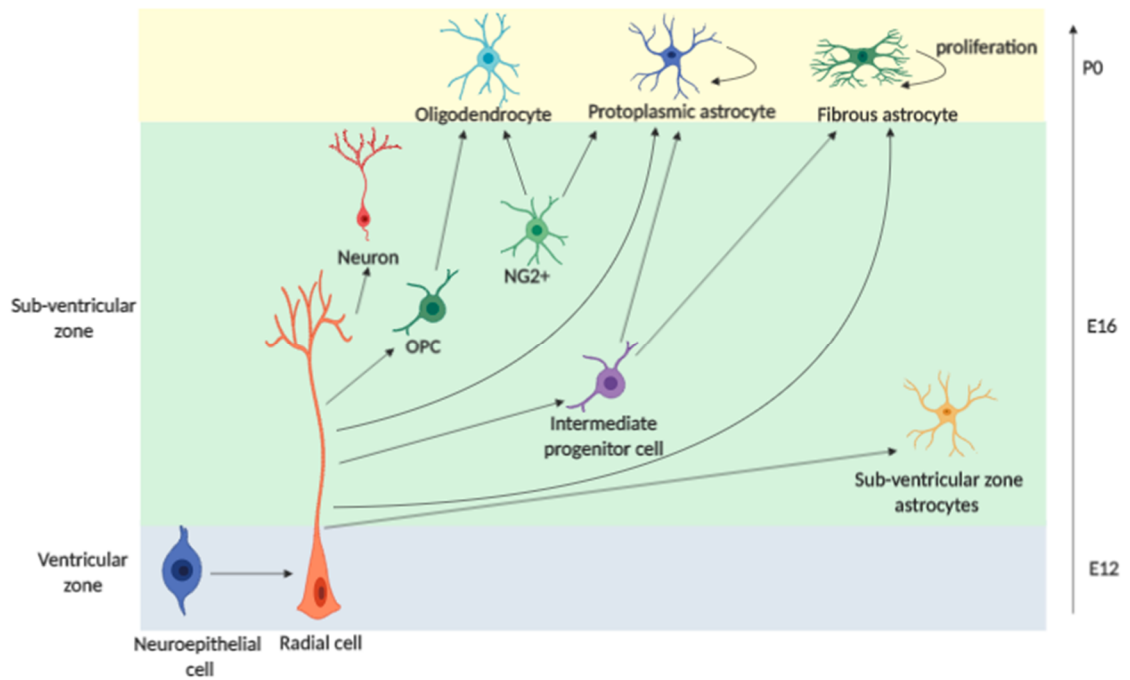


**Figure 1.1 Developmental origins of astrocytes are shown from left to right.** Black arrows indicate differentiation from one cell type to another. The neuroepithelial cell gives rise to a neurogenic radial cell that generates different neuronal subtypes starting from E12 to E16. At later stages of embryogenesis (E16), the neurogenic radial cell starts to become gliogenic and produces astrocytes and oligodendrocyte precursor cells (OPC), which yield oligodendrocytes. Also, radial cells can generate an intermediate progenitor cell that produces astrocytes. NG2<sup>+</sup> glial progenitor cells can create a protoplasmic astrocyte. After birth, the astrocytes begin to differentiate and proliferate.

The current understanding of astrogensis is completed by explaining the factors that affect the transfer from neurons to astrocytes formation. The switch from neurogenesis to gliogenesis is controlled by a combination of their intrinsic factors (e.g., transcription factors and epigenetic factors) and cell-extrinsic factors from the microenvironment around neural stem cells (e.g. cytokines and growth factors). Sonic hedgehog (Shh), neurotrophic cytokine cardiotrophin-1, leukemia inhibitory factor (LIF), a member of the interleukin-6 family (IL-6) and bone morphogenetic proteins (BMPs) are extrinsic morphogenic signals that integrate and bind with neuroepithelial cell populations and activate cell-intrinsic transcription factor expression (Rowitch and Kriegstein, 2010; Sun, Martinowich and Ge, 2003; Holst et al., 2019; Sloan and Barres, 2015; Fukuda et al., 2007; Yang, Higashimori and Morel, 2013). Araújo et al. (2014) found that activation of

the Shh pathway increased proliferation and generation of astroglial cells but not neurons. LIF and ciliary neurotrophic factor (CNTF) can stimulate astroglialogenesis through activation of JAK-STAT signalling (Cao et al., 2010; He et al., 2005; Kim et al., 2010) and act to promote GFAP and S100 $\beta$  genes during the astrocyte differentiation process (Molofsky et al., 2012). In addition, BMP can activate Smad transcription factors, which synergistically stimulate the transcription of glial-specific genes (Vallejo, 2009; Tiwari et al., 2018). However, BMPs have a dual role which can promote neurogenesis in the early stage and astrogenesis during the late period of development, depending on the levels of specific growth factors (Rowitch and Kriegstein, 2010). Moreover, the Notch signalling pathway is another factor that regulates neurogenesis in the beginning, then generates astrocytes in the astroglial phase. Notch is able to activate astroglialogenesis through HES proteins, which inhibit neurogenic bHLH factors, and also through activation of the JAK-STAT pathway (Deneen et al., 2006; Rowitch and Kriegstein, 2010). Several other transcription factors can control the initiation of gliogenesis and the differentiation of astrocytes in a later stage, such as Sox9, which is an HMG box transcription factor, and NFIA transcription factors that bind CAATT boxes (Molofsky et al., 2012; Chaboub and Deneen, 2012; Molofsky and Deneen, 2015). It was found that Notch1 signalling is directly up-regulated by the transcription factor Sox9 (Martini et al., 2013) and NFIA (Tiwari et al., 2018). Benito-Muñoz, Matute and Cavaliere (2016) demonstrated that activation of the A1 receptor by adenosine inhibits adult neurogenesis and promotes astroglialogenesis.

The heterogeneity of astrocytes may relate to the diversity of glial progenitor cells, as mentioned earlier in this section and Figure 1.1. Moreover, it was discovered that spinal cord astrocytes but not cortical could be derived from oligo progenitors, which yield specific astrocyte subpopulations in the spinal cord (Oberheim, Goldman and Nedergaard, 2012). In addition, the extrinsic signals of Shh and BMPs lead to the segmentation of the neuroepithelium into different progenitor

domains (denoted p0, p1 p2, p3 and pMN) (Bayraktar et al., 2015; Rowitch and Kriegstein, 2010). Each domain produces specific progenitor that generate different astrocyte types. Three astrocyte subtypes have been discovered: VA1, VA2 and VA3, each of which expresses different transcription factors and gene expression that may be implicated in astrocyte diversity (Ben Haim and Rowitch, 2016; Chaboub and Deneen, 2012; Rowitch and Kriegstein, 2010) (Figure 1.2). Taken together, the diversity of spinal cord and brain astrocytes is due to distinct subtypes by a homeodomain transcription factor code, diversity of glial progenitors and extrinsic factors that modulate differentiation.

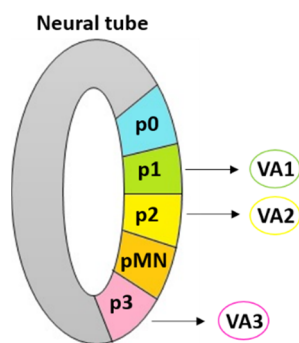


**Figure 1.2 A cross-sectional view of the neural tube.** The neural tube is the origin of the neuroepithelial cell that differentiates into neurons or glial cells, i.e., oligodendrocytes and astrocytes. The neural tube is divided into different segmentations that generate progenitor domains (denoted p0, p1 p2, p3 and pMN). Three astrocyte subtypes have been recognised according to their domains of origin: VA1 astrocytes (derived from p1), VA2 astrocytes (derived from p2) and VA3 astrocytes (derived from p3).

### 1.1.3 Physiological function of mature astrocyte

Mature astrocytes are essential for maintaining the extracellular microenvironment of the CNS. Firstly, they control extracellular ion homeostasis by uptake of  $K^+$  in the extracellular space through potassium channels (Chiang, Sessle and Dostrovsky, 2012). Secondly, the astrocytes clear  $CO_2$  produced by neurons in the brain because they contain carbonic anhydrase enzyme, which synthesises carbonic acid from  $CO_2$  and water then reversibly degrades carbonic acid into  $H^+$  and  $HCO_3^-$  (Benarroch, 2005). Thirdly, they control  $H^+$  to maintain pH in addition to  $Na^+/H^+$  and  $Cl^-/HCO_3^-$  exchanges. Fourthly, astrocytes provide energy for

neurons by converting glucose to lactate during glycolysis, as described by the astrocyte-neuronal lactate shuttle hypothesis (ANLSH); this process is controlled by cotransport of  $H^+$  with lactate on neuron and astrocyte membranes (Kimelberg, 2010). Fifthly, 99% of CNS capillaries are covered by end-feet astrocytes (Verkhatsky et al., 2014), which modulate blood-brain barrier (BBB) permeability (Benarroch, 2005).

Other significant functions of astrocytes include the control of neuronal activity by uptake of neurotransmitters. Glutamate released during synaptic transmission must be cleared to terminate the transient signal. Glial transporters such as GLAST/EAAT1 and GLT1/EAAT2 take up glutamate, maintaining extracellular concentrations at a low level. This prevents excessive activation of neurons, which can lead to excitotoxicity (Paixão and Klein, 2010). One-third of this glutamate enters the tricarboxylic acid cycle (Krebs cycle) to form new glutamate, and the remaining two-thirds is converted into glutamine that is released into the synaptic space then taken up by neurons and used as a glutamate precursor (Chiang, Sessle and Dostrovsky, 2012). In addition, astrocytes participate in GABA uptake using transporters such as GAT3. GAT3 utilises an active process involving the influx of one positive charge via take up of GABA and  $2Na^+$  ions in exchange for  $1Cl^-$  ion per GABA transport cycle (Scimemi, 2019). Dopamine uptake occurs in astrocytes as well via the dopamine transporter (DAT), norepinephrine transporter (NET), organic cation transporter (OCT) and plasma membrane monoamine transporter (PMAT) (Jennings and Rusakov, 2016). Following uptake, the dopamine is metabolised by catechol-O-methyl transferase (COMT) and monoamine oxidase (MAO) (Petrelli et al., 2018). Breakdown of dopamine by MAO produces  $H_2O_2$  that increases  $Ca^{2+}$  release from intracellular stores via activation of phospholipase C (PLC), which causes the release of inositol (1,4,5) trisphosphate ( $IP_3$ ) (Jennings and Rusakov, 2016).

Another consequence of the close association of astrocytes with sites of neurotransmitter release is that they form an essential part of the tripartite synapse (Figure 1.3). They could work bi-directionally by exchanging information between the pre- and postsynaptic cells to regulate synaptic activity, which has also been linked to blood vessel diameter (Paixão and Klein, 2010). Astrocytes can express several receptors in their membrane. A receptor found on neurons has almost certainly been found on astrocytes, too. These receptors include NMDA, AMPA, metabotropic glutamatergic, GABA, neurotrophic tyrosine kinase, neurokinin-1, purinergic (ion channels P2X receptors and metabotropic receptors P2Y), adrenergic, muscarinic, histamine, adenosine, serotonin, dopamine, opioid, cytokine, chemokines receptors and aquaporin channels (Chiang, Sessle and Dostrovsky, 2012; Dorf et al., 2000; Fields, 2009; Hertz et al., 2010; Xu et al., 2018; Miyazaki and Asanuma, 2016; Jennings and Rusakov, 2016; Nam et al., 2018). Activation of metabotropic receptors can trigger the release of  $\text{Ca}^{2+}$  from internal stores on the endoplasmic reticulum (ER), which is the main functional signalling of astrocytes allowing them to detect neurotransmitters and release gliotransmitters such as glutamate, ATP and D-serine (Nedergaard, Rodríguez and Verkhratsky, 2010; Hansen and Malcangio, 2013; Hertz and Zielke, 2004; Coco et al., 2003; Mothet et al., 2005). Following activation of these receptors, phospholipase C (PLC) enzyme hydrolyses phosphatidylinositol bisphosphate ( $\text{PIP}_2$ ) into the intracellular second messenger  $\text{IP}_3$ , which binds to the  $\text{IP}_3$  receptor located in the ER and results in the release of calcium from the ER store. In addition, it appears that other signalling pathways could increase  $\text{Ca}^{2+}$  level in astrocytes by stimulation of  $\text{Ca}^{2+}$ -permeant ionotropic receptors or  $\text{Na}^+/\text{Ca}^{2+}$  exchangers (Volterra, Liaudet and Savtchouk, 2014).

Furthermore, astrocytes can create astroglial networks by cell-to-cell coupling via gap junctions (Orthmann-Murphy, Abrams and Scherer, 2008) such as Connexin-43 (Cx43) (Thompson and Macvicar, 2008; Kang et al., 2008). In summary,

astrocytes are multifunctional cells in CNS that play many roles in controlling neuronal signalling and provide the physiological conditions necessary for the survival of neurons

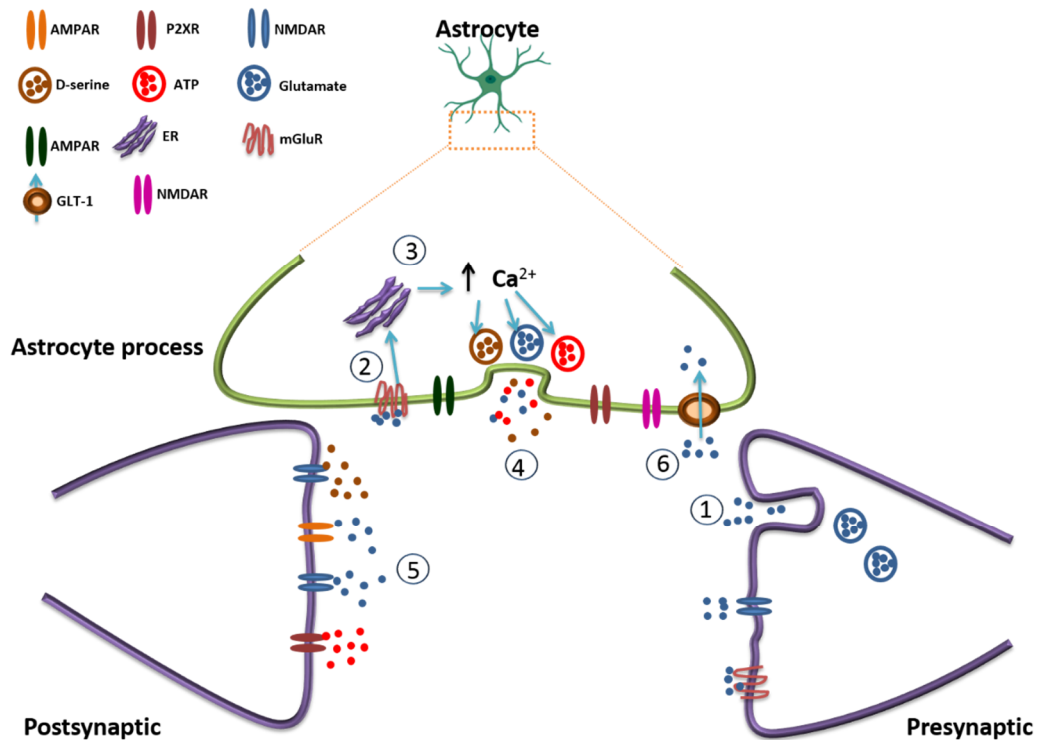


**Figure 1.3 The tripartite synapse.** Neurotransmitters (glutamate) are released from the presynaptic neuron (1), which activate metabotropic glutamate receptors (mGluRs) on astrocytes (2), causing a release of  $\text{Ca}^{2+}$  ions in the astrocyte from the ER (3).  $\text{Ca}^{2+}$  ions trigger the release of gliotransmitters from astrocytes, such as glutamate, ATP and D-serine (4). These gliotransmitters return to act on both presynaptic and postsynaptic neurons. Glutamate released from astrocytes can bind postsynaptically on NMDARs or presynaptically on mGluRs or NMDARs, and the release of D-serine acts on the glycine-binding site of NMDARs. Astrocytic ATP release can act on purinergic P2X and P2Y receptors (5). The excess glutamate can be taken up by the astrocyte again (6).

#### 1.1.4 Role of astrocytes at different developmental stages

Several lines of evidence demonstrate that astrocyte properties are changeable during development due to alteration of their gene expression. Adult astrocytes induce higher *Notch1* expression levels compared with postnatal astrocytes in the cortex, cerebellum and spinal cord (Hu et al., 2019). Cahoy et al. (2008) created a transcriptome database of gene expression in astrocytes from ages P1 to P30. They discovered that early astrocytes express *Sox2*, *Bmpr1a*, *Bmpr1b*, *Bmpr2*, *BMP*, *Shh*, and *Notch1/2/3*, which are essential for astrocyte development.

Moreover, by P17, the development gene profile of astrocytes is complete, and they are demonstrating mature gene expression. Forty-seven gene profiles were conducted by Rusnakova et al. (2013) from age P10 to P50. They concluded that astrocyte populations can be divided into three subpopulations according to their gene expression. They included immature glia from P10, which were characterised by high transcriptional activity of all studied genes, from P20, which were marked by low gene transcript levels, and mature astrocytes mainly from P30 and P50.

Moreover, Clarke et al. (2018) illustrated the expression profile of astrocytes isolated from different brain regions (hippocampus, striatum and cortex) of postnatal day 7 (P7), young adult (P32), mature (10 weeks), middle-age (9.5 months) and aged (2 years) mice. They found that the gene expression of cortical astrocytes was nearly the same during development, while hippocampal and striatal astrocytes have a distinct gene expression pattern. By ageing, hippocampal and striatal astrocytes become more reactive than cortical astrocytes by up-regulating a more significant number of reactive genes, including *C3* and *C4B*, the cytokine pathway (*Cxcl10*), antigen presentation (*H2-D1* and *H2-K1*) and peptidase inhibitor (*Serpina3n*) pathways. They also found that the genes responsible for mitochondrial function and antioxidant protection are down-regulated in aged astrocytes, while the genes encoding the formation and maturation of synapses are unaffected. Orre et al. (2014) indicated that astrocytes isolated from the old mouse cerebral cortex presented increased inflammatory genes compared to young astrocytes.

Similarly, Boisvert et al. (2018) identified gene expression profiles in visual cortex, motor cortex, hypothalamus and cerebellum astrocytes from 4 month- and 2 year-old mice. They demonstrated that all brain regions up-regulated seven genes of reactive astrocytes. In addition, a significant decrease in synapse-inducing genes (*Thbs4* and *Thbs1*) in the ageing hypothalamus and cerebellum was identified, which leads to both synapse impairment by reduction of the synapse formation

and damage to neurons. These results suggest that ageing induces reactivity in astrocytes and may decrease the normal function of astrocytes. Furthermore, the expression of *VEGF* and *FGF-2* and their receptors is reduced in aged astrocytes, which impairs their neuroprotective activity in the CNS (Bernal and Peterson, 2011). It was found that expression of glial glutamate transporter-1 (*GLT1*) and glutamine synthetase, which is the central enzyme for the glutamine-glutamate/GABA shuttle, are reduced during ageing (Cao et al., 2019; Rodríguez-Arellano et al., 2016), and GFAP expression and hypertrophy of astrocytes are increased (Rodríguez-Arellano et al., 2016). Taft, Vertes and Perry (2005) examined the distribution of GFAP<sup>+</sup> astrocytes in regions of the cortex, cerebellum and brainstem of adult and rat pup brains. They discovered a significant difference in GFAP levels across the areas, but similar levels during development.

However, during early postnatal development, secretion of molecules like thrombospondins and glypicans in the cortex plays an essential role in building excitatory synapses (Molofsky and Deneen, 2015). Many important astrocyte genes are up-regulated within three to four weeks after birth, such as glutamate transporter *GLT1*, connexin-43 and 30 and potassium channel *Kir4.1* (Yang, Higashimori and Morel, 2013). Gautron, De Smedt-Peyrusse and Layé (2006) established that signal transducer and activator of transcription 3 (*STAT3*) levels increased with age (P3, P10 and P21). It was also found that each brain region contained unique molecular patterns after studying the gene expression profiles of astrocytes from various developmental stages and regions (Bachoo et al., 2004). For example, *BMP6* is increased in cortex astrocytes with age, and cerebellum astrocytes undergo pro-inflammatory changes with age, with up-regulation of *caspase-1* and *-12* and the chemokine *Cxcl5* genes (Boisvert et al., 2018). Taken together, these results clarify that astrocyte genotype and phenotype can change with development, further contributing to heterogeneity.

## **1.2 Reactive gliosis**

In several CNS insults, including stroke, trauma, growth of a tumour, neurodegenerative disease and pain, the astrocyte can become 'reactive'. This process of astrocyte activation is usually called reactive gliosis or reactive astrogliosis (Pekny and Nilsson, 2005). These reactive astrocytes are characterised by a change in cell morphology, up-regulation or down-regulation of many genes and molecules that change normal astrocyte functions.

### **1.2.1 Features of reactive gliosis**

#### **1.2.1.1 Morphology change**

Overexpression of GFAP, hypertrophy of cellular processes of astrocytes, proliferation and formation of the glial scar are the evident features of reactive gliosis in vivo and in vitro (Pekny and Nilsson, 2005; Matias, Morgado and Gomes, 2019; Neal and Richardson, 2018). The extent of cell hypertrophy and the induction of stellate morphology are variable according to the type of disease, its severity, and the location of the astrocyte relative to a site of injury (Anderson, Ao and Sofroniew, 2014; Sun and Jakobs, 2012). Wilhelmsson et al. (2006) examined the morphology of protoplasmic cortical astrocytes in response to an electrical-induced lesion that causes injury. They found that the astrocyte morphology changed, with an increase in the number of primary processes characterised by a bushier appearance. However, another study examined protoplasmic cortical astrocyte morphology following ischemia and found that the processes of reactive astrocytes became shorter and thicker (Sullivan et al., 2010). Sun et al. (2010) discovered that following an optic nerve injury, reactive fibrous astrocytes showed a reduction in the number of processes and thickening of branching. Changes in astrocyte morphology could slow recovery after injury. Sofroniew (2009) suggests that in mild to moderate situations, reactive astrogliosis has the potential for resolution, while in severe conditions, reactive

astrocytes form a scar; the morphological changes are lasting for a longer time (>2 months).

To understand the mechanism underlying changes to astrocyte morphology, it is important to consider the cytoskeletal organisation of astrocytes in culture and in vivo. Firstly, microtubules form a dense network in mature astrocytes (Potokar et al., 2007). Secondly, the connected, scaffold-like complex in astrocytes is made of different intermediate filament proteins. Astrocyte progenitors express vimentin and nestin, whereas maturing astrocytes express GFAP and vimentin (Pekny and Pekna, 2004). Thirdly, the actin cytoskeleton is responsible for inducing stellate morphologies of astrocytes (Schiweck, Eickholt and Murk, 2018). Fourthly, myosin and the ezrin/radixin/moesin (ERM) proteins have a role in controlling astrocyte morphology (Burgos et al., 2007).

In the case of reactive gliosis, microtubules begin to reorient and connect with intermediate filament proteins to increase and elongate the processes of astrocytes (Schiweck, Eickholt and Murk, 2018). Up-regulation of intermediate proteins can occur in reactive astrocytes, which play a role in maintaining cell polarity, directing movement and control of nuclear positioning and interacting with other filament systems of the cytoskeleton (Schiweck, Eickholt and Murk, 2018). It was found that GFAP/Vim knockdown mice show a reduction of reactive gliosis, impaired formation of the glial scar and develop the characteristic of thickening cellular processes (Hol and Pekny, 2015). These results suggest that intermediate filament up-regulation is an important component of reactive astrogliosis.

The actin cytoskeleton is found around the cell body in reactive astrocytes and plays a role in the extension of the processes and induction of hypertrophy of astrocytes (Schiweck, Eickholt and Murk, 2018). The interaction of actin fibres with myosin-II causes the polygonal shape of astrocytes (John et al., 2004), while

the stellate form of astrocytes is characterised by a lack of actin stress fibres in response to the activation of Arp2/3 dependent actin protein (Murk et al., 2013). It was also found that increased K<sup>+</sup> uptake by astrocytes leads to membrane depolarisation, morphologic changes and cell hypertrophy (Vallejo et al., 2010). This change in astrocytes morphology can be due to changes in the expression of many genes involved in cell morphology, which is controlled by the activation of STAT3 as a transcription factor (Burda and Sofroniew, 2014). Moreover, activation of many signalling pathways such as cAMP, RhoA (Schiweck, Eickholt and Murk, 2018) and fibroblast growth factor (FGF) signalling (Kang et al., 2014) can induce morphological changes in astrocytes, which will be discussed later in this review.

#### **1.2.1.2 Change in the gene expression profile**

In response to CNS diseases in vivo or as a result of inflammatory treatment in vitro, reactive astrocytes express a range of genes that do not occur in normal astrocytes. Zamanian et al. (2012) used Affymetrix GeneChip arrays to identify the gene expression profile of reactive astrocytes after using two mouse injury models, ischemic stroke and neuroinflammation by lipopolysaccharide (LPS). They found that in response to both injuries, the reactive astrocytes expressed two key genes: *Lcn2*, a secreted lipophilic protein that is induced after infection and limits bacterial growth, and *Serpina3n*, a secreted peptidase inhibitor whose expression is induced by inflammation and nerve injury. These two genes were up-regulated on stellate morphology reactive astrocytes and could not be detected in normal astrocytes. In addition, in the case of stroke, the astrocytes up-regulated genes with a beneficial or protective function, whereas LPS treatment induced genes with a harmful role. Zamanian and his group divided gene expression into five groups. Group 1 contained 37 genes that were responsible for proliferation, including late-phase cyclins *b1* and *b2* (*Ccnb1* and *Ccnb2*), *Cdk1*, *Top2a* and the proliferation marker *Ki67*. Group 2 contained 44 genes, including the classic reactive gliosis marker *vimentin* *galectins* *Lgals3* and *Lgals1* and *osteopontin* (*Spp1*). Group 3 was

the largest and contained 135 genes, including *Lcn2*, *Serpina3n*, tweak receptor (*Tnfrsf12a*), *S1pr3* and *all Ptx3*. Group 4 contained 22 genes, such as chemokines *CXCL1*, *CXCL2*, and *CXCL1* as well as reactive gliosis marker *GFAP*. Group 5 contained 65 genes, including *Bdnf*, the oncostatin M receptor (*Osmr*) and transcription factor tumour suppressor *klf6*. Similarly, up-regulation of *Serpina3n*, *Cxcl10* and *C4B* in reactive astrocytes in the hippocampus, striatum and cortex was detected following the LPS injection in mice (Clarke et al., 2018). In addition, Pang, Cai and Rhodes (2001) classified the up-regulation of genes expressed after LPS treatment into transcription factors (*STAT3*, *NFκB* and *cAMP response element-binding protein*), cytokines and chemokines, growth factors and metabolic enzyme-related proteins. Treatment of primary mouse astrocytes with tumour necrosis factor-alpha (TNFα) up-regulated NFκB pathway-related genes, such as *ccl2* and *lcn2* (Birck et al., 2016). Injection of adult mice with LPS increased the mRNA expression of *IL-1β*, *IL-6* and *TNFα* in astrocytes. It also caused a decrease in the mRNA expression of *TGFβ*, but no change was noticed in *IL-10* (Norden et al., 2016). IL-1β activated human fetal astrocytes in culture and led to up-regulation of cytokines and chemokines gene expression (John et al., 2005).

Using cDNA arrays, 268 genes were detected in human adult astrocytes stimulated with TNFα, IL-1β and IFNδ. TNFα increased expression of several genes, including those encoding the chemokines *CCL2*, *CCL5* and *CXCL8*, growth factors including *BMP2A*, *BMP3*, neuromodulin (*GAP43*), *BDNF* and *G-CSF*, and receptors such as the *CRF* receptor, the calcitonin receptor (*CTR*) and *TKT*. The response to IL-1β involved the same range of genes, but the level of expression was lower compared with TNFα, while IFNδ had no effects on the expression of any of the 268 genes (Meeuwsen et al., 2003). Combination treatment of cortical astrocytes with TGFβ1, LPS and IFNδ significantly induced reactive gliosis, which is characterised by the up-regulated expression of chemokines and growth factors. Also, several genes

for G-protein-coupled receptors (GPCRs) involved in calcium signalling were significantly down-regulated, such as *Cxcr4*, *Adra2a*, *Ednra*, *P2y1*, *Gnao1* and *Gng7*, or up-regulated, such as *P2y14*, *P2y6*, *Ccr12* and *Gnb4* (Hamby et al., 2012). Inducing a spinal cord injury in mice produced *Cdh2*, *Sox9*, *Xylt1*, *Chst11*, *Csgalnact1*, *Acan*, *Pcan* and *Slit2* genes, which play a role in scar-forming in astrocytes (Okada et al., 2018).

### **1.2.1.3** Molecular regulators of astrogliosis

Reactive astrogliosis can be regulated by extracellular signals or via the intrinsic signalling pathway of astrocytes (Table 1.1 and Figure 1.4) (Colombo and Farina, 2016; Sofroniew and Vinters, 2010; Rossi, 2015; Sofroniew, 2015; Kang and Hébert, 2011). Each of these molecular signals plays a role in reactive gliosis, as summarised in Table 1.2 (Colombo and Farina, 2016; Sofroniew, 2017; Sofroniew, 2009).

One of the intrinsic signalling pathways involved in reactive gliosis is the MAPKs cascade. It is branched into three different types: ERK, p38 and c-JNK (Gosselin et al., 2010). Some studies have found that the p38 pathway is activated in microglia (Chang et al., 2010), and the c-JNK is stimulated in astrocytes and activated by cytokines such as TNF $\alpha$  and increased the expression of the chemokine of CCL2 by astrocytes (Tian et al., 2017; Zhuang et al., 2006). This evidence established that blocking these pathways in both microglia and astrocytes prevents the induction of IL-1 $\beta$ , TNF $\alpha$  and IL-6 (Wang et al., 2009; Zhuang et al., 2006; Wen et al., 2009).

NF $\kappa$ B and SOCS3 are pro-inflammatory transcription factors that regulate the release of CCL2 and CXCL10 from astrocytes (Sofroniew, 2017; Colombo and Farina, 2016). NF $\kappa$ B can modulate anti-apoptotic proteins, cell adhesion molecules, glial fibrillary acidic protein, inducible nitric oxide synthase and neurotrophic factors (Colombo and Farina, 2016). In addition, vasoactive

endothelial growth factor (VEGF) can be released from astrocytes in response to IL-1 $\beta$  and increase blood-brain barrier permeability and promote leukocyte extravasation (Sofroniew, 2017). Inflammatory gene induction of IL-17 in astrocytes is mediated by the Act1 signalling pathway (Sofroniew, 2017; Colombo and Farina, 2016). Increased release of ATP leads to activation of P2Y and P2X receptors, which activate mitogen-activated protein kinase (MAPK), extracellular signal-regulated kinases (ERKs) and Ca<sup>2+</sup> signalling pathways, promoting inflammation (Franke and Illes, 2014).

Furthermore, up-regulation of the expression of toll-like receptors (TLR2 and TLR4) in reactive astrocytes is controversial. It was found that reactive astrocytes can activate MAPKs and NF $\kappa$ B signalling pathways through the activation of toll-like receptors which are responsible for inducing the release of pro-inflammatory chemokines and cytokines, including IL-1 $\beta$ , TNF $\alpha$ , IL-6 and nitric oxide (NO) synthase (Fellner et al., 2013; Gorina et al., 2011; Lukin et al., 2017; Nakano et al., 2015; Sofroniew, 2017; Sofroniew, 2009; Vallejo et al., 2010). However, other studies have demonstrated that microglia, but not astrocytes, express TLR4 (Holm, Draeby and Owens, 2012; Facci et al., 2014).

In contrast to these pro-inflammatory signals, TGF $\beta$  and A20 are intracellular molecules released from astrocytes that support the resolution of inflammation by inhibiting NF $\kappa$ B signalling (Sofroniew, 2017; Colombo and Farina, 2016). Similarly, the STAT3 signalling pathway controls the anti-inflammatory function of astrocytes by mediating scar formation and preventing the spread of leukocytes and microbial pathogens after CNS injury (Sofroniew, 2017; Colombo and Farina, 2016). However, translocation of p-STAT3 from the cytoplasm to the nucleus starts the transcription of many genes involved in the release of pro- or anti-inflammatory cytokines and chemokines (Sofroniew, 2009; Sofroniew, 2017; Hol and Pekny, 2015).

Shh and Olig2 regulate the proliferation of reactive astrocytes, and deletion of Olig2 in astrocytes diminishes their proliferation (Buffo, Rolando and Ceruti, 2010; Kang and Hébert, 2011). Mutants in BMP1 specifically in astrocytes after spinal injury are associated with decreased hypertrophy of the astrocytes and lower levels of GFAP compared to controls (Kang and Hébert, 2011). In addition, the elevation of inhibitory factor chondroitin sulfate proteoglycans (CSPGs) could be an indicator of reactive gliosis, which plays a role in limiting the regrowth of injured axons (East, Golding and Phillips, 2009; Beckerman et al., 2015; Kerstetter and Miller, 2012). Increasing excitatory neurotransmitter in the synapse can occur due to the reduction of glutamate uptake and down-regulation of the glutamate transporter (GLAST and GLT1), leading to increased neuron excitability (Milligan and Watkins, 2009; Vallejo et al., 2010). Additionally, many gliotransmitters such as prostaglandins, GDNF, ATP, nitric oxide, D-serine and glutamate could be increased in the extracellular space and increase the expression of many receptors on glial cells which enhance Ca<sup>2+</sup> signalling pathways in astrocytes and neuron excitability (Milligan and Watkins, 2009; Old, Clark and Malcangio, 2015; Vallejo et al., 2010). This range of signalling pathways linked to the dramatic phenotypic changes of reactive gliosis further contribute to astrocyte heterogeneity.

**Table 1.1 Molecular regulators of reactive gliosis**

Type	Source	Example
<b>Extracellular molecular signals</b>		
Damage-associated molecular patterns (DAMPs)	Cell damage	ATP, nitric oxide
Neurotransmitters	Neurons	Glutamate, noradrenaline
Hormones	Neurodegeneration	$\beta$ -amyloid ( $A\beta$ )
Cytokines and growth factors	Other glial cells and immune cells	IL-1 $\beta$ , TNF $\alpha$ , INF $\delta$ , IL-6, CNTF, LIF, TGF $\beta$ , IL-10, epidermal growth factor (EGF), FGF2, Shh
Pathogen associated molecular patterns (PAMPs)	Microbes	LPS
Hypoxia and metabolic stress	Ischemia	Oxygen deprivation, glucose deprivation
<b>Astrocyte-produced molecules</b>		
Intracellular signalling pathways	Astrocytes	STAT3, JAK2, NF $\kappa$ B, SOCS3, MAPK, Olig2, cAMP, Ca <sup>2+</sup> , Nuclear receptor related 1(Nurr1), c-Jun N-terminal kinases (JNK), PKA, PKC, ERK, Act1, A20
Cytokines		IL-1 $\beta$ , IL-6, IL-11, IL-15, IL-17, TNF $\alpha$ , TGF $\beta$ , INF $\delta$ , IL-6, IL-10, IL-11, IL-19, IL-27
Chemokines		CCL2, CCL5, CCL7, CCL8, CCL12, CXCL1, CXCL9, CXCL10, CXCL12, CXCL16
Growth factors		Brain-derived neurotrophic factor (BDNF), Nerve growth factor (NGF), glial cell line-derived neurotrophic factor (GDNF), BMP1, VEGF, CNTF
Extracellular matrix		chondroitin sulfate proteoglycans (CSPG)
Intermediate filaments		GFAP, vimentin, nestin Intermediate filaments
Transmitters		Glutamate, D-serine
Small molecules		nitric oxide , prostaglandin E, ATP

**Table 1.2 Role of different molecules in reactive gliosis**

<b>Signalling pathways and molecules</b>	<b>Function</b>
STAT3, NFκB, cAMP, Rho-kinase	Structural modulation
STAT3, BMP1, NFκB	Astrocyte hypertrophy and scar formation
Olig2, JNK/c-Jun, Shh, STAT3	Astrocyte proliferation
CSPG, TGFβ, SOX9	Scar related axon growth inhibitors
NFκB, MAPKs, SOCS3, CCL2, CCL5, CCL7, CCL8, CCL12, CXCL1, CXCL9, CXCL10, CXCL12, CXCL16, IL-1β, IL-6, IL-11, IL-15, IL-17, TNFα, VEGF, Act1	Pro-inflammatory
STAT3, TGFβ, INFδ, IL-6, IL-10, IL-11, IL-19, IL-27, A20, BDNF, Nurr1	Anti-inflammatory

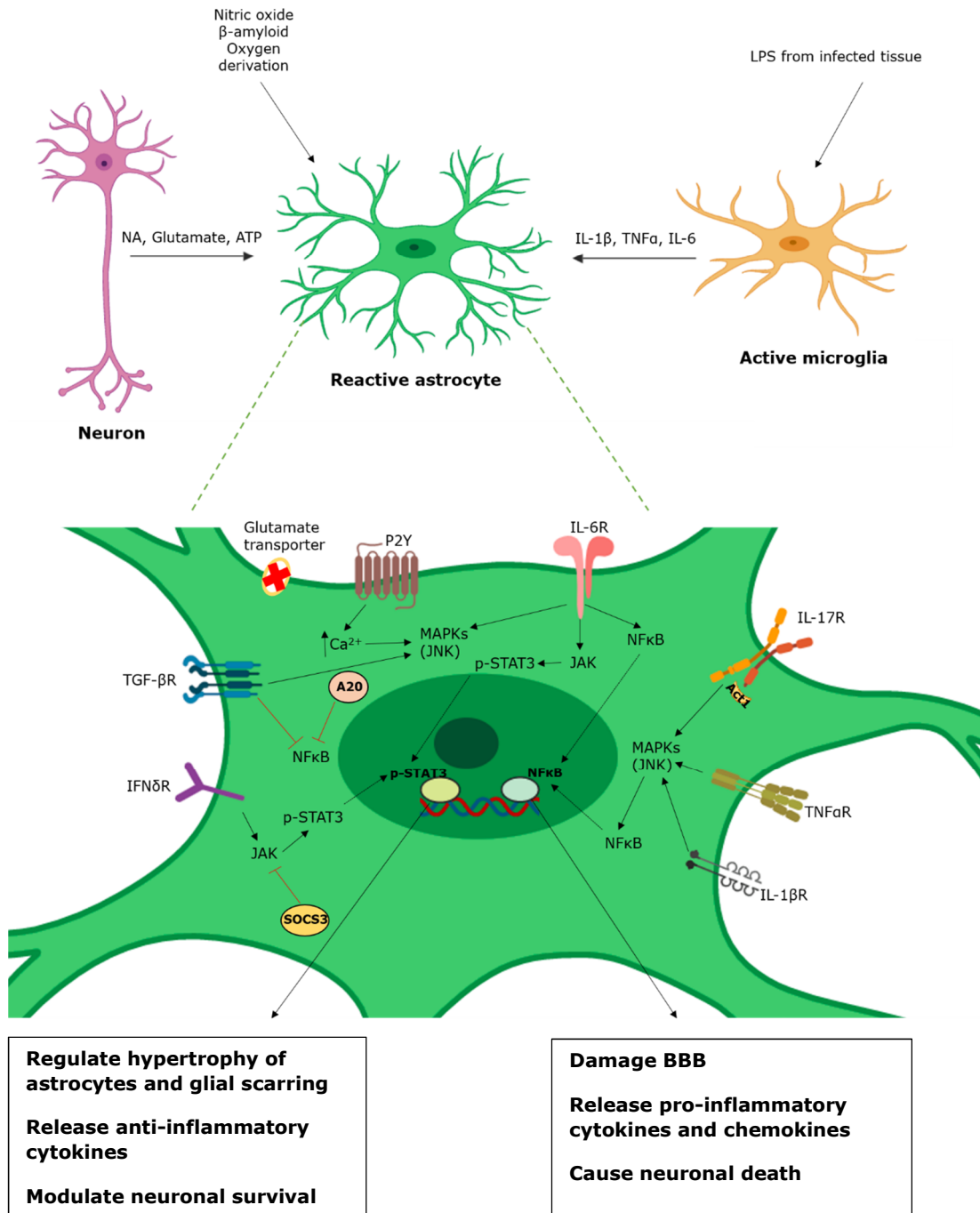


**Figure 1.4 Schematic diagram showing the interaction of an astrocyte with microglia and neurons under pathological conditions.** Increased release of neurotransmitters from neurons, the presence of nitric oxide,  $\beta$ -amyloid and oxygen deprivation as well as release of cytokines from active microglia cause astrocyte reactivity, leading to down-regulation of the glutamate transporter, and up-regulation of cytokines receptors in astrocytes that activate MAPKs, NF $\kappa$ B and STAT3 signalling pathways. MAPKs and NF $\kappa$ B have detrimental roles, while STAT3 plays a protective role in reactive astrocytes.

### **1.2.2 Heterogeneity of reactive astrocytes**

Reactive gliosis also varies with age and brain region. Astrocytes respond differently according to several sites and during development. After a stroke, TGF $\beta$  signalling is increased with age in 5- and 18-month-old mice brains (Doyle et al., 2010). Furthermore, astrocytes treated with LPS to induce reactive gliosis have a greater increase in the level of GFAP, IL-1 $\beta$  and TNF $\alpha$  with age compared with young rats (Lynch et al., 2010). Following nerve injury, microglia and astrocytes play a role in the maintenance of neuropathic pain. It was found that they have a weak response in young animals compared with adults, which could explain the absence of neuropathic allodynia in young animals (Vega-Avelaira, Moss and Fitzgerald, 2007). Yoon et al. (2017) demonstrated that after focal demyelinating injury, the level of GFAP, IL-6 and STAT3 is higher in the spinal cord compared to brain astrocytes and is increased during development.

Following brain injury, distinct changes to reactive gliosis morphology have been detected in vivo in other brain regions (Hill, Barbarese and McIntosh, 1996). Morga, Faber and Heuschling (1999) investigated the level of IL-6 and TNF $\alpha$  production in response to LPS in primary rat astrocytes from five different brain regions (cortex, hippocampus, striatum, septum and brainstem). They established that the septum, striatum and brainstem have much higher levels of IL-6 production than the cortex and hippocampus, while TNF $\alpha$  production in the septum and striatum is higher than the cortex, hippocampus and brainstem.

Moreover, the role of reactive astrogliosis in many diseases differs and is a subject of debate. Many studies have found that reactive astrocytes are harmful because they can inhibit axon regeneration after CNS injury, which worsens spinal cord injuries by activation of NF $\kappa$ B (Brambilla et al., 2009), leading to the release of pro-inflammatory cytokines and chemokines (Luo et al., 2016). Also, in many neurodegenerative diseases, astrocytes can impair their physiological function (Verkhratsky et al., 2014). Conversely, a considerable amount of research has

identified that the formation of a glial scar from a reactive astrocyte has the ability to remove pathogens and repair the nervous tissue in several diseases such as spinal cord injury, CNS trauma, ischemia and experimental autoimmune diseases of the CNS (Faulkner et al., 2004; Voskuhl et al., 2009; Sofroniew, 2017; Huang et al., 2019).

Reactive astrocytes have recently been classified into the A1 and A2 subtype (Liddelow et al., 2017). A1 reactive astrocytes are proposed to be induced by activated microglia releasing IL-1 $\alpha$ , TNF $\alpha$  and C1q cytokines and triggering neuroinflammation, leading to activation of the NF $\kappa$ B signalling pathway to secrete neurotoxins that cause the rapid death of neurons. A1 astrocytes are characterised with an increase in the up-regulation of *C3*, *CFB* and *MX1S* genes. They lose many normal functions, such as the promotion of neuronal survival and outgrowth as well as the induction of fewer and weaker synapses compared with healthy astrocytes. In contrast, A2 reactive astrocytes are induced by ischaemia. They demonstrate a neuroprotective role and tissue reparative effects induced by the secretion of several neurotrophic factors via STAT3-mediation. The A2 astrocyte-related gene *S100A10* is essential for cell proliferation, membrane repair, and inhibition of cell apoptosis. Moreover, A2 astrocytes promote the expression of anti-inflammatory cytokine TGF $\beta$ , which participates in synaptogenesis and plays a neuroprotective role (Liddelow et al., 2017; Liddelow and Barres, 2017; Li et al., 2019). In addition, Sofroniew (2009) proposed that reactive astrocytes could be classified according to mild-moderate or severe astrogliosis. Mild-moderate cells have a resolving role that returns to healthy cells phenotype; however, severe reactive astrocytes cause a glial scar in response to inflammatory stimuli.

By considering these results, it becomes apparent that astrocytes have dual beneficial and harmful roles which depend on the nature of the injury or disease. In addition, microglia can modulate active astrocytes during injury and disease (Matias, Morgado and Gomes, 2019).

### **1.3 Astrocyte stellation signalling pathway**

The previous section outlined the complex neuroinflammatory signalling environment of reactive gliosis. What is less well understood is how this environment causes changes to astrocyte morphology during reactive gliosis.

Astrocytes display a branching cell shape *in vivo*. In the case of reactive astrocytes under pathological conditions, they are characterised by longer branching, thickening of processes and somatic hypertrophy cell shape (Pekny and Nilsson, 2005; Matias, Morgado and Gomes, 2019; Neal and Richardson, 2018); however, culturing astrocytes in standard serum-containing medium leads to cells exhibiting a flat, polygonal cell morphology (Ramakers and Moolenaar, 1998).

Activation of many signalling pathways such as cAMP, p-STAT3 or inhibition of RhoA can induce a more stellate shape of astrocytes resembling their morphology *in vivo* (Masaki et al., 2000; Ramakers and Moolenaar, 1998; Fedoroff et al., 1984; Tiryaki et al., 2015; Fahrig and Sommermeyer, 1993; Sands et al., 2006; Renault-Mihara et al., 2017; Renault-Mihara and Okano, 2018; Perez et al., 2005; Washburn and Neary, 2006) (Figure 1.5). Stellation is characterised by shrinking of the cytoplasm and formation of thin processes by loss of actin stress fibres (Ramakers and Moolenaar, 1998). Morphology changes of astrocytes by formation of the processes seems to modify the signals and the interaction between the astrocyte and neuron *in vivo* (Zeug et al., 2018). Therefore, stellation of astrocytes may play significant roles in CNS physiology and pathology.

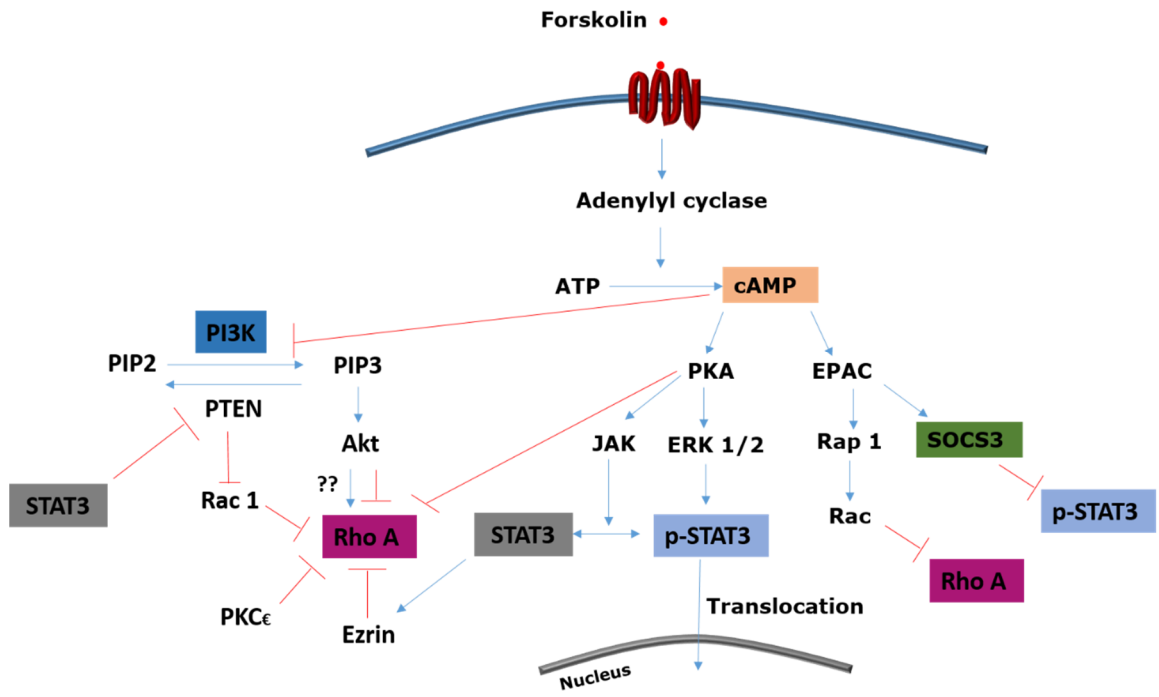


**Figure 1.5 Schematic diagram showing the proposed signalling pathways stimulated with forskolin that controls the stellation of astrocyte morphology.**

### 1.3.1 cAMP-induced stellation

Stimulation of adenylyl cyclase with  $\beta$ -adrenergic stimulators, adenosine, neuromodulators (serotonin, dopamine and histamine), forskolin and neuropeptides such as vasoactive intestinal peptide (VIP) and pituitary adenylyl cyclase-activating polypeptide (PACAP) (Zhou, Ikegaya and Koyama, 2019) can convert ATP to cAMP in many neural cells (Sadana and Dessauer, 2009). This cAMP plays a role in synaptic plasticity, learning, memory, sensitisation of nociceptors and neurodegeneration (Tanabe, Kozawa and Iida, 2016). In pain, it was found that increasing the level of cAMP in neurons leads to hyperalgesia (Hucho and Levine, 2007), while the absence of cAMP reduces the pain response (Sadana and Dessauer, 2009). Also, the cAMP pathway can maintain the pain through activation of PKA, the GDP/GTP exchange factor Epac and  $Ca^{2+}$  signalling pathway as well (Hucho and Levine, 2007; Zhou, Ikegaya and Koyama, 2019).

Treatment of astrocytes *in vitro* with cAMP-increasing stimuli can change the astrocyte morphology to a stellate cell shape (Abe and Misawa, 2003; Dagainakatte

et al., 2008; Fang et al., 2012; Vardjan, Kreft and Zorec, 2014) by the reorganisation of the cytoskeleton with decrease the phosphorylation in light chain of myosin (MLC) and actin-depolymerising factor leading to loss the actin stress fibres (Won and Oh, 2000; Baorto, Mellado and Shelanski, 1992). In addition, cAMP activates the PKA signalling pathway, leading to the increased expression of the monopolar spindle-one-binder (Mob) family of zinc-binding proteins, which controls cellular processes (Fang et al., 2012). Also, stellation seems to depend on the actin-binding protein profilin 1 (PFN1), which is regulated by PKA phosphorylation (Schweinhuber et al., 2015; Zeug et al., 2018). It was found that inhibiting the Arp2/3 complex causes rapid expansion of astrocyte cell bodies and reduces branching of processes (Murk et al., 2013).

Cyclic AMP has diverse roles in reactive astrocytes. Dagainakatte et al. (2008) tested gene expression in two different models of reactive gliosis by treating the astrocyte with dibutyryl cAMP (dbcAMP) as the first model and exposure to combined IL-1 $\beta$ /IFN $\delta$  as a second model. They demonstrated that both models shared 44 differentially expressed genes related to a stellate astrocyte morphology as well as increased levels of GFAP expression and the release of pro-inflammatory mediators. However, Paco et al. (2016) discovered that treating neonatal cortical astrocytes with a cAMP analog up-regulates genes which are responsible for homeostatic control, metabolic and structural support to neurons and antioxidant defence while down-regulating the genes associated with astrocyte activation, such as cytoskeletal rearrangement, triggering of immunological reactions and production of scar components. Wandosell, Bovolenta and Nieto-Sampedro (1993) claimed that the cultured astrocytes treated with a cAMP analog had a different biochemical function than reactive astrocytes in vivo because it did not express epidermal growth factor receptor (EGFR), microtubular associate protein 2 and  $\beta$  amyloid precursor protein.

Moreover, it was discovered that cAMP can play an anti-inflammatory role by suppressing NF $\kappa$ B activation (Gavrilyuk et al., 2002) and inducing the expression of A20 (Tumor necrosis factor alpha-induced protein 3), which is rapidly induced by the tumor necrosis factor and has been shown to inhibit NF $\kappa$ B activation (Laureys et al., 2014), leading to lowered IL-6 secretion, up-regulated IL-10 expression (Christiansen et al., 2011; Paco et al., 2016) and decreased levels of CCL5 (Gavrilyuk et al., 2002). Nevertheless, cAMP in combination with TNF $\alpha$  can increase the expression of IL-6 (McNamee et al., 2010).

Collectively, cAMP induces astrocyte stellation by controlling many mechanisms and seems to have the anti-inflammatory roles sometimes associated with reactive astrocytes.

### **1.3.2 Role of RhoA and ROCK in stellation**

Astrocytes express monomeric small G proteins that can be divided into groups according to their structure: the Rho, Ras, Rab, Arf, Ran and RGK families. The Rho family, including RhoA, Rac1 and Cdc42, plays an important role in regulating a variety of cellular functions such as gene transcription and controlling the shape of astrocytes by adjusting the actin cytoskeleton (Zeug et al., 2018). Activation of RhoA can induce the release of inflammatory mediators from astrocytes, such as COX2, IL-6 and VEGF (Dusaban et al., 2017). Studies demonstrate that inhibiting the RhoA-ROCK signalling pathway induces astrocyte stellation (Abe and Misawa, 2003; Zeug et al., 2018; Racchetti, D'Alessandro and Meldolesi, 2012; Ramakers and Moolenaar, 1998). Similarly, it was found that overexpression of Rac1 causes stellation by inhibiting RhoA (Zeug et al., 2018). Racchetti, D'Alessandro and Meldolesi (2012) discovered that knockdown or inhibited Rac1 with blockers led to a reduction or elimination of the stellation process.

Others kinase families can link to RhoA and affect astrocyte morphology. Burgos et al. (2007) found that protein kinase C (PKC), especially PKC $\epsilon$ , can inhibit RhoA activity, leading to stellation. Perez et al. (2005) also discovered that stellation of

the astrocyte treated with forskolin (a cAMP-raising agent) was significantly blocked in astrocytes with an active mutant of RhoA. This blocking occurred in a PKA-independent manner because a PKA blocker cannot inhibit stellation in the presence of forskolin. The PI3K blocker inducing stellation was blocked in an active mutant of RhoA astrocytes. These results suggest that forskolin causing stellation is due to the inhibition of PI3K that is linked to RhoA (Perez et al., 2005). In addition, AMP-activated protein kinase (AMPK) can induce stellation in astrocytes, which is prevented in activated RhoA-transfected astrocytes (Favero and Mandell, 2007). This suggests the involvement of RhoA in astrocyte morphological changes.

### **1.3.3 p-STAT3 and reactive gliosis**

STAT3 is a transcription factor that regulates the transcription of many genes in response to extracellular signals. These signals lead to phosphorylation of STAT3 to the active forms, including tyrosine and serine p-STAT3 (Figure 1.6), followed by translocation to the nucleus to start gene transcription (Coulombe et al., 2003; Dimri, Sukanya and De, 2017; Debidda et al., 2005; Huang et al., 2015; Lin et al., 2014; New and Wong, 2007; Renault-Mihara and Okano, 2018; You et al., 2015; Yu et al., 2014; Hazan-halevy, Harris and Chen, 2010).

STAT3 plays a key role in astrocyte proliferation. It regulates proliferation of the neuronal precursor cells during development (Kim et al., 2010) and in reactive astrocytes following ATP treatment (Washburn and Neary, 2006) and after neuropathic pain (Tsuda et al., 2011). It was found that the number of newly formed astrocytes within the glial scar are decreased in STAT3 knockdown mice (Wanner et al., 2013). In addition, STAT3 induces GFAP expression (Hol and Pekny, 2015). The level of GFAP was significantly decreased after inhibiting STAT3 with a genetic mutant or pharmacological drugs following injury (Ben Haim et al., 2015b; Herrmann et al., 2008; Wanner et al., 2013; Sriram et al., 2004; Nobuta et al., 2012).

STAT3 regulates the release of many inflammatory cytokines and chemokines (CCL20, CX3CL1, CXCL5 and CXCL10) *in vivo* and *in vitro* after LPS stimulation (Liu et al., 2013; O'Callaghan et al., 2014). Decreasing the release of these inflammatory mediators by up-regulation of SOCS3 expression, a specific inhibitor of the JAK–STAT3 pathway, led to decreased microglial activation (Ben Haim et al., 2015b). However, STAT3 demonstrates anti-inflammatory roles as well by the increased expression of CSPGs (Anderson et al., 2016), which aid in injured axon regeneration and release anti-inflammatory cytokines in many diseases (Colombo and Farina, 2016). Genetic inhibition of STAT3 can limit migration of reactive astrocytes, increase the spread of inflammatory cells and cause neural disruption and demyelination, which worsens the spinal cord injury (Okada et al., 2006).

STAT3 in reactive astrocytes controls the expression of thrombospondin-1 (TSP1), which plays a role in the recovery of excitatory synapses onto axotomised motor neurons *in vivo*, and high levels of TSP1 have beneficial roles in neuronal survival and plasticity during astrogliosis *in vitro* (Tyzack et al., 2014). These results suggest that STAT3 has both a protective and harmful role.

Furthermore, STAT3 can modulate the morphology of reactive astrocytes. Several lines of evidence suggest that the formation of a glial scar and change the astrocytes morphology by striking cytoplasm and formation of processes are regulated by STAT3 after spinal cord injury *in vivo* (Kang and Hébert, 2011; Herrmann et al., 2008; Wanner et al., 2013; Sloan and Barres, 2015; Nobuta et al., 2012). It was found that GAP43 expression is mediated by STAT3 in cultured astrocytes, leading to an increase in the number and length of astrocyte processes (Hung et al., 2016).

Overall, these studies indicate that STAT3 is a 'master regulator' in reactive astrocytes by controlling the release of pro- and anti-inflammatory mediators, regulating the expression of GFAP and proliferation, as well as modulating the morphology changes of reactive astrocytes *in vivo*.

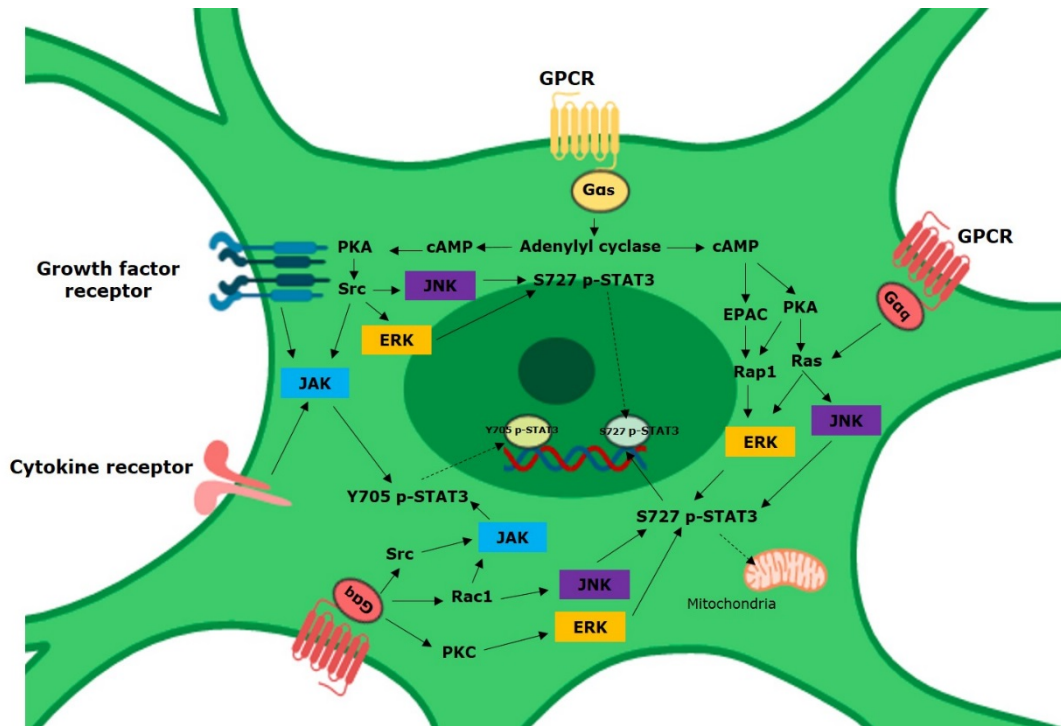


**Figure 1.6 Schematic diagram showing the extracellular signals that activate STAT3 signalling pathways.** Activation of Janus kinases (JAKs) with cytokines, hormones or growth receptors and GPCRs (G $\alpha$ s and G $\alpha$ q) can phosphonate STAT3 to Tyr705-phospho-STAT3, which translocates into the nucleus to activate target genes. Moreover, tyrosine kinase and cytoplasmic kinases like Src kinase are involved in tyrosine p-STAT3 activation. STAT3 can also be phosphorylated at serine 727 (S727) by extracellular signal-regulated kinases (ERK) and c-Jun N-terminal kinase (JNK), which can also trigger translocation from cytoplasm to the nucleus and mitochondria.

#### **1.4 Aim and objective**

The main aim of this project is to investigate the mechanisms of reactive gliosis astrocytes in vitro. The strategy employed in this research depends on four specific objectives:

Firstly, an optimised protocol for pure astrocyte cell cultures from the spinal cord. Secondly, developing a quantitative assay for reactive astrogliosis based on morphological analysis. Thirdly, discovering the difference in the reactive astrocytes according to their regions in the CNS and during development. Finally, exploring the role of p-STAT3 in the morphological changes of reactive astrocyte.

## **Chapter 2 Materials and methods**

## **2.1 Animals**

Postnatal day P2 and embryonic E18 Wistar rats (Charles River, UK) were used. All animals were housed in the Biological Services Unit (BSU) at the University of Nottingham. Rats and pups were kept under standard housing environments (12 h/12 h dark-light cycle) and supplied with food and water throughout. Experiments were conducted according to the guidelines defined in the code of practice for humane killing under Schedule 1 of the UK Home Office Animals (Scientific Procedures) Act 1986. All animals were killed by cervical dislocation, and post-mortem tissue was isolated immediately. Experiments were performed according to policies on the care and use of laboratory animals of the British Home Office and were approved by The University of Nottingham Animal Welfare and Ethical Review Body.

## **2.2 Pharmacology**

Forskolin, lipopolysaccharides (LPS), noradrenaline (NA), IL-6, glutamate, ATP, Akti-1/2 trifluoroacetate salt hydrate (Akt inhibitor 1/2) and Uridine diphosphate glucose (UDP-glucose) were purchased from Sigma-Aldrich (St. Louis, MO, USA). Dibutyryl-cAMP sodium salt, substance P, histamine, KT5720 (PKA inhibitor), Y27632 di-hydrochloride (RhoA inhibitor), LY294002 hydrochloride (PI3K inhibitor), prazosin, propranolol and stattic (STAT3 inhibitor) were obtained from Tocris Bioscience (Abingdon, UK). Tumor necrosis factor-alpha (TNF $\alpha$ ) was acquired from R&D Systems (Minneapolis, USA). WP1066 (JAK inhibitor) was bought from Selleckchem (USA). All drugs were prepared as stock solutions in PBS, except forskolin, which was made in DMSO. IL-6 was reconstituted in 10mM HCl, and 100 $\mu$ M of ascorbic acid was added to noradrenaline stock to prevent oxidation. All stock solutions were aliquoted and stored at -20°C. All compounds were diluted in an imaging buffer or culture media depending on an experiment.

## 2.3 Antibodies

The primary and secondary antibodies used are listed in Table 2.1

**Table 2.1 Overview of the primary and secondary antibodies used.**

Antibody	Source	Dilution	
		Immunocytochemistry	Western blot
<b>Primary antibodies</b>			
Rabbit anti-Iba-1	Wako (019-19741)	1:500	
Rabbit anti-glial fibrillary acidic protein (GFAP)	Abcam (ab7260)	1:1000	
Mouse anti-glial fibrillary acidic protein (GFAP)	Thermo Fisher (MS-1376-P1)	1:100	
Rabbit Anti-STAT3 (phospho S727) antibody	Abcam (ab86430)	1:250	1:250
Rabbit Anti-STAT3 (phospho Y705) antibody	Abcam (ab76315)	1:500	1:1000
Mouse anti-total Stat3	Santa Cruz Biotechnology (sc-8019)	1:500	
Mouse anti-GAPDH	Thermo Fisher (MA5-15738)		1:1000
<b>Secondary antibodies</b>			
Donkey anti-Rabbit IgG (H+L) Secondary Antibody, Alexa Fluor® 488 conjugate	Thermo Fisher (A21206)	1:250	
Donkey anti-Mouse IgG (H+L) Secondary Antibody, Alexa Fluor® 488 conjugate	Thermo Fisher (A21202)	1:250	
Donkey anti-Mouse IgG (H+L) Secondary Antibody, Alexa Fluor® 568 conjugate	Thermo Fisher (A10037)	1:250	
IRDye® 680LT Donkey anti-Mouse IgG (H + L)	Li-cor (925- 68022)		1:5000
IRDye® 800CW Goat anti-Rabbit IgG (H + L)	Li-cor (925- 32211)		1:5000

## **2.4 Primary astrocyte isolation and culturing**

Primary astrocyte cultures were obtained from rats of different ages. Neonatal rat P2 days old or E18 rat embryos were used. Under sterile conditions, the spinal cords and cortices were dissected with a dissection microscope. The meninges were removed from the brain and spinal cord. Afterwards, they were pooled in an ice-cold glial medium containing: Dulbecco's Modified Eagle Medium (DMEM) (Sigma Aldrich, USA), 10% fetal bovine serum (FBS) (Gibco, USA), 0.5% penicillin and streptomycin and 50µg/ml L-proline. Whole spinal cords and cortices were then transferred to two separate 15 ml conical centrifuge tubes with a pipette and incubated for 40 minutes with 15µg/ml papain (Worthington, USA) dissolved in 5 ml of glial medium. Following this process, 0.5 ml of DNase solution (20 mg/ml) (AppliChem Panreac, Barcelona, Spain) was added, and the tissue was triturated with 1-mm bore Pasteur pipette 20 times to dissociate the cells.

After this first stage of trituration, the tissue was centrifuged for 6 minutes at 212 g. The supernatant was discarded, and the pellet was re-suspended with 2 ml of glial medium and 0.5 ml of DNase, then triturated 20 times with 1-mm bore Pasteur pipette. The tube was spun again at 182 g for 3 minutes. At this point, the supernatant was collected in a new universal tube, and 10 ml of medium was added to the pellet then triturated with 4-mm bore Pasteur pipette for 20 cycles and spun again, as previously described. This step was repeated once more, and the supernatant was collected. At the end of these steps, the collected supernatant was centrifuged for 6 min at 212 g. The pooled supernatant was removed, and the pellet was re-suspended in 5 ml of glial medium. The final suspension was then passed through a 100-µm cut-off cell strainer.

Cells were counted on a haemocytometer and dispensed into T-75 flasks with a density of  $1 \times 10^6$  cell/ml each. Each flask was filled with 20 ml of the glial medium and placed in a humidified incubator at 37 °C with 5% CO<sub>2</sub> for 24 hours. Afterwards, the flask was shaken overnight at 300 rpm on an orbital shaker

(Starlab, UK) to remove contaminating cells (Kerstetter and Miller, 2012). Several washes were performed with the medium, then the flasks were filled with 20 ml of the glial medium and returned to the incubator for two weeks. The medium was changed every three days thereafter to allow cells to grow until they achieved confluence.

### **2.5 Subculture and treatment of primary astrocyte**

After two weeks, the cells in the flask were washed with PBS, then incubated in 2 ml of 0.05% trypsin-0.02% EDTA solution (Sigma Aldrich, USA) for 5 minutes. Following this, the detachment of the cells was checked every 5 minutes, and astrocyte detachment was enforced by hitting the flask against the palm of a hand (2-3 times). After astrocytes were detached from the culture flask, the trypsin was deactivated by adding 8 ml of the medium. The cell suspensions were collected in a universal tube and centrifuged at 212 g for 6 minutes. The supernatant was removed, and the pellet was re-suspended with 5 ml of the glial medium.

The neonatal and embryonic astrocyte cells were plated in a 6-well plate containing 22-mm diameter coverslips (for immunocytochemistry and epifluorescence live-cell  $\text{Ca}^{2+}$  imaging) at a density of  $2.5 \times 10^4$  cell/ml. Cells were also plated in a 96-well plate and 24-well plate at a density of 5,000 cells/ml and  $1.25 \times 10^4$  cell/ml, respectively, and used for immunocytochemistry. For the Western blot and hit hunter cAMP assay, the cells were sub-cultured directly in a 6-well plate without coverslips at a density of  $3 \times 10^5$  cell/ml. All plates were coated with 100 $\mu$ l-300 $\mu$ l poly-L-lysine (0.1mg/ml). The cells were used for experiments after 48 hours of plating.

The astrocytes were treated with glutamate (100 $\mu$ M) (Xi et al., 2011), ATP (100 $\mu$ M) (Yang et al., 2016) and UPD-glucose (100 $\mu$ M) (Hamby et al., 2012) to produce the  $\text{Ca}^{2+}$  response. To induce reactive gliosis, the astrocytes were treated with forskolin (10 $\mu$ M) (Barres, Chun, and Corey, 1989), LPS (1 $\mu$ g/ml) (Lin et al.,

2008), TNF $\alpha$  (200ng/ml) (Lee et al., 2017), noradrenaline (10 $\mu$ M) (Gavin Norris and Benveniste, 1993; Junker et al., 2002), cAMP analog (1mM) (Abe, K and Saito, 1997), histamine (100 $\mu$ M) (Kubo et al., 1991), substance P (100nM) (Miyano et al., 2010) and IL-6 (100ng/ml) (März et al., 1999). Inhibitors like propranolol (10 $\mu$ M) (Junker et al., 2002), prazosin (10 $\mu$ M) (Muyderman et al., 2001), PKA inhibitor (100nM) (Schweinhuber et al., 2015; Fang et al., 2012), RhoA inhibitor (10 $\mu$ M) (Abe and Misawa, 2003), PI3K inhibitor (20 $\mu$ M) (Perez et al., 2005), Akt inhibitor (10 $\mu$ M) (Hu et al., 2012), stattic (10 $\mu$ M) (Schust et al., 2006; Han et al., 2014) and WP1066 (5 $\mu$ M) (Masliantsev et al., 2018) were added 1 hour before adding the reactive astrocyte inducers.

## **2.6 Epifluorescence live cell Ca<sup>2+</sup> imaging**

Cultured astrocytes on coverslips were transferred to petri dishes and incubated with 1 $\mu$ M fluo-5F AM (Invitrogen, UK) in 20% pluronic in 3 ml of imaging buffer for 30 minutes in the dark at room temperature. The standard imaging buffer contained NaCl (135mM), KCl (3mM), HEPES (10mM), glucose (15mM), MgSO<sub>4</sub> (1mM) and CaCl<sub>2</sub> (2mM), then NaOH was added to achieve pH 7.4. The astrocytes were then moved to another petri dish with an imaging buffer alone and stored in the dark for an additional 30 minutes to allow the remaining fluo-5F AM to de-esterify. After de-esterification, coverslips with loaded cells were transferred to pre-greased imaging chambers in imaging buffer. The chamber was mounted on the stage of a Brunel SP981 inverted fluorescent microscope, and a vacuum line (Dymax 5 by Charles Austen) was placed at the surface of the bathing solution.

Fluorescence microscopy was performed on the coverslips. Images were captured using a Zyla 4.2 sCMOS camera (Andor Technology, Belfast, UK) with an Olympus 10X lens. An appropriate imaging setting was established by using a micromanager software. The usual setting applied was 100 millisecond exposure time to an LED source (470 nm peak, Cool LED pE2) and 4 $\times$ 4 binning. The images were acquired at 1 frame/second and 1200 frames (20 minutes). Agonists were

added at the specified concentrations by manual displacement with an excess of solution into the chamber after 120 seconds.

### **2.7 Real-time morphology imaging**

Cultured astrocytes on coverslips were transferred to petri dishes and incubated for 30 minutes in the dark at room temperature with 1 $\mu$ M calcein-AM (Invitrogen, UK) in 20% pluronic in 3 ml of imaging buffer (see section 2.6 above), followed by 30 minutes in buffer alone for de-esterification. After de-esterification, coverslips with loaded cells were transferred to pre-greased imaging chambers. The chamber was mounted on the stage of Nikon-Eclipse Ti-E fluorescent microscope, and a vacuum line (Dymax 5 by Charles Austen) placed at the surface of the bathing solution.

Fluorescence microscopy was performed on the coverslips. Images were captured using a Zyla 4.2 sCMOS camera (Andor Technology, Belfast, UK) with an Olympus 10X lens. An appropriate imaging setting was established by using micromanager software. The usual setting applied was 500 millisecond exposure time to an LED source (470 nm peak, Cool LED pE2) and 1 $\times$ 1 binning. The images were acquired at 1 frame/minute and 120 frames (2 hours). Agonists were added at the specified concentrations by manual displacement with an excess of solution into the chamber after 10 minutes.

### **2.8 Immunocytochemistry**

Cells were rinsed with Dulbecco's phosphate-buffered saline (PBS 0.1M) and then fixed with 4% paraformaldehyde (pre-warmed at 37 °C) for 10 minutes at room temperature. They were then washed three times with PBS. To increase the permeability of the cells, 0.01% Triton X-100 was added to the cells for 10 minutes and followed by three washes with PBS. The cells were incubated in bovine serum albumin (BSA) 0.5% for 1 hour at room temperature to block non-specific binding sites.

The cells were subsequently incubated at 4 °C overnight with primary antibodies diluted in 0.5% BSA dissolved in PBS. The cells were then washed with PBS three times and incubated for 45 minutes at room temperature with specific secondary antibodies diluted with 0.5% BSA dissolved in PBS. The samples were then rinsed three times in PBS. For a co-staining experiment, cells were blocked again with 0.5% BSA, then another primary antibody was incubated followed by PBS washes and specific secondary antibody incubation. All nuclei were stained with blue fluorescence DAPI (1µg/ml) for 15 minutes, and the cells were rinsed twice in PBS. Next, the cells were cultured in coverslips, which were mounted on slides with mounting media.

The antibodies used in immunocytochemistry are summarised in Table 2.1. All images were taken by the image Xpress ultra-confocal microscope with a Nikon 40X objective (Molecular Devices, Sunnyvale, USA) or a Nikon-Eclipse Ti-E fluorescent microscope with a Zyla 4.2 sCMOS camera (Andor Technology, Belfast, UK) and an Olympus 10X objective lens.

## **2.9 Protein preparation and Western blotting**

### **2.9.1 Protein preparation from astrocytes**

After plating the astrocytes and treating them with specific stimuli, the medium was removed and the cells were washed with PBS. To lyse cells, 200 µl of Radioimmunoprecipitation assay buffer (RIPA) (Table 2.2) and a 1:100 protease and phosphatase inhibitor cocktail (Sigma Aldrich, USA) were added (Sarafian et al., 2010). Cells were scraped out of the plates and collected (3 wells of 6-well plates per sample) to increase protein concentration. Samples were sonicated by the Sonics Vibra-Cell sonicator (Sonics & materials inc, USA) twice for 10 seconds on ice at 40% amplitude. The protein was either immediately used for Western blotting or stored at -20 °C for later processing.

### **2.9.2 Western Blots**

Protein concentration was measured by using the Bicinchoninic acid (BCA) protein assay (Thermo Fischer, UK). Samples were diluted in (1:1) 2X Laemmli buffer (Table 2.2) then vortexed and boiled for 5 minutes. The samples were spun at 12000 X g for 5 minutes. Next, 20 µg samples were loaded into a 12% acrylamide gel. To estimate protein size, a pre-stained protein ladder (Bio-Rad Laboratories Ltd., UK) was loaded along with the samples.

After loading, the protein was separated using PowerPac HC hardware (Bio-Rad Laboratories, UK) connected with the Mini-Protean Tetra Vertical Electrophoresis Cell (Bio-Rad Laboratories, UK) and filled with Tris-glycine-SDS (TGS) running buffer (Table 2.2). The electrophoresis was done at 125V for 1.5 hours. After running the samples, the protein was transferred to a nitrocellulose membrane in Mini Trans-Blot Cell filled with chilled Tris-glycine (TG) blotting buffer (Bio-Rad Laboratories, UK) (Table 2.2) for 2 hours at 80V. The remaining binding sites on the membrane were blocked during a 1 hour incubation in 5% skimmed milk in Tris-buffered saline (TBS) with 0.005% Tween. After blocking, the membrane was incubated with primary antibodies in a blocking buffer overnight on a shaker at 4 °C (Table 2.1). After three washes for 10 minutes, each with TBST (Tris-buffered saline, 0.005% Tween), the membrane was incubated in secondary antibodies diluted in blocking buffer (Table 2.1) for 1 hour on the shaker. The nitrocellulose membrane was washed three times with TBST, then imaged using a Li-cor Odyssey scanner. Quantification was completed using the Image J software. The intensity of each band was measured and normalised against the corresponding GAPDH band and then normalised to the control sample.

**Table 2.2 Buffers used in Western blots**

<b>Buffer</b>	<b>Concentration</b>
<b>RIPA buffer</b>	
NaCl	150mM
Tris-HCl pH 7.6	25mM
NP-40	1%
Na- deoxycholate	1%
SDS	0.1%
Na <sub>3</sub> VO <sub>4</sub>	1mM
NaF	10mM
<b>2X Laemmli buffer</b>	
Tris/Cl pH 6.8	100mM
SDS	4%
DTT	0.1M
Glycerol	20%
EDTA	1mM
Bromphenol Blue	0.2mg/ml
<b>10X TGS running buffer</b>	
Tris, pH 8.6	0.25M
Glycine	1.92M
SDS	1%
Dilute 1 in 10 to give 1X	
<b>1X TG blotting buffer</b>	
Tris	25mM
Glycine	192mM
Methanol	20%
<b>10X TBS</b>	
NaCl	3M
Tris	0.4M
pH to 7.3	
Dilute 1 in 10 to give 1X	

## **2.10 Cell lysis and Hit-Hunter cAMP assay**

### **2.10.1 Cell lysis**

After astrocytes were grown to confluence in 6-well plates, the cells received a different treatment to induce a level of cAMP. Following treatments, the bathing medium was removed by a vacuum, and cells were rapidly washed with PBS. After washing, cells were lysed by scraping the well in the presence of 100 µl of ice-cold 70% ethanol (Moldrich et al., 2002). Once each well dried, 100 µl of 50mM Tris-1mM EDTA solution (Moldrich et al., 2002) was added to it. The wells were then agitated to re-suspend cell contents, which were then transferred to a tube and stored at -20 °C or used immediately to measure cAMP levels with the Hit-Hunter

cAMP assay for small molecules (DiscoverX, USA). The protein content was determined using the BCA protein assay (Thermo Fischer, UK).

### 2.10.2 Hit-Hunter cAMP assay

cAMP levels were measured using the Hit-Hunter cAMP assay (DiscoverX, Fremont, CA). For this assay, 96-well half-area plates were used in this assay. To prepare the standards, serial dilutions in an 11-point series of 3-fold dilutions of the standard were made. The highest concentration of cAMP standard was obtained by diluting the cAMP standard stock  $2.5 \times 10^4$  M in a 1:9 ratio.

After preparing standards, 10  $\mu$ L of cAMP assay buffer was added to all wells in the assay plate. Following the buffer, 7.5  $\mu$ L was added from each sample and standard in different wells. Afterwards, 5  $\mu$ L of cAMP antibody reagent and 30  $\mu$ L of cAMP working detection solution (19-parts of cAMP lysis buffer, 5-parts of substrate reagent 1, 1-part of substrate reagent 2 and 25-parts of cAMP solution D) were added to all wells and incubated for 1 hour at room temperature in the dark for the immunocompetition reaction to occur. Finally, 30  $\mu$ L of cAMP solution A was added to all wells of the assay plate and incubated for 3 hours at room temperature in the dark.

Luminescence signals were detected using the Fluoroskan Ascent™ Microplate Fluorometer (Thermo Scientific, UK) with a 5,000 millisecond integrated time between wells. All measurements of cAMP accumulation were performed six times. The values were calculated by non-linear regression analysis using a fit to the assay standard curve with the hyperbolic equation ( $Y = B_{max} * X / (K_d + X)$ ), where **X** is concentration, **Y** is fluroskan Luminescence signal and **B<sub>max</sub>** is the maximum luminescence signal in the same units as Y. **K<sub>d</sub>** is the equilibrium binding constant in the same units as X and represents the cAMP concentration needed to achieve half-maximum luminescence at equilibrium. Finally, the cAMP concentration for each sample was then normalised to protein concentration.

### **2.11 Accell siRNA transfection of STAT3**

Cells were plated in 96-well plates with a 5,000 cells/ml density and a medium supplemented with 2% fetal bovine serum. The cells were incubated at 37 °C with 5% CO<sub>2</sub> for 48 hours until confluent.

A 100µM STAT3 siRNA solution (Horizon Discovery, UK) in a RNase-free buffered solution was prepared as stock. An appropriate volume of RNase-free solution was added into the siRNA solution (according to manufacturer's instructions), then it was pipetted up and down 3-5 times. The solution was placed on an orbital mixer/shaker for 30 minutes at room temperature and centrifuged to collect the solution at the bottom of the tube.

The growth medium was removed and replaced with 1µM Accell siRNA in a low-serum or serum-free medium (100 µl per well) in 96-well plates. The plates were incubated at 37 °C with 5% CO<sub>2</sub> for 72 hours and 96 hours. The 10% serum was added after 48 hours. Following knockdown, the cells were treated with 10µM forskolin for 3 hours. To assess knockdown and stellation, immunocytochemistry was conducted by staining the astrocytes with total STAT3 and GFAP antibodies (Figure 2.1).

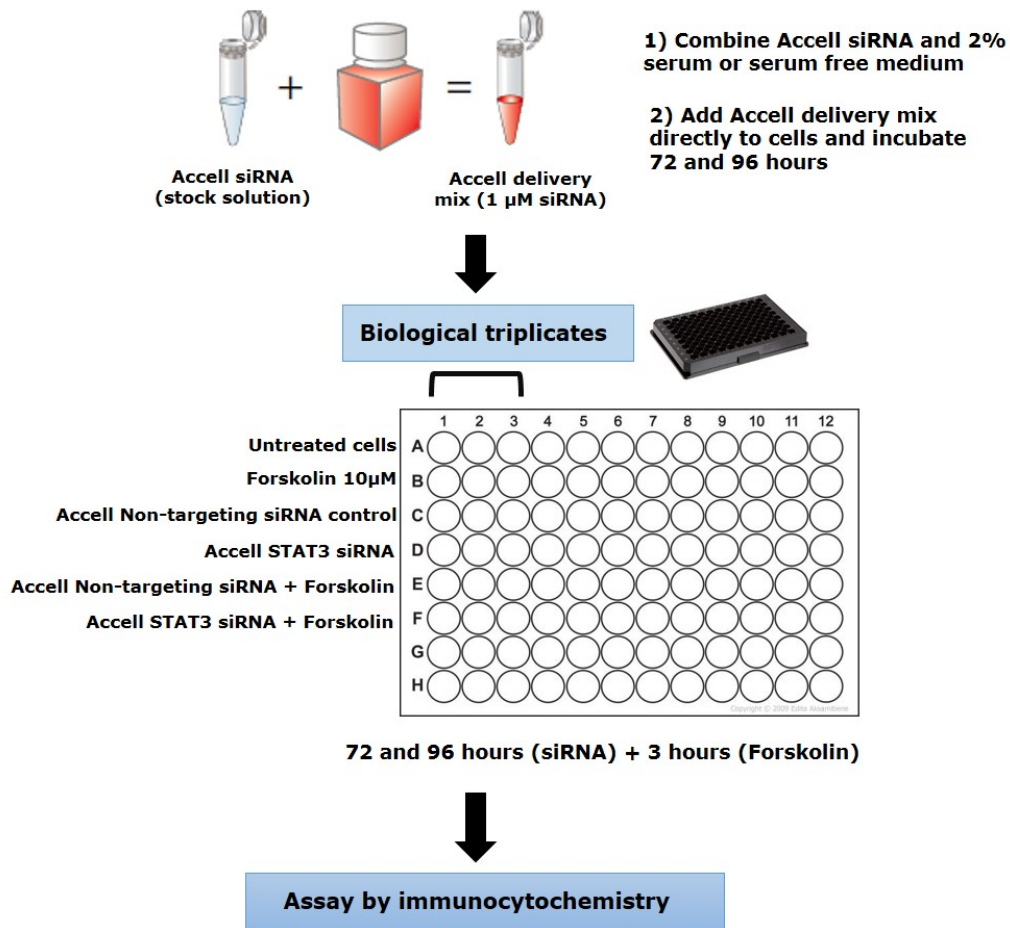


**Figure 2.1 Experimental workflow for Accell siRNA-mediated gene knockdown.**

### 2.12 Image analysis

For  $\text{Ca}^{2+}$  imaging data, Image J software was used with a time-series analyser plugin to manually select regions of interest (ROIs) centred on the cell nucleus. Matlab R2015a software with Calcium GUI was applied to analyse mean fluorescence intensity in each cell. The mean fluorescence intensity within each ROI was quantified and expressed as the ratio of fluorescence at time  $t$  divided by mean intensity for 0-120 seconds before the addition of the agonist ( $F/F_0$ ). If mean  $F/F_0$  exceeded 1.045 fold, the cells were defined as responding to the stimulus by increased  $\text{Ca}^{2+}$ . Area under the curve (AUC) was calculated as the integral of fluorescence intensity during the 18-minute time window after adding the agonist. The percentage of cells responding was also calculated.

To determine the purity of the astrocyte culture, the number of positive GFAP and Iba1 positive cells was measured. Image J software was used to differentiate between the positive and background fluorescence. GFAP and Iba1 staining were green, and DAPI displayed a magenta colour. A time series analyser plugin was provided to select the ROIs. Count the positive GFAP and Iba1 cells was done manually. The positive astrocyte cells were defined with green GFAP labelling, and the microglia were identified with Iba1 labelling.

For the stellation assay, astrocytes were treated with pharmacological compounds (as specified in relevant sections), then labelled with a GFAP antibody. Cells were defined as stellate if they had clearly distinct fibres radiating from the soma, a spiky star shape with defined processes, a small soma and the GFAP label was intense. This contrasts with protoplasmic cells, which have diffuse, web-like labelling throughout the cell body. Image J and a time series analyser plugin were used to mark the ROIs. The stellate cells were manually and blindly counted, and the percentage of cells stellation was measured.

Another way to assess the morphology change of astrocytes was by loading the cells with calcein-AM for real-time imaging. The cell was analysed with Image J by manually drawing a line around the cell perimeter in the first and the last frames of the real-time imaging. Shape measures, such as area and perimeter, were calculated using the Image J of the same cell before and after treatment. Next, the circularity was calculated using this equation:  $(4 * \pi * \text{area}) / (\text{perimeter}^2)$ , where  $\pi = 3.14$ .

To quantify translocation of S727 p-STAT3 and Y705 p-STAT3 from the cytoplasm to the nucleus, Matlab R2016a software with Gliosis analysis GUI was used to isolate the nuclei from the rest of the image based on the DAPI signal and to measure the intensity of S727 p-STAT3 and Y705 p-STAT3 in the nuclear compartment. To measure the total STAT3 intensity in the siRNA experiment,

Gliosia analysis GUI was used to identify each cell by DAPI and measure the intensity in the cytoplasm and nucleus.

### **2.13 Statistical analysis**

All experiments (immunocytochemistry, Ca<sup>2+</sup> imaging, real-time imaging and intensity measures (S727 p-STAT3 and Y705 p-STAT3) in the nucleus) were obtained from three independent experiments. Each coverslip or well had greater than a hundred cells analysed, which gave a mean value that was used for the statistical analysis. Western blot samples were repeated three times from different cultures, except for IL-6 with stattic and WP1066, which were done once. Each sample of the cyclic AMP assay was done from one well. The sample was repeated six to twelve times and independently stimulated and assayed, but the samples from each experiment were from one litter of rats cultured together. The Accell siRNA STAT3 transfection experiment was repeated once in each condition. All statistical tests were completed with the Graph Pad Prism software. All data are presented as a mean  $\pm$  standard error of the mean (SEM). The statistical significance was determined using the t-test (Mann Whitney test, Paired t-test and Wilcoxon test) and one way ANOVA, where  $P < 0.05$  was considered statistically significant.

**Chapter 3 Optimising astrocyte culture and characterisation of different assays of reactive gliosis.**

### **3.1 Introduction**

Astrocytes are a class of glial cells that play many essential functions in the CNS. They control extracellular ion homeostasis (Chiang, Sessle and Dostrovsky, 2012), uptake CO<sub>2</sub> that is produced by neurons (Benarroch, 2005), modulate synaptic activity by releasing gliotransmitter via Ca<sup>2+</sup> signalling (Rossi, 2015) and uptake glutamate from the synaptic cleft to prevent excessive activation of neurons, which can lead to excitotoxicity (Paixão and Klein, 2010). It has been found that 99% of CNS capillary covered by end-feet astrocyte (Verkhatsky et al., 2014) that gave the ability for an astrocyte to modulate blood-brain barrier (BBB) permeability (Benarroch, 2005).

Astrocytes have been traditionally classified into two groups according to their morphology in vitro. The first group is the protoplasmic astrocytes, which are found in the grey matter. They have a rounded shape with several main branches that engage 50–60% of the cytoplasmic and envelop about 80% of the surface area of the cell (Rossi, 2015). The second group is the fibrous astrocytes that present in the white matter. They are a fibrous structure with long processes (Allen and Eroglu, 2017; Guillamón-Vivancos, Gómez-Pinedo and Matías-Guiu, 2015; Oberheim, Goldman, and Nedergaard, 2012; Rossi, 2015). In contrast to this simple classification, Emsley and Macklis (2006) described many types of astrocyte by using GFAP and S100β immunostaining across different CNS regions including Bergmann glia, ependymal glia, fibrous astrocytes, marginal glia, perivascular glia, protoplasmic astrocytes, tanycytes, and velate glia.

Under pathological conditions, the release of excitatory neurotransmitters in the synapse, and the release of cytokines and chemokines from reactive microglia leads to reactive gliosis. Reactive gliosis has a harmful or supporting activity. Liddel et al. (2017) demonstrated that reactive gliosis astrocytes could be classified to A1 and A2 astroglia, based on gene expression profile. A1 reactive astrocytes are destructive and are induced by activated microglia. While A2

astrogliosis had protective roles, which leads to up-regulation of many neurotrophic factors. In addition, Sofroniew (2009) divided the reactive astrocyte to mild-moderate or severe astrogliosis. Mild to moderate cells have a mechanism of resolving and return to healthy cells phenotype. However, severe reactive astrocytes formed in response to inflammation and cause a glial scar.

The hallmark of reactive gliosis in CNS involves a morphological change, cell migration, proliferation and up-regulation of glial markers such as GFAP (Ji, Berta and Nedergaard, 2013; Pekny et al., 2019). Changing of the glial functions and formation of the glial scars seem to be the main indicators of reactive gliosis (Gao and Ji, 2010; Verkhratsky et al., 2014). In addition, CSPGs could be an indicator for reactive gliosis because it is an inhibitory factor that releases from glial scars in the reactive astrocyte to limit the regrowth of injured axons (East, Golding and Phillips, 2009; Beckerman et al., 2015; Kerstetter and Miller, 2012). The reduction of glutamate uptake and down-regulation of the glutamate transporter could be another indicator of reactive gliosis, leading to increased neuron excitability (Milligan and Watkins, 2009). Furthermore, reactive gliosis can increase the expression of many receptors such as toll-like receptors (TLR2 and TLR4) which can activate MAPKs and NF $\kappa$ B signalling pathways responsible for inducing the release of pro-inflammatory chemokines and cytokines, including IL-1 $\beta$ , TNF $\alpha$  and IL-6 (Fellner et al., 2013; Gorina et al., 2011; Lukin et al., 2017; Nakano et al., 2015; Sofroniew, 2017; Sofroniew, 2009). However, it was found that astrocytes do not express TLR4 and the presence of TLR4-positive microglia with astrocytes determines the astrocytes response to LPS (Holm, Draeby and Owens, 2012; Facci et al., 2014). Liu et al. (2013) discovered that activate STAT3 pathways and translocation of p-STAT3 as transcription factor from the cytoplasm to the nucleus could be the initial marker for a reactive astrocyte. Therefore, p-STAT3 can bind with DNA and transcript other genes that are involved in proliferation, astrocyte hypertrophy and release of pro or anti-inflammatory cytokines and chemokines

(Sofroniew, 2009; Sofroniew, 2017; Hol and Pekny, 2015). Gene expression data showed that reactive astrocytes up-regulated *Nes*, *Ctnnb1*, *Axin2*, *Plaur*, *Mmp2*, *Mmp13*, *Cdh2*, *Sox9*, *Xylt1*, *Chst11*, *Csgalnact1*, *Acan*, *Pcan*, *Slit2*, and these were defined as the marker genes of scar-forming astrocytes after spinal cord injury (Okada et al., 2018). Another study discovers that in the case of reactive gliosis, numerous genes for GPCRs, such as *P2ry14* gene for P2Y<sub>14</sub> receptor, were increased and these genes can be involved in calcium signalling which leads to an increase in intracellular calcium levels in 50% of the cells after adding a specific agonist of the P2Y<sub>14</sub> receptor, e.g., UDP-glucose ligand (Hamby et al., 2012).

### **Aim**

In this chapter, culture methods for spinal cord astrocytes were optimised, and different methods tested for the quantification of reactive gliosis. Neonatal cortical astrocytes were used as the standard for comparison, given the extensive previous literature using this preparation. The hypothesis of this chapter is to find quantitative assays of reactive gliosis after treating cells with different stimulants known to induce gliosis. The reactive astrogliosis was quantified by calculating the percentage of stellate cells, determining the circularity of reactive cells, examining the sensitivity of cells to the P2Y<sub>14</sub> receptor agonist UDP-glucose, as this receptor is up-regulated in reactive astrocytes and measuring the intensity of p-STAT3 in the nucleus using a confocal microscope.

## 3.2 Results

### 3.2.1 Optimising spinal astrocyte culture

#### 3.2.1.1 Purity of spinal astrocyte culturing

As it was described in section 2.4, the cells were cultured in flasks for two weeks, and they were split into 6-well plates for use in imaging and immunocytochemical experiments. To determine the purity of astrocyte culture, cells were stained with 2 different antibodies: GFAP (astrocyte selective marker) and Iba1 (a microglial marker) (Ito et al., 2001) at 4 days and 11 days after cell splitting. The percentage of both GFAP and Iba1 positive cells are shown in Table 3.1. High microglia contamination was indicated in neonatal spinal astrocytes (Figure 3.1)

	<b>GFAP</b>	<b>Iba1</b>
<b>4 days</b>	83±3% (200)	17±2.5% (156)
<b>11 days</b>	71±4% (358)	33±3.5% (210)

**Table 3.1 The mean±SEM (total number of cells counted) percentage of positive staining of two antibodies.** GFAP is represented in the astrocyte while positive Iba1 staining shows the presence of microglia.

As a first strategy to remove the contaminating cells, the flasks were placed on a plate shaker within the incubator overnight at 300 rpm, 24 hours after the day of isolation. Astrocytes are strongly adherent, and so shaking is intended to remove the less adherent microglia. The cell identity markers demonstrated a decrease in the percentage of Iba1 staining compared with the previous protocol (Table 3.2 & Figure 3.2)

	<b>GFAP</b>	<b>Iba1</b>
<b>4 days</b>	97±0.7% (863)	15±2.4% (578)
<b>11 days</b>	97±1.2% (753)	5.7±2.13% (589)

**Table 3.2 The mean±SEM (total number of cells counted) percentage of positive staining of two antibodies.** GFAP is represented in the astrocyte while positive Iba1 staining shows the presence of microglia.

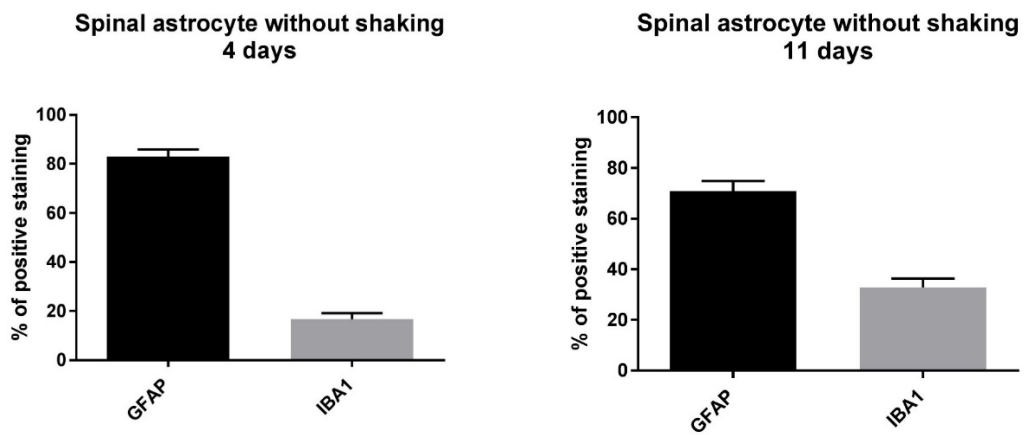
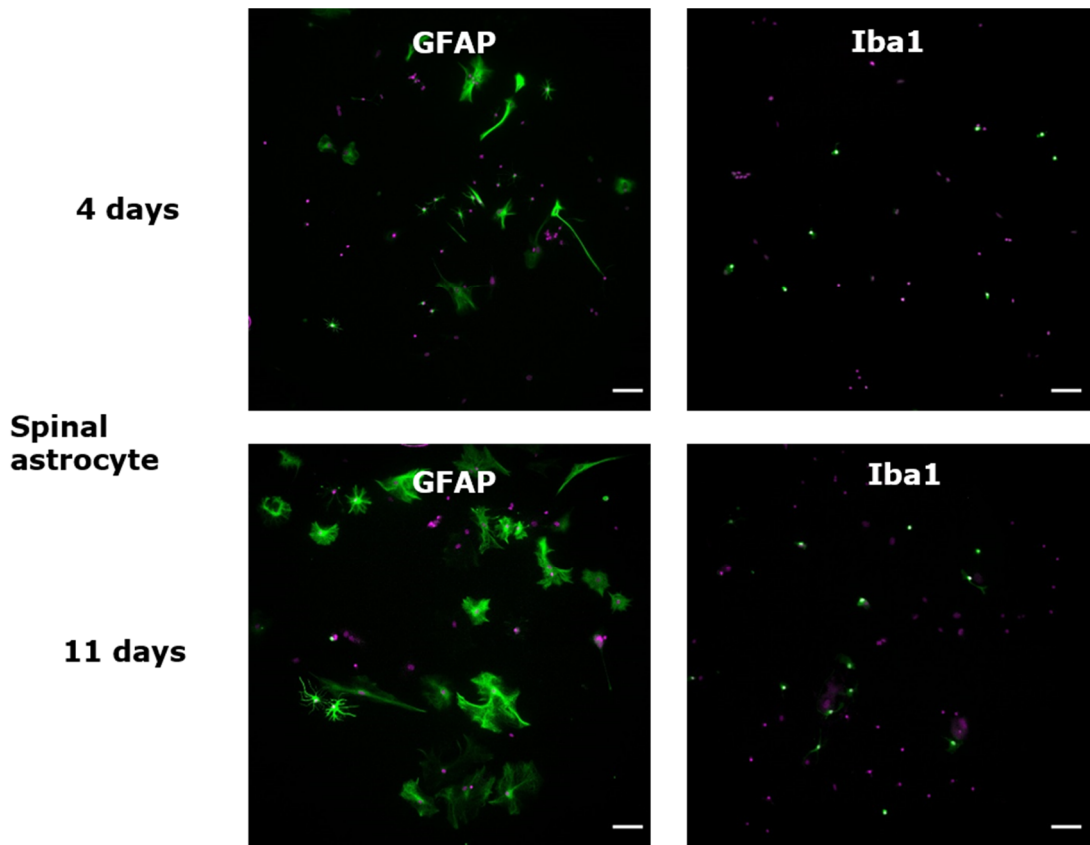


**Figure 3.1 Cell identity of astrocytes in culture from neonatal rats.** Neonatal cells prepared from spinal cord were seeded without shaking and then splitting at a density of  $2.5 \times 10^4$  cells, the test was done at 4 days (upper panels) and 11 days (lower panels) after cell splitting. Immunocytochemistry for GFAP, and Iba1 expression (green) and nuclear staining with DAPI (magenta) was used to determine the percentage of GFAP, and Iba1 positive cells. Scale bar=500 $\mu$ m. The graphs represent means $\pm$ SEM attained from three different experiments.

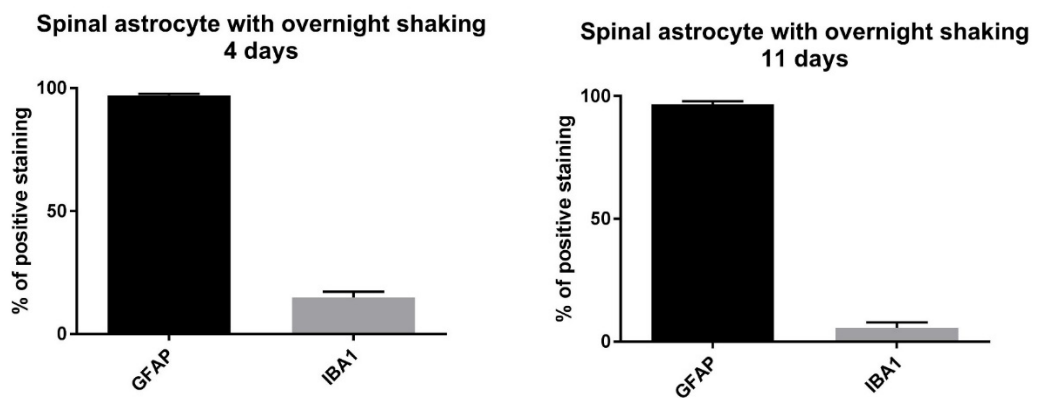
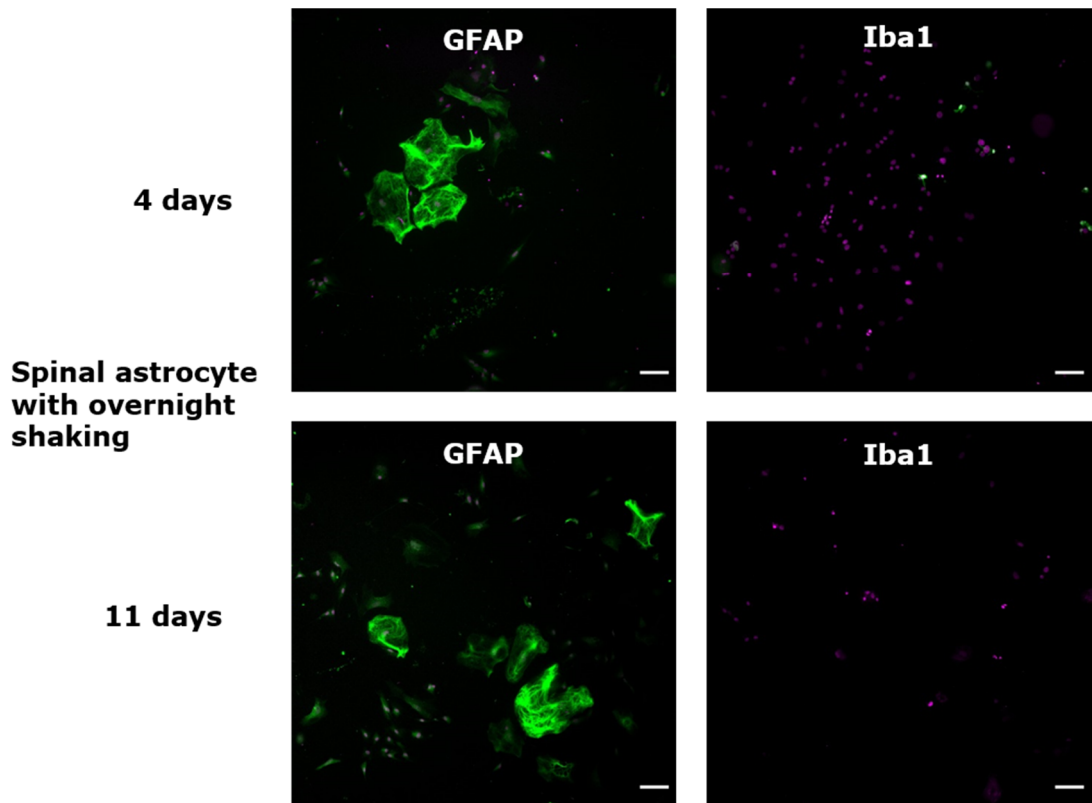


**Figure 3.2 Cell identity of astrocytes in culture from neonatal rats.** Neonatal cells prepared from spinal cord were seeded after shaking and then splitting at a density of  $2.5 \times 10^4$  cells, the test was done at 4 days (upper panels) and 11 days (lower panels) after cell splitting. Immunocytochemistry for GFAP, and Iba1 expression (green) and nuclear staining with DAPI (magenta) was used to determine the percentage of GFAP, and Iba1 positive cells. Scale bar=500 $\mu$ m. The graphs represent means $\pm$ SEM acquired from three different experiments.

**3.2.1.2** Establish the functional response in astrocytes by measuring Ca<sup>2+</sup> responses

To establish the functional response to receptor activation in astrocytes, the Ca<sup>2+</sup> responses were examined on neonatal spinal cells by adding 100µM ATP and 100µM glutamate. Without shaking, it was found that the percentage of cells responding to glutamate is 10%, while 46% of the cells responded to ATP (P=0.001). There is a significant difference for AUC between ATP and glutamate (P <0.001) (Figure 3.3). However, after shaking cells, the percentage of cells responding to glutamate and ATP is higher, with 82% of cells in the case of ATP and 42% after adding glutamate (P= 0.03). There is a significant difference for AUC between ATP and glutamate (P= 0.001) (Figure 3.4). Comparing the percentages of cells responding, there are increases in cell responses, especially with ATP after cell shaking (Table 3.3). Glutamate can induce Ca<sup>2+</sup> due to activate the metabotropic glutamate receptor, and ATP can release Ca<sup>2+</sup> in response to P2X or P2Y, but the main reason for a rapid ATP effect because it's rapidly degraded.

	<b>ATP</b>	<b>Glutamate</b>
<b>Neonatal without shaking</b>	46%	10%
<b>Neonatal with shaking</b>	82%	42%

**Table 3.3 Summary table of Ca<sup>2+</sup> responses.** Data have presented the percentage of respond cells on neonatal astrocytes without shaking between glutamate (n=64) and ATP (n=420) and with shaking between glutamate (n=161) and ATP (n=326). N represents the total number of cells.

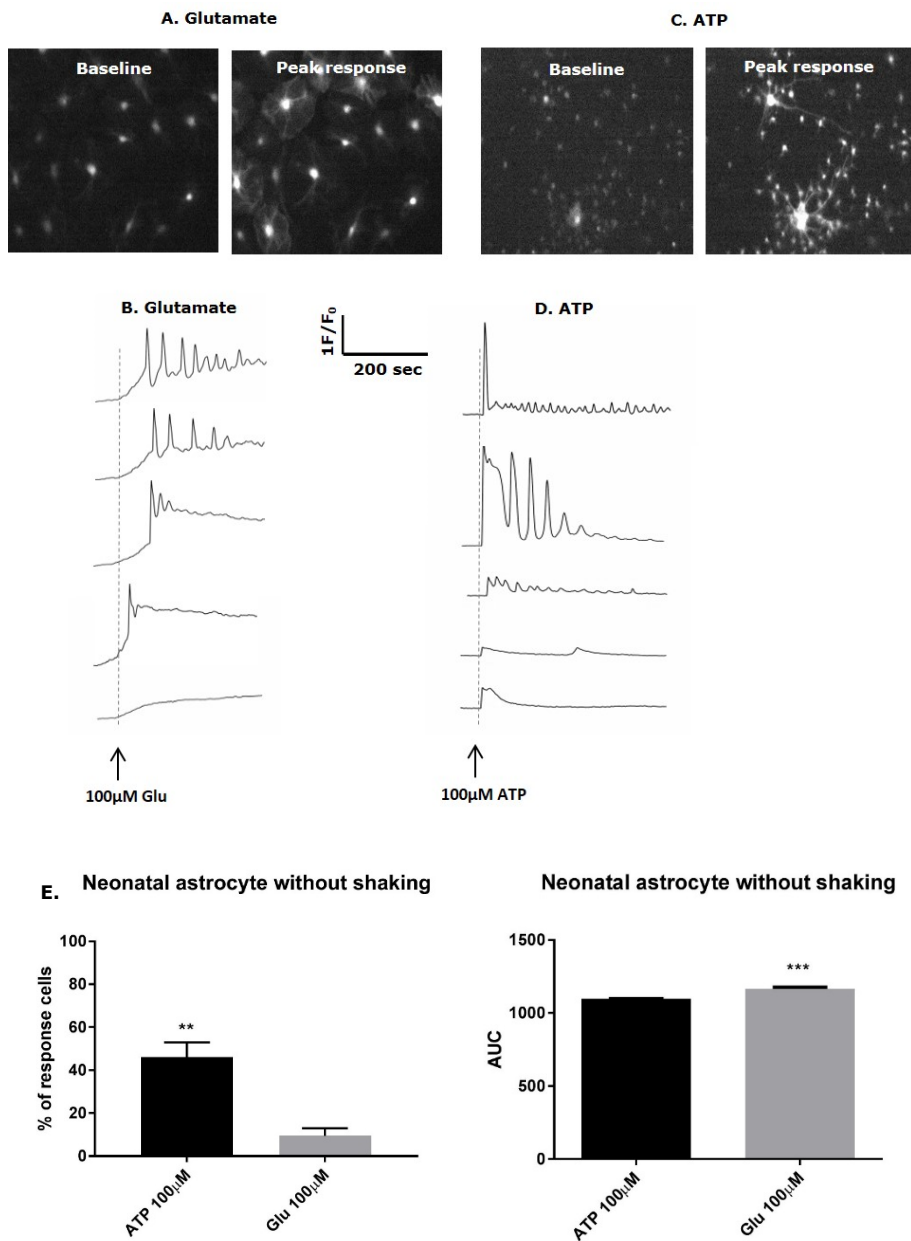


**Figure 3.3 Ca<sup>2+</sup> response of neonatal astrocyte without shaking by adding glutamate and ATP.** A) Two images show Fluo-5F fluorescence intensity at the baseline and after 10 minutes of adding glutamate. B & D) Representative traces of Fluo-5F fluorescence intensity for five individual cells. C) Two images are representing the Fluo-5F fluorescence intensity at the baseline and the peak of response after 6 seconds of adding ATP. E) Aggregate data of area under the curve and the percentage of response cells between glutamate and ATP. Data are presented as a mean  $\pm$  standard error (SEM) obtained from three independent experiments. The statistical significance was determined using the Mann-Whitney test, where (\*\* $P < 0.01$  and \*\*\* $P < 0.001$ ) was considered statistically significant.

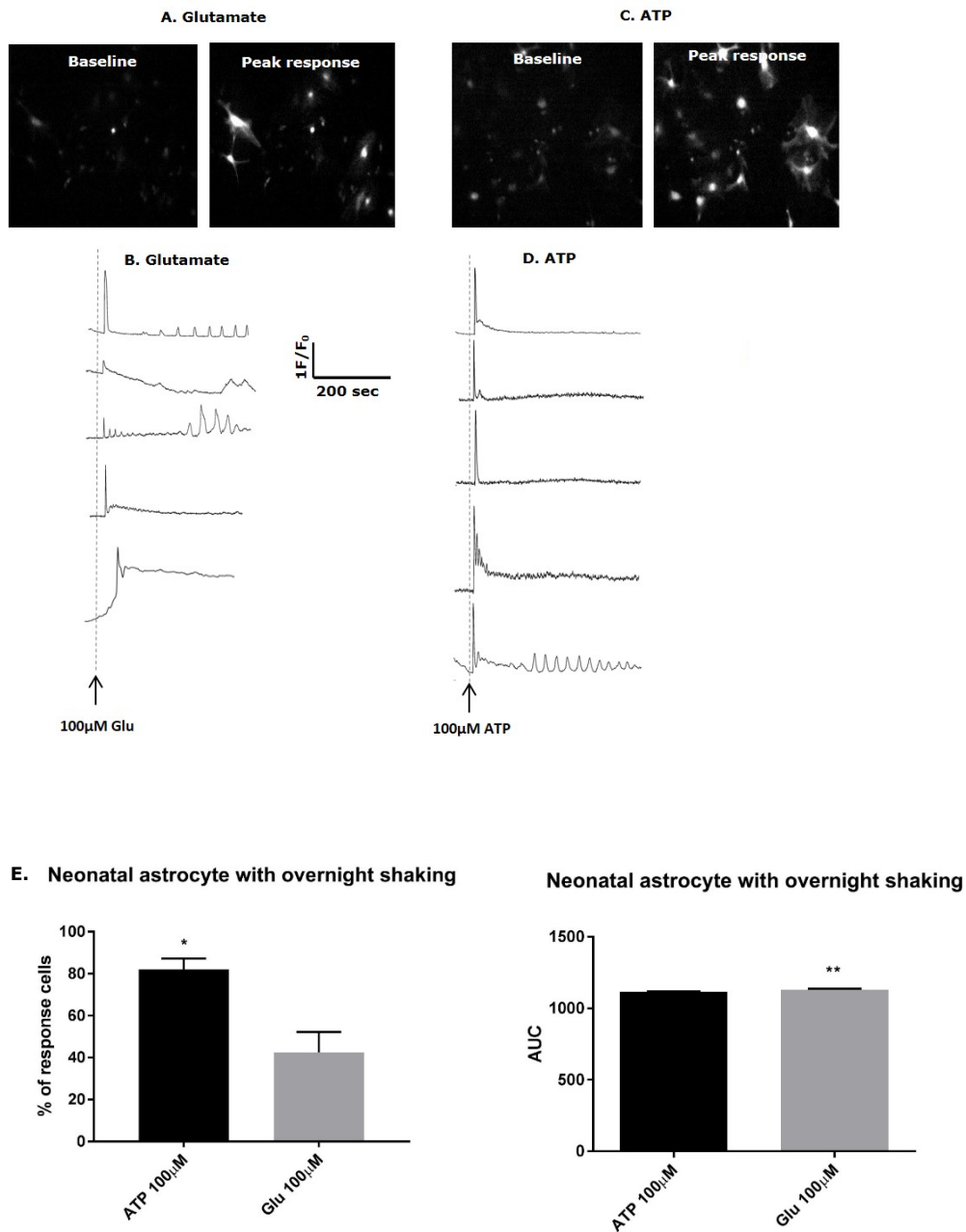


**Figure 3.4  $\text{Ca}^{2+}$  response of neonatal astrocyte with shaking by adding glutamate and ATP.** A) Two images show Fluo-5F fluorescence intensity at the baseline and after 5 seconds of adding glutamate. B & D) Representative traces of Fluo-5F fluorescence intensity for five individual cells. C) Two images are representing the Fluo-5F fluorescence intensity at the baseline and the peak of response after 5 seconds of adding ATP. E) Aggregate data of area under the curve and the percentage of response cells between glutamate and ATP. Data are presented as a mean  $\pm$  standard error (SEM) obtained from three independent experiments. The statistical significance was determined using the Mann-Whitney test, where (\* $P < 0.05$  and \*\* $P < 0.01$ ) was considered statistically significant.

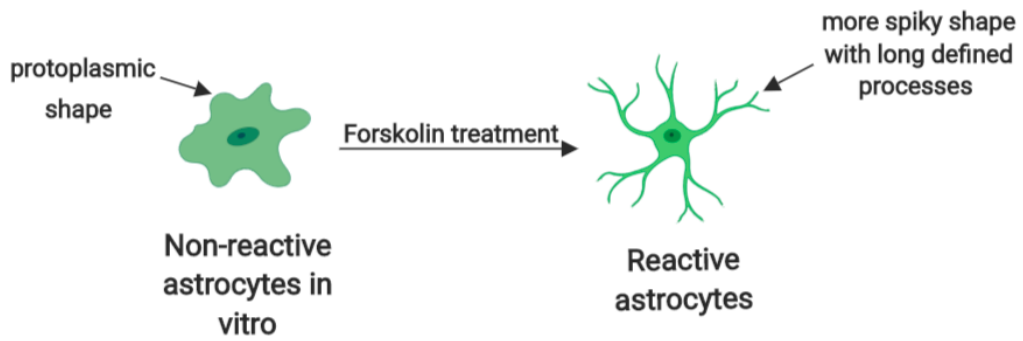
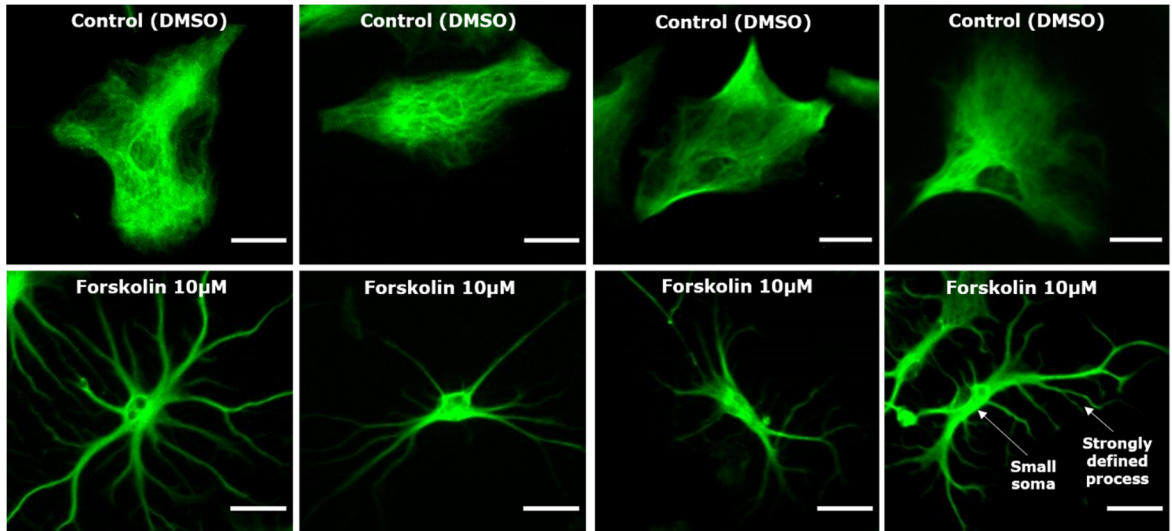
Given this immunocytochemical and functional evidence, all future preparations used this modified protocol with shaking to increase astrocyte purity in the primary cultures. The next aim was to test different potential assays of reactive gliosis.

### **3.2.2 Characterisation of different assays of reactive gliosis in cortical neonatal astrocyte**

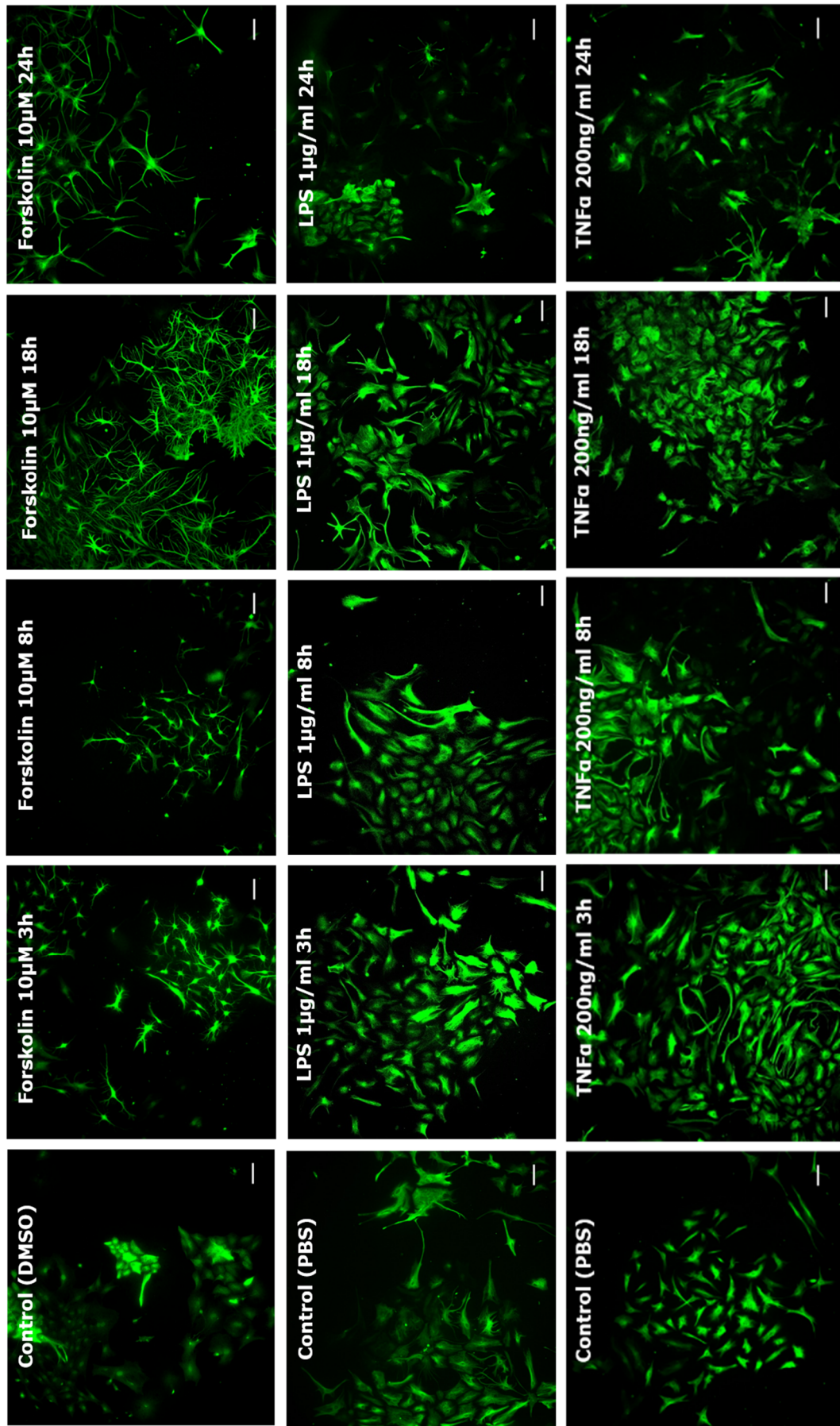
#### **3.2.2.1** Assess the morphological change (stellation) with GFAP immunocytochemistry

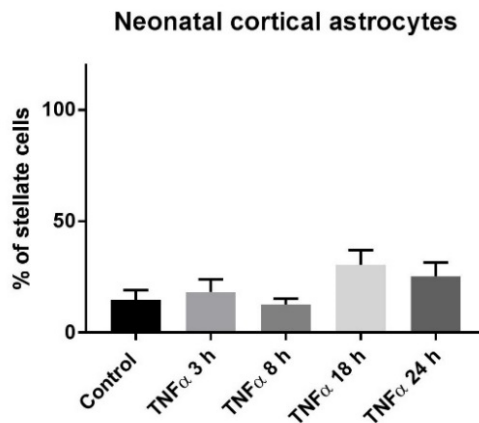
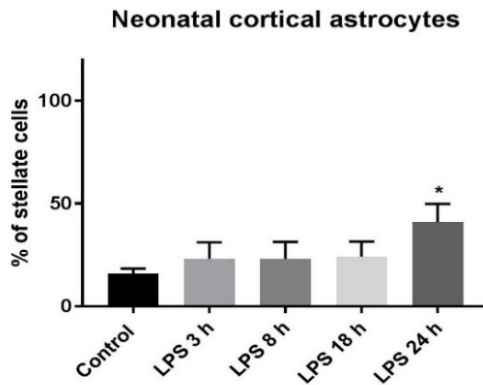
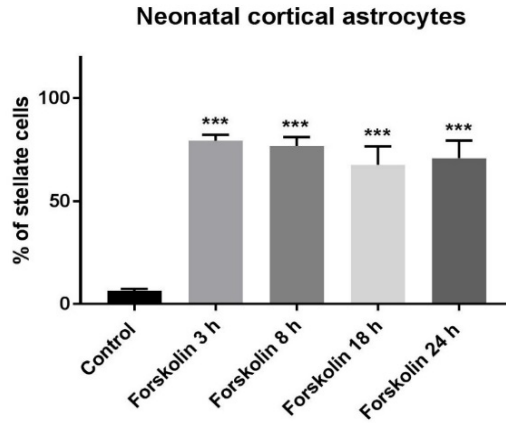
Morphological changes in cell structure were assessed using immunocytochemistry. Morphological changes of astrocytes are the most apparent sign of reactive gliosis in vivo and vitro. The reactive gliosis has a heuristic classification changes such as a change in the classic morphology of the astrocytes from a protoplasmic cell to a more-spiky elaborate shape with defined processes, decrease the size of the soma and increases the density of GFAP (Figure 3.5).

The neonatal cortical astrocytes responded to forskolin treatment with readily detectable morphological changes, starting from 3 hours of incubation with 79% of stellate cells until the end of the experiment ( $P < 0.001$ ). In the case of LPS, only 40% of cells become stellate after 24 hours ( $P=0.015$ ). However, no significant stellation was detected after TNF $\alpha$  treatment (Figure 3.6). Because forskolin gives a considerable percentage of stellate cells, other drugs that activate adenylyl cyclase the same as forskolin were tested. The result shows that noradrenaline can induce stellation with 37% of cells becoming stellate after 3 hours ( $P < 0.001$ ), but other potential cAMP-linked agonists, histamine and substance P, had no detectable effect (Figure 3.7).

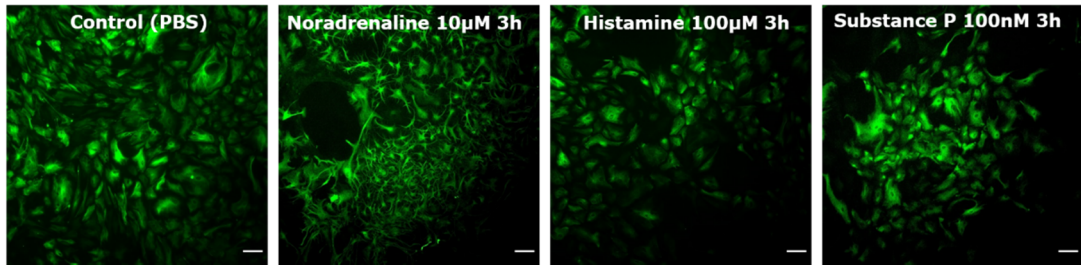


**Figure 3.5 Identify morphology change in astrocytes.** Images: staining with GFAP. The upper images represent untreated protoplasmic cells, and lower images represent stellate cells with many processes after treatment with forskolin. Scale bar=20µm.

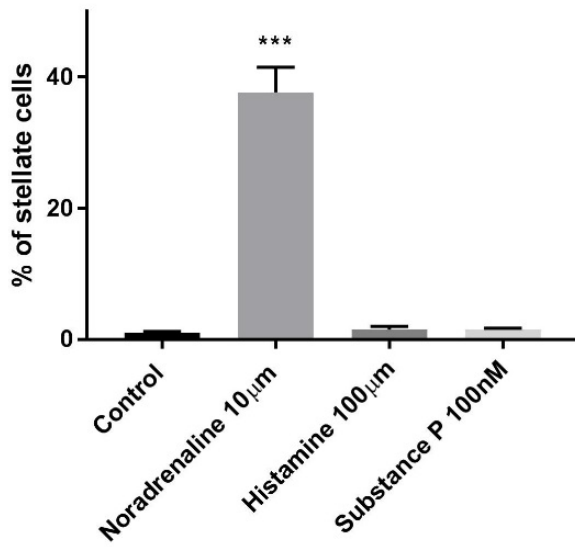




**Figure 3.6 Stellation response of neonatal cortical astrocytes.** Images: staining with GFAP after treatment with forskolin, LPS and TNF $\alpha$  at different time intervals, as indicated. Scale bar=500 $\mu$ m. Aggregate data represent the percentage of stellate cells for each treatment and time interval. Data are presented as a mean  $\pm$  SEM attained from three different experiments. The statistical significance was determined using the one way ANOVA with Dunnett's multiple comparisons test, where (\*P < 0.05 and \*\*\* P < 0.001) was considered statistically significant.



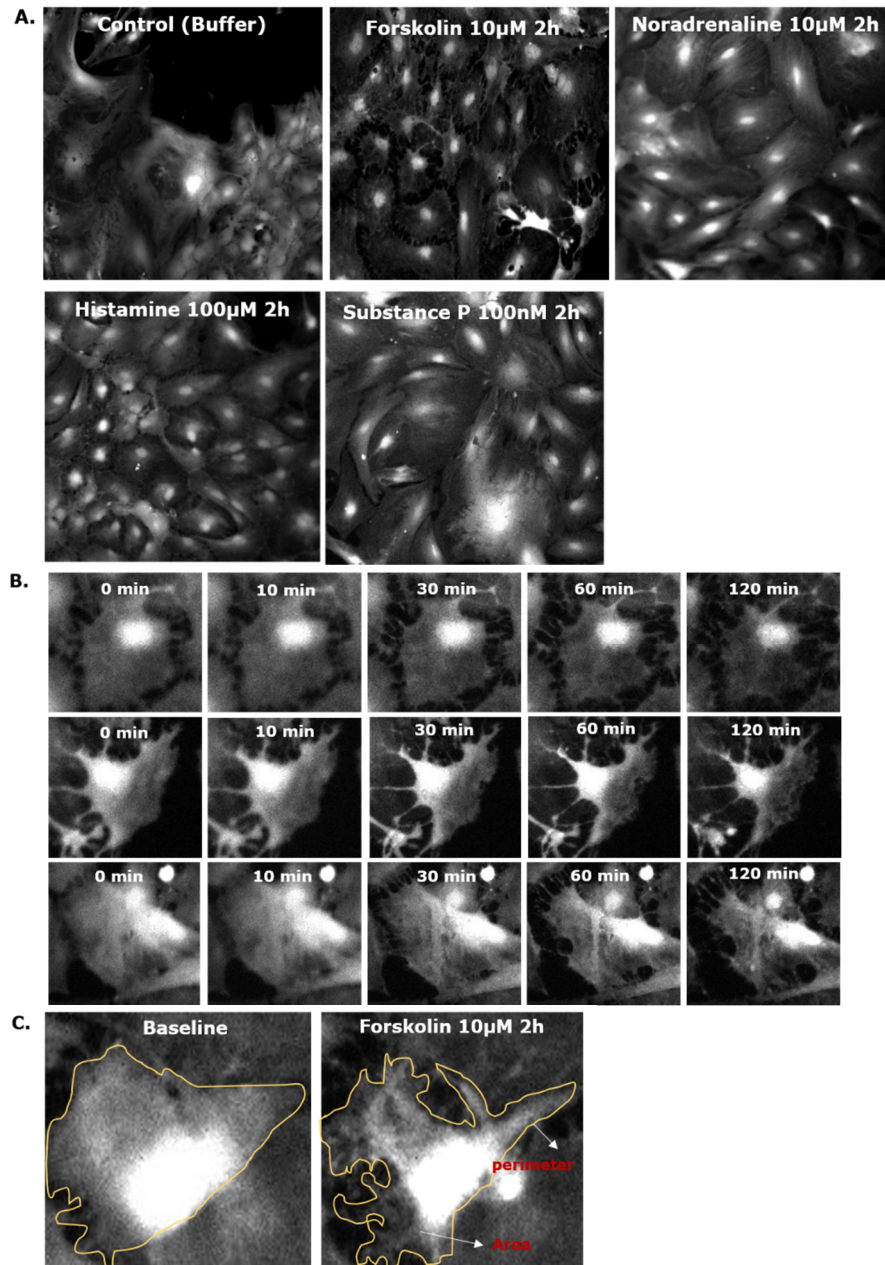
### Neonatal Cortical astrocytes



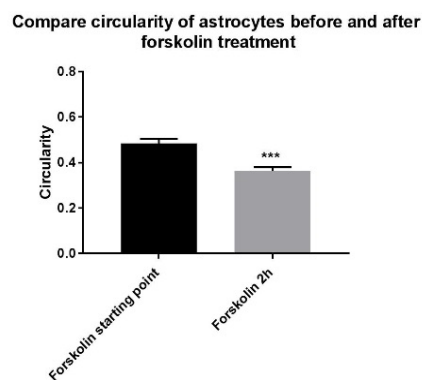
**Figure 3.7 Stellation model on neonatal cortical.** Images: staining with GFAP after treatment with noradrenaline, histamine and substance P for 3hours. Scale bar=500µm. Aggregate data represent the percentage of stellate cells for each treatment. Data are presented as a mean ± SEM attained from three different experiments. The statistical significance was determined using the one way ANOVA with Dunnett's multiple comparisons test, where (\*\*\*)  $P < 0.001$  was considered statistically significant.

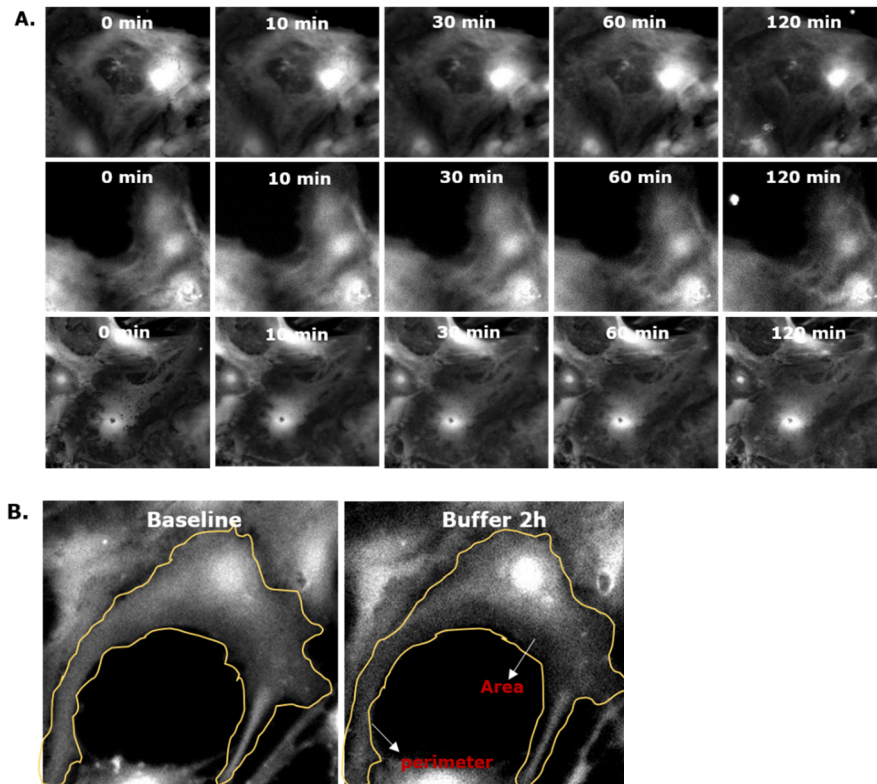
### **3.2.2.2** Assess the morphological change (stellation) with calcein-AM real-time imaging

Another way to assess the morphology change of astrocytes is by loading the astrocyte with calcein-AM for real-time live-cell imaging. The main reasons for using this indicator are to get out to use antibody labelling with GFAP in fixed cells and use another assess by observing stellation happening in live cells. In this assay, area and perimeter were measured to calculate the circularity using this equation  $(4 * \pi * \text{area}) / (\text{perimeter}^2)$  where  $\pi = 3.14$ . A value of 1 indicates that the feature is a perfect circle, and 0 indicates that it is a line (elongated). The result shows that circularity of the cells treated with forskolin was significantly decreased to 0.36 compared with the baseline 0.5 ( $P < 0.001$ ) (Figure 3.8). Where the circularity of cells treated with other drugs does not show significant differences. The circularity of cells treated with a buffer for 2 hours is 0.6, and the baseline is 0.56 (Figure 3.9). In addition, in the case of noradrenaline. The circularity after 2 hours is 0.55 and at the baseline is 0.52 (Figure 3.10). Before and after histamine treatment, the circularity is similar, and it equals 0.65 (Figure 3.11). The starting point circularity in case of substance P equals 0.6 and after 2 hours is 0.66 (Figure 3.12).



**Figure 3.8 Stellation assays of neonatal cortical astrocytes,** A) Cells were stained with calcein-AM and treatment with buffer as control, forskolin, noradrenaline, histamine and substance P. B) The real-time imaging duration was 2 hours after forskolin treatment. C) Images represent the area and perimeter change of astrocyte at the baseline and after 2 hours of treatment. Aggregate data show circularity of 10 cells of each condition at the beginning and the end of imaging. Data are presented as a mean  $\pm$  SEM. The statistical significance was determined using the paired t-test, where (\*\*\*)  $P < 0.001$  was considered statistically significant.





Compare circularity of astrocytes before and after buffer treatment

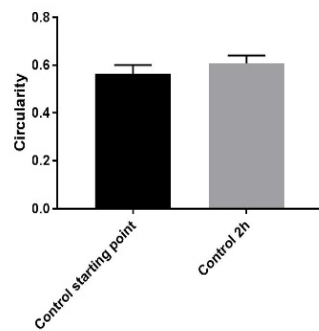
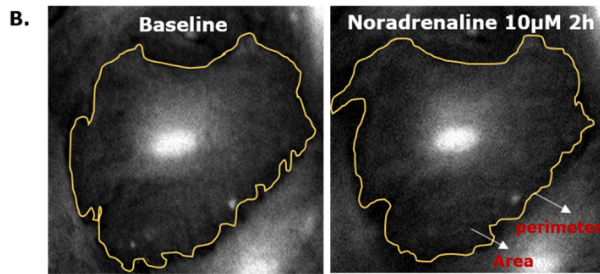
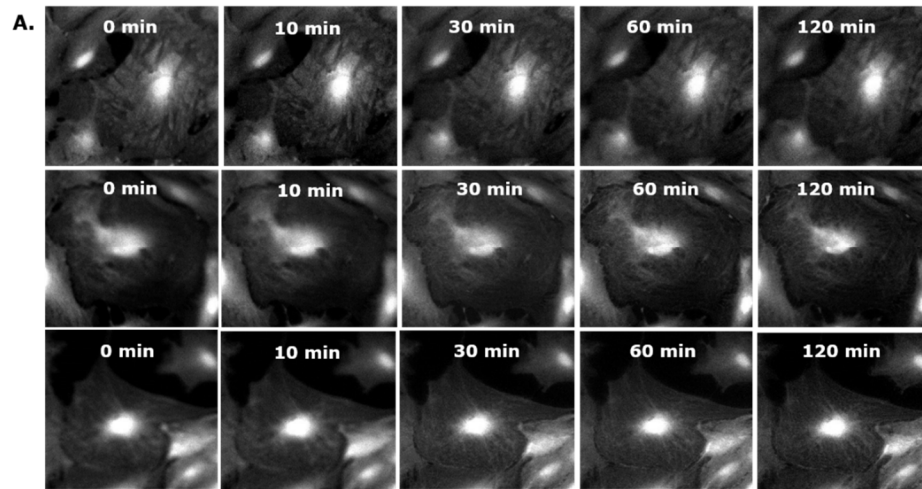


**Figure 3.9 Stellation assays of neonatal cortical astrocytes**, cells were stained with calcein-AM and treatment with buffer as control. A) The real-time imaging duration was 2 hours after adding the buffer. B) Images represent the area and perimeter change of astrocyte at the baseline and after 2 hours of treatment. Aggregate data show circularity of 10 cells of each condition at the beginning and the end of imaging. Data are presented as a mean  $\pm$  SEM. No statistically significant differences were determined using the paired t-test.



Compare circularity of astrocytes before and after noradrenaline treatment

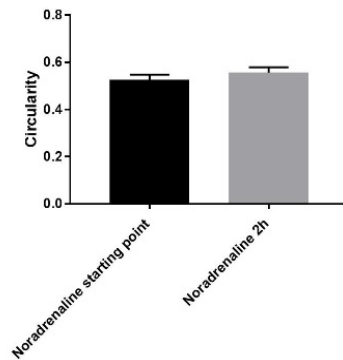
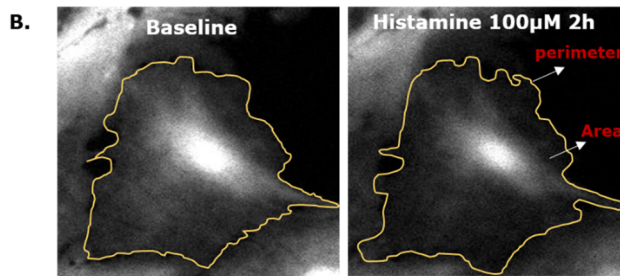
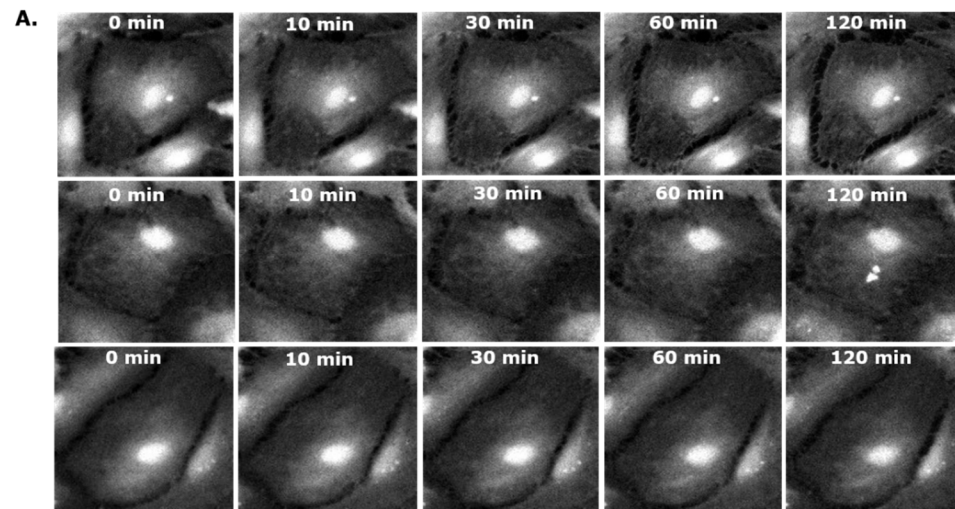


**Figure 3.10 Stellation assays of neonatal cortical astrocytes**, cells were stained with calcein-AM and treatment with noradrenaline. A) The real-time imaging duration was 2 hours after noradrenaline treatment. B) Images represent the area and perimeter change of astrocyte at the baseline and after 2 hours of treatment. Aggregate data show circularity of 10 cells of each condition at the beginning and the end of imaging. Data are presented as a mean  $\pm$  SEM. No statistically significant differences were determined using the paired t-test.



Compare circularity of astrocytes before and after histamine treatment

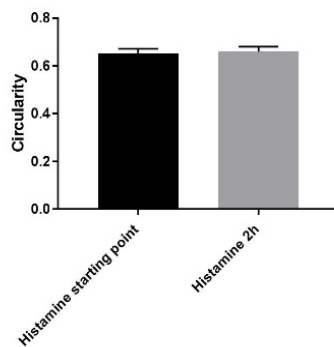
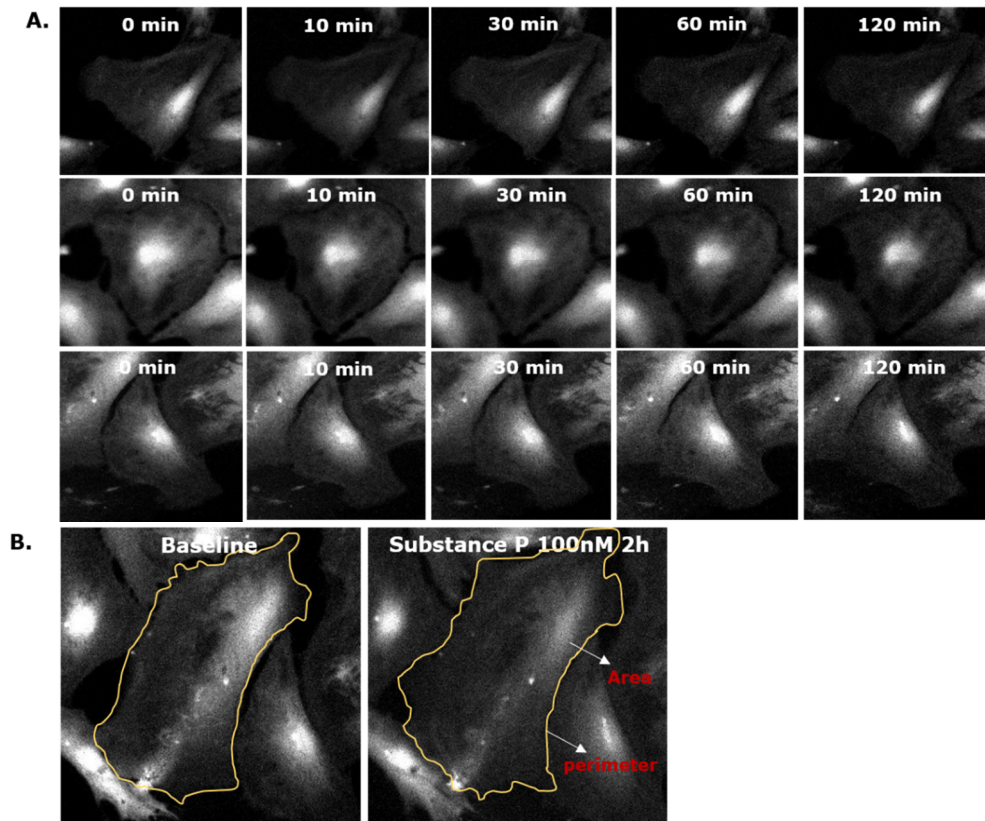


**Figure 3.11 Stellation assays of neonatal cortical astrocytes**, cells were stained with calcein-AM and treatment with histamine. A) The real-time imaging duration was 2 hours after histamine treatment. B) Images represent the area and perimeter change of astrocyte at the baseline and after 2 hours of treatment. Aggregate data show circularity of 10 cells of each condition at the beginning and the end of imaging. Data are presented as a mean  $\pm$  SEM. No statistically significant differences were determined using the paired t-test.



Compare circularity of astrocytes before and after substance P treatment

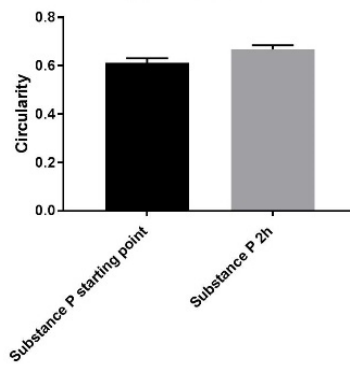


**Figure 3.12 Stellation assays of neonatal cortical astrocytes**, cells were stained with calcein-AM and treatment with substance P. A) The real-time imaging duration was 2 hours after substance P treatment. B) Images represent the area and perimeter change of astrocyte at the baseline and after 2 hours of treatment. Aggregate data show circularity of 10 cells of each condition at the beginning and the end of imaging. Data are presented as a mean  $\pm$  SEM. No statistically significant differences were determined using the paired t-test.

### **3.2.2.3** Release of $\text{Ca}^{2+}$ after stimulation of the $\text{P2Y}_{14}$ receptor

Change the function of astrocyte is also another parameter of reactive gliosis in parallel with the morphology change. Here, the functional assay of reactive astrocytes was measured by loading the astrocyte with another calcium indicator (Fluo-5F). To induce reactive gliosis and up-regulate  $\text{P2Y}_{14}\text{R}$  in the astrocytes, cells were incubated for 24 hours with forskolin, LPS and TNF $\alpha$ . The calcium imaging was done to test for the expression of  $\text{P2Y}_{14}\text{R}$  in the astrocytes before and after treatment of reactive gliosis inducer; cells were stimulated with the receptor-selective and endogenous ligand, which is UDP-glucose. The result shows that the addition of UDP-glucose caused calcium signalling in 18% of cells, and the time courses of these responses were highly variable (Figure 3.13). Responding cells typically showed oscillations in calcium concentration, but the pattern of oscillation was also variable. However, there was no significant difference observed in the percentage of cells responding to UDP-glucose between the treated cells with forskolin ( $P=0.240$ ), LPS ( $P=0.937$ ) or TNF $\alpha$  ( $P=0.387$ ) and the control cells with 37%, 28%, and 16%, respectively (Figure 3.13).

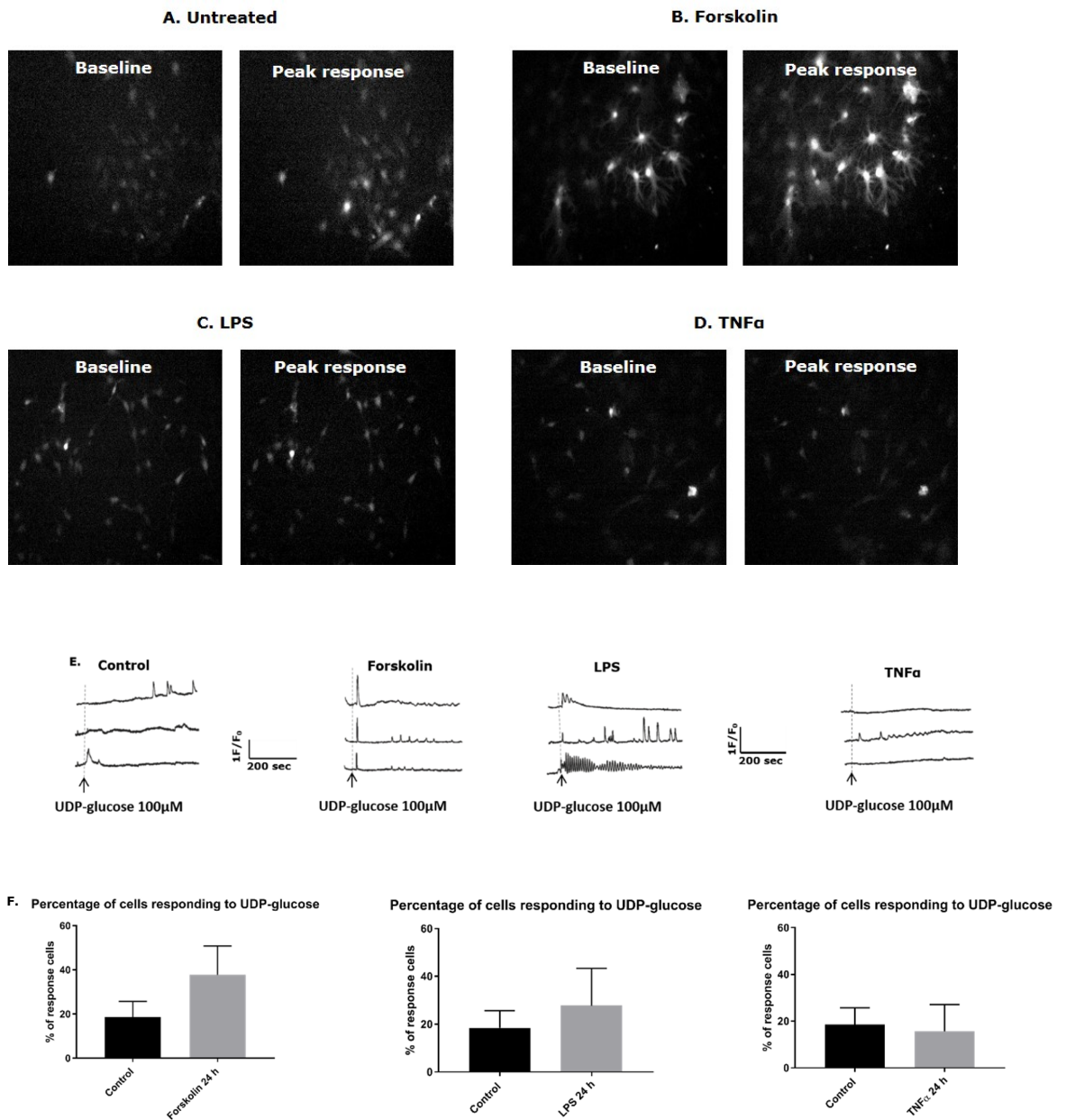


**Figure 3.13 Ca<sup>2+</sup> response of neonatal cortical by adding UDP-glucose.** A) Two images show Fluo-5F fluorescence intensity at the baseline and after 9 seconds of adding UDP-glucose in untreated cells. B) Two images show Fluo-5F fluorescence intensity at the baseline and after 5 minutes of adding UDP-glucose in cells treated with forskolin. C) Two images show Fluo-5F fluorescence intensity at the baseline and after 2 seconds of adding UDP-glucose in cells treated with LPS. D) Two images show Fluo-5F fluorescence intensity at the baseline and after 8 minutes of adding UDP-glucose in cells treated with TNF $\alpha$ . E) Representative traces of Fluo-5F fluorescence intensity for three individual cells in each group. F) Aggregate data above represent the percentage of cells responding in the control (n = 291) and the test groups (forskolin: n = 255, LPS: n = 260 and TNF $\alpha$ : n = 300). Data are presented as a mean  $\pm$  standard error (SEM). No statistically significant differences were determined using the Mann-Whitney test. The experiment was repeated three times.

#### **3.2.2.4** Measure intensity of p-STAT3 in the nucleus with confocal microscopy

Another functional assay of reactive gliosis has quantified the intensity of p-STAT3 in the nucleus. P-STAT3 seems to be the master regulator signalling pathway in reactive gliosis. In this section, the intensity was examined by performing immunocytochemistry with double staining of two types of p-STAT3 (serine and tyrosine) and GFAP antibodies. The results determine the same change of cell morphology compared with the previous experiment. In the case of forskolin treatment, the result demonstrates a significant increase in the intensity of S727 p-STAT3 in the nucleus after 3 hours ( $P=0.041$ ), and it decreases after 24 hours (Figure 3.14). Also, the intensity of S727 p-STAT3 is increase after treating astrocytes with LPS for 24 hours ( $P=0.015$ ) but not with 3 hours (Figure 3.15). There is a significant increase in nucleus intensity after treating astrocytes with TNF $\alpha$  for 3 hours ( $P=0.037$ ) and 24 hours ( $P=0.014$ ) (Figure 3.16). No detection of the high intensity of Y705 p-STAT3 in the nucleus is determined after forskolin and LPS treatment for 3 hours and 24 hours (Figure 3.17, Figure 3.18). However, there is a significant increase in tyrosine intensity after treat astrocytes with TNF $\alpha$  for 24 hours ( $P=0.001$ ) (Figure 3.19).

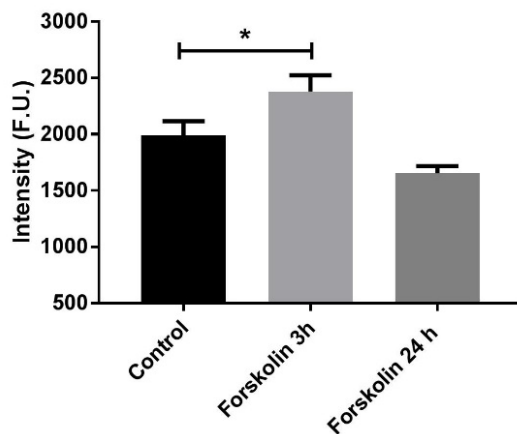
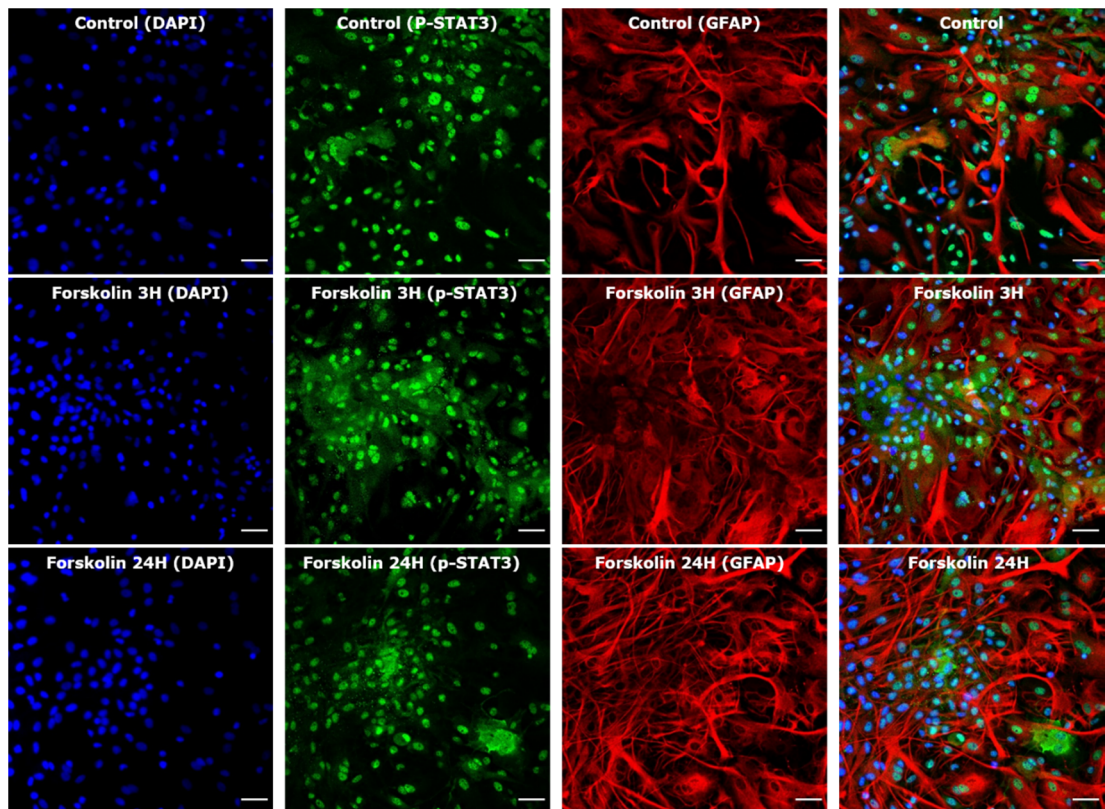


**Figure 3.14 Intensity of S727 p-STAT3 on neonatal cortical astrocytes with confocal microscopy,** cells are stained with GFAP in red, S727 p-STAT3 in green and DAPI in blue. Cells are treated with forskolin 10 $\mu$ M at 3 hours (middle panels) 24 hours (lower panels). The scale bar = 40 $\mu$ m. Aggregate data represent the mean of S727 p-STAT3 intensity per pixel in the nucleus. Data are presented as a mean  $\pm$  SEM completed from three different experiments. The statistical significance was determined using the one way ANOVA (Dunnett's multiple comparisons test) by comparing treated groups with control, where (\*P < 0.05) was considered statistically significant.

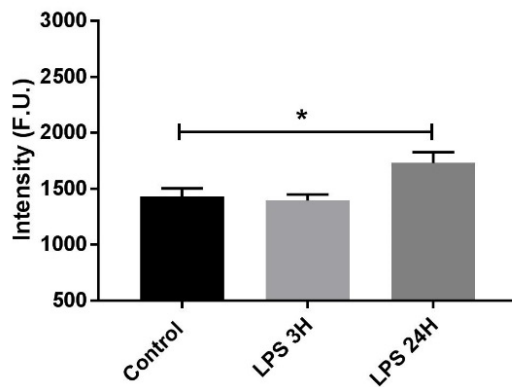
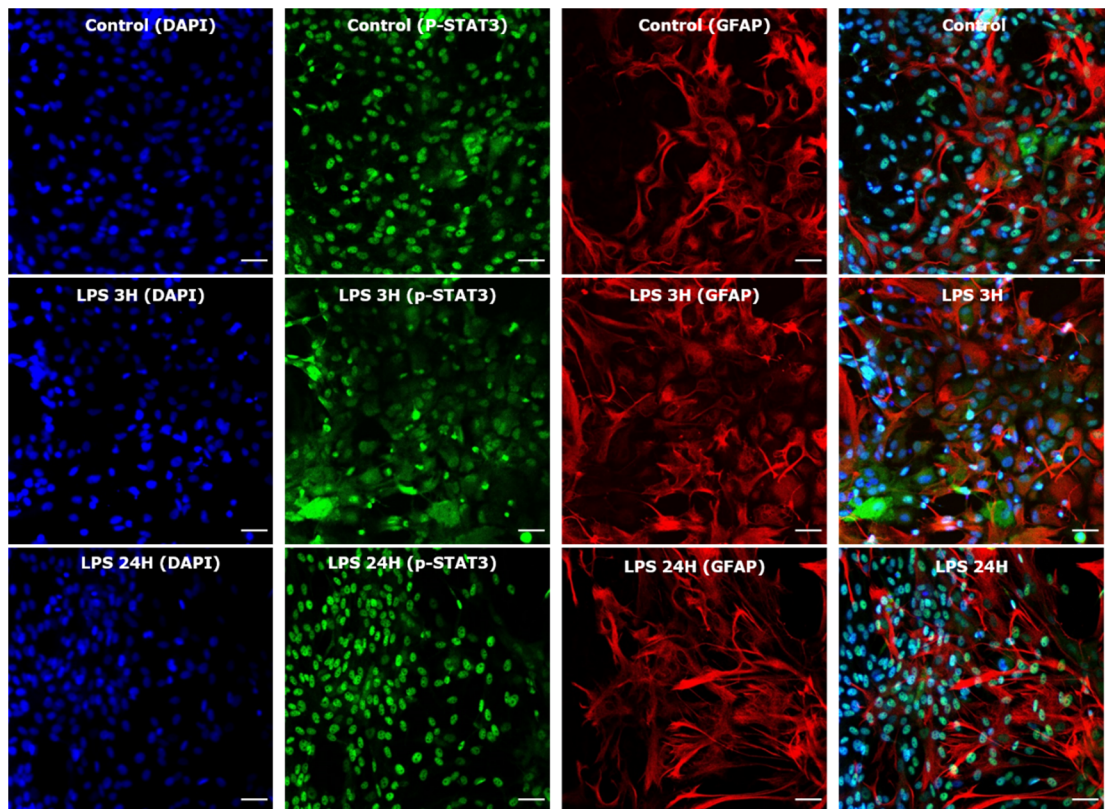


**Figure 3.15 Intensity of S727 p-STAT3 on neonatal cortical astrocytes with confocal microscopy,** cells are stained with GFAP in red, S727 p-STAT3 in green and DAPI in blue. Cells are treated with LPS 1 $\mu$ g/ml at 3 hours (middle panels) 24 hours (lower panels). The scale bar = 40 $\mu$ m. Aggregate data represent the mean of S727 p-STAT3 intensity per pixel in the nucleus. Data are presented as a mean  $\pm$  SEM completed from three different experiments. The statistical significance was determined using the one way ANOVA (Dunnett's multiple comparisons test) by comparing treated groups with control, where (\*P < 0.05) was considered statistically significant.

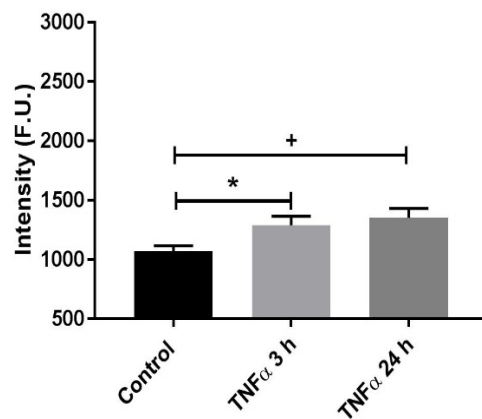
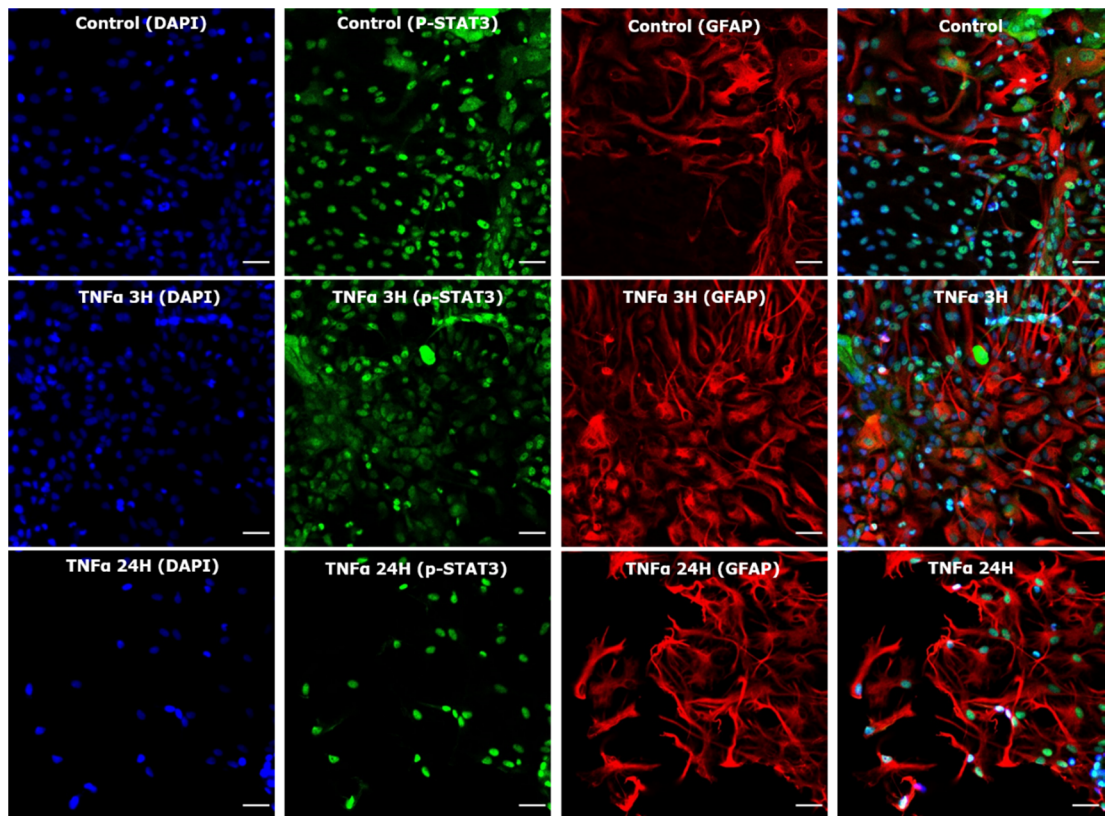


**Figure 3.16 Intensity of S727 p-STAT3 on neonatal cortical astrocytes with confocal microscopy**, cells are stained with GFAP in red, S727 p-STAT3 in green and DAPI in blue. Cells are treated with TNF $\alpha$  200ng/ml at 3 hours (middle panels) 24 hours (lower panels). The scale bar = 40 $\mu$ m. Aggregate data represent the mean of S727 p-STAT3 intensity per pixel in the nucleus. Data are presented as a mean  $\pm$  SEM completed from three different experiments. The statistical significance was determined using the one way ANOVA (Dunnett's multiple comparisons test) by comparing treated groups with control, where (\*P < 0.05) was considered statistically significant.

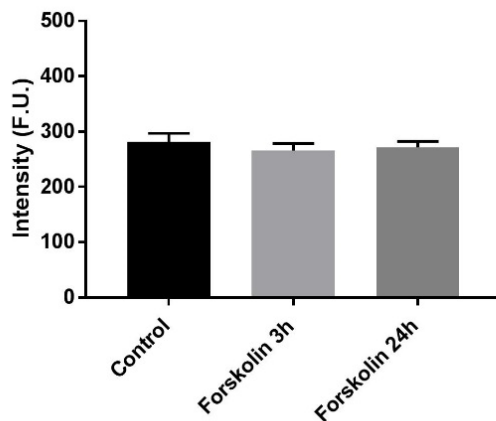
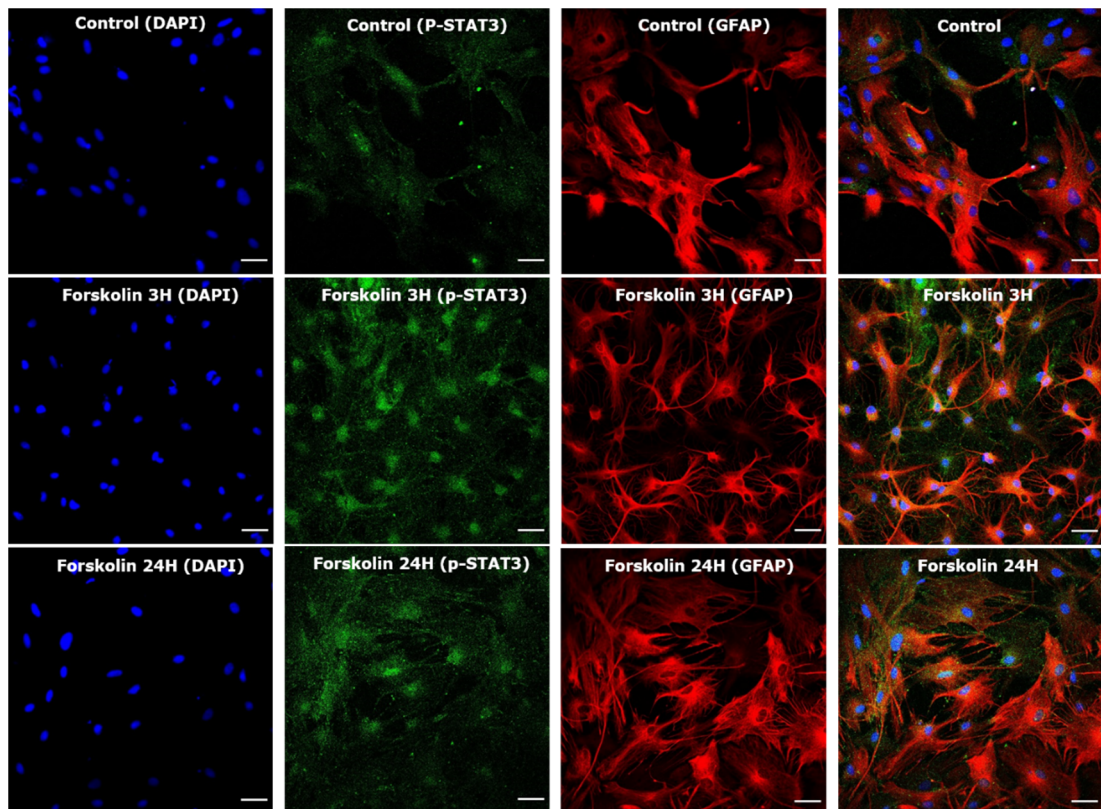


**Figure 3.17 Intensity of Y705 p-STAT3 on neonatal cortical astrocytes with confocal microscopy**, cells are stained with GFAP in red, tyrosine p-STAT3 in green and DAPI in blue. Cells are treated with forskolin 10 $\mu$ M at 3 hours (middle panels) 24 hours (lower panels). The scale bar = 40 $\mu$ m. Aggregate data represent the mean of Y705 p-STAT3 intensity per pixel in the nucleus. Data are presented as a mean  $\pm$  SEM completed from three different experiments. No statistically significant differences were determined using the one way ANOVA (Dunnett's multiple comparisons test) by comparing treated groups with control.

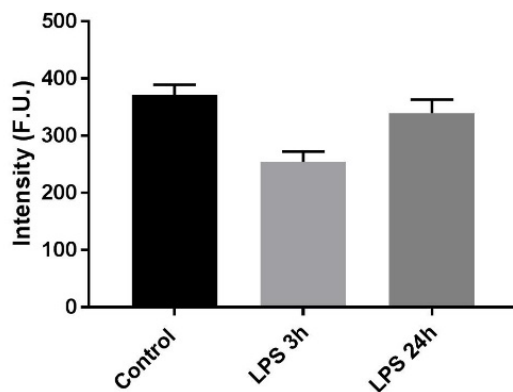
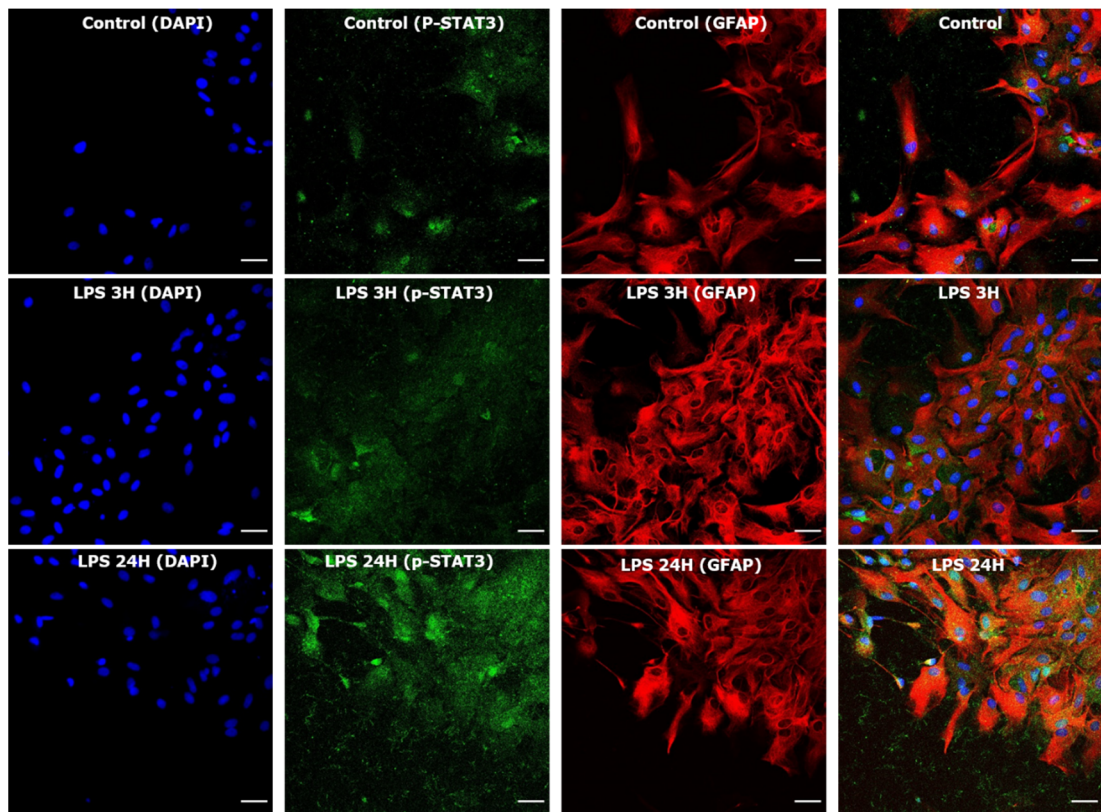


**Figure 3.18 Intensity of Y705 p-STAT3 on neonatal cortical astrocytes with confocal microscopy,** cells are stained with GFAP in red, tyrosine p-STAT3 in green and DAPI in blue. Cells are treated with LPS 1 $\mu$ g/ml at 3 hours (middle panels) 24 hours (lower panels). The scale bar = 40 $\mu$ m. Aggregate data represent the mean of Y705 p-STAT3 intensity per pixel in the nucleus. Data are presented as a mean  $\pm$  SEM completed from three different experiments. No statistically significant differences were determined using the one way ANOVA (Dunnett's multiple comparisons test) by comparing treated groups with control.

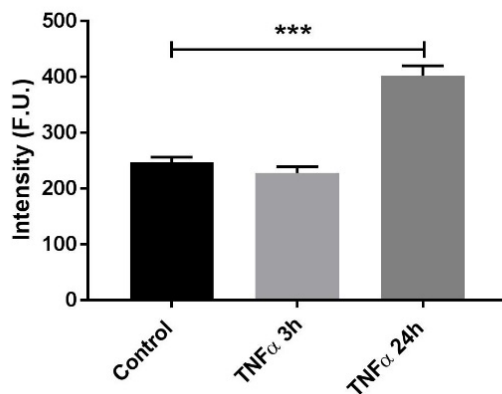
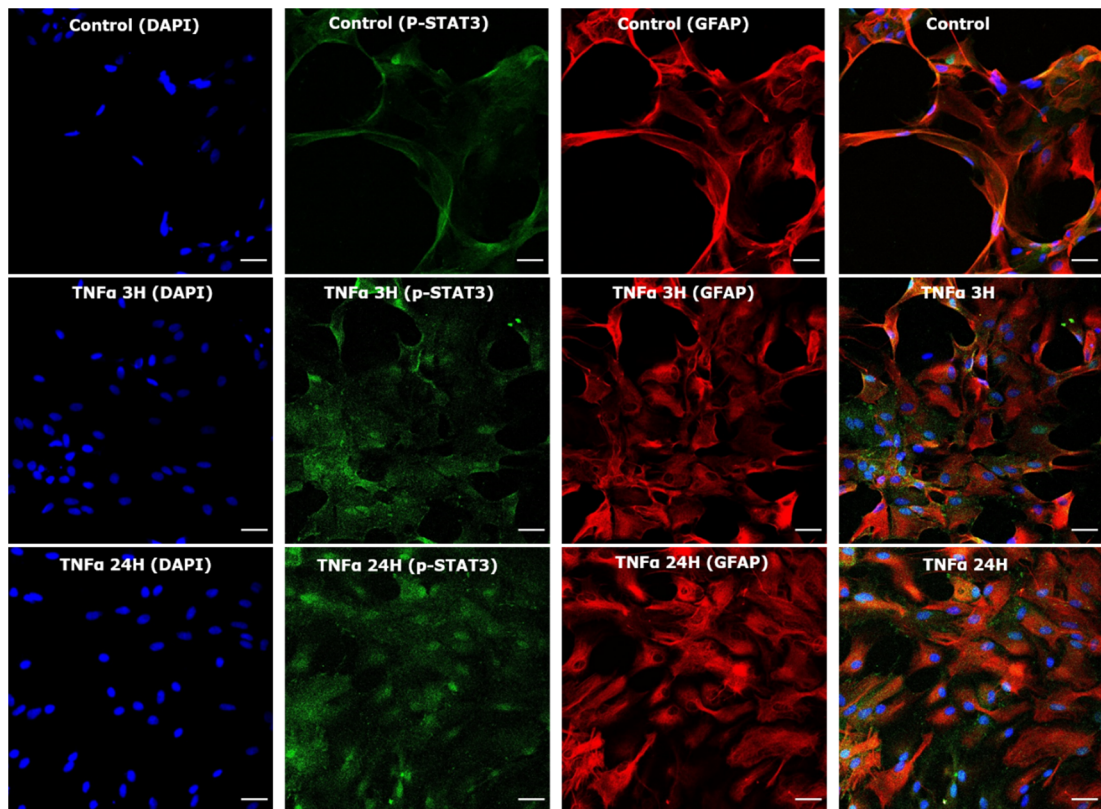


**Figure 3.19 Intensity of Y705 p-STAT3 on neonatal cortical astrocytes with confocal microscopy,** cells are stained with GFAP in red, tyrosine p-STAT3 in green and DAPI in blue. Cells are treated with TNF $\alpha$  200ng/ml at 3 hours (middle panels) 24 hours (lower panels). The scale bar = 40 $\mu$ m. Aggregate data represent the mean of Y705 p-STAT3 intensity per pixel in the nucleus. Data are presented as a mean  $\pm$  SEM completed from three different experiments. The statistical significance was determined using the one way ANOVA (Dunnett's multiple comparisons test) by comparing treated groups with control, where (\*\*\*)  $P < 0.001$  was considered statistically significant.

### **3.3 Discussion**

In vitro investigations of astrocyte function depend on obtaining a pure astrocyte culture after removing contaminating cells, and having reliable assays for changes in cell morphology and phenotype due to reactive gliosis. Most studies of astrocytes have used neonatal primary astrocytes isolated from the cerebral cortex as they are easier to isolate and culture than the spinal cord. In this chapter, we adapted this method for the culture of spinal cord astrocyte in different conditions to find the best protocol that would give us pure astrocyte cultures that respond to neurotransmitters (ATP and glutamate) with  $\text{Ca}^{2+}$  responses. It was found that GFAP-positive cells predominate after two weeks in vitro, but that a significant number of contaminating microglia cells are also present when cells are cultured in flasks. Removing the contaminating cells by shaking the flasks improved the purity of the astrocyte culture because astrocytes are more adherence cells (Tamashiro, Dalgard and Byrnes, 2012; Kerstetter and Miller, 2012). This refinement reduced the number of Iba1 positive cells by more than half.

There are other existing methods for culturing pure astrocyte. Other studies have demonstrated that using a modified chemically defined medium (MCM) by replacing glucose and D-valine with sorbitol and L-valine in growth media (Yang et al., 2007) or adding a mitotic inhibitor for 5-6 days to cells, then treated with l-leucine methyl ester after becoming confluent, could remove other contaminating cells but it takes a longer time (Gingras et al., 2007; Hamby et al., 2006). Moreover, culturing rat spinal cord astrocytes on glass coverslips seem to be a quick and easy way to get pure astrocyte because astrocytes adhere to the glass while other cells not (Silva et al., 1998), but total cell numbers are less.

Regarding the induction of reactive astrogliosis: it is possible to get reactive gliosis to occur in the commonly used of cortical astrocyte model (Lin et al., 2008; Barres, Chun, and Corey, 1989). We used a range of drugs that are known to evoke gliosis

in culture models with these doses forskolin (10 $\mu$ M) (Barres, Chun, and Corey, 1989), LPS (1 $\mu$ g/ml) (Lin et al., 2008), TNF $\alpha$  (200ng/ml) (Lee et al., 2017), noradrenaline (10 $\mu$ M) (Gavin Norris and Benveniste, 1993; Junker et al., 2002), histamine (100 $\mu$ M) (Kubo et al., 1991) and substance P (100nM) (Miyano et al., 2010). We attempted to measure four assays: morphological change with GFAP immunocytochemistry, live imaging of cells stained with calcein-AM, Ca<sup>2+</sup> response by adding UDP-glucose which is the agonist of P2Y<sub>14</sub>R and measure the intensity of p-STAT3 in the nucleus.

Immunocytochemistry is an essential method about helping us identify and characterise the morphology of the cells. However, the use of subjective measurements for both cell identity and morphology during reactive gliosis is a major limiting factor. Weak antibody staining is the main problem that we faced during cell identification, and it affected our results. Besides, the variation of GFAP expression and staining is the second issue. It has been reported that GFAP expression level depends on culture conditions, the location of astrocyte in vivo and the age of the animals (Khakh and Sofroniew, 2015; Middeldorp and Hol, 2011).

Moreover, it is possible that changed GFAP intensity may result from the accessibility of the antibody or a change in the structure of the cytoskeleton, rather than an increase in GFAP expression level. Thus, it can make classifying cells by GFAP expression challenging, and it is difficult to classify astrocyte by GFAP alone. However, measuring the GFAP intensity and GFAP protein level are the most common assays for reactive gliosis (Eriksson et al., 2002; Formichella et al., 2014; Kang et al., 2014; Liddelow et al., 2017; Sriram et al., 2004 ). We found that assessing the GFAP fluorescence intensity may not be suitable in our experiment because many variable factors could affect this intensity, and we were not able to control for them. Quantified the reactive gliosis by measuring the morphological change in astrocytes could be the best method. Counting the percentage of stellate

cells is one of the popular techniques to assess morphology change in astrocytes and to identify the numbers of reactive astrocytes (Brozzi et al., 2009; Murk et al., 2013). However, the time is taken for manual assessment, or need for specialist software to automatically calculate the percentage of stellation, are the main drawbacks in this assay. In addition, measuring the stellation index (total process area/cell body area) (Beckerman et al., 2015), the ratio between the cell outline and the cell area (Murk et al., 2013), the perimeter of cell staining (East, Golding, and Phillips, 2008), changes in morphology can be quantified. Here, we measured the cell circularity by using the equation  $(4 * \pi * \text{area}) / (\text{perimeter}^2)$  where the value close to zero indicates astrocyte stellation, which occurs after forskolin treatment. These different approach work because we can look at and observing stellation in live cells during the time, which gives us a geometric assessment of morphology. However, it is not usually more efficient than immunocytochemistry. It does not add any particular value because we are still using the manual counting of the geometric circularity, and automate the analysis is very reliable to save the analysis time.

Culturing primary astrocytes in serum-containing medium, show a flat, morphology without processes. Treat astrocyte with different drugs that activate different signalling pathway have a various response. Forskolin, noradrenaline can induce stellation (a star-shaped morphology) while LPS, TNF $\alpha$ , histamine and substance P did not. This indicates the involvement of adenylyl cyclase to cause morphology change and reactive gliosis (Daginakatte et al., 2008; Fedoroff et al., 1984; Masaki et al., 2000; Tiryaki, Ayres, et al., 2015) because both forskolin and noradrenaline activate adenylyl cyclase (Donnell et al., 2013; Tanabe, Kozawa and Iida, 2016). High percentage of stellate cells after forskolin treatment (79%) but not with noradrenaline (39%) indicate the direct activation of adenylyl cyclase in case of forskolin (Tanabe, Kozawa and Iida, 2016) while noradrenaline work through the balance between activation of  $\alpha$  and  $\beta$  receptor in astrocytes (Donnell

et al., 2013). Culturing astrocytes in serum cause protoplasmic morphology, and the stellation is happening through the depolymerisation of actomyosin stress fibres in response to drugs (Perez et al., 2005). In addition, the presence of serum in astrocytes culture media reduces the level of Mob protein which regulates cell morphogenesis in alteration of the actin cytoskeleton arrangement and treats the cells with cAMP lead to increase in Mob2 expression and cause stellation (Fang et al., 2012).

GFAP assay is not enough assays for reactive gliosis because we are not going to consider on GFAP to be a sole marker (Sofroniew and Vinters, 2010; Liddelow and Barres, 2017). We tried to use multiple markers for reactive gliosis. For example, Zamanian et al. (2012) determined that there is an increase in the expression of two genes (*Lcn2* and *Serpina3n*) in case of reactive astrocytes that could be reliable markers for reactive gliosis. Another significant functional assay we can use as the assay of reactive gliosis is by measuring  $Ca^{2+}$  signalling and gene expression of multiple GPCRs after adding GPCR-specific ligands. There is a study found that induction of reactive gliosis after treatment of astrocyte with inflammatory stimuli such as LPS, TGF $\beta$ 1 and IFN $\delta$  can significantly increase the expression level of *P2ry14* gene for P2Y<sub>14</sub> receptor. These lead to increase in intracellular calcium levels in 50% of the cells after adding UDP-glucose ligand that binds with a purinergic receptor on astrocyte (P2Y<sub>14</sub>) while this ligand did not have any detection of  $Ca^{2+}$  response in physiological astrocyte (Hamby et al., 2012). Another study was demonstrate that UDP-glucose can increase the intracellular calcium levels in 11% of physiological cortical astrocytes (Fumagalli et al., 2003). Our result found that the neonatal cortical astrocytes treated with forskolin have an increase in mean  $Ca^{2+}$  release but this was not statistically significant due to the variation between groups. We hypothesised that forskolin might be involved in the signalling pathway, which leads to up-regulate this gene in the GPCR and affects the calcium release, but this may not be correct as it is a

different stimulus used than the original report (Hamby et al., 2012). A combinational treatment of inflammatory stimuli may be essential to change the level of the P2Y<sub>14</sub> receptor and increase Ca<sup>2+</sup> signalling (Hamby et al., 2012), which make an account for our variable responses with individual inflammatory stimuli.

It was discovered that P2Y<sub>14</sub> receptor known to be involved in another process like cell infection and neuroinflammation (Abbracchio et al., 2003; Moore et al., 2003; Lazarowski and Harden, 2015). However, the tonic level of P2Y<sub>14</sub> receptor can inhibit the astrocytes remodelling and knockdown this receptor increases the release of TNF $\alpha$  that lead to increase the expression of matrix metalloprotease-9 (MMP9) which is responsible for cell remodelling (Kinoshita et al., 2013). There is evidence discovered that overnight expression of LPS in microglia increases the expression of the P2Y<sub>14</sub> receptor as well as increase the Ca<sup>2+</sup> signalling in response to UDP-glucose (Bianco et al., 2005). Taken together, this indicates the involvement of this receptor in inflammatory neurological diseases, and it seems to be that the P2Y<sub>14</sub> receptor is a promising candidate assay for reactive gliosis.

Franke and Illes (2014) found that release ATP from neurons lead to activate both P2X<sub>7</sub> and P2Y<sub>1,2</sub> subtypes receptors during astrogliosis. These receptors lead to induce reactive gliosis through activation of a STAT3 signalling pathway (Washburn and Neary, 2006). Also, it was found that up-regulation on the level of STAT3 and activate STAT3 pathway could be the initial marker for reactive astrocyte (Liu et al., 2013; Sofroniew, 2009; Zhang et al., 2013). Here, the localisation of p-STAT3 was measured. It discovers a significant increase of S727 p-STAT3 intensity in the nucleus after forskolin, LPS and TNF $\alpha$  while only TNF $\alpha$  can increase the localisation of Y705 p-STAT3 in the nucleus.

In summary, neonatal cortical induce reactive gliosis in response to different stimuli. Change the astrocytes morphology form polygonal shape to stellate was detected after forskolin and noradrenaline with a high percentage of stellate cells.

Assay of the morphology change during live imaging indicated that the only forskolin reduces the astrocytes circularity comparing with others. Up-regulation of P2Y<sub>14</sub> seemed variable but was not statistically significant after forskolin, while LPS and TNF $\alpha$  had no observable effect. In this chapter, it was found an increase in the intensity of p-STAT3 in the nucleus. These results indicate that p-STAT3 is involved in inducing reactive gliosis and may relate to stellation.

**Chapter 4 Characterisation of stellation in different CNS regions and at various developmental stages**

#### **4.1 Introduction**

Embryonic and postnatal astrocytes are different according to their morphology and function. The astrocytes are divided into three stages cells: progenitor (which occurs in the embryonic stage), a maturing postnatal astrocyte, and an adult astrocyte (Molofsky et al., 2012). At the embryonic stage, neural stem cells convert from neurogenesis to gliogenesis in a process called the gliogenic switch to form astrocyte precursors. It's reported that this step happens around E12.5 in spinal cord and E16-18 in the cortex (Molofsky and Deneen, 2015). Moreover, astrocytes can rise from four different sources including radial glia, astrocyte progenitor population, NG2<sup>+</sup> glial progenitor cells, or the proliferation of newly born astrocytes (Ge et al., 2012; Sloan and Barres, 2015; Sohn et al., 2015). The astrocytes are functionally mature during the postnatal stage. Cahoy et al. (2008) were demonstrated that astrocytes express the mature gene profile by P17. On the other hand, Rusnakova et al. (2013) found that P30 mainly represent the mature astrocyte genes. Mature astrocytes can express many markers, such as GFAP, S100 $\beta$ , Aldh1L1, and aquaporin4 (Chaboub and Deneen, 2013).

The role of astrocytes is distinct in different regions in CNS and developmental stages (Bayraktar et al., 2015; Cahoy et al., 2008; Taft, Vertes and Perry, 2005; Zhang and Barres, 2010). These differences according to the changes in astrocyte genes profiles. Clarke et al. (2018) discovered that aged brain astrocytes have more A1 reactive astrocytes function and reactive gliosis genes expression are up-regulated in hippocampal and striatal than cortical astrocytes. Increase GFAP, TNF $\alpha$  and IL-1 $\beta$  expression in hippocampus rat tissue are age-related (Lynch et al., 2010). Yoon et al. (2017) established a significantly higher level of GFAP, IL-6 and STAT3 proteins in the spinal cord than the brain in postnatal and adult mice. Production of cytokines and chemokines in reactive astrocytes are regions difference (Morga, Faber and Heuschling, 1999; Fitting et al., 2010). It was found that increasing the expression of astrocytes markers and microglia markers after

nerve injury in the spinal cord is developmentally depended (Vega-Avelaira, Moss and Fitzgerald, 2007) and neuropathic pain mainly occurs in late stages following neonatal nerve injury (Vega-Avelaira et al., 2012).

However, TGF $\beta$  signalling is increased by age in response to post-stroke, which regulates glial scar formation and the immune response (Doyle et al., 2010). A study identifies the expression of Notch1 signalling, which is controlling neuronal reprogramming in different CNS regions and age. They found that spinal astrocytes expressed more *Notch1* level than cortical astrocytes in neonatal animal and it is increased in adults, and proliferation rate of neonatal spinal astrocyte is higher than cortical astrocytes (Hu et al., 2019)

Won and Oh (2000) found heterogeneity in the ability of cAMP to induce stellation in neonatal astrocytes from six different regions of the rat brain. However, the cAMP level was the same in both ages (Abe and Saito, 1997). Gautron, De Smedt-Peyrusse and Layé (2006) measured the STAT3 level in different ages (P3, P10, and P21). The amount of total STAT3 was increased by age. Phosphorylated-serine STAT3 was lower at P3 but increased at later stages while phosphorylated STAT3 on tyrosine 705 increased at P3 and P10 and then decreased at P21.

### **Aim**

The reactive gliosis phenomena of neonatal and embryonic astrocytes isolated from rat brain and spinal cord were evaluated. Most developmental studies were focused on testing the difference between neonatal and adults astrocytes, while the difference between neonatal and embryonic is still not understood. This chapter investigated the hypothesis that neonatal and embryonic astrocytes may differ in their ability to induce reactive gliosis and morphology change in response to different stimuli within the brain and spinal cord.

## **4.2 Results**

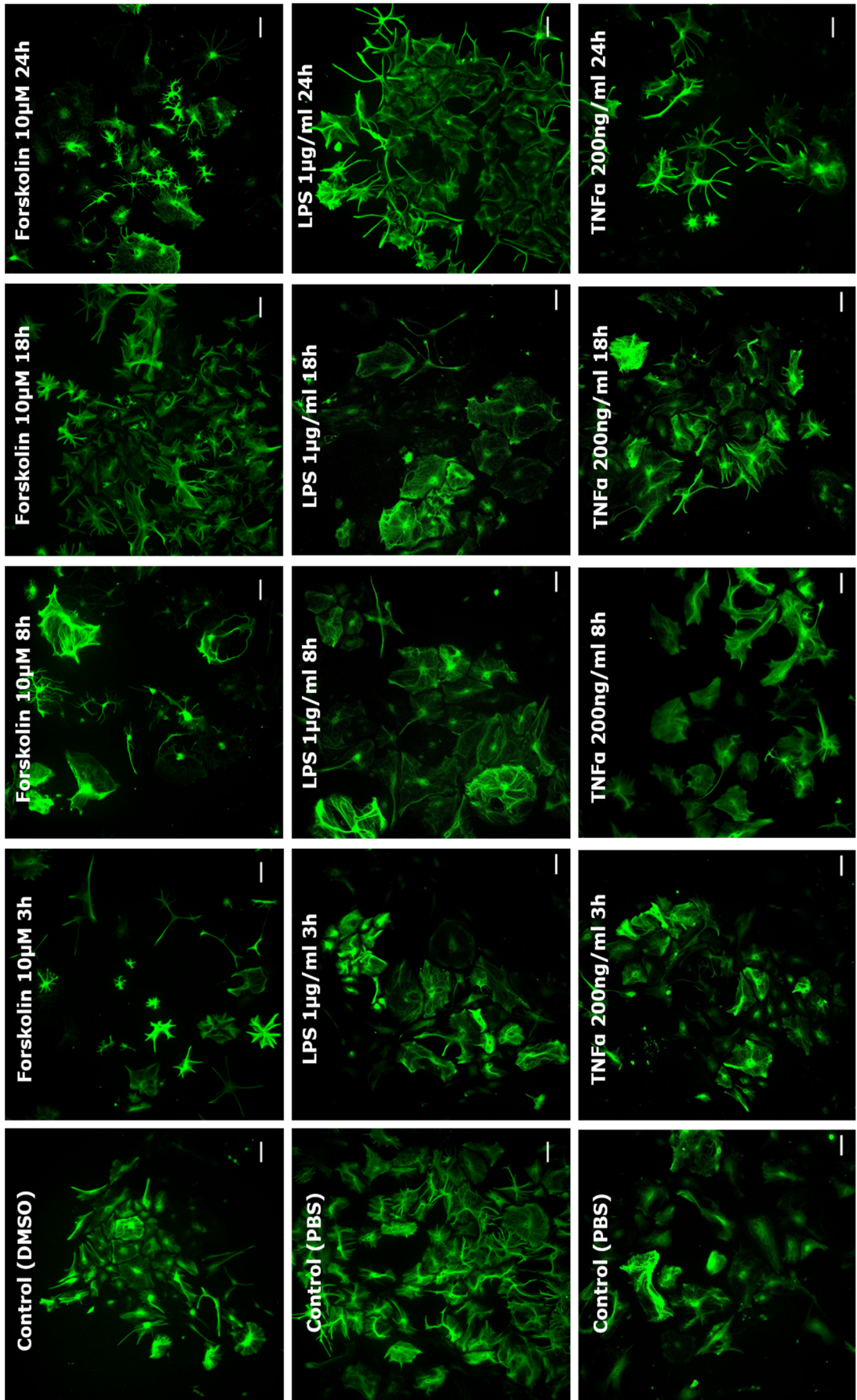
### **4.2.1 Neonatal spinal vs Neonatal cortical astrocytes**

**4.2.1.1** Assess the morphological change (stellation) with GFAP immunocytochemistry

In the previous chapter, many assays for reactive gliosis were tested using cortical astrocytes. Next, we used these assays to investigate the response of primary astrocytes isolated from the spinal cord.

Morphology change of spinal astrocytes was measured after treating them with forskolin, LPS and TNF $\alpha$  at different time intervals. The results demonstrate that 40% of cells became stellate after 3 hours and 8 hours of forskolin treatment ( $P=0.0001$ ), but the percentage dropped after 18 and 24 hours to 29 % ( $P=0.01$ ) compared with a control group. However, no significant differences were discovered in the case of LPS treatment ( $P=0.972$ ). There is a significant difference only after 18 hours of TNF $\alpha$  treatment with 34% of stellation ( $P=0.049$ ) compared with the control cells (Figure 4.1).

Neonatal cortical astrocytes (data of cortical stellation shown in details in Figure 3.6) were therefore significantly more likely than spinal astrocytes to respond to forskolin by inducing stellation ( $P < 0.001$ ). However, no differences were discovered between cortical and spinal astrocyte in the case of LPS ( $P=0.578$ ) and TNF $\alpha$  treatment ( $P=0.540$ ) (Figure 4.2).



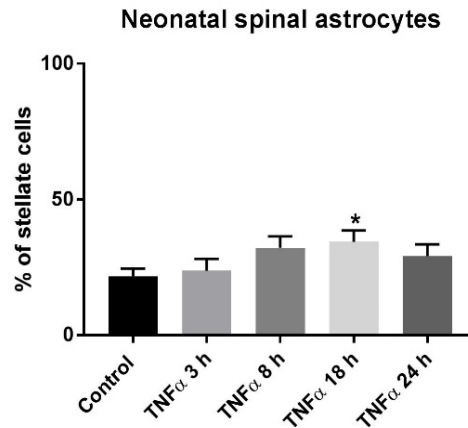
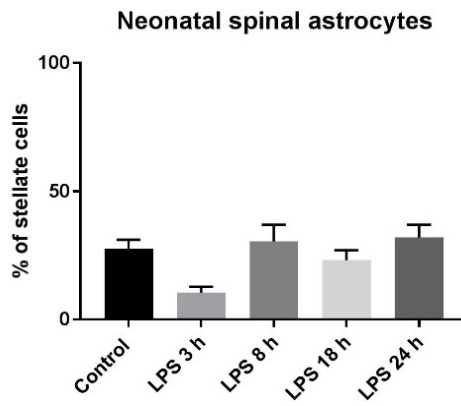
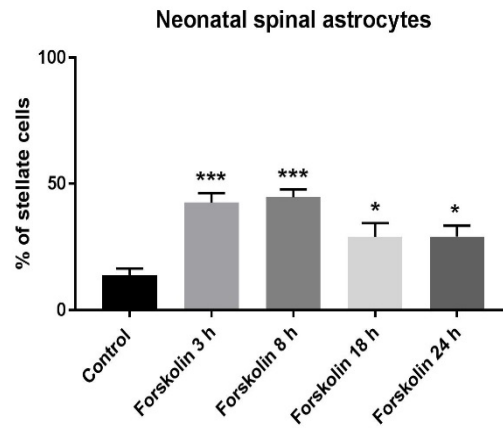
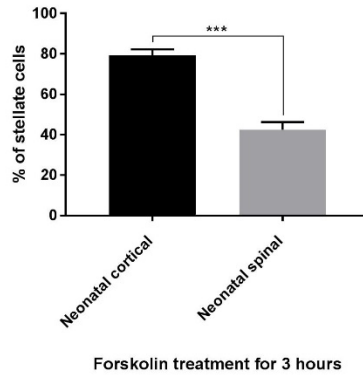
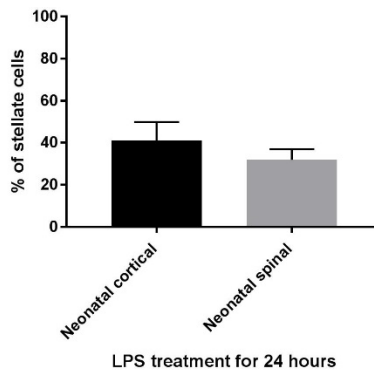


**Figure 4.1 Stellation response of neonatal spinal astrocytes.** Images: staining with GFAP after treatment with forskolin, LPS and TNF $\alpha$  at different time intervals, as indicated. Scale bar=500 $\mu$ m. Aggregate data represent the percentage of stellate cells for each treatment and time interval. Data are presented as a mean  $\pm$  SEM obtained from three independent experiments. The statistical significance was determined using the one way ANOVA followed by Dunnett's multiple comparisons test, where (\*P < 0.05 and \*\*\* P < 0.001) was considered statistically significant.

Comparison between neonatal cortical and spinal astrocytes in stellation



Comparison between neonatal cortical and spinal astrocytes in stellation



Comparison between neonatal cortical and spinal astrocytes in stellation

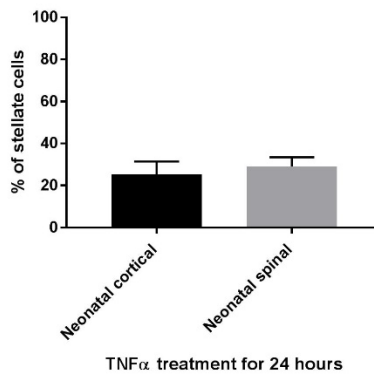
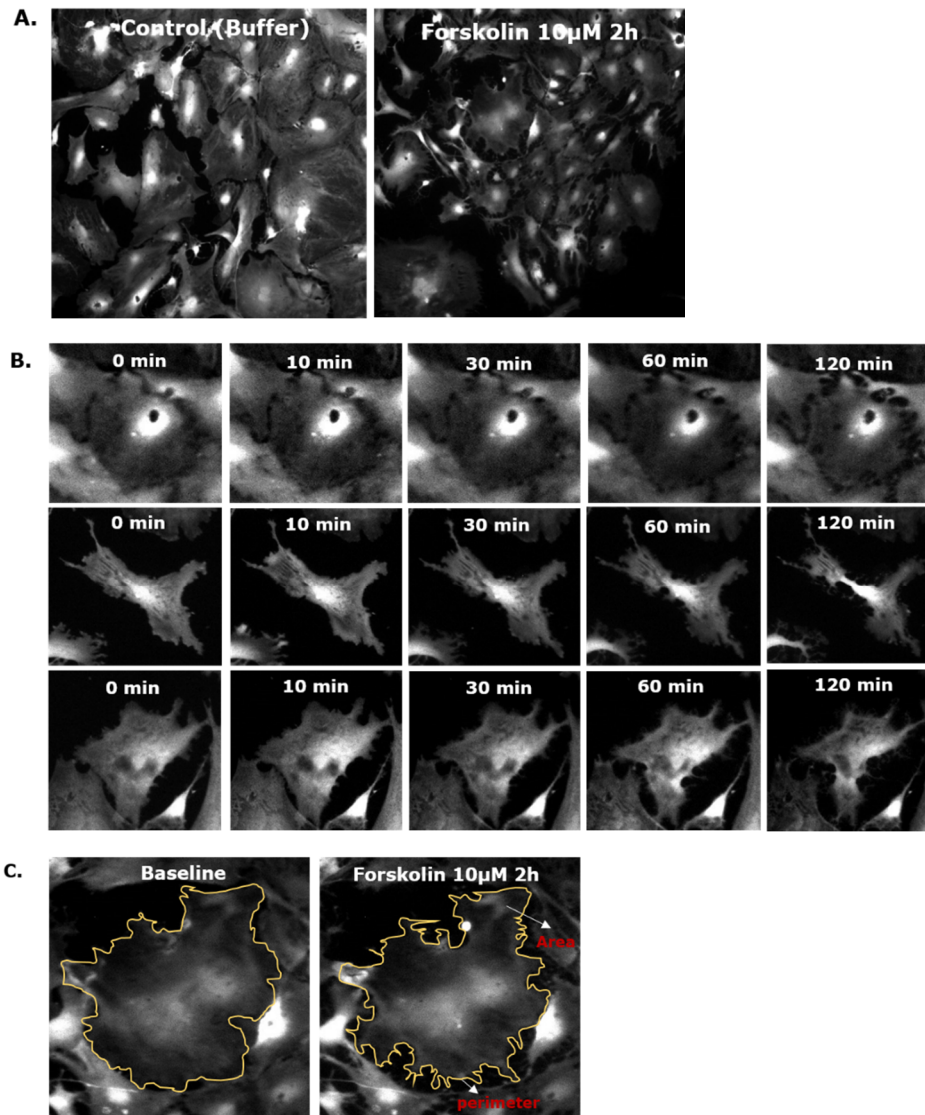


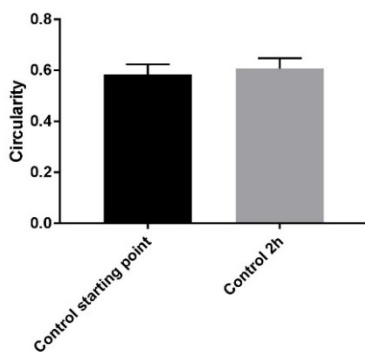
**Figure 4.2 Comparison between neonatal cortical and spinal astrocytes in stellation**, after treatment with forskolin for 3 hours, LPS and TNF $\alpha$  for 24 hours. Aggregate data represent the percentage of stellate cells. Data are presented as a mean  $\pm$  SEM and obtained from three independent experiments. The statistical significance was determined using the Mann-Whitney test, where (\*\*\*) P < 0.001) was considered statistically significant.

#### **4.2.1.2** Assessing morphological change (stellation) with calcein-AM real-time imaging

After loading spinal cord astrocytes with calcein-AM, the cells were treated with imaging buffer and forskolin to assist the morphology change during 2 hours of real-time imaging. There is no significant difference after adding the buffer from the starting point and after 2 hours ( $P=0.187$ ). The mean of circularity is 0.584 at the first image and 0.606 at the end of imaging. However, the circularity of cells treated with forskolin decreased from 0.483 to 0.397 ( $P < 0.001$ ) (Figure 4.3). By comparing the circularity between cortical (data are shown in details in chapter 3) and spinal astrocytes, there is no significant difference between cortical and spinal after 2 hours of forskolin treatment ( $P=0.529$ ) (Figure 4.4).



Compare circularity of astrocytes before and after buffer treatment



Compare circularity of astrocytes before and after forskolin treatment

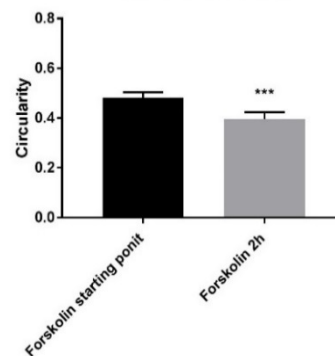


**Figure 4.3 Stellation assays of neonatal spinal astrocytes,** A) Cells were stained with calcein-AM and treated with forskolin. B) The real-time imaging duration was 2 hours. C) Images represent the area and perimeter changes of astrocyte at the baseline and after 2 hours of treatment. Aggregate data show circularity of 10 cells of each condition at the beginning and the end of imaging. Data are presented as a mean  $\pm$  SEM. The statistical significance was determined using the paired t-test, where (\*\*\*)  $P < 0.001$  was considered statistically significant.

### Comparison between neonatal cortical and spinal astrocytes in circularity

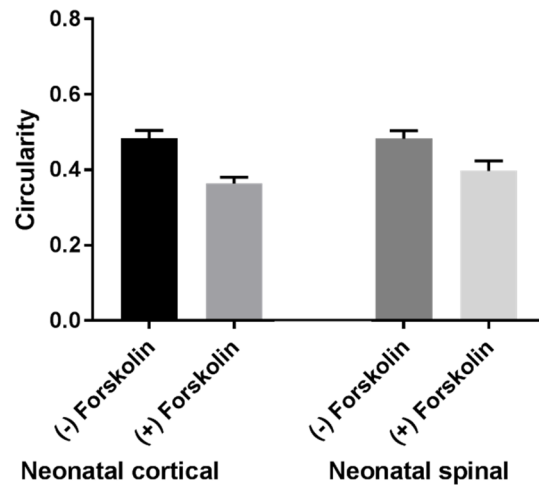


**Figure 4.4 Comparison between neonatal cortical and spinal astrocytes in stellation,** after treatment with forskolin for 2 hours. Aggregate data represent circularity of 10 cells of each condition at the beginning and the end of real-time imaging. Data are presented as a mean  $\pm$  SEM and obtained from three independent experiments. The statistical significance was determined using the Mann-Whitney test. No significant difference was discovered.

#### **4.2.1.3** Release of $\text{Ca}^{2+}$ after stimulation of the $\text{P2Y}_{14}$ receptor

The spinal cord astrocytes were treated with forskolin, LPS and TNF $\alpha$  for 24 hours to test for up-regulation of  $\text{P2Y}_{14}$  receptor. The receptor activity was determined by measuring  $\text{Ca}^{2+}$  release in response to UDP-glucose. It was found that 26% of the untreated neonatal spinal astrocytes respond to UDP-glucose while just 13%, 18% and 8% of the astrocytes were responsive after forskolin, LPS and TNF $\alpha$  treatment, respectively. There were no significant differences between control and treated groups (forskolin  $P=0.814$ , LPS  $P=0.922$  and TNF $\alpha$   $P=0.567$ ) (Figure 4.5). By comparing the  $\text{Ca}^{2+}$  response between cortical (data are shown in details in Figure 3.13) and spinal astrocytes, there was no statistically significant difference between them (forskolin  $P=0.179$ , LPS  $P=0.554$  and TNF $\alpha$   $P=0.567$ ) (Figure 4.6).

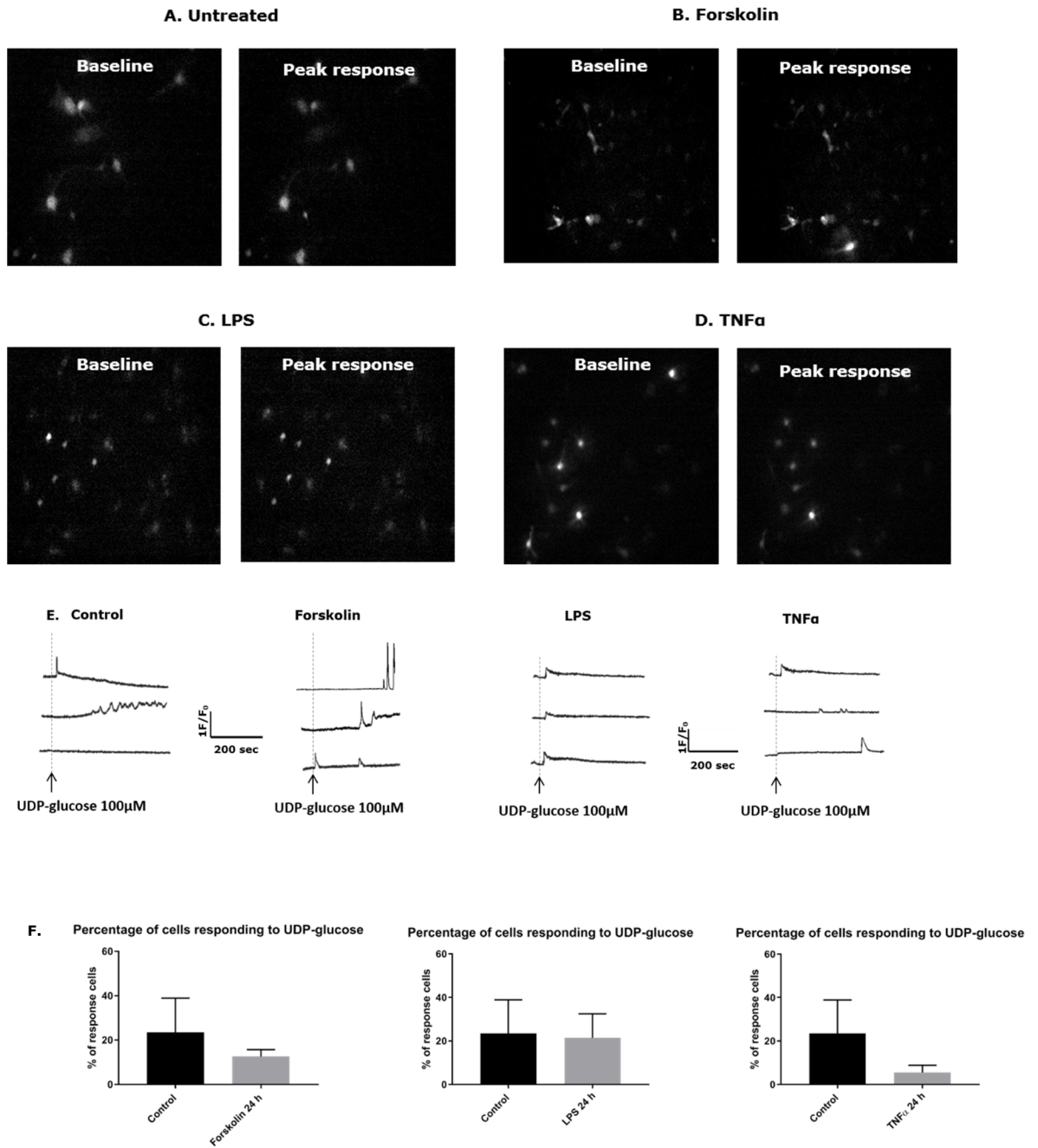
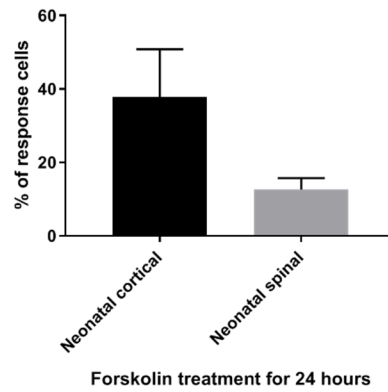
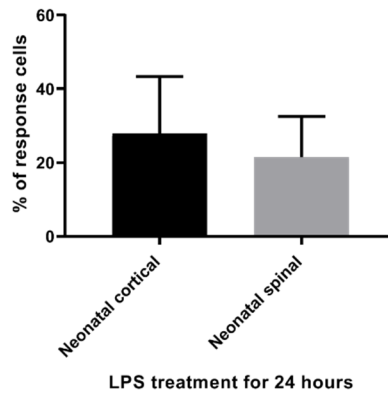


**Figure 4.5 Ca<sup>2+</sup> response of neonatal spinal by adding UDP-glucose.** A) Two images show Fluo-5F fluorescence intensity at the baseline and after 13 minutes of adding UDP-glucose in untreated cells. B) Two images show Fluo-5F fluorescence intensity at the baseline and after 4 minutes of adding UDP-glucose in cells treated with forskolin. C) Two images show Fluo-5F fluorescence intensity at the baseline and after 17 minutes of adding UDP-glucose in cells treated with LPS. D) Two images show Fluo-5F fluorescence intensity at the baseline and after 14 minutes of adding UDP-glucose in cells treated with TNF $\alpha$ . E) Representative traces of Fluo-5F fluorescence intensity for three individual cells in each group. F) Aggregate data above represent the percentage of cells responding in the control (n = 190) and the test groups (forskolin: n = 169, LPS: n = 294 and TNF $\alpha$ : n = 131). Data are presented as a mean  $\pm$  standard error (SEM). No statistically significant differences were determined using the Mann-Whitney test. The experiment was repeated three times.

Compare the percentage of cells responding to UDP-glucose between neonatal cortical and spinal astrocytes



Compare the percentage of cells responding to UDP-glucose between neonatal cortical and spinal astrocytes



Compare the percentage of cells responding to UDP-glucose between neonatal cortical and spinal astrocytes

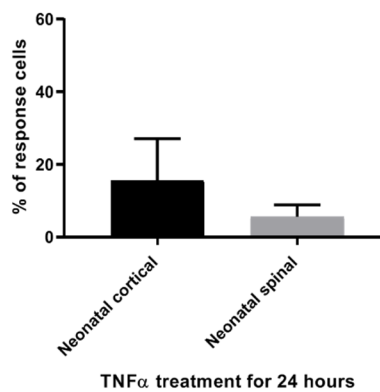


**Figure 4.6** Ca<sup>2+</sup> response of neonatal cortical and spinal astrocytes by adding UDP-glucose after treating the cells with Forskolin, LPS and TNF $\alpha$  for 24 hours. Data are presented as a mean  $\pm$  standard error (SEM). No statistically significant differences were determined using the Mann-Whitney test.

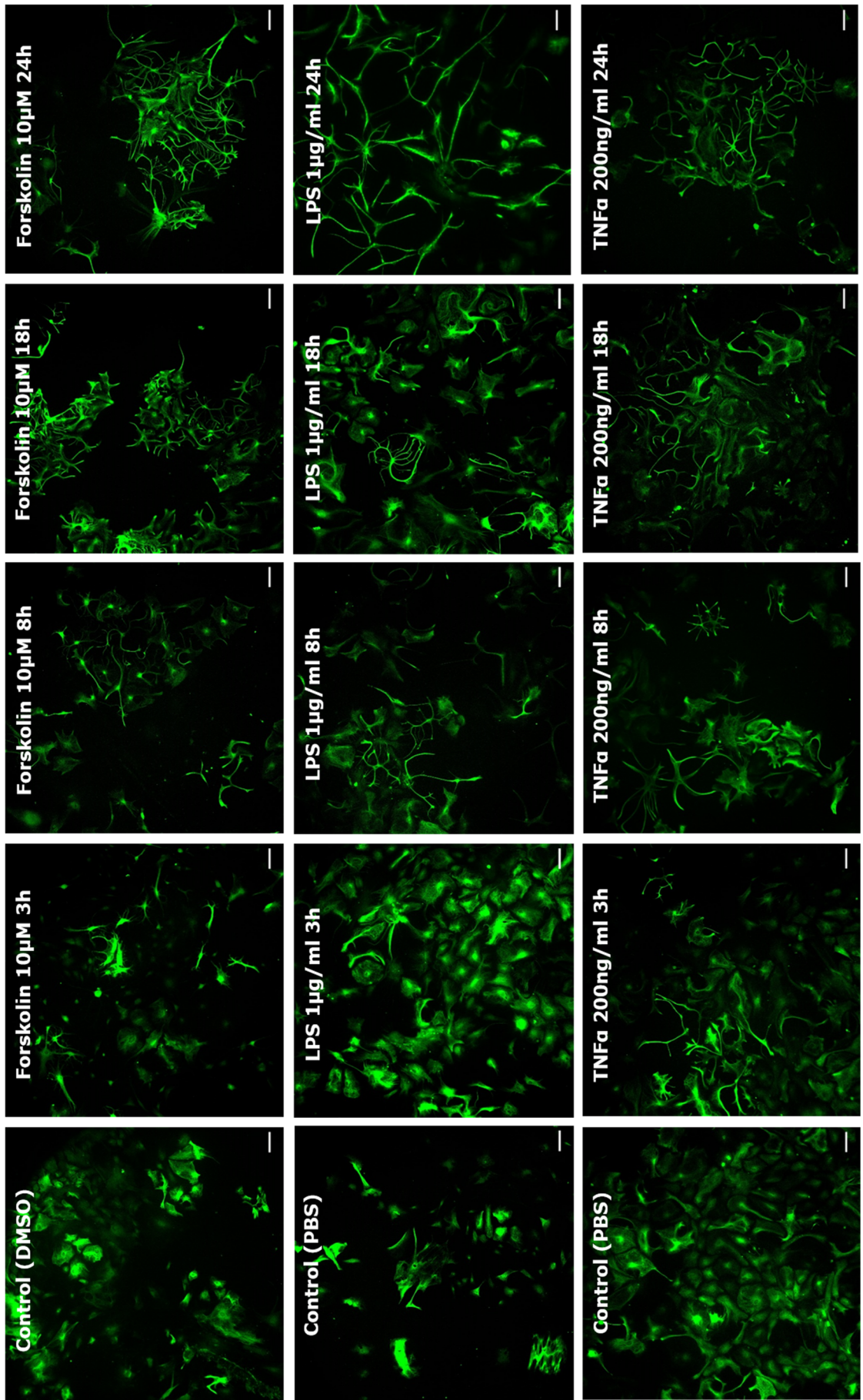
## **4.2.2 Neonatal cortical vs Embryonic cortical astrocytes**

**4.2.2.1** Assess the morphological change (stellation) with GFAP immunocytochemistry

The next stage was to investigate whether there was a difference between astrocytes obtained from postnatal rats and embryonic rats.

To induce stellation in embryonic cortical cells, we treated with forskolin, LPS and TNF $\alpha$  as usual. In the case of embryonic cortical, forskolin treatment led to the appearance of branched cells after 3 hours incubation with 28% of cells showing stellation ( $P=0.023$ ) with only 7% of untreated cells. Then, it is decreased after 8 hours treatment to 22% ( $P=0.151$ ) and increased again to 30% and 36% after 18 hours ( $P=0.001$ ) and 24 hours ( $P=0.0001$ ). For LPS and TNF $\alpha$ , no significant increase in cell stellation was determined in both treatments (LPS  $P=0.193$  and TNF $\alpha$   $P=0.349$ ) compared with the control group (Figure 4.7).

This contrasts with neonatal cortical astrocytes, which demonstrate time-dependent gliosis. Comparing neonatal with embryonic cortical, results show there is a significant difference between groups in stellation after forskolin and LPS but not with TNF $\alpha$ . The percentage of stellate neonatal cortical astrocyte after forskolin treatment is 76%, which is higher than embryonic cortical with 28% ( $P<0.001$ ). In the case of LPS, 41% of neonatal cortical became stellate, and only 16% of embryonic cortical changed into stellate cells ( $P=0.046$ ). They are inducing stellation after TNF $\alpha$  treatment was nearly equal with 25% in the case of neonatal cortical and 29% in the case of embryonic cortical astrocyte ( $P=0.613$ ) (Figure 4.8).



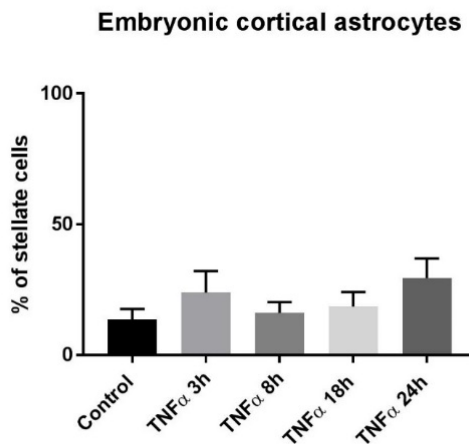
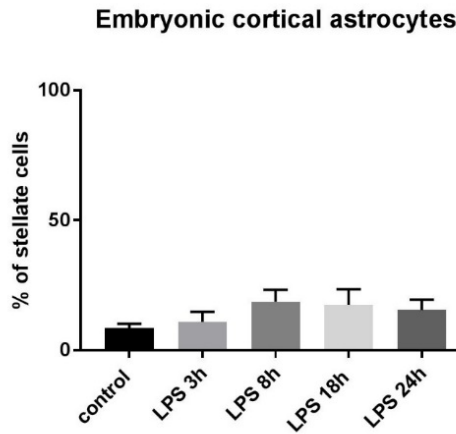
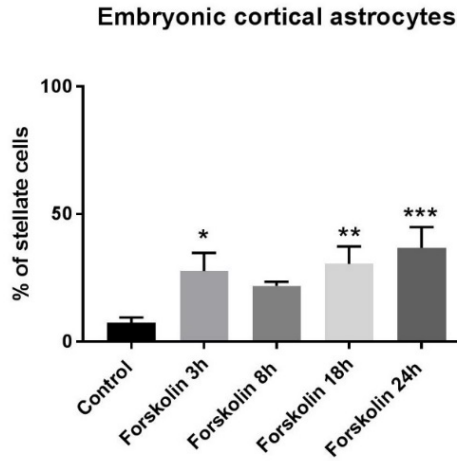
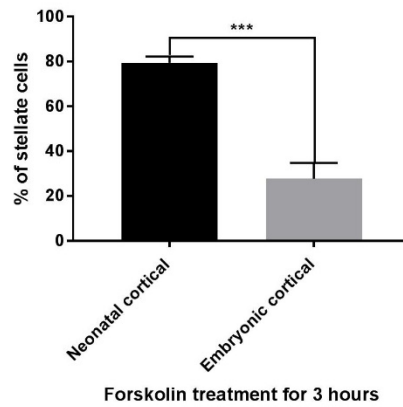
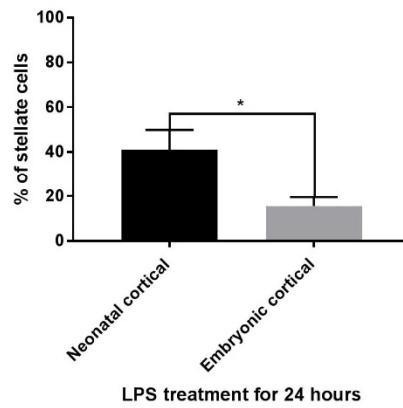


**Figure 4.7 Stellation response of embryonic cortical astrocytes.** Images: staining with GFAP after treatment with forskolin, LPS and TNF $\alpha$  at different time intervals, as indicated. Scale bar=500 $\mu$ m. Aggregate data represent the percentage of stellate cells for each treatment and time interval. Data are presented as a mean  $\pm$  SEM obtained from three independent experiments. The statistical significance was determined using the one way ANOVA followed by Dunnett's multiple comparisons test, where (\*P < 0.05, \*\*P<0.01 and \*\*\* P < 0.001) was considered statistically significant.

Comparison between neonatal and embryonic cortical astrocytes in stellation



Comparison between neonatal and embryonic cortical astrocytes in stellation



Comparison between neonatal and embryonic cortical astrocytes in stellation

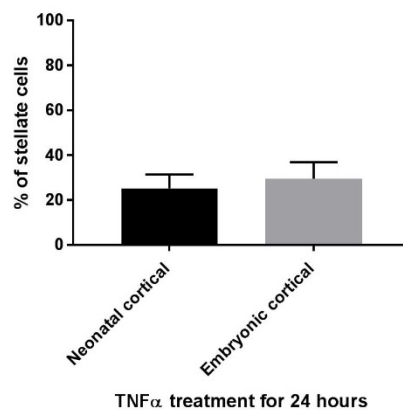
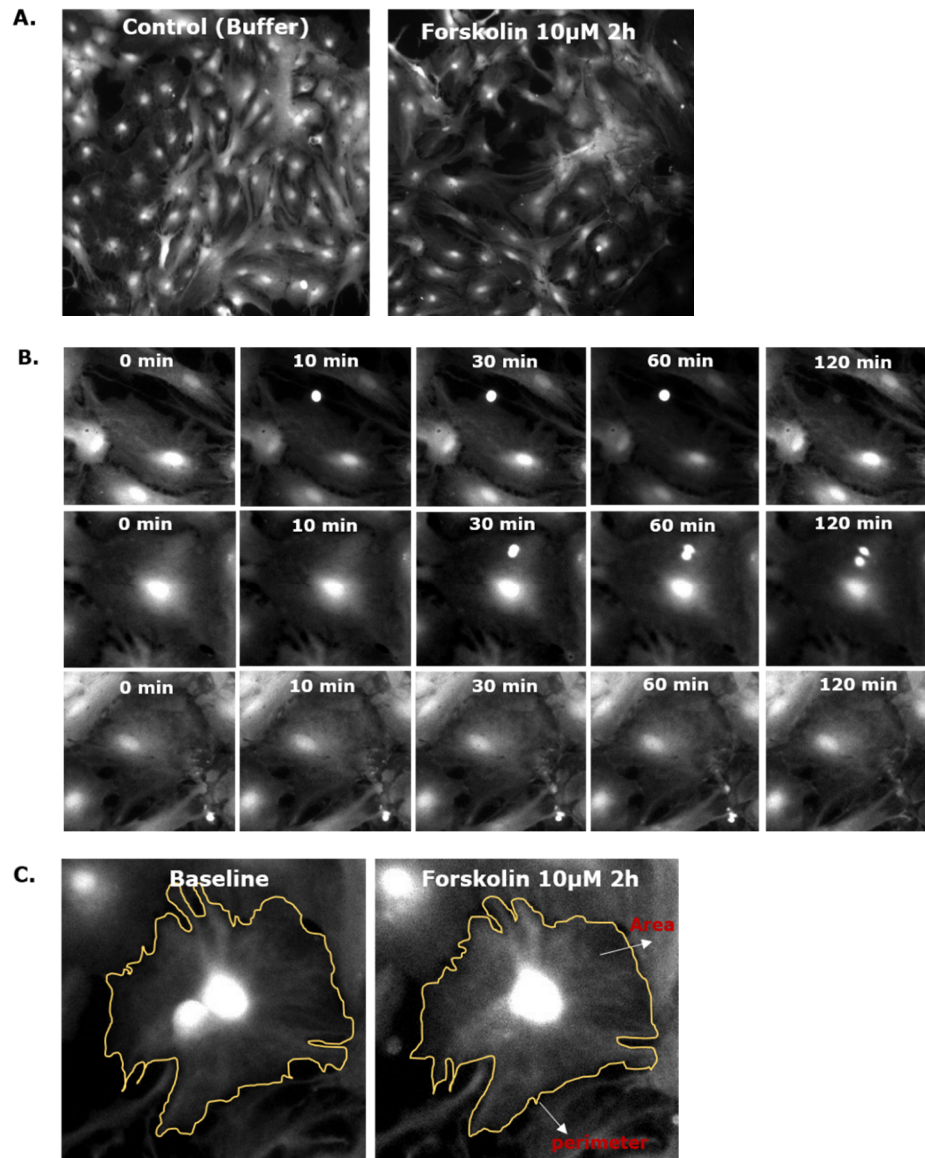


**Figure 4.8 Comparison between neonatal and embryonic cortical astrocytes in stellation**, after treatment with forskolin for 3 hours, LPS and TNF $\alpha$  for 24 hours. Aggregate data represent the percentage of stellate cells. Data are presented as a mean  $\pm$  SEM and obtained from three independent experiments. The statistical significance was determined using the Mann-Whitney test, where (\* P < 0.05 and \*\*\* P < 0.001) was considered statistically significant.

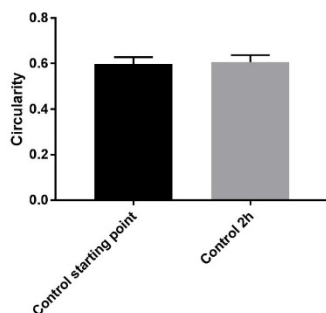
#### **4.2.2.2** Assessing the morphological change (stellation) with calcein-AM real-time imaging

Real-time imaging experiments did not show any significant change in embryonic cortical astrocyte circularity after the cells treated with buffer ( $P=0.659$ ). The circularity of astrocytes at the beginning of imaging equal 0.59, and after 2 hours imaging was 0.6. However, there is a significant increase in astrocytes circularity after 2 hours of forskolin treatment ( $P=0.02$ ) with 0.5 to 0.6 (Figure 4.9).

Comparison between neonatal (shown in details in section 3.2.2.2) and embryonic cortical in stellation assay of calcein-AM loading showed that the circularity of neonatal cortical astrocyte after forskolin was significantly lower than embryonic cortical with 0.36 in case of neonatal and 0.55 in case of embryonic astrocytes ( $P<0.001$ ). This result indicates that the neonatal cortical became more stellate than embryonic cortical astrocytes (Figure 4.10).



Compare circularity of astrocytes before and after buffer treatment



Compare circularity of astrocytes before and after forskolin treatment

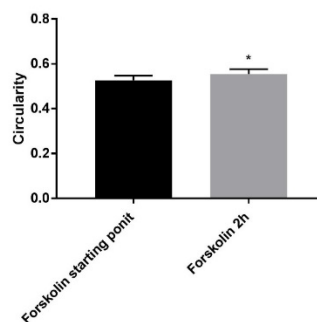


**Figure 4.9 Stellation assays of embryonic cortical astrocytes**, A) Cells were stained with calcein-AM and treated with forskolin. B) The real-time imaging duration was 2 hours. C) Images represent the area and perimeter changes of astrocyte at the baseline and after 2 hours of treatment. Aggregate data show circularity of 10 cells of each condition at the beginning and the end of imaging. Data are presented as a mean  $\pm$  SEM. The statistical significance was determined using the paired t-test, where (\*  $P < 0.05$ ) was considered statistically significant.

### Comparison between neonatal and embryonic cortical astrocytes in circularity

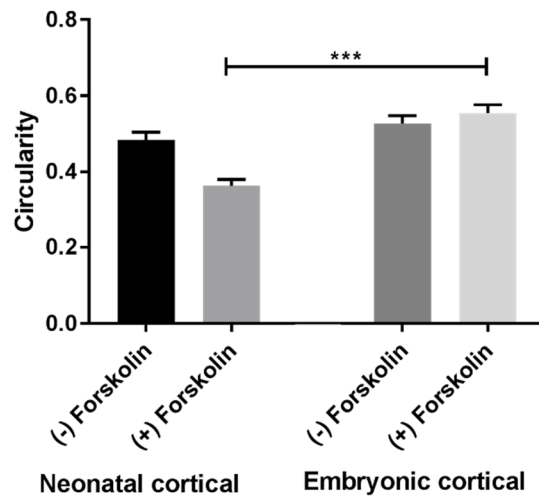


**Figure 4.10 Comparison between neonatal and embryonic cortical astrocytes in stellation**, after treatment with forskolin for 2 hours. Aggregate data represent circularity of 10 cells of each condition at the beginning and the end of real-time imaging. Data are presented as a mean  $\pm$  SEM and obtained from three independent experiments. The statistical significance was determined using the Mann-Whitney test, where (\*\*\*)  $P < 0.001$  was considered statistically significant.

#### **4.2.2.3** Release of Ca<sup>2+</sup> after stimulation of the P2Y<sub>14</sub> receptor

The result of neonatal cortical astrocytes regarding the up-regulation of P2Y<sub>14</sub> receptor is described in details in section 3.2.2.3 and Figure 3.13 for neonatal cortical. The same experiment was done on embryonic cortical and neonatal spinal astrocytes to measure Ca<sup>2+</sup> release after up-regulation of P2Y<sub>14</sub> receptor.

The results show no significant difference of cells response to UDP-glucose for embryonic cortical astrocytes treated with buffer control, forskolin (P >0.999), LPS (P=0.568) or TNF $\alpha$  treatment (P=0.563) (Figure 4.11).

Response to UDP-glucose is higher in neonatal cortical astrocyte with 38% of cells respond to UDP-glucose after forskolin treatment, while only 17% of cells response in the case of embryonic cortical (Figure 4.12). In addition, treating neonatal cortical astrocytes with LPS increase the percentage of cells response to 28%, which is higher than embryonic cortical with only 21% of cells response. However, the percentage of cells responding to UDP-glucose after TNF $\alpha$  treatment is more in embryonic with 26% than neonatal cortical astrocyte with 16%. Due to high variation between cells, no significant differences were detected (forskolin P=0.089, LPS P=0.554 and TNF $\alpha$  P=0.562) (Figure 4.12).

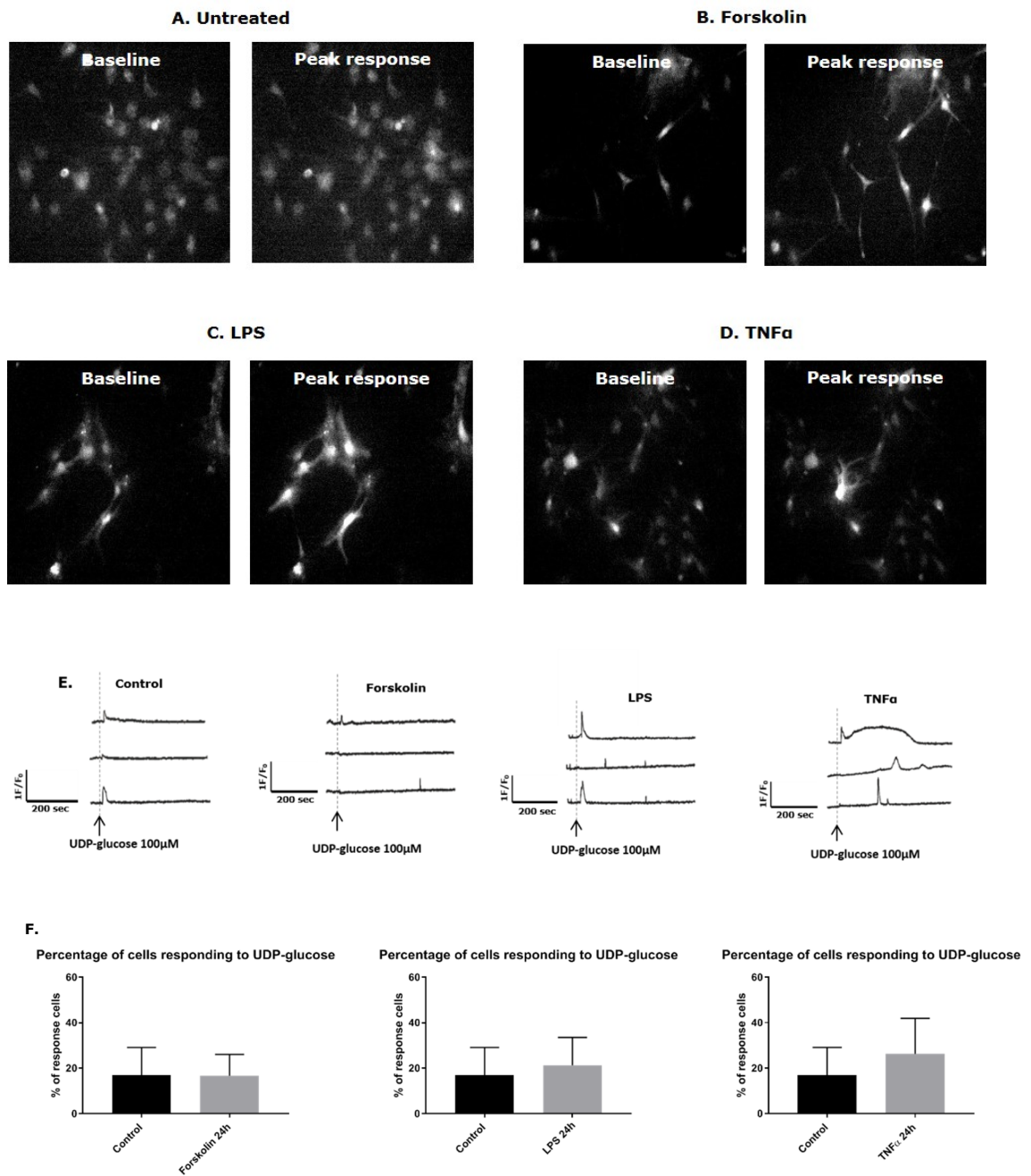
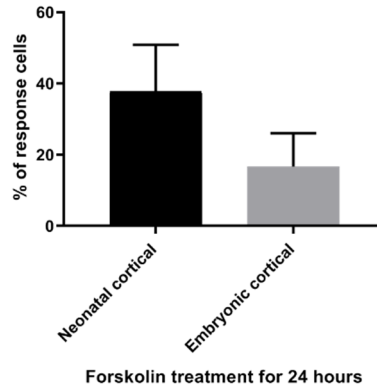
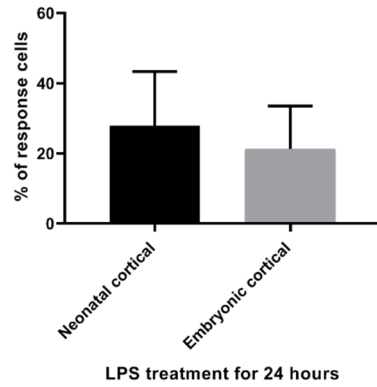


**Figure 4.11 Ca<sup>2+</sup> response of embryonic cortical astrocytes by adding UDP-glucose.** A) Two images show Fluo-5F fluorescence intensity at the baseline and after 9 minutes of adding UDP-glucose in untreated cells. B) Two images show Fluo-5F fluorescence intensity at the baseline and after 3 minutes of adding UDP-glucose in cells treated with forskolin. C) Two images show Fluo-5F fluorescence intensity at the baseline and after 3 minutes of adding UDP-glucose in cells treated with LPS. D) Two images show Fluo-5F fluorescence intensity at the baseline and after 2 minutes of adding UDP-glucose in cells treated with TNF $\alpha$ . E) Representative traces of Fluo-5F fluorescence intensity for three individual cells in each group. F) Aggregate data above represent the percentage of cells responding in the control (n = 194) and the test groups (forskolin: n = 130, LPS: n = 111 and TNF $\alpha$ : n = 150). Data are presented as a mean  $\pm$  standard error (SEM). No statistically significant differences were determined using the Mann-Whitney test. The experiment was repeated three times.

Compare the percentage of cells responding to UDP-glucose between neonatal and embryonic cortical astrocytes



Compare the percentage of cells responding to UDP-glucose between neonatal and embryonic cortical astrocytes



Compare the percentage of cells responding to UDP-glucose between neonatal and embryonic cortical astrocytes

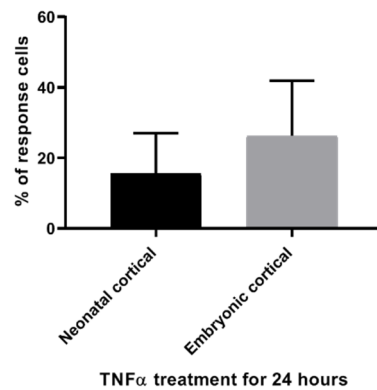


**Figure 4.12**  $\text{Ca}^{2+}$  response of neonatal and embryonic cortical astrocytes by adding **UDP-glucose** after treating the cells with Forskolin, LPS and  $\text{TNF}\alpha$  for 24 hours. Data are presented as a mean  $\pm$  standard error (SEM). No statistically significant differences were determined using the Mann-Whitney test.

There is a clear difference between cortical and spinal astrocytes or neonatal cortical and embryonic cortical astrocytes in their responses. In the following section, we try to test the main reasons for these differences. We hypothesise that either they generate less cAMP in response to the stimuli, or the ability of cAMP to trigger stellation is changed according to age and regions. The way to do this is measuring the stellation assays in the presence of cAMP analog in all different classes of astrocytes and quantify the level of cAMP.

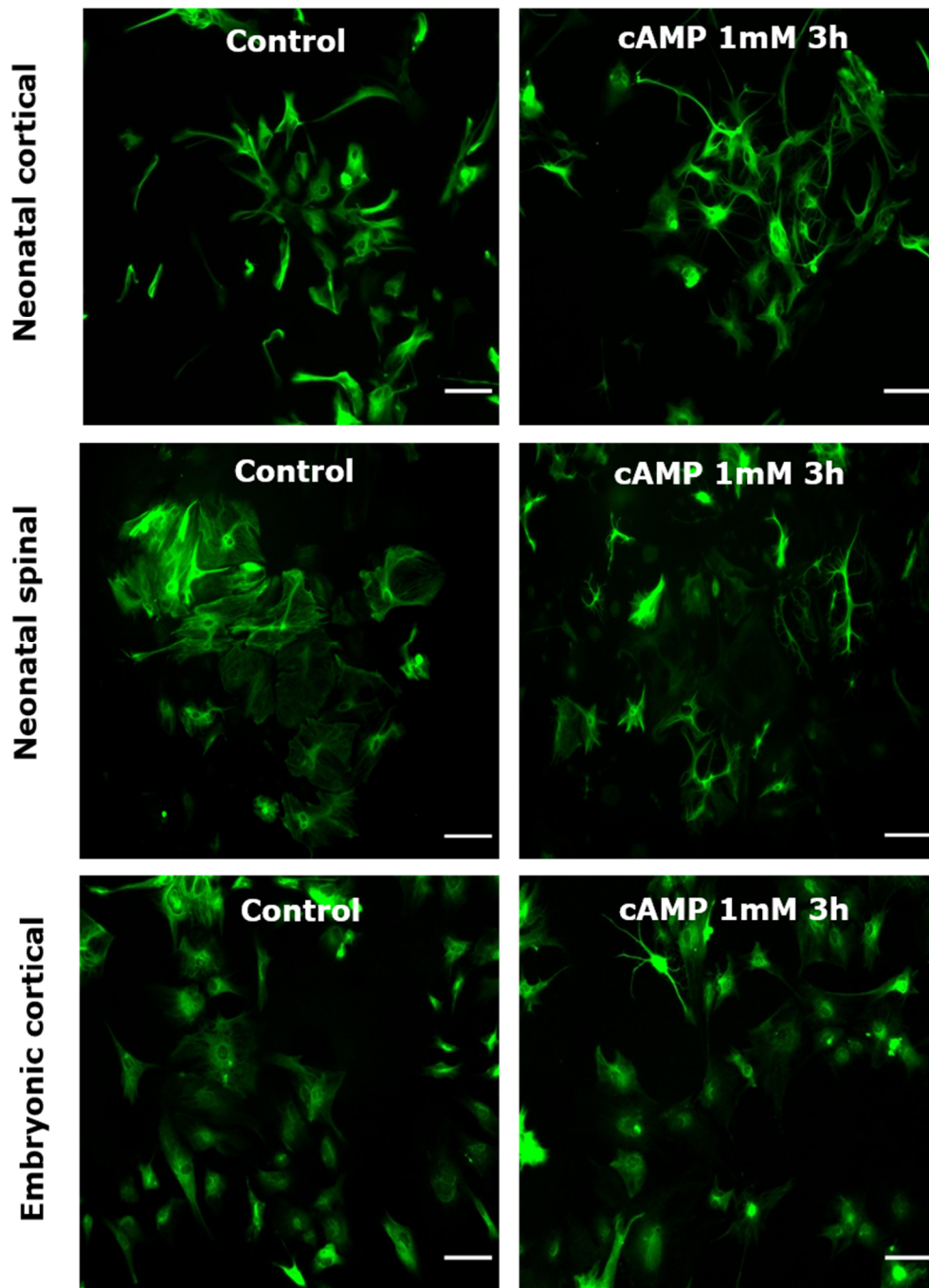
#### **4.2.3 Cyclic AMP involvement in stellation difference according to site and age**

**4.2.3.1** Assess the stellation with GFAP immunocytochemistry in response to a cAMP analog

To test the hypothesis, stellation was measured in response to a cAMP analog, dibutyryl-cAMP sodium salt for 3 hours in all different groups of astrocytes. This treatment would not depend on expression levels of receptors or adenylyl cyclase, and should directly activate downstream effectors.

Addition of the analog cause significant increased the number of stellate cells in cortical astrocytes compared with control, reaching 50% of the cell population ( $P < 0.001$ ) (Figure 4.13). In the case of spinal astrocytes, there is also a significant increase in the percentage of the stellate cell compared with the control, which equals 26% ( $P < 0.001$ ) (Figure 4.13). In contrast, after treating embryonic cortical astrocyte with cAMP analog for 3 hours, only 6% of cells became stellate ( $P = 0.007$ ) (Figure 4.13).

Comparing cortical with spinal astrocyte, it was found that cortical astrocytes are significantly more likely to be stellate than spinal astrocytes ( $P < 0.001$ ) (Figure 4.14). Moreover, there is a significant difference in the percentage of stellate cells between neonatal cortical (50%) and embryonic cortical (6%;  $P < 0.001$ ) (Figure 4.14).



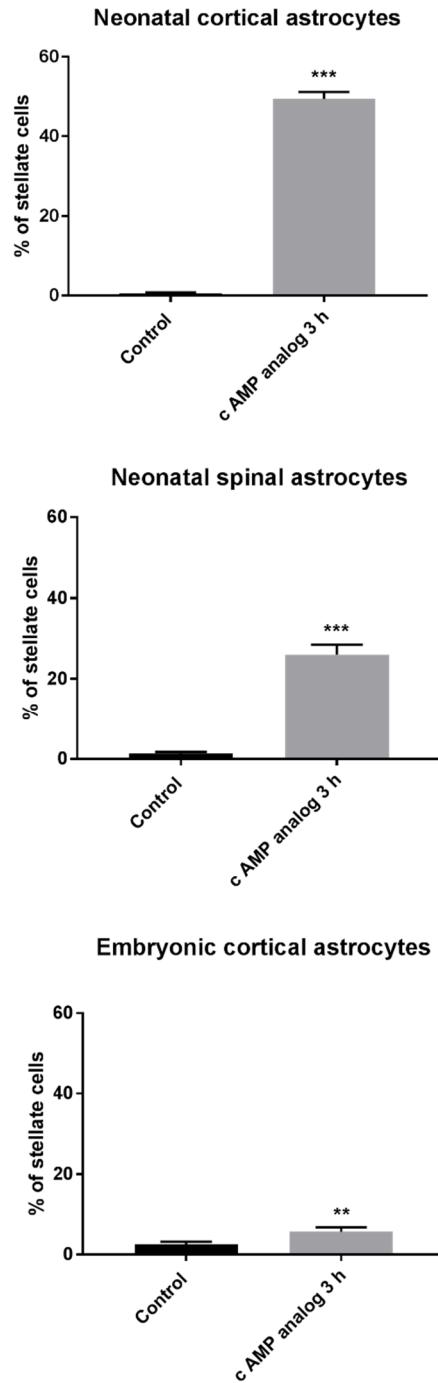
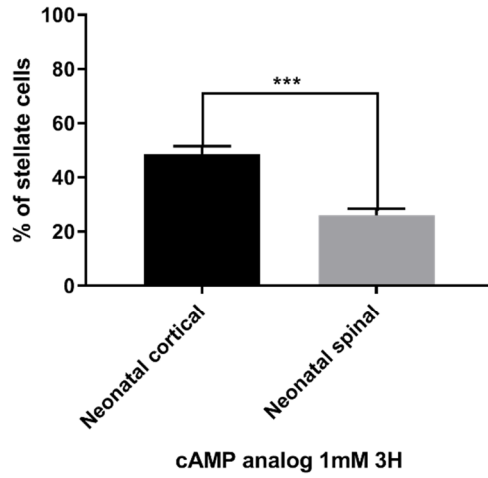


**Figure 4.13 Stellation assay on neonatal cortical, neonatal spinal and embryonic cortical astrocytes.** Images: staining with GFAP after treatment with cAMP analog for 3 hours. Scale bar=50µm. Aggregate data represent the percentage of stellate cells. Data are presented as a mean ± SEM obtained from three different experiments. The statistical significance was determined using the Mann-Whitney test, where (\*\*p<0.01 and \*\*\* P < 0.001) was considered statistically significant.

**Comparison between neonatal cortical and spinal astrocytes in stellation**



**Comparison between neonatal and embryonic cortical astrocytes in stellation**

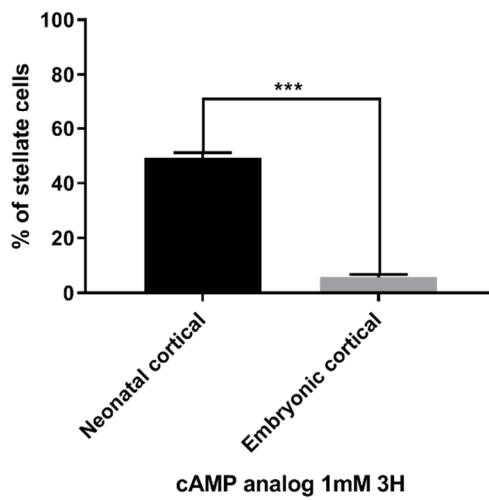


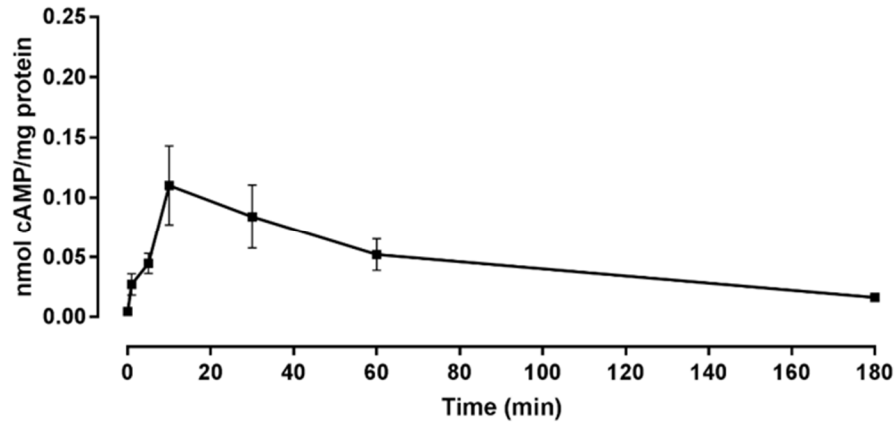
**Figure 4.14 Comparison between neonatal cortical and spinal or embryonic cortical astrocytes in stellation**, after treatment with cAMP analog for 3 hours. Aggregate data represent the percentage of stellate cells. Data are presented as a mean  $\pm$  SEM. The statistical significance was determined using the Mann-Whitney test, where (\*\*\*)  $P < 0.001$  was considered statistically significant.

#### **4.2.3.2** Measuring cAMP accumulation

##### **4.2.3.2.1** *Optimising the cAMP level measurement in neonatal cortical astrocytes*

We next tested how much cAMP level was generated in each cell class after stimulation with forskolin and noradrenaline. In the beginning, a preliminary experiment was done to determine the time course of cAMP accumulation in response to forskolin and noradrenaline in neonatal cortical astrocytes. The results show that forskolin and noradrenaline produced maximum cAMP concentration after 10 minutes incubation with 0.11 nmol/mg protein in case of forskolin and 0.190 nmol/mg protein after noradrenaline incubation (Figure 4.15).

Time course of cAMP response to forskolin in neonatal cortical astrocytes



Time course of cAMP response to noradrenaline in neonatal cortical astrocytes

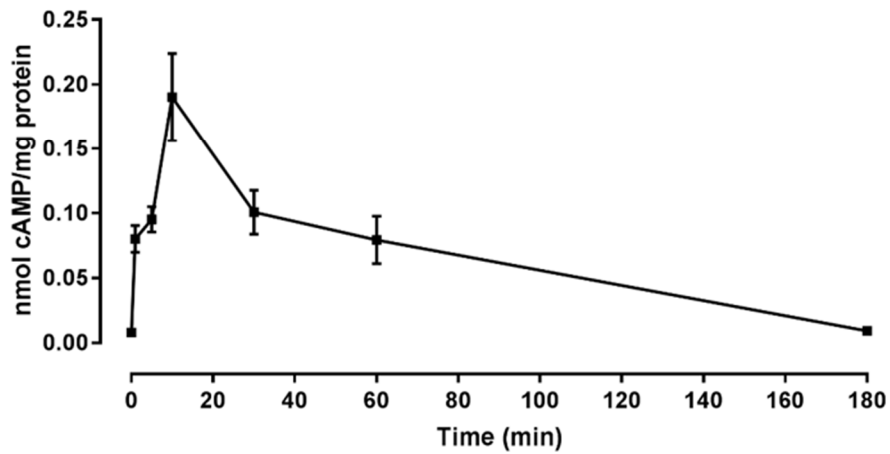


**Figure 4.15 Time course of cAMP response to forskolin and noradrenaline in astrocytes.** Cells were treated by addition of forskolin and noradrenaline (both 10 $\mu$ M) at time = 0. The data was shown mean $\pm$ SEM values from 6 individual experiments.

#### **4.2.3.2.2** *cAMP level measurement in all groups*

The cAMP concentration at 10 minutes was measured in all neonatal cortical, spinal and embryonic cortical astrocytes after forskolin and noradrenaline treatment. In the case of neonatal cortical astrocytes, there is an increase of cAMP level in both treated groups compared with control (Figure 4.16). The mean of the cAMP level after forskolin incubation was  $0.1 \pm 0.02$  nmol/mg protein. Moreover, noradrenaline increases the cAMP level to  $0.173 \pm 0.02$  nmol/mg protein.

In the case of spinal astrocytes, cAMP concentration is also higher after forskolin treatment and noradrenaline incubation (Figure 4.16). Comparing cAMP accumulation between neonatal cortical and spinal astrocytes, it was found that the neonatal cortical astrocytes were significantly higher than spinal astrocytes in response to both forskolin ( $P=0.009$ ) and noradrenaline ( $P=0.0004$ ) (Figure 4.17).

Finally, cAMP concentration was measured in embryonic cortical astrocytes. The result demonstrated that a little increase was discovered after forskolin ( $0.018 \pm 0.006$ ) treatment compared with control ( $0.001 \pm 0.0002$ ). However, noradrenaline can increase the level of cAMP to  $0.81 \pm 0.02$  (Figure 4.16). Comparing the age difference of the cAMP level; it was discovered that the neonatal astrocyte produced cAMP more than embryonic in case of both forskolin ( $P=0.001$ ) and noradrenaline ( $P=0.008$ ) (Figure 4.17).

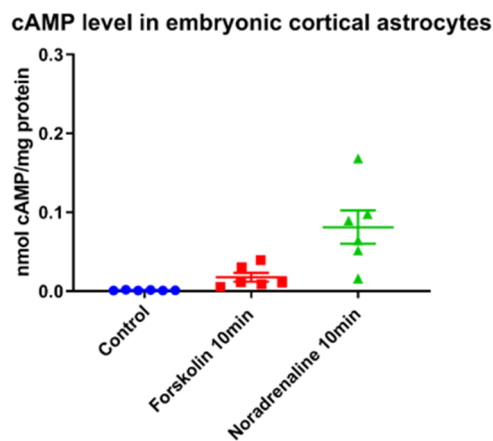
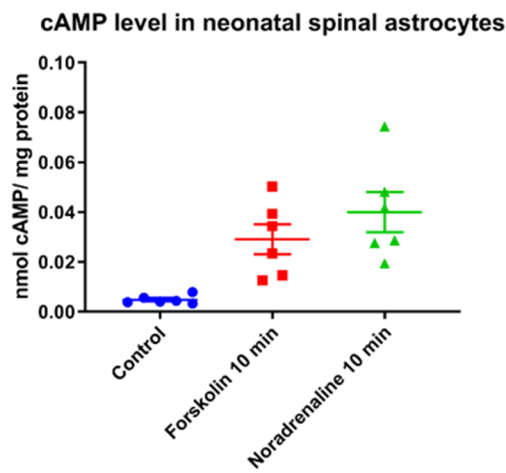
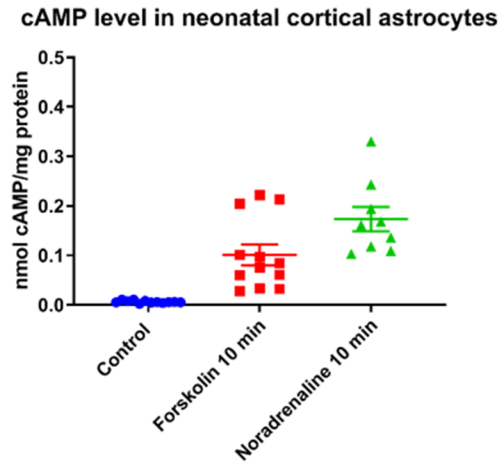
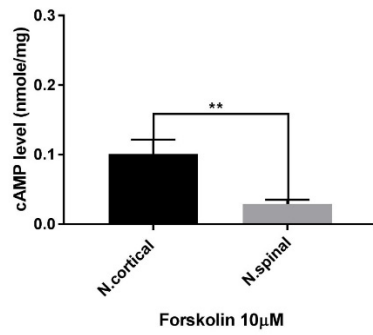
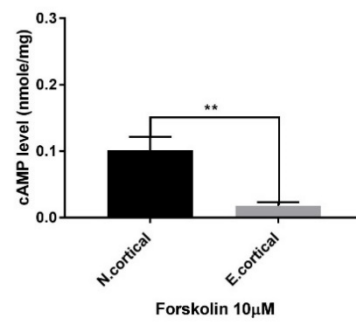


**Figure 4.16 Effect of forskolin and noradrenaline 10 $\mu$ M on the cAMP accumulation in neonatal cortical, spinal and embryonic cortical astrocytes.** Cells were pre-treated with drugs for 10 minutes. At the end of the incubation period, the assay was started by the addition of lysis buffer and the relative levels of cAMP determined using the Hit-Hunter assay kit. The data shown represent mean  $\pm$  SEM values from 6 individual experiments in each condition except for neonatal cortical the data obtained from 12 individual experiments in case of forskolin and 9 individual experiments in case of noradrenaline.

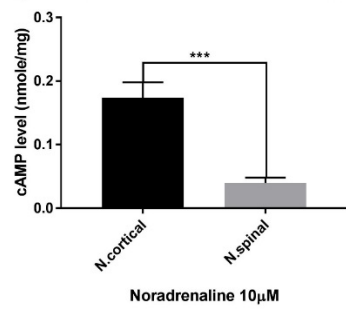
Compare cAMP level after Forskolin treatment



Compare cAMP level after Forskolin treatment



Compare cAMP level after noradrenaline treatment



Compare cAMP level after noradrenaline treatment

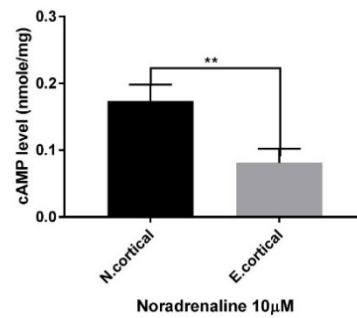


**Figure 4.17 Comparison of cAMP concentration between neonatal cortical and spinal astrocytes or between neonatal and embryonic cortical astrocytes.** Cells were pre-treated with forskolin and noradrenaline for 10 minutes. The data shown represent mean  $\pm$  SEM values. The statistical significance was determined using the Mann-Whitney test, where (\*\* $P < 0.01$  and \*\*\*  $P < 0.001$ ) was considered statistically significant.

### 4.3 Discussion

Astrocytes are heterogeneous cells and assays of reactive gliosis appear to be challenging to assess due to the considerable variation in responses seen even within control populations. Nevertheless, in this chapter, the data presents a significant change of reactive astrocytes morphology and function during development and between cortex and spinal cord.

We were used a combination of  $\text{Ca}^{2+}$  imaging, immunocytochemistry and cAMP assay. Stellation showed significant differences between CNS region (cortical versus spinal) and at the development stage (embryonic versus postnatal). This was most obvious with forskolin and Camp analog treatment. LPS and TNF $\alpha$  generally only caused low levels of stellation in all cases. For  $\text{Ca}^{2+}$  responses, there were not many obvious trends. Again, there was variation between CNS region and developmental stage, but none of the gliosis-evoking stimuli consistently altered the response to UDP-glucose.

It is important to assess the difference between embryonic and postnatal astrocytes according to their morphology and function to understand how reactive gliosis may vary with age and brain region. Regarding the morphological change: two assays were used to test astrocytes stellation. It is possible to obtain an elaborate spike shape to occur in the commonly-used neonatal cortical astrocyte model (Lin et al., 2008; Barres, Chun and Corey, 1989). However, it was found that the stellation was much less pronounced with the spinal cord and the cortical embryonic cultures.

The measuring circularity of individual cells did not show any difference in stellation between neonatal cortical and spinal after forskolin treatment. But this could be attributed to the smaller number of cells that were assayed and the variance within the population, meaning only a fraction of cells displayed prominent stellation reactions. While this assay is useful for recording morphology

changes in real-time for a single cell, it is less helpful in detecting population-level changes.

cAMP signalling pathway regulates many functions in normal or reactive astrocyte by trigger glycogenolysis-related energy supply, regulate homeostasis and regulates cytokine and inflammatory factor release (Zhou, Ikegaya and Koyama, 2019). Moreover, cAMP has been shown to induce stellation and reactive gliosis (Daginakatte et al., 2008; Fedoroff et al., 1984; Masaki et al., 2000; Tiryaki, Ayres, et al., 2015). Here this study shows the ability of cells to stellate after cAMP analog treatment was different (bypassing receptors and adenylyl cyclase) related to age and region heterogeneity. Cyclic AMP analog produced high cells stellation with neonatal cortical, but it's lower in neonatal spinal and embryonic cortical. These findings are comparable with Won and Oh (2000) study. They tested possible of neonatal brain astrocyte regional heterogeneity in morphological changes in response to cAMP stimulation in vitro. They found that hypothalamic astrocytes are less stellate than other cells types. These indicate that astrocytes derived from different regions produce different levels of stellation in response to cAMP. Thus, regional and age-related heterogeneity of astrocyte stellation may be linked to the differential expression level of cytoskeletal and cytoskeletal protein-modifying protein, or each cell type has a different sensitivity to cAMP. In addition, in the current study, it was found that the level of cAMP is regional and developmentally different after forskolin and noradrenaline treatment. Cyclic AMP concentration was higher in neonatal cortical than others. These change of cAMP levels are correlated with the different of astrocyte stellation outcomes and suggesting that spinal and embryonic cells were both less able to generate cAMP and less sensitive to it.

However, Abe and Saito (1997) demonstrate that the difference between E18 and P2 astrocytes stellation after  $\beta$ -adrenoceptor stimulation is not related to cAMP level. They found that cAMP production was similar in E18 and P2 and only the

cAMP sensitivity controlling different of E18 and P2 astrocytes. Taken together, these implying that astrocyte reactivity and maturation increase after birth.

Variance in reactive astrocytes morphology has also been detected in a different brain region in vivo and vitro (Hill, Barbarese and McIntosh, 1996; Tsai et al., 2014; Zhang and Barres, 2010) and during development (Testen et al., 2019). Wanner et al. (2013) demonstrate that spinal cord injury leads to activation of astrocytes into two broad categories which there are differences in structure. The heterogeneity of astrocytes morphology in vivo it may due to the environment surrounding the astrocyte, status of neurons, neuronal subtypes and properties (Hill, Barbarese and McIntosh, 1996; Ben Haim and Rowitch, 2016) and a distance of astrocytes from the site of injury (O'Callaghan et al., 2014). However, this study discovered that different cAMP production and sensitivity of the cells to cAMP are consistency with the astrocytes induces stellation in vitro.

Moving to the function assay, intracellular  $Ca^{2+}$  signalling is an essential aspect of astrocyte function. Activating the neonatal cortical astrocytes by a combination of inflammatory stimuli significantly modulates astrocytes calcium signalling by up-regulation of the *P2y14* gene, which is one of the GPCR genes found in reactive astrocytes (Hamby et al., 2012). In the previous chapter, there is some evidence demonstrating that this assay is useful. However, testing for the up-regulation of this receptor in a different type of astrocytes after forskolin, LPS and TNF $\alpha$  incubation separately, demonstrated a slightly higher level of expression in the neonatal cortical astrocytes compared with spinal and embryonic brain astrocytes, but no significant difference was detected. However, increased responses to UDP-glucose after treatment with forskolin, LPS, and TNF $\alpha$  were not consistently observed in our experiments, in contrast to the results of Hamby et al. (2012). This experiment was shown less reliability and did not identify the pattern that recognises the change in different regions and during development. Clearly, it is not a useful general assay for reactive gliosis.

The origin of astrocytes heterogeneity might be due to the variation of glial progenitor cells that produce astrocytes (Ge et al., 2012). Spinal cord astrocytes but not cortical could originate from Oligo progenitors, that lead to providing specific subpopulations in the spinal cord astrocyte (Oberheim, Goldman and Nedergaard, 2012). The extrinsic signals, such as Shh and BMPs, have the ability to form different progenitor domains (Bayraktar et al., 2015; Rowitch and Kriegstein, 2010). These domains produce different astrocyte progenitors that give different astrocytes subtypes which express different transcription factor and gene expression that led to astrocyte diversity (Ben Haim and Rowitch, 2016; Chaboub and Deneen, 2012; Rowitch and Kriegstein, 2010).

Involving a cAMP signalling pathway in reactive gliosis is controversial. Paco et al. (2016) discovered that genes that responsible for astrocytes activation, such as cytoskeletal rearrangement, scar components and immunological mediators, were inhibited by cAMP. cAMP can suppress NF $\kappa$ B activation (Gavrilyuk et al., 2002) by inducing the expression of A20 in cultured astrocytes (Laureys et al., 2014) and decrease A20 can cause gliosis in both astrocytes and microglia (Voet et al., 2018; Guedes et al., 2014). However, treating astrocyte with dibutyryl cAMP (dbcAMP) or any drugs activate cAMP in vitro significantly changed astrocyte morphology, increased GFAP expression (Abe and Misawa, 2003; Dagainakatte et al., 2008; Fang et al., 2012; Vardjan, Kreft and Zorec, 2014) and up-regulated or down-regulated 44 genes that involving in reactive gliosis (Dagainakatte et al., 2008). On the other hand, it was found that treating cells with cAMP analog changed the morphology to reactive cells that do not share many properties of reactive astrocytes in vivo (Wandosell, Bovolenta and Nieto-Sampedro, 1993).

In summary, astrocyte show distinct responses to induce stellation in the early postnatal and embryonic periods from different CNS regions. It was found that cortical astrocytes produce a high number of stellate cells and high cAMP concentration compared with spinal astrocytes. Regarding age-dependent change,

the neonatal stage is more able to induce reactive gliosis than embryonic according to morphology change and increase the level of cAMP. Studying the difference of astrocytes according to different age and region in their morphology and function in response to various stimuli in vitro may let us understand the roles of these cells in normal and pathological conditions in CNS at specific age and site. These differences will need to be taken into account in the design of targeted therapies.

## **Chapter 5 Role p-STAT3 in astrocytes stellation**

## 5.1 Introduction

The signal transducer and activator of transcription 3 (STAT3) is a transcription factor that regulates genes which are involving in cell differentiation, proliferation, development, apoptosis and inflammation (Dimri, Sukanya and De, 2017; Huang et al., 2015; You et al., 2015). STAT3 is activated in response to a wide variety of receptors. Activation of Janus kinases (JAK) with cytokines, hormones or growth receptors and GPCRs (Gas and Gaq) can phosphorylate STAT3 to Tyr705-phospho-STAT3 that translocates into the nucleus, where it activates target genes. Also, tyrosine kinase and cytoplasmic kinases like Src kinase are also involved in tyrosine p-STAT3 activation (Ceyzériat et al., 2016; Dimri, Sukanya and De, 2017; Huang et al., 2015; Lin et al., 2014; New and Wong, 2007; Renault-Mihara and Okano, 2018; You et al., 2015; Yu et al., 2014).

STAT3 can also be phosphorylated at serine 727 (S727) and translocate from cytoplasm to nucleus and mitochondria. The phosphorylation of STAT3 at serine 727 can be activated by MAPKs such as c-JNK, PKC family including PKC $\delta$ , PKC $\epsilon$  (Ceyzériat et al., 2016; Dimri, Sukanya and De, 2017; Hazan-halevy, Harris and Chen, 2010; Huang et al., 2015; You et al., 2015). Washburn and Neary (2006) found that P2Y receptors (GPCR) can activate STAT3 to S727-phospho-STAT3 and Y705-phospho-STAT3 via ERK. Moreover, Rac1 and Rho can produce tyrosine p-STAT3 via JAK activation by GPCRs (Coulombe et al., 2003) and serine p-STAT3 (Debidia et al., 2005). However, Epac leads to accumulation of Rac1, which cause up-regulation of SOCS3 via ERK-dependent pathway, which down-regulates activation of JAK-STAT pathway and inhibit STAT3 activation (Sands et al., 2006). Overall, it is clear that there are lots of mechanisms for STAT3 phosphorylation that are relevant to induce reactive gliosis.

Several lines of evidence on STAT3 has revealed that this protein is essential to induce reactive astrocytes in vivo. Sriram et al. (2004) found that injecting mice with a dopaminergic neurotoxic agent and 1-methyl-4-phenyl-1,2,3,6-

tetrahydropyridine (MPTP), can activate JAK2/STAT3 signalling and induce astrogliosis. In addition, causing cortex lesion in adult rat activated STAT3, which is localised in astrocytes (Xia et al., 2002). Activation of STAT3 in adult mice astrocytes (O'Callaghan et al., 2014) or the postnatal rat astrocytes (Acarin, González and Castellano, 2000) induced by neurotoxic administration in the brain.

Knockout of STAT3 in astrocytes after spinal cord injury can decrease GFAP labelling, failure of astrocyte hypertrophy, prevention of astroglial scar formation and loss of neurons (Herrmann et al., 2009; Kang and Hébert, 2011; Nobuta et al., 2012; Wanner et al., 2013). It also decreased the migration of reactive astrocyte and increased demyelination of neurons (Okada et al., 2006). Moreover, it was found that increase CSPGs like laminin through activating STAT3 after spinal cord injury have a role in axon regeneration (Anderson et al., 2016).

Moreover, inhibition of the JAK/STAT3 pathway in astrocytes leads to decreased levels of mRNA GFAP, reduced microglial activation and increased the number of a neuropathological hallmark in two transgenic mouse models of Alzheimer's disease (Ben Haim et al., 2015b). STAT3 in reactive astrocytes regulates the expression of TSP1, which is responsible for the recovery of excitatory synapses onto axotomised motor neurons in vivo (Tyzack et al., 2014). It also has beneficial roles in neuronal survival and plasticity during astrogliosis in vitro (Hung et al., 2016). However, activation of STAT3 produced astrocyte proliferation and maintained allodynia in rats with peripheral nerve injury (Tsuda et al., 2011). LPS administration activated STAT3 in reactive spinal astrocytes, which up-regulated the expression of inflammatory chemokines, including CX3CL1, CXCL5, CXCL10 and CCL20 that contributed to pain modulation (Liu et al., 2013). In summary, STAT3 has been recognised as playing a central role in the induction of reactive gliosis in a wide variety of brain regions and pathological conditions.

**Aim**

STAT3 activation is a master regulator of reactive gliosis. In chapter 3, we described changes in p-STAT3 levels in the nucleus of astrocytes exposed to forskolin. In this chapter, we investigate whether p-STAT3 has a role in astrocyte stellation.

## **5.2 Results**

### **5.2.1 Effect of p-STAT3 and JAK inhibitors on astrocyte stellation**

#### **5.2.1.1 Neonatal cortical astrocytes**

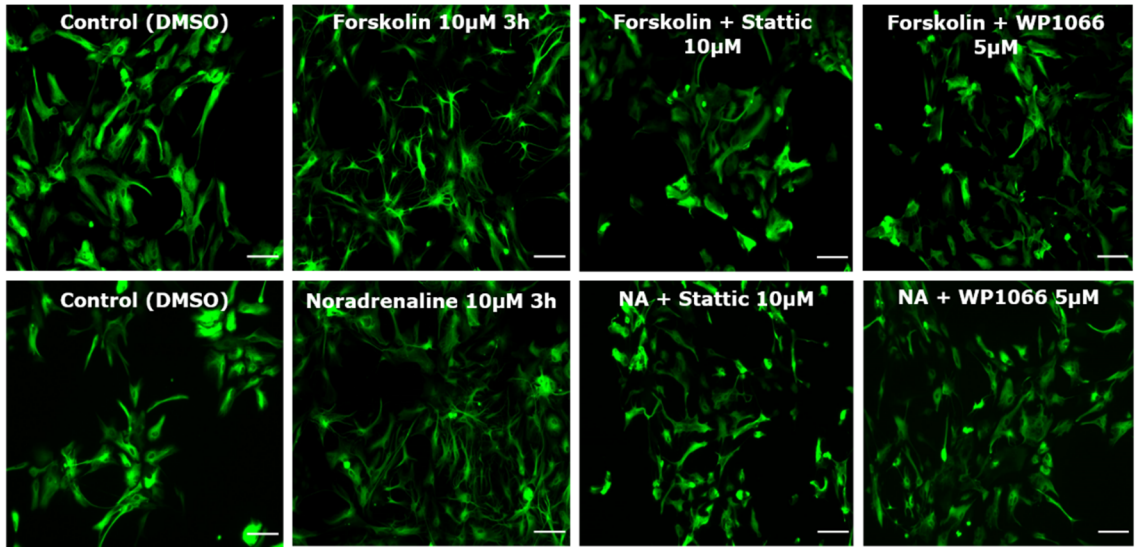
P-STAT3 was inhibited by pre-treating the cells with two types of inhibitors p-STAT3 inhibitor (stattic) and JAK inhibitor (WP1066) for 1 hour before induction of stellation by forskolin or noradrenaline treatment for 3 hours.

As with previous experiments, the results demonstrated a significant increase in the percentage of stellate cells after forskolin treatment to 70% compared with the control, which is just 4% ( $P < 0.001$ ). However, the percentage of the stellate cell is dramatically reduced after treating the cells with stattic (12%,  $P < 0.001$ ) and WP1066 (13%,  $P < 0.001$ ) (Figure 5.1).

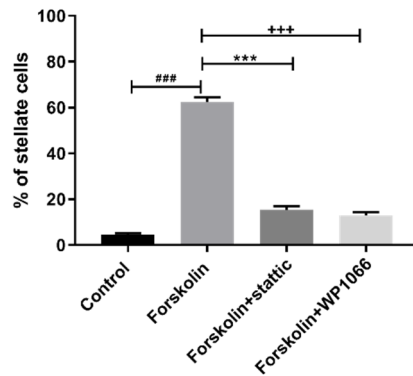
In the case of noradrenaline, there was a significant increase in the percentage of stellate cells to 48%. But the inhibitors significantly decreased the percentage of stellate cells to 14% in the case of stattic ( $P < 0.001$ ) and 27% in the present of WP1066 ( $P < 0.001$ ) (Figure 5.1).

#### **5.2.1.2 Neonatal spinal astrocytes**

The response of stattic was tested in neonatal spinal astrocytes as well. The result showed that forskolin increased the percentage of stellate cells to 23% ( $P = 0.018$ ) compared with the control of 0.8%. Pre-treatment of the cells with stattic before forskolin significantly reduced stellation to 2.4% of stellate cells compared with forskolin alone ( $P = 0.037$ ) (Figure 5.2).



Effect of p-STAT3 and JAK inhibitors in neonatal cortical stellation



Effect of p-STAT3 and JAK inhibitors in neonatal cortical stellation

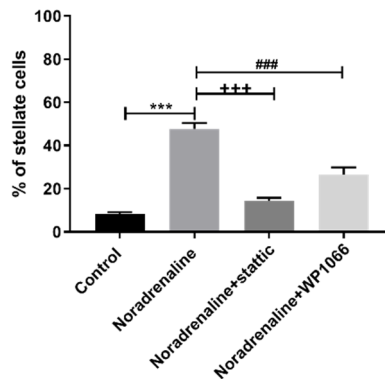
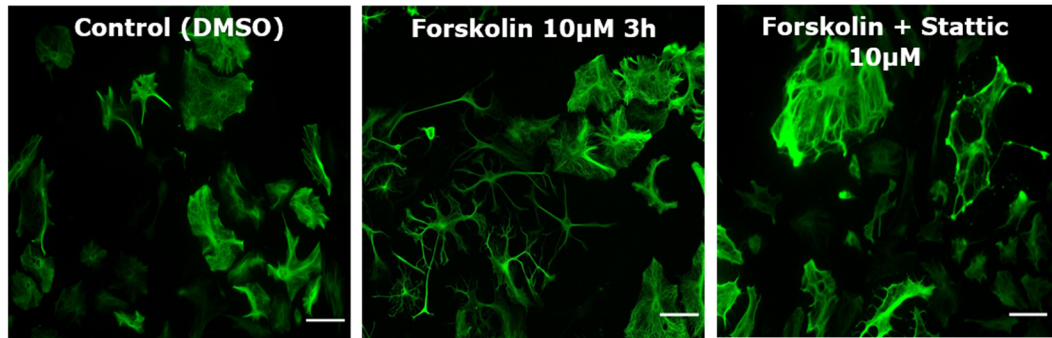


**Figure 5.1 Effect of p-STAT3 and JAK inhibitors on stellation of neonatal cortical astrocytes.** Images: staining with GFAP after treatment with inhibitors (stattic and WP1066) for 1 hour and forskolin and noradrenaline for 3 hours. Scale bar=50µm. Aggregate data represent the percentage of stellate cells. Data are presented as a mean ± SEM obtained from three independent experiments. The statistical significance was determined using the one way ANOVA followed by Tukey's multiple comparisons test, where (\*\*\*) P < 0.001) was considered statistically significant.



**Effect of p-STAT3 inhibitor in neonatal spinal stellation**

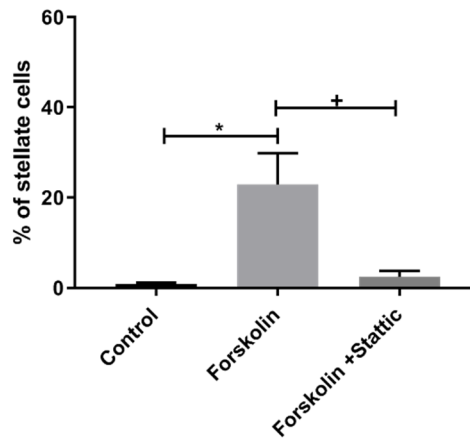


**Figure 5.2 Effect of p-STAT3 inhibitor on stellation of neonatal spinal astrocytes.** Images: staining with GFAP after treatment with stattic for 1 hour and forskolin for 3 hours. Scale bar=50µm. Aggregate data represent the percentage of stellate cells. Data are presented as a mean ± SEM obtained from three independent experiments. The statistical significance was determined using the one way ANOVA followed by Tukey's multiple comparisons test, where (\*  $P < 0.05$ ) was considered statistically significant.

## **5.2.2 Effect of different inhibitors on neonatal cortical astrocyte stellation**

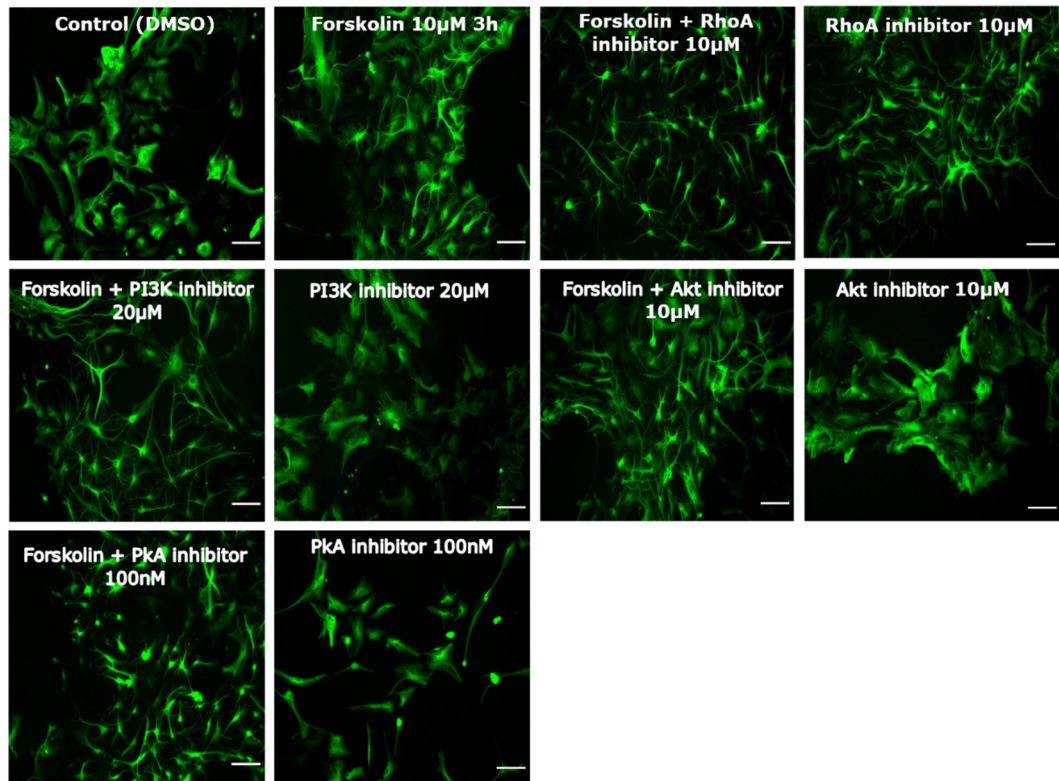
### **5.2.2.1 Kinase inhibitors**

Pharmacological screening of other inhibitors was tested to find the link between signalling pathways known to influence STAT3 activation, and astrocyte stellation. Many kinase inhibitors were assessed, to block putative upstream kinases that may be involved in STAT3 activation during stellation like PKA or known to cause astrocytes stellation like PI3K, Akt and RhoA.

The cells were incubated with RhoA, PI3K, Akt and PKA inhibitors for 1 hour following by 3 hours forskolin treatment or the inhibitors alone. The result discovered that none of them even PKA that affect STAT3 activation did significantly decrease stellation after forskolin treatment. In addition, treat the astrocytes with the inhibitors alone did not induce stellation except for RhoA inhibitor, which can increase the percentage of the stellate cell to 60% ( $P < 0.001$ ) (Figure 5.3).

### **5.2.2.2 Adrenergic receptors blockers**

$\alpha$  and  $\beta$  receptor blockers were added to astrocytes to measure the stellation assay in the presence of noradrenaline. It was demonstrated that propranolol ( $\beta$  blocker) significantly block stellation after noradrenaline treatment to 6% ( $P < 0.001$ ). However, prazosin, which is an  $\alpha$  receptor blocker, did not affect the astrocyte stellation with 45% of stellate cells ( $P = 0.46$ ) (Figure 5.4). This confirms the involvement of  $\beta$  receptor activation of adenylyl cyclase in stellation, in cells stimulated with noradrenaline.



Effect of kinase inhibitors in neonatal cortical stellation

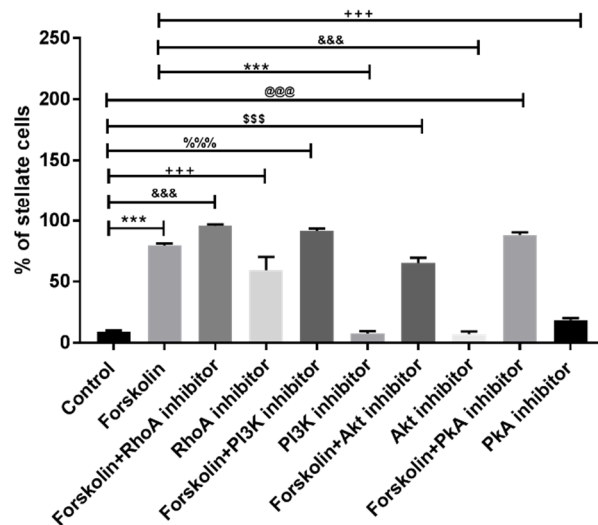
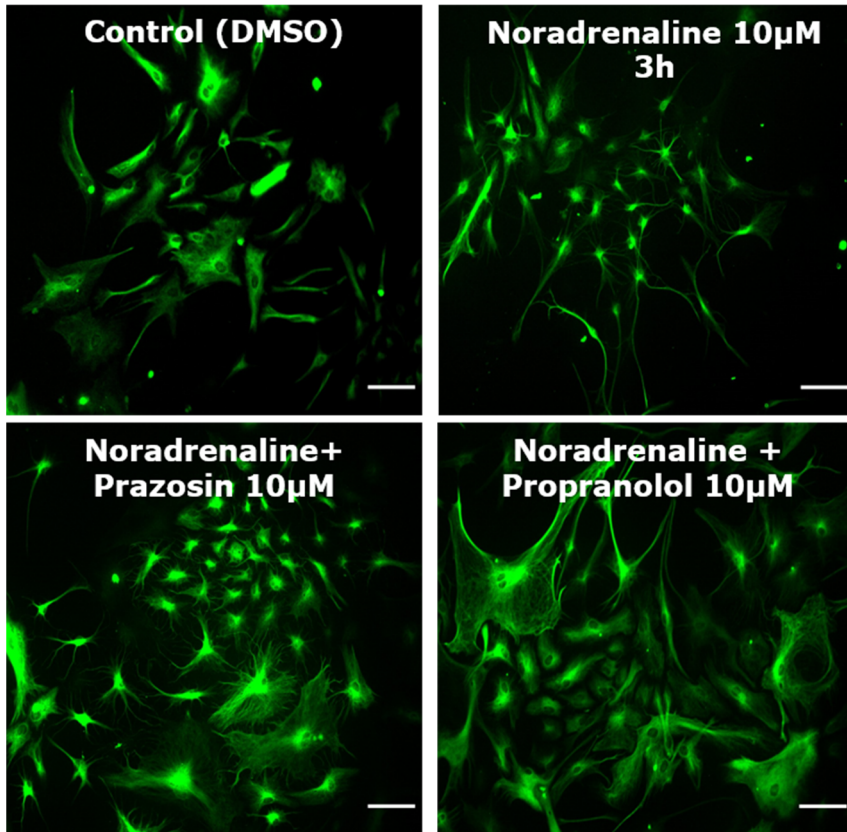


**Figure 5.3 Effect of different kinase inhibitors on the stellation of neonatal cortical astrocytes.** Images: staining with GFAP after treatment with inhibitors (Y27632 dihydrochloride RhoA inhibitor, LY294002 hydrochloride PI3K inhibitor, Akt inhibitor 1/2 and KT5720 PKA inhibitor) for 1 hour and forskolin for 3 hours. Scale bar=50µm. Aggregate data represent the percentage of stellate cells. Data are presented as a mean  $\pm$  SEM obtained from three independent experiments. The statistical significance was determined using the one way ANOVA followed by Tukey's multiple comparisons test, where (\*\*\*) $P < 0.001$  was considered statistically significant.



Effect of  $\alpha$  &  $\beta$  blockers in neonatal cortical astrocytes stellation

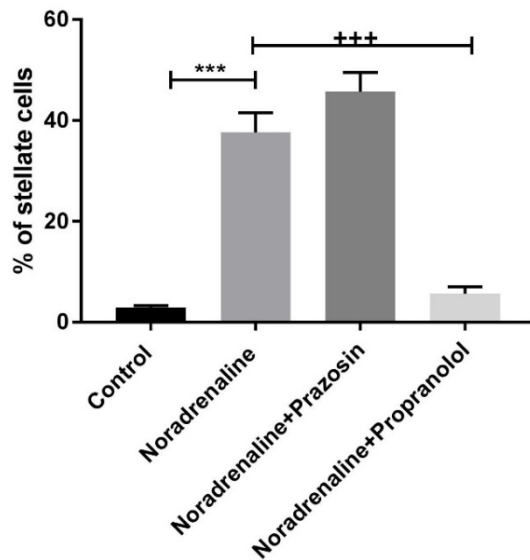


**Figure 5.4 Effect of adrenergic receptor blockers on the stellation of neonatal cortical astrocytes.** Images: staining with GFAP after treatment with inhibitors (prazosin and propranolol) for 1 hour and noradrenaline for 3 hours. Scale bar=50 $\mu$ m. Aggregate data represent the percentage of stellate cells. Data are presented as a mean  $\pm$  SEM obtained from three independent experiments. The statistical significance was determined using the one way ANOVA followed by Tukey's multiple comparisons test, where (\*\*\*) $P < 0.001$  was considered statistically significant.

### **5.2.3 Measuring Ca<sup>2+</sup> release in astrocytes treated with stattic (p-STAT3 inhibitor)**

It is possible that the effects of stattic and WP1066 on stellation are indirect – for example if inhibition of STAT3 compromises cell viability or metabolism. To test the functional state of astrocytes after stattic incubation, Ca<sup>2+</sup> imaging was done to measure the Ca<sup>2+</sup> release with or without stattic in response to ATP and noradrenaline. The result determined that the astrocytes normally respond to Ca<sup>2+</sup> mobilising agonists after stattic incubation for 1 hour. The percentage of cells responding to ATP was 100% in the presence and absence of stattic (P>0.999). In the case of noradrenaline too, no significant difference was detected between noradrenaline alone with 97.8% of cells responding and noradrenaline pre-treated with stattic (97.7%) (P>0.999) (Figure 5.5).

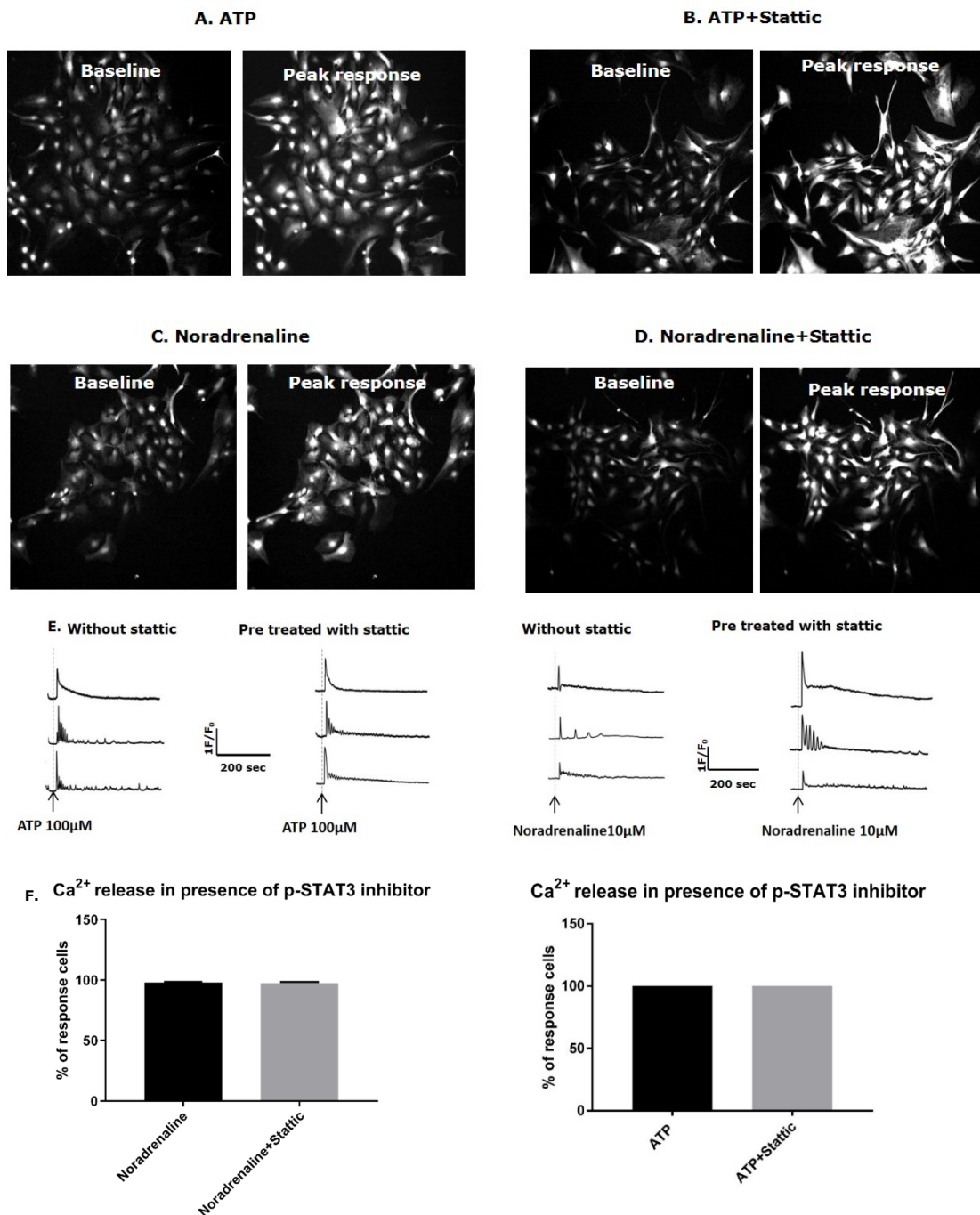


**Figure 5.5 Ca<sup>2+</sup> response of neonatal cortical to ATP and noradrenaline in the presence and absence of static 10 $\mu$ M incubation for 1 hour before imaging.** A) Two images show Fluo-5F fluorescence intensity at the baseline and after 3 minutes of adding ATP in the absence of static. B) Two images show Fluo-5F fluorescence intensity at the baseline and after 3 minutes of adding ATP in the presence of static. C) Two images show Fluo-5F fluorescence intensity at the baseline and after 2 minutes of adding noradrenaline in the absence of static. D) Two images show Fluo-5F fluorescence intensity at the baseline and after 2 minutes of adding noradrenaline in the presence of static. E) Representative traces of Fluo-5F fluorescence intensity for three individual cells in each group. F) Aggregate data above represent the percentage of cells responding in the ATP (n = 348), ATP+static (n=376), noradrenaline (n=275) and noradrenaline+ static (n=323). Data are presented as a mean  $\pm$  standard error (SEM). No statistically significant differences were determined using the Mann-Whitney test.

## **5.2.4 Measuring cAMP accumulation**

### **5.2.4.1 Effect of p-STAT3 and JAK inhibitors in cAMP level**

The cAMP level was measured in response to forskolin and noradrenaline after incubating the cells with stattic and WP1066 for 1 hour. The goal of this experiment is to test if the inhibitors directly affect the level of cAMP.

It was found that forskolin increased the cAMP concentration to  $0.262 \pm 0.038$  nmol/mg compared with untreated cells  $0.005 \pm 0.001$  nmol cAMP/mg protein. Pre-treating the cells with stattic and WP1066 decreased the cAMP level (Figure 5.6). The level of cAMP in presence of stattic was  $0.031 \pm 0.005$  nmol/mg and after WP1066 incubation was  $0.149 \pm 0.039$  nmol/mg.

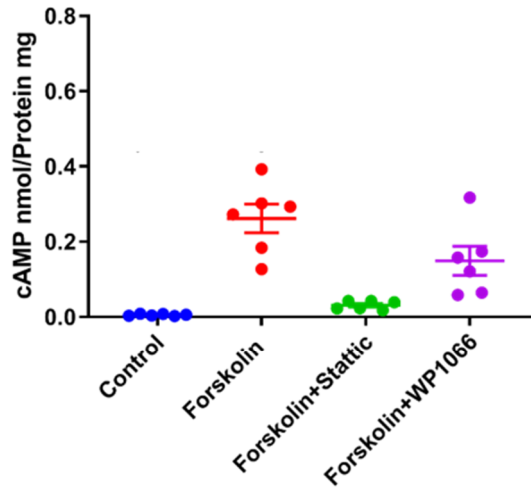
In cell treated with noradrenaline, the level of cAMP was increased to  $0.213 \pm 0.067$  nmol cAMP/mg protein. However, in contrast to the results with forskolin, no significant decrease was identified after p-STAT3 and JAK inhibitors incubation. Stattic slightly decreased the cAMP level with  $0.161 \pm 0.035$  after stattic treatment and with nearly no change in case of WP1066 ( $0.196 \pm 0.035$ ) compared with noradrenaline alone (Figure 5.6).

### **5.2.4.2 Effect of adrenergic receptor blockers in cAMP level**

Because p-STAT3 and JAK inhibitors failed to affect the level of cAMP in response to noradrenaline,  $\alpha$  and  $\beta$  blocker were used to confirm the earlier results on stellation correlated with reduced cAMP levels.

The results demonstrated that propranolol but not prazosin decreased the level of cAMP. The level in the presence of propranolol was  $0.004 \pm 0.0004$ . While the concentration of cAMP after prazosin incubation was  $0.135 \pm 0.021$  compared with noradrenaline ( $0.105 \pm 0.021$ ) (Figure 5.7).

cAMP level in presence of p-STAT3 and JAK inhibitors



cAMP level in presence of p-STAT3 and JAK inhibitors

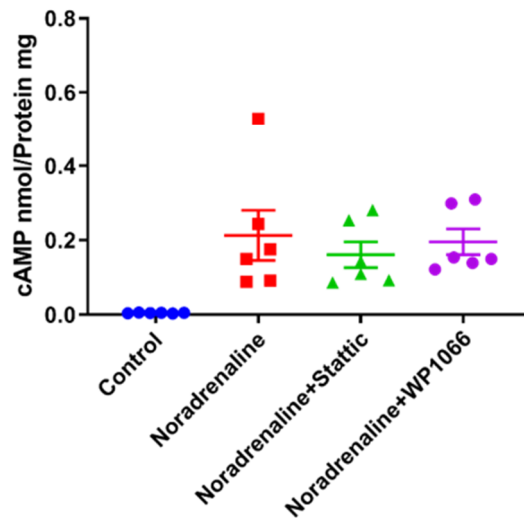


**Figure 5.6 Measuring the level of cAMP of neonatal cortical astrocytes treated with inhibitors for 1 hour and forskolin or noradrenaline for 10 minutes.** Aggregate data represent the level of cAMP normalised to protein in nmol/mg. Data are presented as a mean  $\pm$  SEM values from 6 individual experiments in each condition.

### cAMP level in presence of $\alpha$ and $\beta$ blockers

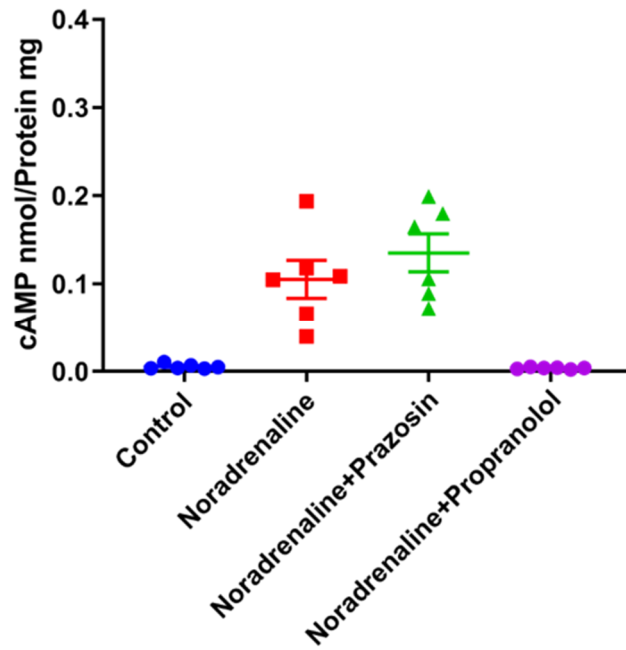
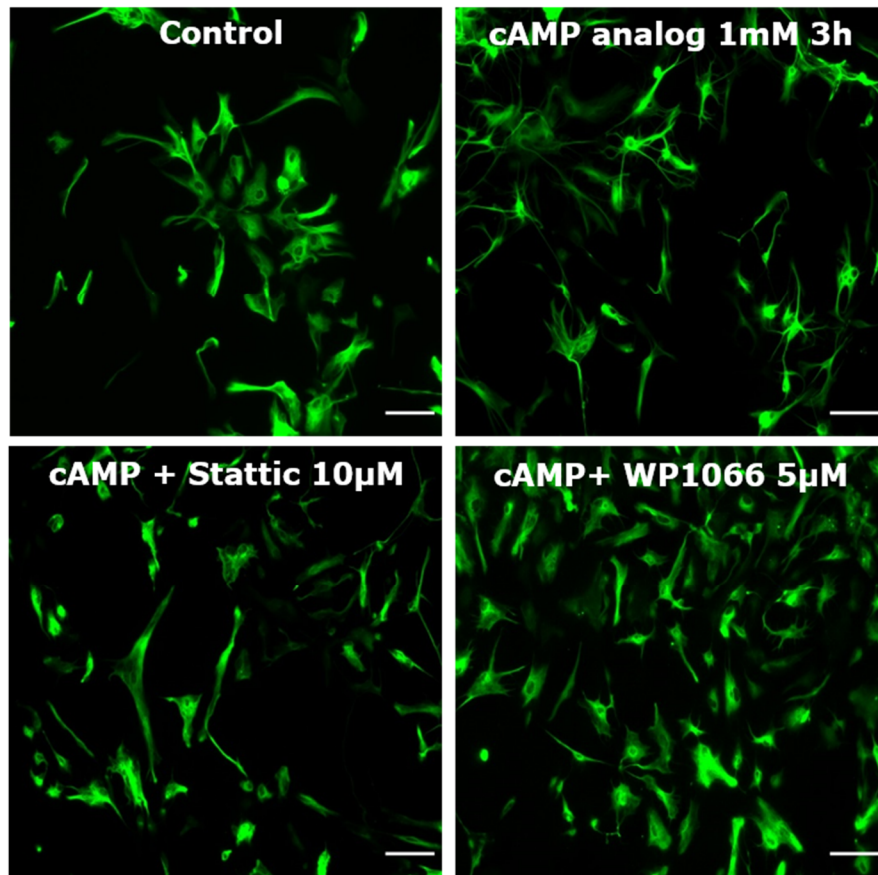


**Figure 5.7 Measuring the level of cAMP of neonatal cortical astrocytes treated with inhibitors for 1 hour and noradrenaline for 10 minutes.** Aggregate data represent the level of cAMP normalised to protein in nmol/mg. Data are presented as a mean  $\pm$  SEM values from 6 individual experiments in each condition.

### **5.2.5 Stellation assay of neonatal cortical astrocytes treated with cAMP analog in the presence of p-STAT3 and JAK inhibitors**

The percentage of stellate cells was calculated after cAMP analog treatment in the presence of p-STAT3 and JAK inhibitors, to test if the presence of cAMP even with the blockers can cause stellation. The results show there was a significant increase in the percentage of stellate cells after dibutyryl-cAMP sodium salt incubation ( $P < 0.001$ ). Pre-treating the cells with inhibitors significantly decreased the percentage of cell stellation. Stattic reduced the percentage to 17% ( $p < 0.001$ ) and 14% of cells became stellate in case of WP1066 ( $P < 0.001$ ) (Figure 5.8).



Effect of p-STAT3 and JAK inhibitors in neonatal cortical stellation

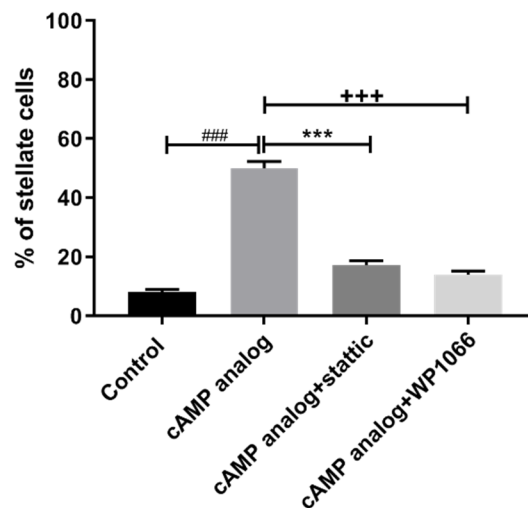


**Figure 5.8 Effect of p-STAT3 and JAK inhibitors on stellation of neonatal cortical astrocytes.** Images: staining with GFAP after treatment with inhibitors for 1 hour and cAMP analog (dibutyryl-cAMP, sodium salt) for 3 hours. Scale bar=50µm. Aggregate data represent the percentage of stellate cells. Data are presented as a mean  $\pm$  SEM obtained from three independent experiments. The statistical significance was determined using the one way ANOVA followed by Tukey's multiple comparisons test, where (\*\*\*)  $P < 0.001$  was considered statistically significant.

## **5.2.6 Effect of IL-6 in astrocytes stellation**

### **5.2.6.1 Neonatal cortical astrocytes**

We next tested whether known upstream stimuli for activating STAT3 phosphorylation would themselves trigger cell stellation. IL-6 is a cytokine responsible for phosphorylating STAT3 via JAK kinase (Tanabe, Kozawa and Iida, 2016). The cells were treated with IL-6 over different time intervals. The result showed no significant increase in the percentage of stellate cells at any time ( $P=0.05$ ). The mean percentage of control was 0.7%, 3 hours was 1%, 8 hours was 2%, 18 hours was 1.9% and 24 hours was 2.3% (Figure 5.9).

### **5.2.6.2 Neonatal spinal astrocytes**

Similar treatment of neonatal spinal astrocytes with IL-6 also failed to induce stellation for different intervals time ( $P=0.514$ ). 3% of untreated cells became stellate, while 4% after 3 hours, 5% after 8 hours, 3.6% after 18 hours and 5% after 24 hours incubation of IL-6 (Figure 5.10).

### **5.2.6.3 Embryonic cortical astrocytes**

Finally, to test the effect of IL-6 in induce stellation on embryonic cortical astrocytes, the cells were treated for IL-6 the same as neonatal cortical and spinal astrocytes. It was discovered that no significant increase was detected in the number of stellate cells ( $P=0.305$ ) with only 2.6% of control cells, 3.5% in case of 3 hours IL-6 treatment, 2.8% after 8 hours then it was increased to 5% after 18 hours and dropped off again to 3.8% after 24 hours incubation (Figure 5.11).

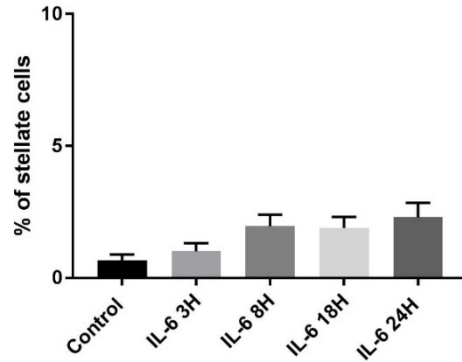
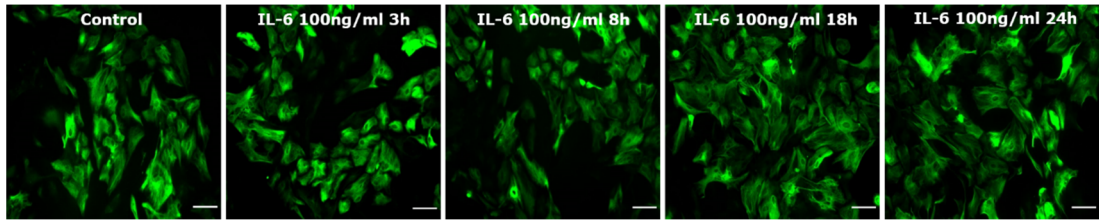


**Figure 5.9 Stellation assay of neonatal cortical astrocytes.** Images: staining with GFAP after treatment with IL-6 for different intervals time. Scale bar=50µm. Aggregate data represent the percentage of stellate cells. Data are presented as a mean  $\pm$  SEM obtained from three independent experiments. No statistically significant differences were determined using the one way ANOVA followed by Dunnett's multiple comparisons test.

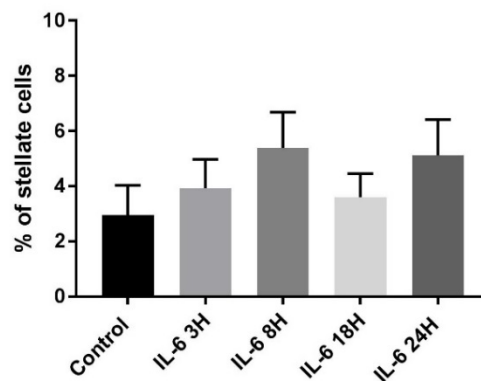
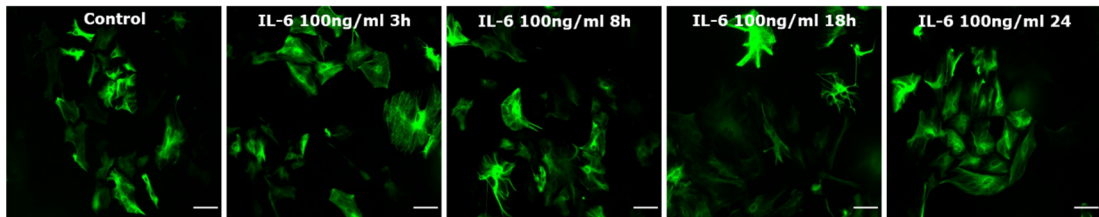


**Figure 5.10 Stellation assay of neonatal spinal astrocytes.** Images: staining with GFAP after treatment with IL-6 for different intervals time. Scale bar=50µm. Aggregate data represent the percentage of stellate cells. Data are presented as a mean  $\pm$  SEM obtained from three independent experiments. No statistically significant differences were determined using the one way ANOVA followed by Dunnett's multiple comparisons test.

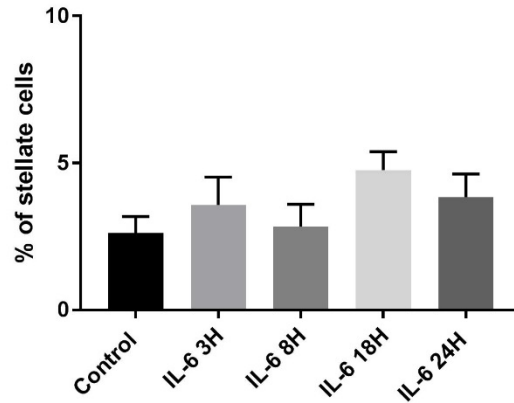
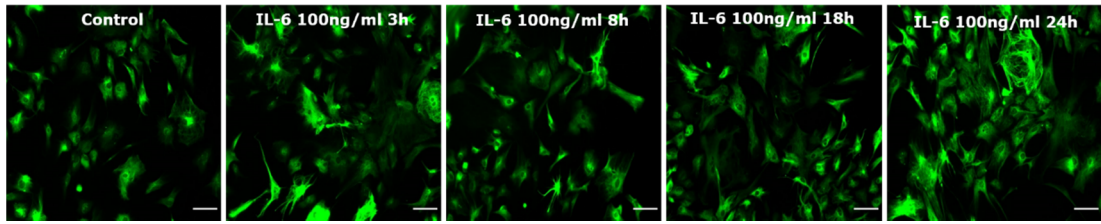


**Figure 5.11 Stellation assay of embryonic cortical astrocytes.** Images: staining with GFAP after treatment with IL-6 for different intervals time. Scale bar=50 $\mu$ m. Aggregate data represent the percentage of stellate cells. Data are presented as a mean  $\pm$  SEM obtained from three independent experiments. No statistically significant differences were determined using the one way ANOVA followed by Dunnett's multiple comparisons test.

## **5.2.7 Measuring intensity of p-STAT3 in the nucleus with confocal microscopy**

### **5.2.7.1 Neonatal spinal astrocytes**

The intensity of serine (S727) and tyrosine (Y705) p-STAT3 in spinal astrocytes nuclei was measured. Cells were treated with forskolin, LPS, and TNF $\alpha$  for 3 and 24 hours. Cells were stained with GFAP and different p-STAT3 antibodies. It was found that there was no significant increase in serine p-STAT3 intensity after treating astrocytes with forskolin for 3 hours and 24 hours (Figure 5.12). However, the intensity of S727 p-STAT3 was significantly increased after 24 hours of LPS treatment ( $P=0.005$ ) but not after 3 hours ( $P=0.067$ ) (Figure 5.13). In addition, treating astrocytes with TNF $\alpha$  for 24 hours increased the nucleus intensity ( $P=0.0001$ ), but not for 3 hours of treatment ( $P=0.37$ ) (Figure 5.14). Regarding Y705 p-STAT3, none of the treatments increased the intensity in nucleus (forskolin 3 hours  $P= 0.09$  and 24 hours  $P= 0.569$ ) (Figure 5.15), (LPS 3 hours  $P= 0.939$  and 24 hours  $P= 0.995$ ) (Figure 5.16), and (TNF $\alpha$  3hours  $P= 0.241$  and 24 hours  $P= 0.351$ ) (Figure 5.17).

Overall, the changes in nuclear intensity were small and variable, suggesting that neither of the treatments tested had a major impact on STAT3 translocation.

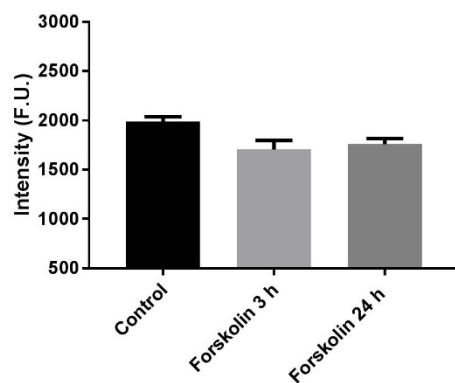
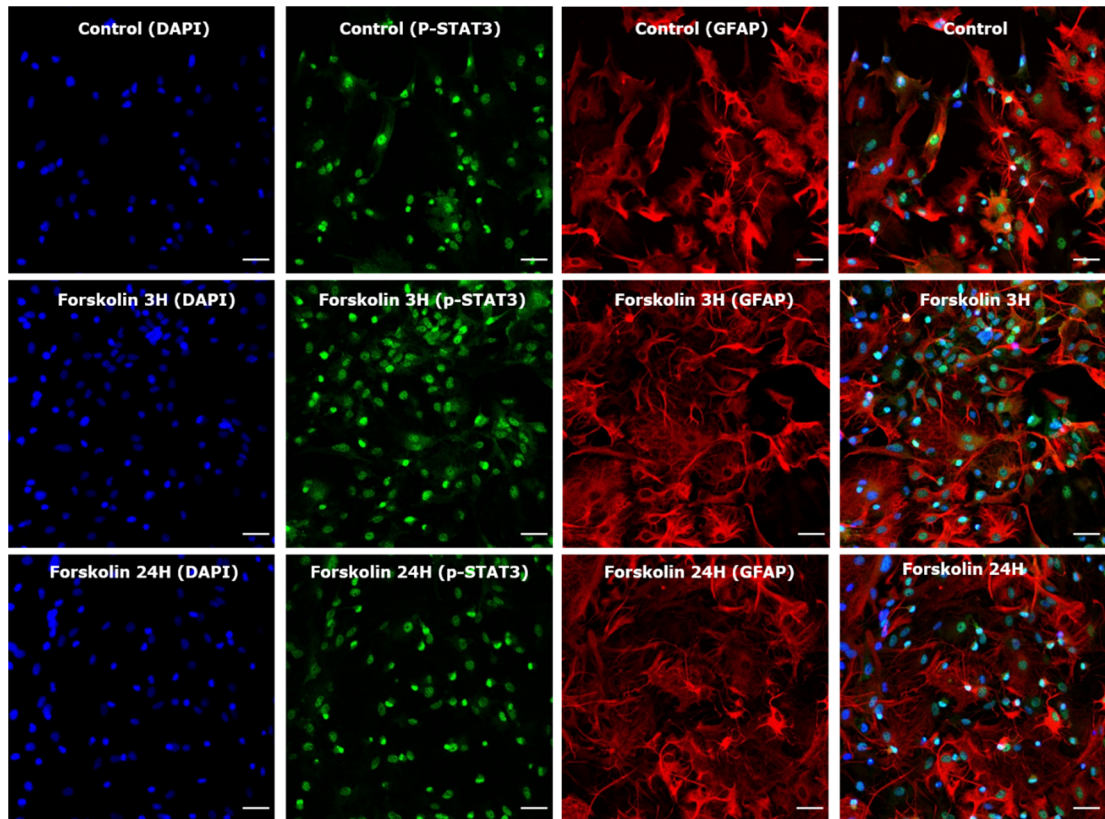


**Figure 5.12 Intensity of S727 p-STAT3 on neonatal spinal astrocytes with confocal microscopy**, cells are stained with GFAP in red, serine p-STAT3 in green and DAPI in blue. Cells are treated with forskolin 10 $\mu$ M at 3 hours (middle panels) 24 hours (lower panels). The scale bar = 40 $\mu$ m. Aggregate data represent the mean of p-STAT3 intensity per pixel in the nucleus. Data are presented as a mean  $\pm$  SEM completed from three different experiments. No statistically significant differences were determined using the one way ANOVA (Dunnett's multiple comparisons test) by comparing treated groups with control.

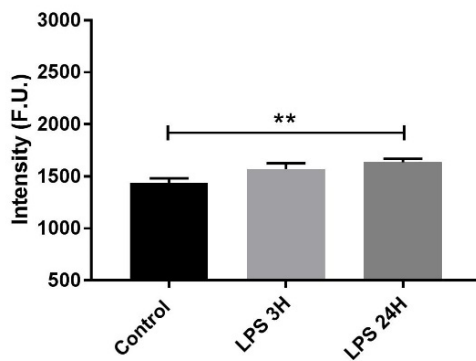
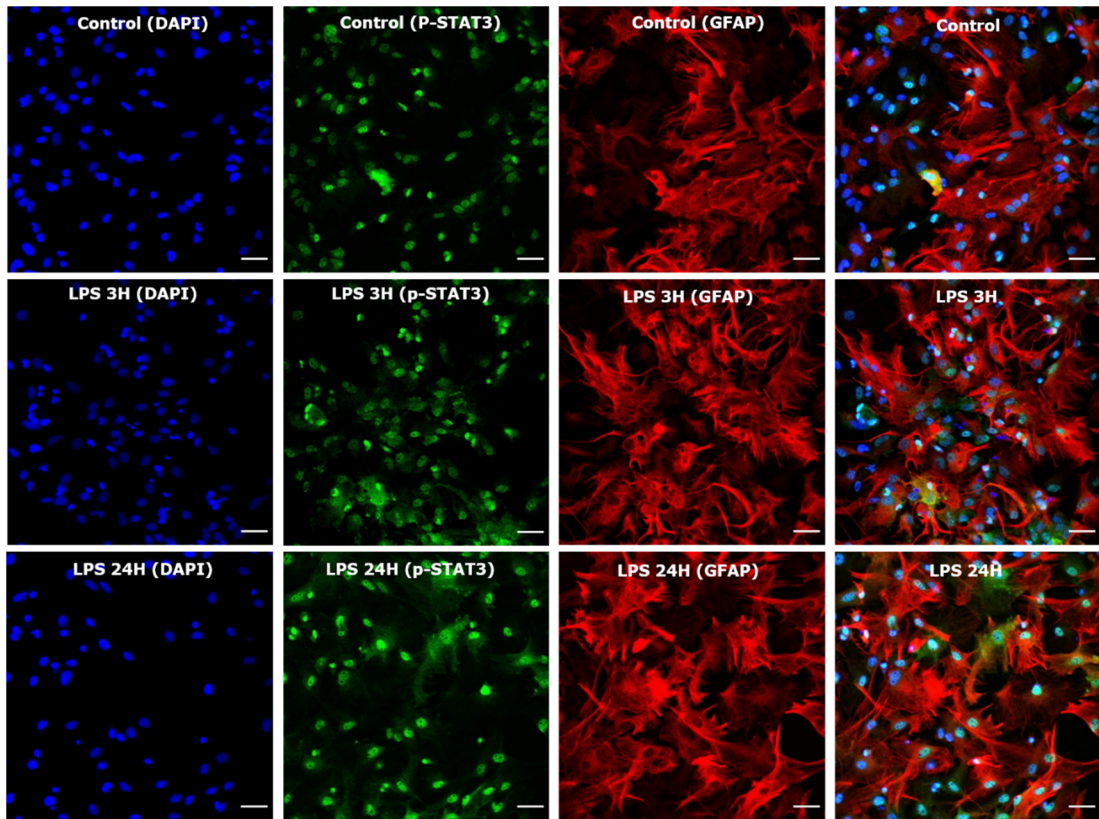


**Figure 5.13 Intensity of S727 p-STAT3 on neonatal spinal astrocytes with confocal microscopy**, cells are stained with GFAP in red, serine p-STAT3 in green and DAPI in blue. Cells are treated with LPS 1 $\mu$ g/ml at 3 hours (middle panels) 24 hours (lower panels). The scale bar = 40 $\mu$ m. Aggregate data represent the mean of p-STAT3 intensity per pixel in the nucleus. Data are presented as a mean  $\pm$  SEM. The statistical significance was determined using the one way ANOVA (Dunnett's multiple comparisons test) by comparing treated groups with control, where (\*\*P < 0.01) was considered statistically significant. The experiment was repeated three times.

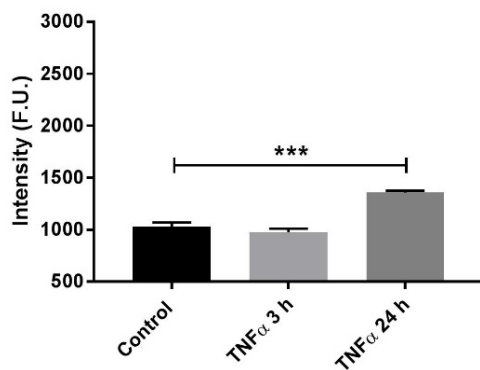
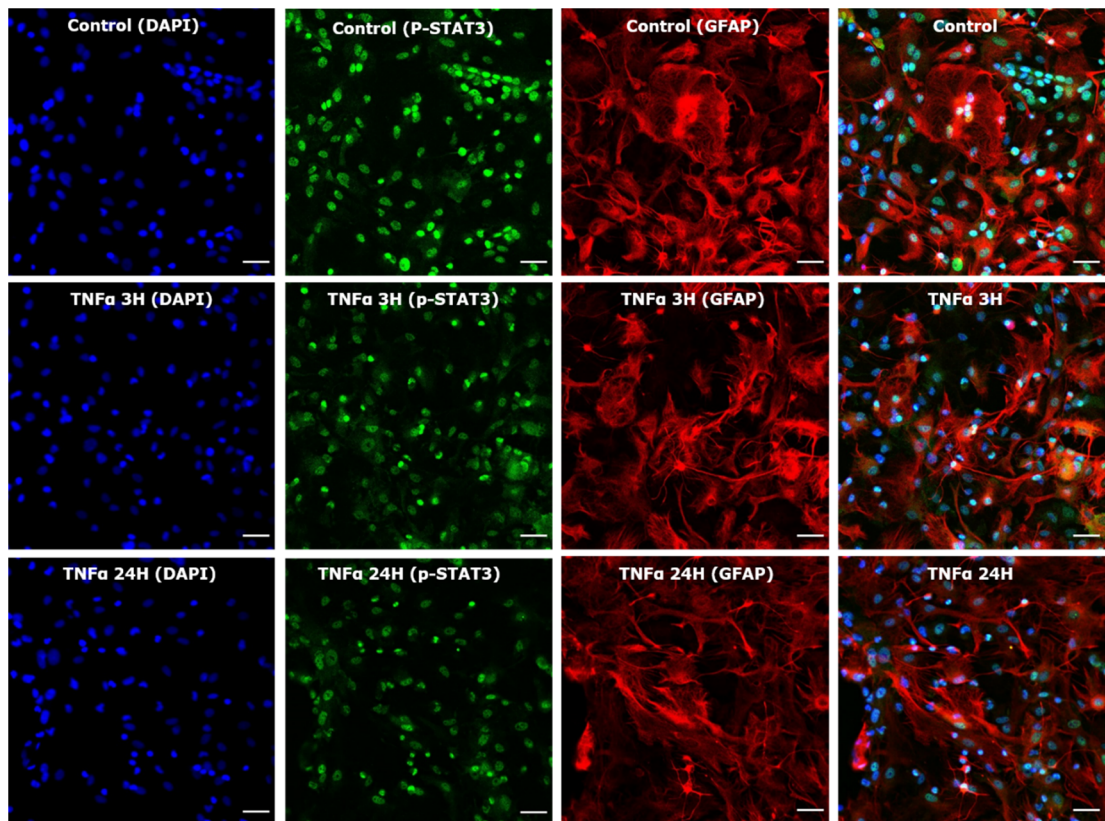


**Figure 5.14 Intensity of S727 p-STAT3 on neonatal spinal astrocytes with confocal microscopy**, cells are stained with GFAP in red, serine p-STAT3 in green and DAPI in blue. Cells are treated with TNF $\alpha$  200ng/ml at 3 hours (middle panels) 24 hours (lower panels). The scale bar = 40 $\mu$ m. Aggregate data represent the mean of p-STAT3 intensity per pixel in the nucleus. Data are presented as a mean  $\pm$  SEM. The statistical significance was determined using the one way ANOVA (Dunnett's multiple comparisons test) by comparing treated groups with control, where (\*\*\*) $P < 0.001$  was considered statistically significant. The experiment was repeated three times.

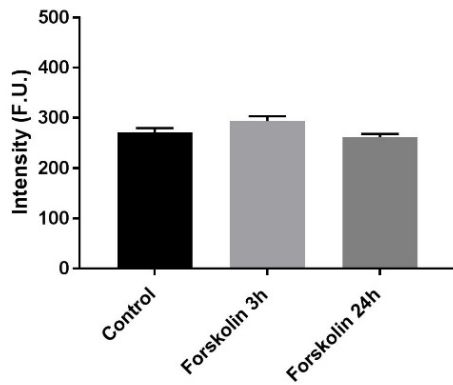
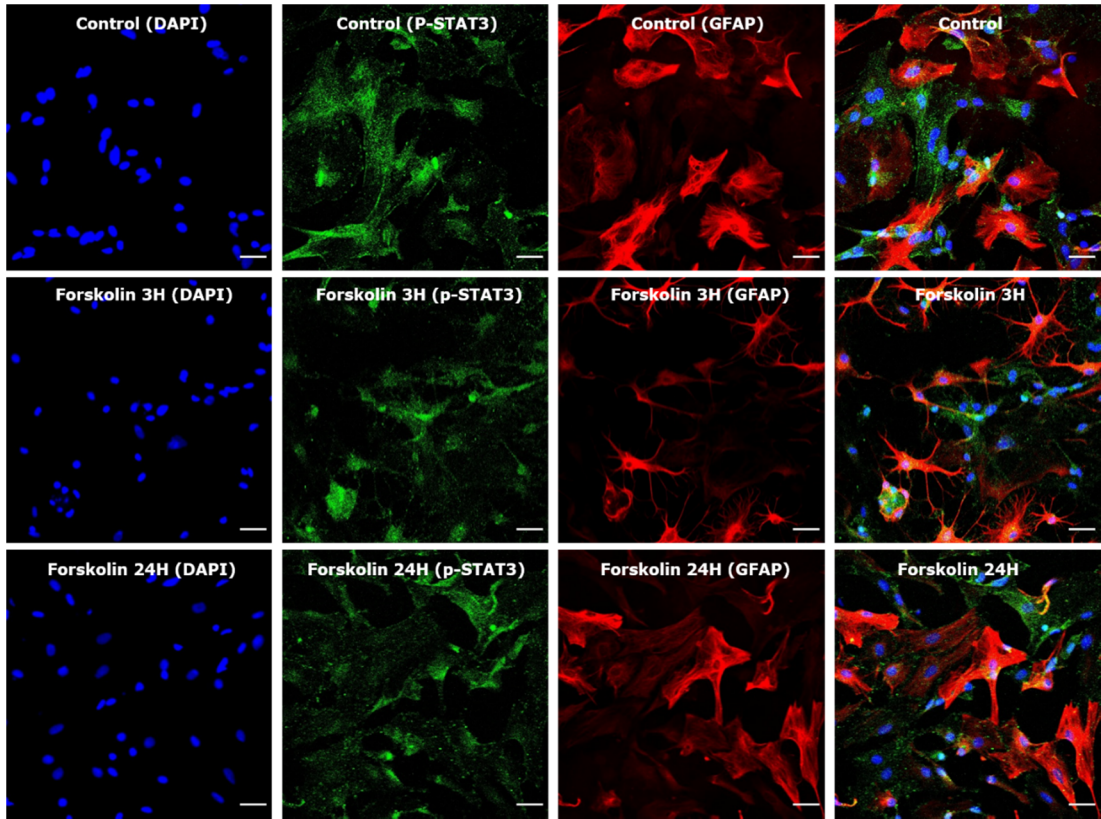


**Figure 5.15 Intensity of Y705 p-STAT3 on neonatal spinal astrocytes with confocal microscopy**, cells are stained with GFAP in red, tyrosine p-STAT3 in green and DAPI in blue. Cells are treated with forskolin 10 $\mu$ M at 3 hours (middle panels) 24 hours (lower panels). The scale bar = 40 $\mu$ m. Aggregate data represent the mean of Y705 p-STAT3 intensity per pixel in the nucleus. Data are presented as a mean  $\pm$  SEM completed from three different experiments. No statistically significant differences were determined using the one way ANOVA (Dunnett's multiple comparisons test) by comparing treated groups with control.

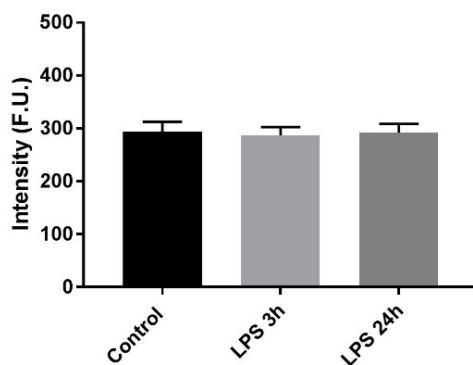
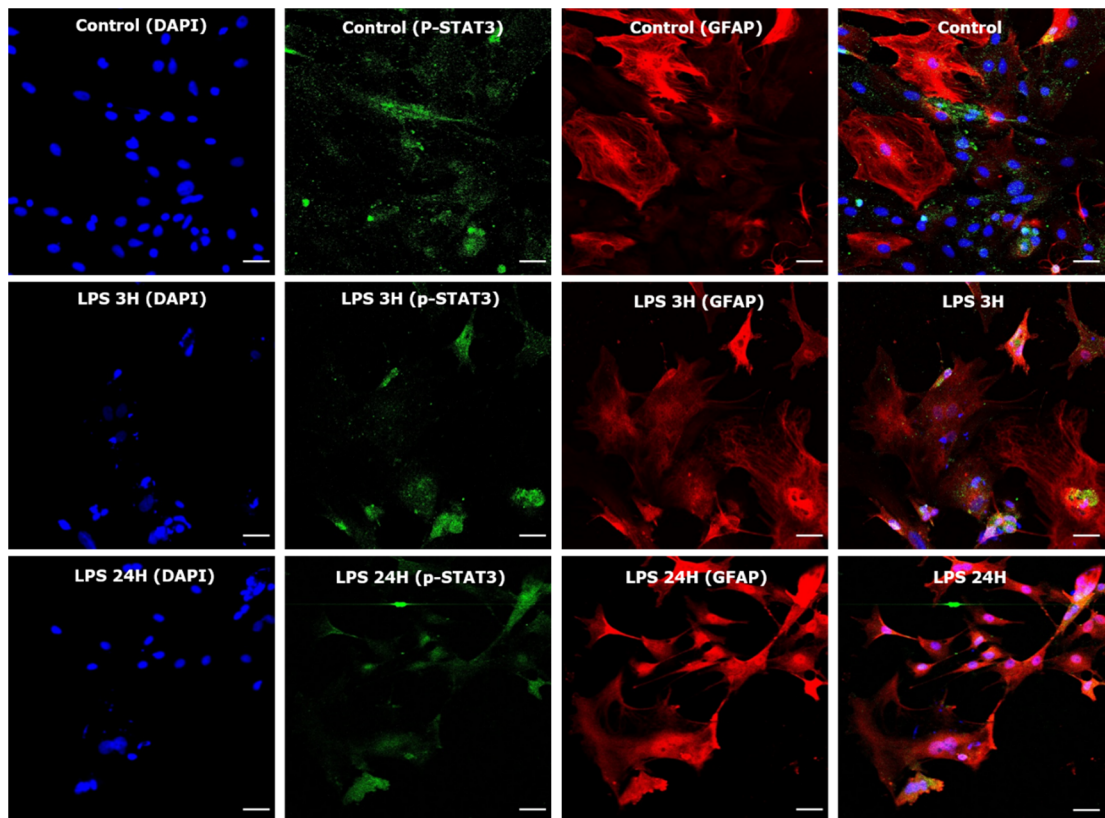


**Figure 5.16 Intensity of Y705 p-STAT3 on neonatal spinal astrocytes with confocal microscopy**, cells are stained with GFAP in red, tyrosine p-STAT3 in green and DAPI in blue. Cells are treated with LPS 1 $\mu$ g/ml at 3 hours (middle panels) 24 hours (lower panels). The scale bar = 40 $\mu$ m. Aggregate data represent the mean of Y705 p-STAT3 intensity per pixel in the nucleus. Data are presented as a mean  $\pm$  SEM completed from three different experiments. No statistically significant differences were determined using the one way ANOVA (Dunnnett's multiple comparisons test) by comparing treated groups with control.

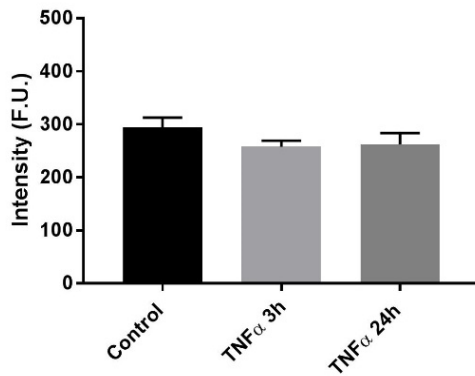
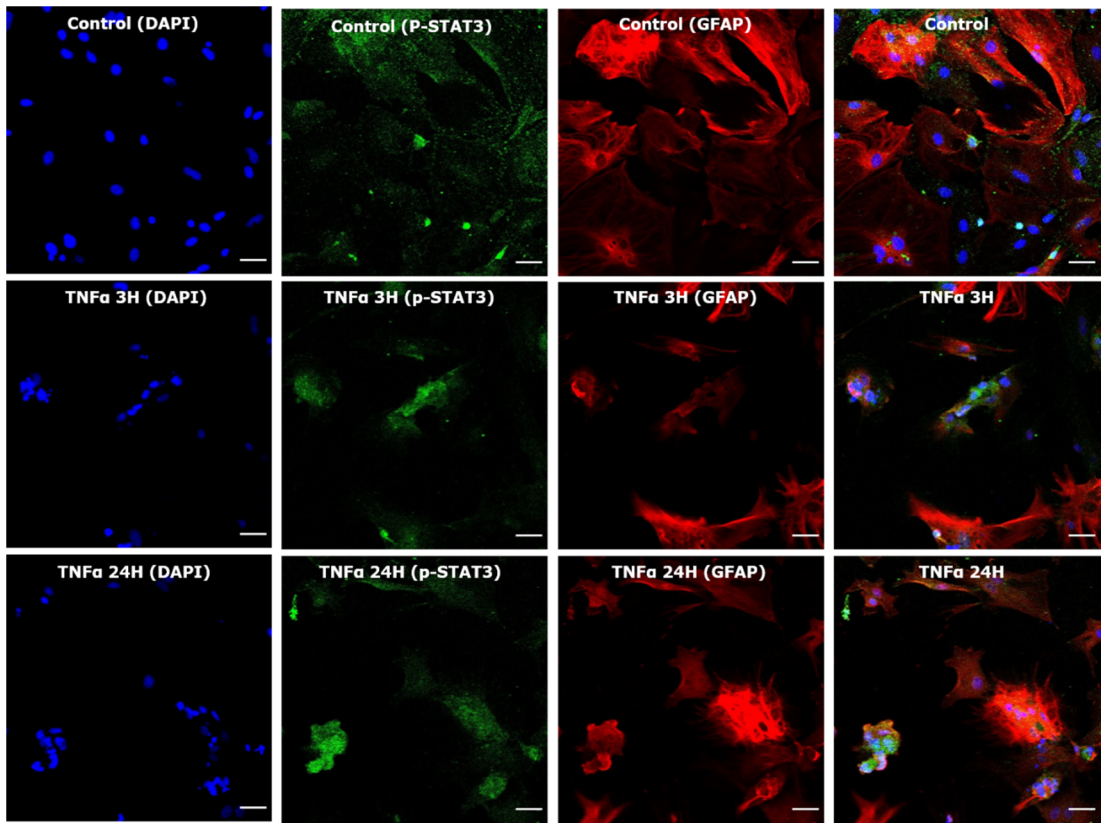


**Figure 5.17 Intensity of Y705 p-STAT3 on neonatal spinal astrocytes with confocal microscopy**, cells are stained with GFAP in red, tyrosine p-STAT3 in green and DAPI in blue. Cells are treated with TNF $\alpha$  200ng/ml at 3 hours (middle panels) 24 hours (lower panels). The scale bar = 40 $\mu$ m. Aggregate data represent the mean of Y705 p-STAT3 intensity per pixel in the nucleus. Data are presented as a mean  $\pm$  SEM completed from three different experiments. No statistically significant differences were determined using the one way ANOVA (Dunnett's multiple comparisons test) by comparing treated groups with control.

### **5.2.7.2 Embryonic cortical astrocytes**

Embryonic cortical astrocytes were also treated with forskolin, LPS and TNF $\alpha$  to quantify the intensity of serine p-STAT3 in the nucleus. The results demonstrated that forskolin does not increase the intensity of serine p-STAT3 for 3 hours (P=0.944) or 24 hours (P=0.904) compared with the untreated cells (Figure 5.18). In the case of LPS, no significant difference was discovered after 3 hours (P=0.577) or 24 hours treatment (P=0.053) (Figure 5.19). In addition, treating the cells with TNF $\alpha$  failed to increase the level of p-STAT3 in the nucleus for both 3 hours (P=0.492) and 24 hours (P=0.996) (Figure 5.20).

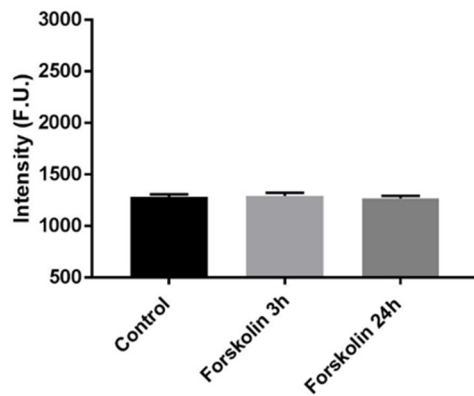
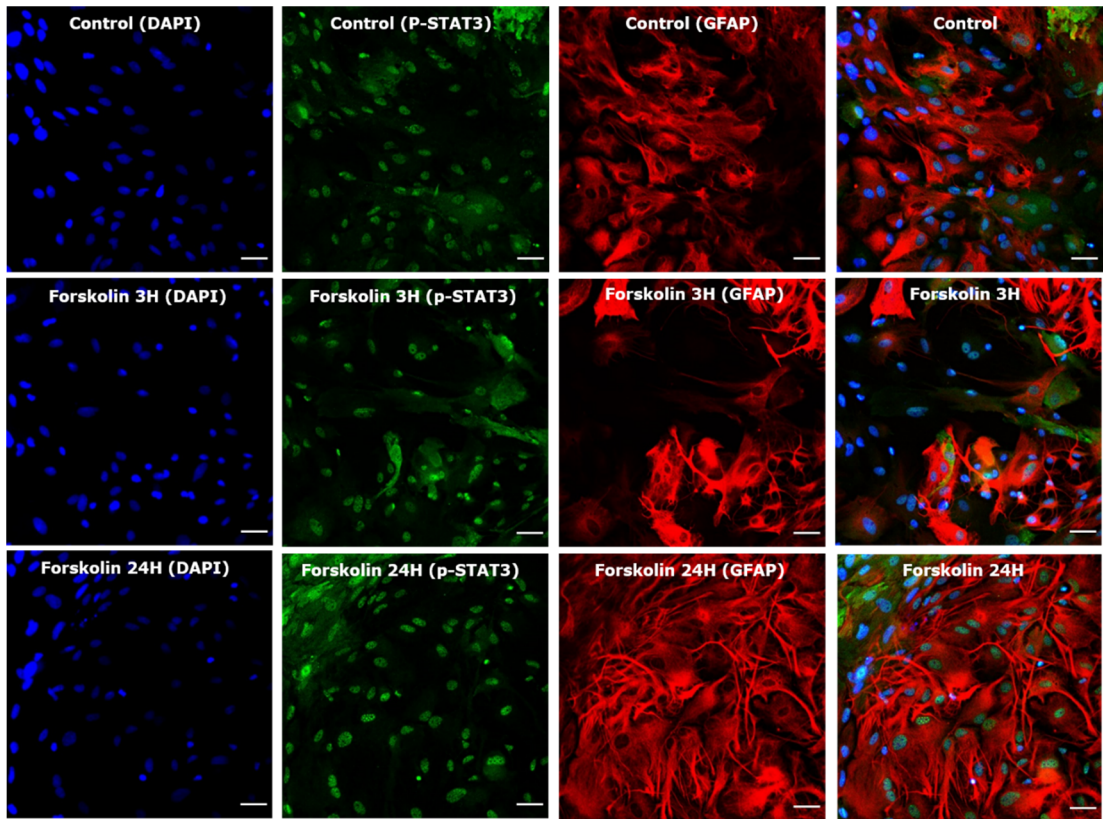


**Figure 5.18 Intensity of S727 p-STAT3 on embryonic cortical astrocytes with confocal microscopy**, cells are stained with GFAP in red, serine p-STAT3 in green and DAPI in blue. Cells are treated with forskolin 10 $\mu$ M at 3 hours (middle panels) 24 hours (lower panels). The scale bar = 40 $\mu$ m. Aggregate data represent the mean of S727 p-STAT3 intensity per pixel in the nucleus. Data are presented as a mean  $\pm$  SEM completed from three different experiments. No statistically significant differences were determined using the one way ANOVA (Dunnett's multiple comparisons test) by comparing treated groups with control.

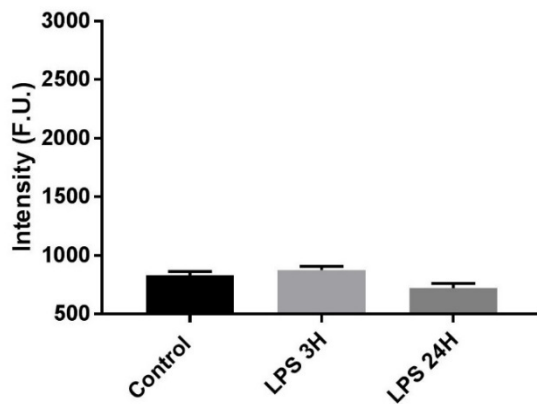
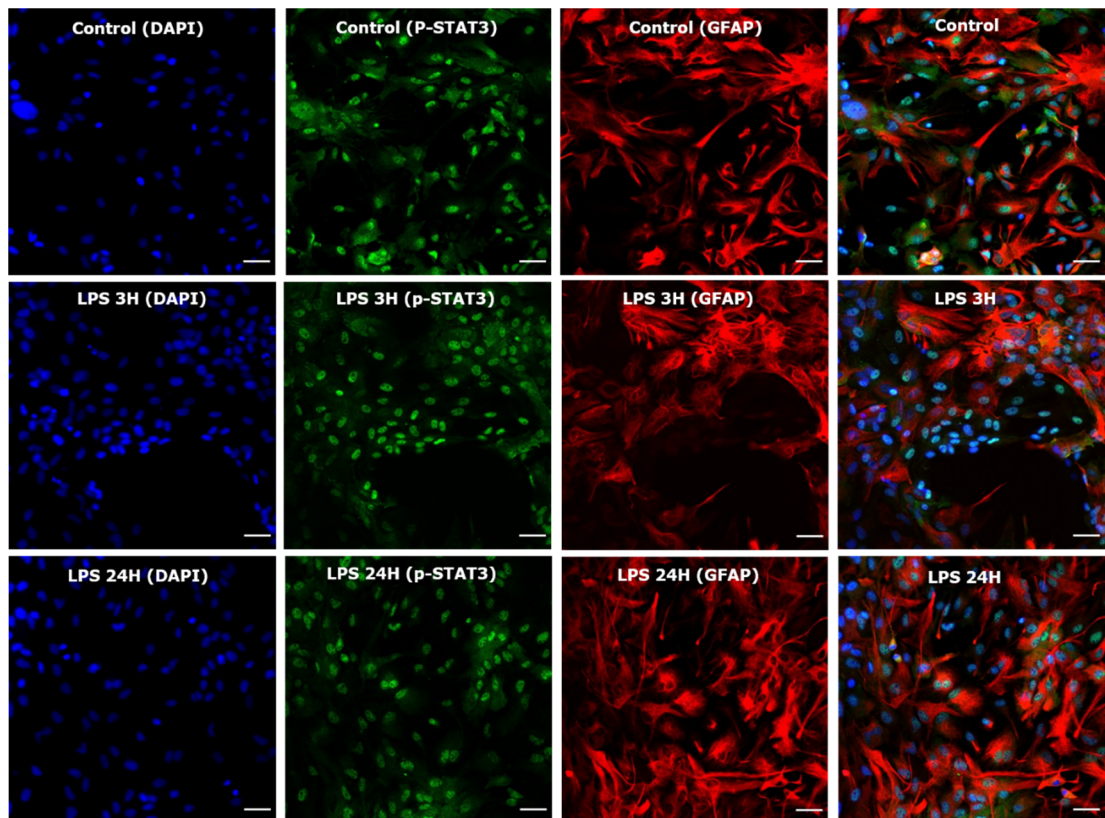


**Figure 5.19 Intensity of S727 p-STAT3 on embryonic cortical astrocytes with confocal microscopy,** cells are stained with GFAP in red, serine p-STAT3 in green and DAPI in blue. Cells are treated with LPS 1 $\mu$ g/ml at 3 hours (middle panels) 24 hours (lower panels). The scale bar = 40 $\mu$ m. Aggregate data represent the mean of S727 p-STAT3 intensity per pixel in the nucleus. Data are presented as a mean  $\pm$  SEM completed from three different experiments. No statistically significant differences were determined using the one way ANOVA (Dunnett's multiple comparisons test) by comparing treated groups with control.

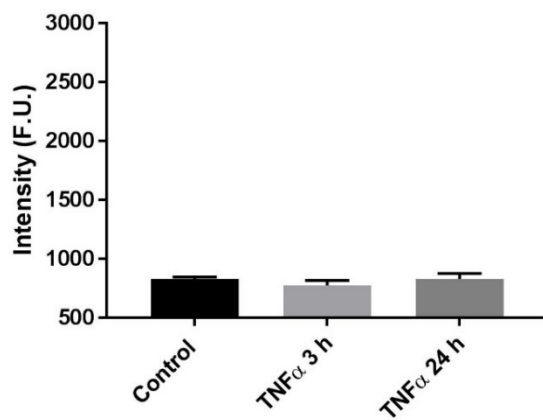
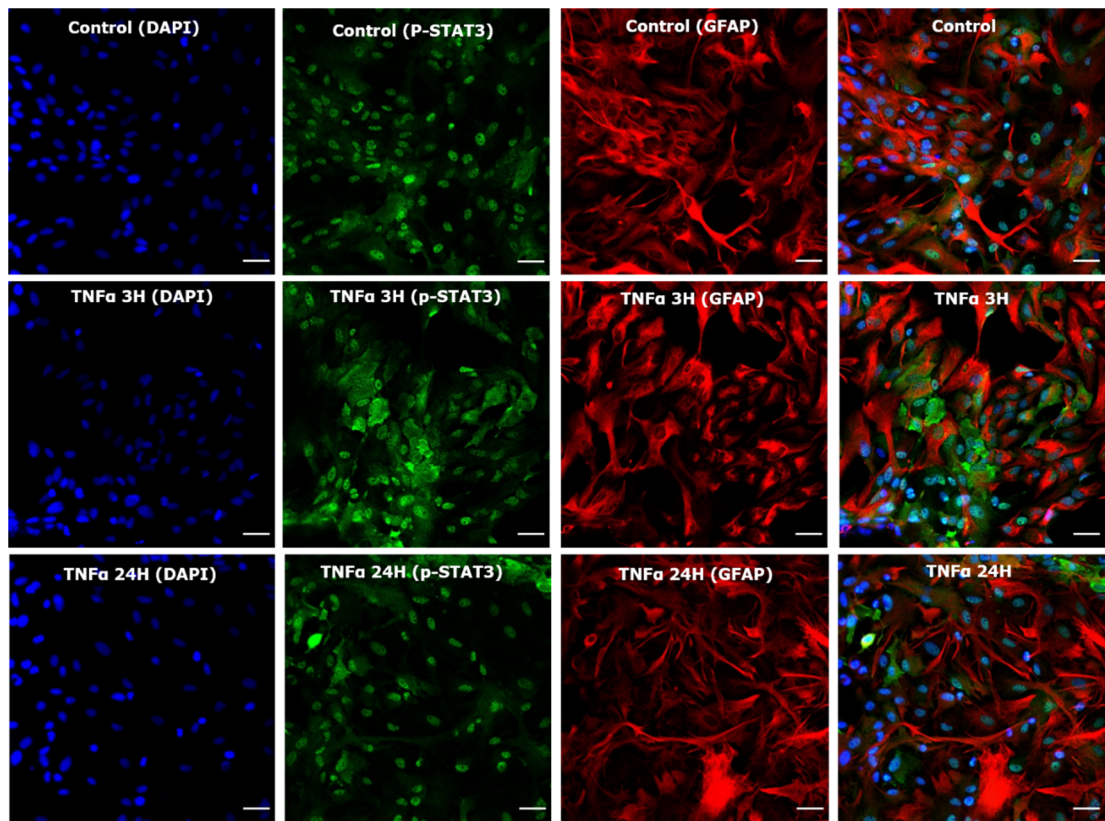


**Figure 5.20 Intensity of S727 p-STAT3 on embryonic cortical astrocytes with confocal microscopy**, cells are stained with GFAP in red, serine p-STAT3 in green and DAPI in blue. Cells are treated with TNF $\alpha$  200ng/ml at 3 hours (middle panels) 24 hours (lower panels). The scale bar = 40 $\mu$ m. Aggregate data represent the mean of S727 p-STAT3 intensity per pixel in the nucleus. Data are presented as a mean  $\pm$  SEM completed from three different experiments. No statistically significant differences were determined using the one way ANOVA (Dunnett's multiple comparisons test) by comparing treated groups with control.

<b>Time and treatment</b>	<b>Neonatal cortical astrocytes</b>		<b>Neonatal spinal astrocytes</b>		<b>Embryonic cortical astrocytes</b>	
<b>Forskolin</b>	<b>S727 p-STAT3</b>	<b>Y705 p-STAT3</b>	<b>S727 p-STAT3</b>	<b>Y705 p-STAT3</b>	<b>S727 p-STAT3</b>	<b>Y705 p-STAT3</b>
Untreated cells	1991±125	281±15	1989±49	271±8	1282±25	-
3 hours	2379±145	265±13	1706±92	294±9	1292±30	-
24 hours	1654±64	271 ±11	1759±56	262±6	1268±24	-
<b>LPS</b>	<b>S727 p-STAT3</b>	<b>Y705 p-STAT3</b>	<b>S727 p-STAT3</b>	<b>Y705 p-STAT3</b>	<b>S727 p-STAT3</b>	<b>Y705 p-STAT3</b>
Untreated cells	1428±75	372±17	1439±43	294±19	823±33	-
3 hours	1395±55	255±18	1572±54	287±16	875±32	-
24 hours	1730±97	339±24	1637±33	292±17	722±38	-
<b>TNF<math>\alpha</math></b>	<b>S727 p-STAT3</b>	<b>Y705 p-STAT3</b>	<b>S727 p-STAT3</b>	<b>Y705 p-STAT3</b>	<b>S727 p-STAT3</b>	<b>Y705 p-STAT3</b>
Untreated cells	1072±46	248±9	1032±38	284±18	827±19	-
3 hours	1290±76	228±11	979±34	258±11	776±42	-
24 hours	1353±78	402±18	1357±18	263±21	830±45	-

**Table 5.1 Summary of the intensity of p-STAT3 in the nucleus** after forskolin, LPS and TNF $\alpha$  treatment of neonatal cortical, neonatal spinal and embryonic cortical astrocytes. Data are presented as a mean  $\pm$  SEM.

## **5.2.8 Measuring protein expression of p-STAT3 with Western blots**

### **5.2.8.1 Optimising the p-STAT3 protein detection**

To measure p-STAT3 protein expression in astrocytes in a different way, we used Western blotting to assess p-STAT3 levels after treatment with forskolin and noradrenaline.

Cells were treated with forskolin and noradrenaline for 0 minute, 1 minute, 5 minutes, 10 minutes, 30 minutes, 1 hour and 3 hours. Serine and tyrosine p-STAT3 antibodies were used. It was found that forskolin treatment failed to activate serine p-STAT3. However, forskolin-induced phosphorylation of STAT3 on tyrosine in a time-dependent manner (Figure 5.21).

Western blotting is a semi-quantitative method, and so we tried to normalise p-STAT3 levels in two ways: by comparison to another protein (GAPDH) and by normalisation to control levels before the addition of forskolin or noradrenaline.

Treating the cells with noradrenaline and forskolin did not significantly increase the levels of p-tyrosine-STAT3 compared to control ( $P=0.25$ ) (Figure 5.21 and Figure 5.22). But the maximum level of p-STAT3 was detected after 30 minutes of forskolin treatment and 10 minutes of noradrenaline treatment.

GAPDH is an unreliable normalisation method due to so much of variations occur. However, it better to do it in the base of how much p-STAT3 in there by normalised to control.

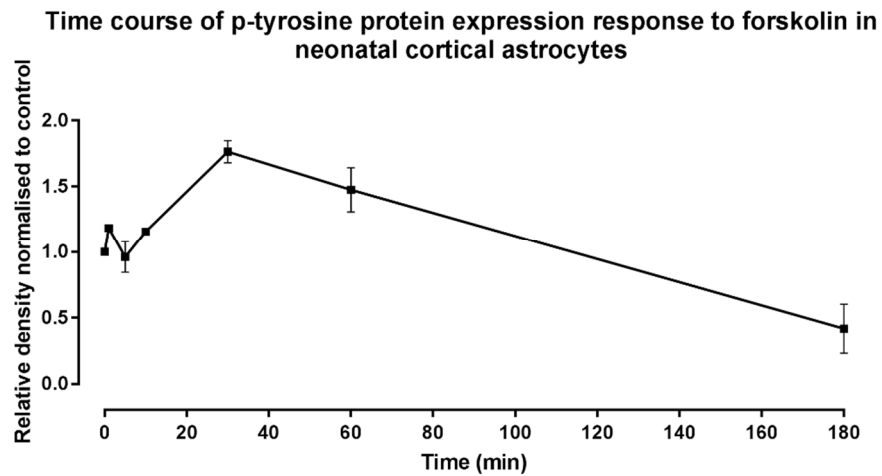
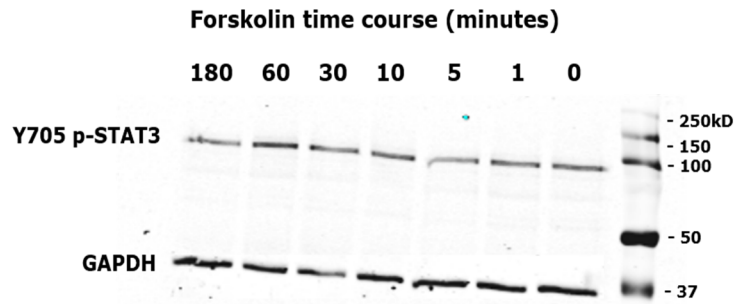
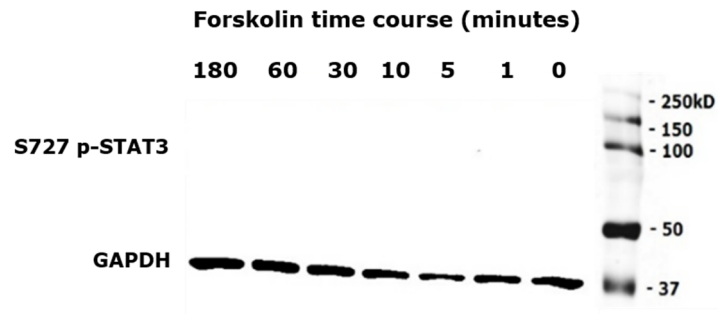
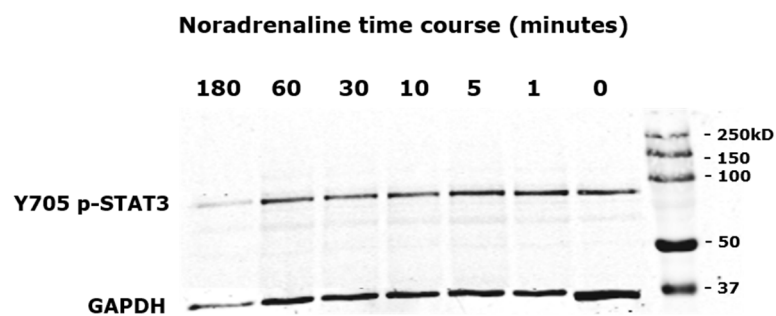


**Figure 5.21 Western blot of S727 p-STAT3 and Y705 p-STAT3 protein in neonatal cortical astrocytes after 10 $\mu$ M forskolin treatment.** Aggregate data represent the relative density of each band normalised to the control. Data are presented as a mean  $\pm$  SEM. No statistically significant differences were determined using the Wilcoxon test with control normalisation and by comparing the peak with control. The experiment was repeated three times.



**Time course of p-tyrosine protein expression response to noradrenaline in neonatal cortical astrocytes**

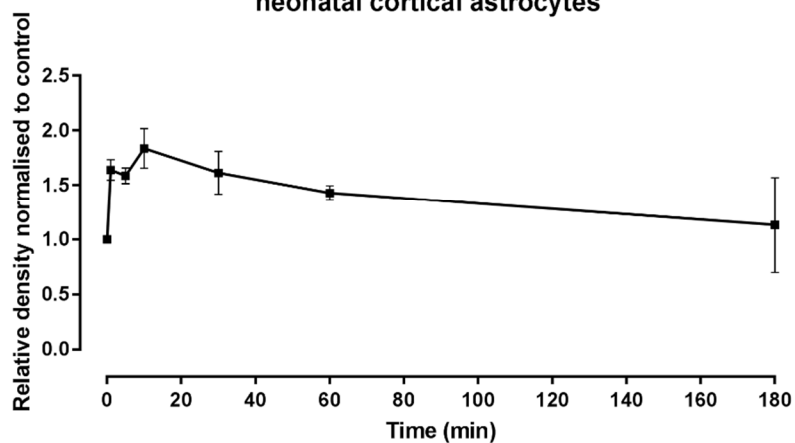


**Figure 5.22 Western blot of Y705 p-STAT3 protein in neonatal cortical astrocytes after 10µM noradrenaline treatment.** Aggregate data represent the relative density of each band normalised to GAPDH as reference protein and the control. Data are presented as a mean  $\pm$  SEM. No statistically significant differences were determined using the Wilcoxon test with control normalisation and by comparing the peak with control. The experiment was repeated three times.

#### **5.2.8.2** Tyrosine p-STAT3 activation in different types of astrocytes

To investigate phosphorylation of STAT3 in more detail, we next tested forskolin responses in all astrocyte types (spinal, cortical and embryonic) and compared these to responses evoked by a positive control, IL-6, which is known to be linked to tyrosine phosphorylation of STAT3

Normalised to GAPDH and control, IL-6 caused a significant increase in all cases but forskolin was ineffective. Normalised to GAPDH, there were differences between forskolin induce Y705 p-STAT3 between neonatal cortical and spinal ( $P=0.003$ ) and between neonatal spinal and embryonic cortical ( $P=0.028$ ). No difference was determined between neonatal and embryonic cortical astrocytes after forskolin treatment ( $P=0.1$ ) (Figure 5.23).

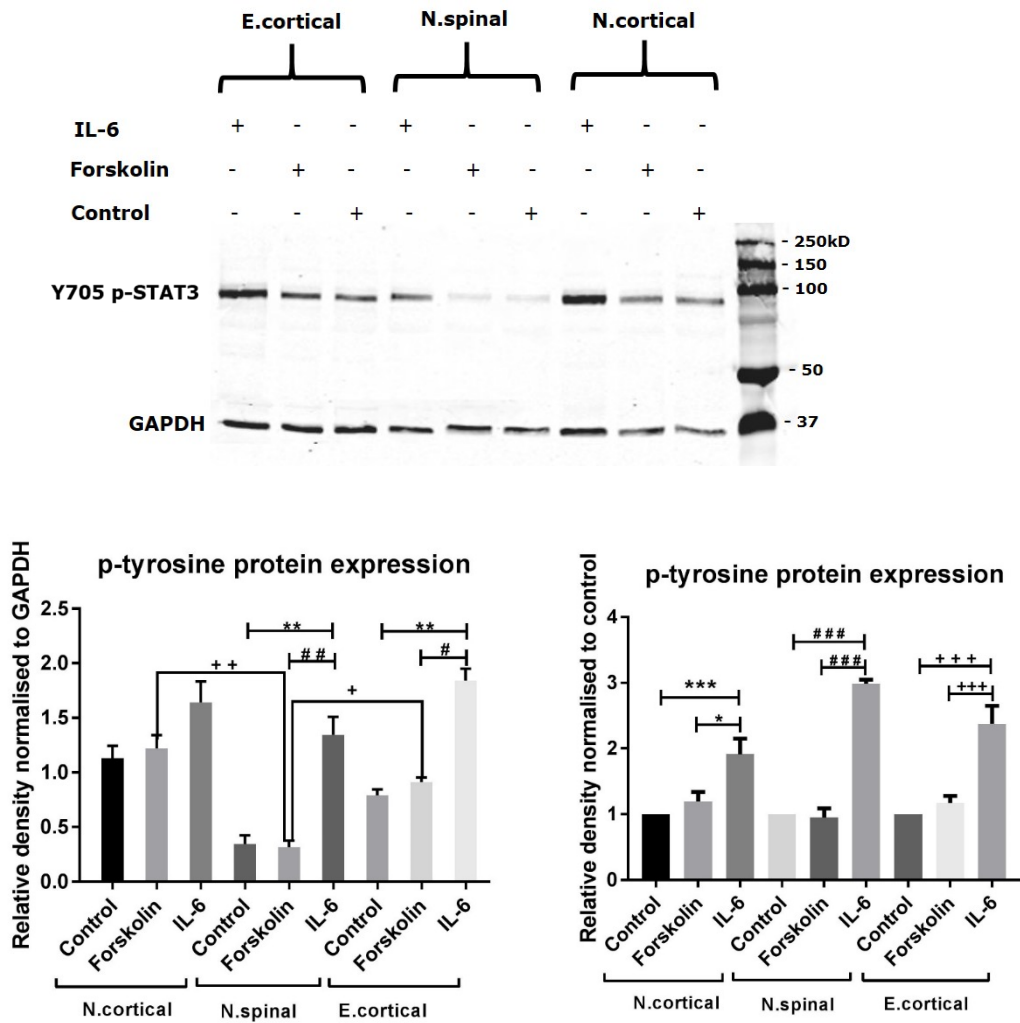


**Figure 5.23 Western blot of Y705 p-STAT3 protein in neonatal cortical, spinal and embryonic cortical astrocytes after 30 minutes of 10 $\mu$ M forskolin and 10 minutes of 100ng/ml IL-6 treatment.** Aggregate data represent the relative density of each band normalised to GAPDH as reference protein and the control. Data are presented as a mean  $\pm$  SEM. The statistical significance was determined using the one way ANOVA (Tukey's multiple comparisons test) and the Mann-Whitney test to compare between forskolin group in each cells type, where (\* $P < 0.05$ , \*\* $P < 0.01$  and \*\*\* $P < 0.001$ ) was considered statistically significant. The experiment was repeated three times.

**5.2.8.3** Tyrosine p-STAT3 protein levels in the presence of p-STAT3 and JAK inhibitors

Neonatal cortical astrocytes were treated with forskolin, noradrenaline and IL-6 in the presence of stattic and WP1066. Stattic ( $P=0.003$ ) and WP1066 ( $P=0.015$ ) were decreased Y705 p-STAT3 relative to control in the cells treated with forskolin (Figure 5.24). However, treat cells with stattic and noradrenaline was significantly reduced the level of tyrosine p-STAT3 ( $P=0.005$ ), but this was not the case with WP1066 ( $P=0.186$ ) (Figure 5.25). Treat the cells with stattic and WP1066 alone were significantly decreased the Y705 p-STAT3 level, compared with forskolin (Figure 5.24), noradrenaline (Figure 5.25), and IL-6 (Figure 5.26). The main problem in this experiment was with normalisation, which impacts on stats. To improve this problem, all data were normalised to control.

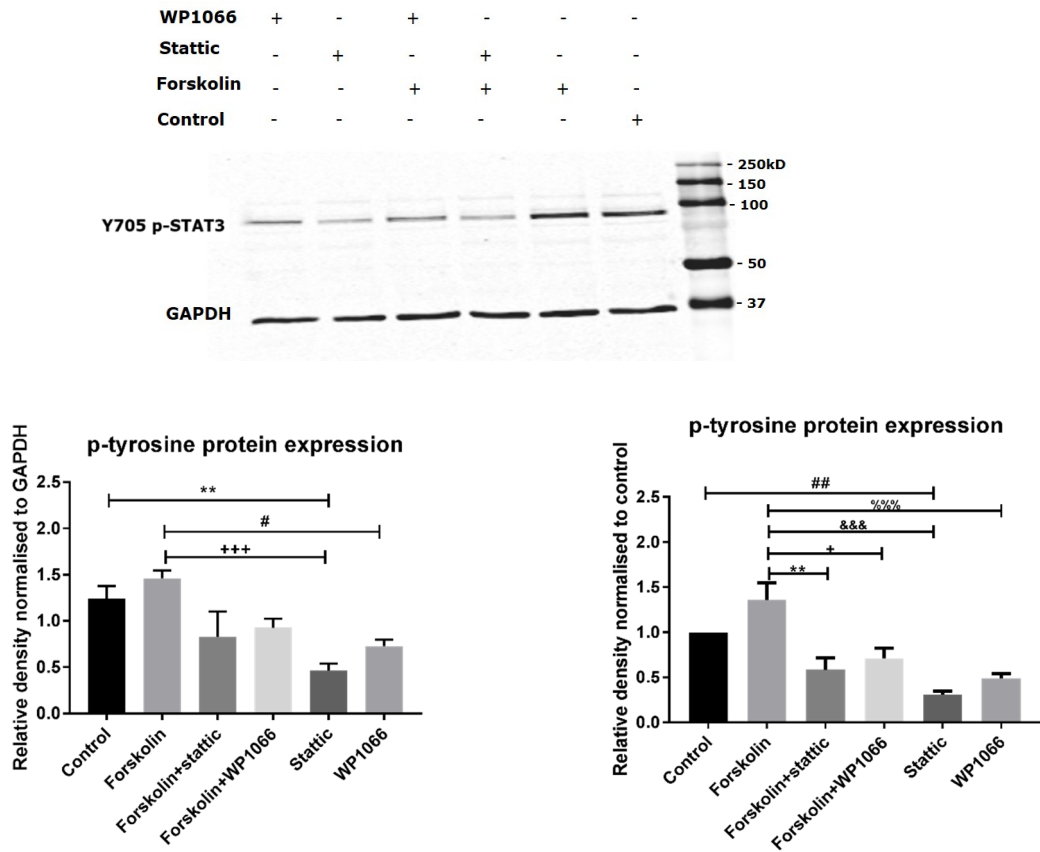


**Figure 5.24 Western blot of Y705 p-STAT3 protein in neonatal cortical astrocytes after treated with p-STAT3 and JAK inhibitors for 1 hour and 10 $\mu$ M forskolin for 30 minutes.** Aggregate data represent the relative density of each band normalised to GAPDH as reference protein and the control. Data are presented as a mean  $\pm$  SEM. The statistical significance was determined using the one way ANOVA followed by Tukey's multiple comparisons test, where (\* $P$ <0.05 and \*\* $P$ <0.01) was considered statistically significant. The experiment was repeated three times.

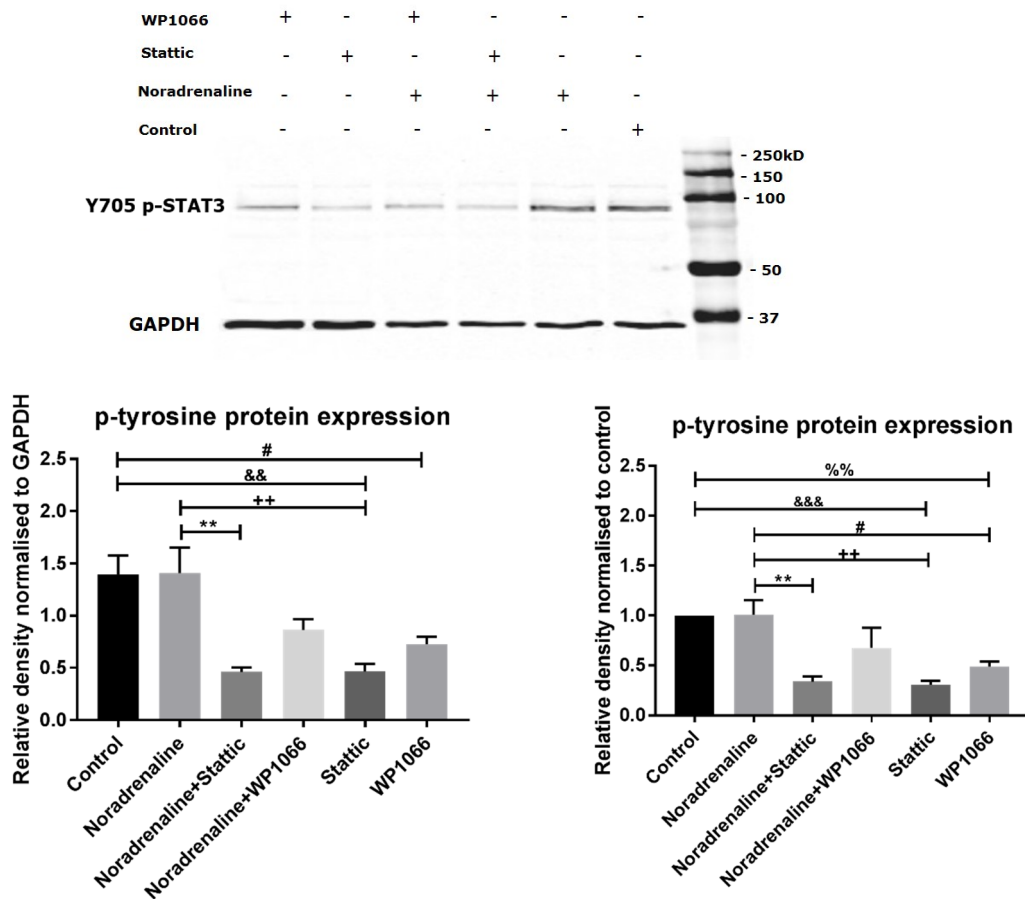


**Figure 5.25 Western blot of Y705 p-STAT3 protein in neonatal cortical astrocytes after treated with p-STAT3 and JAK inhibitors for 1 hour and 10 $\mu$ M noradrenaline for 10 minutes.** Aggregate data represent the relative density of each band normalised to GAPDH as reference protein and the control. Data are presented as a mean  $\pm$  SEM. The statistical significance was determined using the one way ANOVA followed by Tukey's multiple comparisons test, where (\*\* $P < 0.01$ ) was considered statistically significant. The experiment was repeated three times.

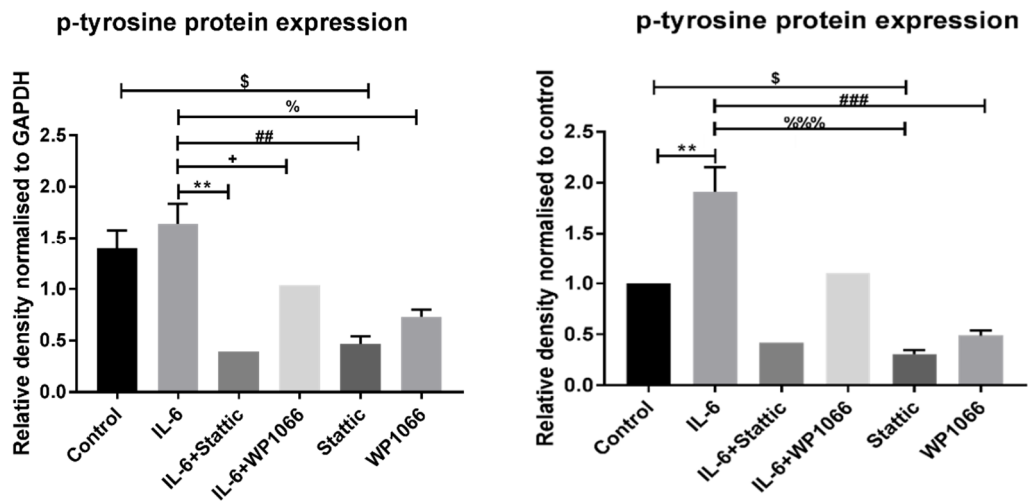
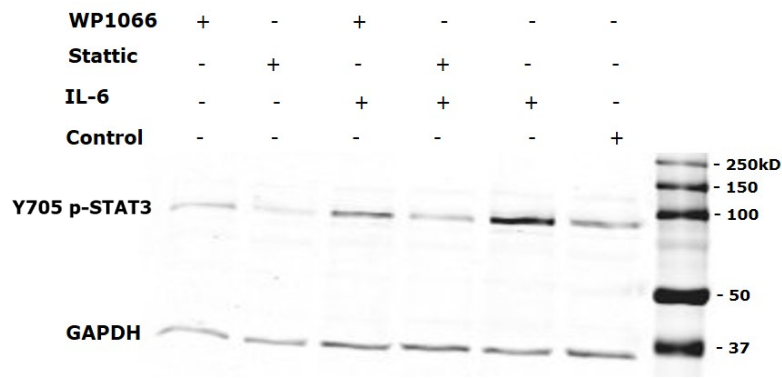


**Figure 5.26 Western blot of Y705 p-STAT3 protein in neonatal cortical astrocytes after treated with p-STAT3 and JAK inhibitors for 1 hour and 100ng/ml IL-6 for 10 minutes.** Aggregate data represent the relative density of each band normalised to GAPDH as reference protein and the control. Data are presented as a mean  $\pm$  SEM. The statistical significance was determined using the one way ANOVA followed by Tukey's multiple comparisons test, where (\* $P < 0.05$  and \*\* $P < 0.01$ ) was considered statistically significant. The experiment was repeated three times, except for IL-6 with stattic and WP1066 were done once.

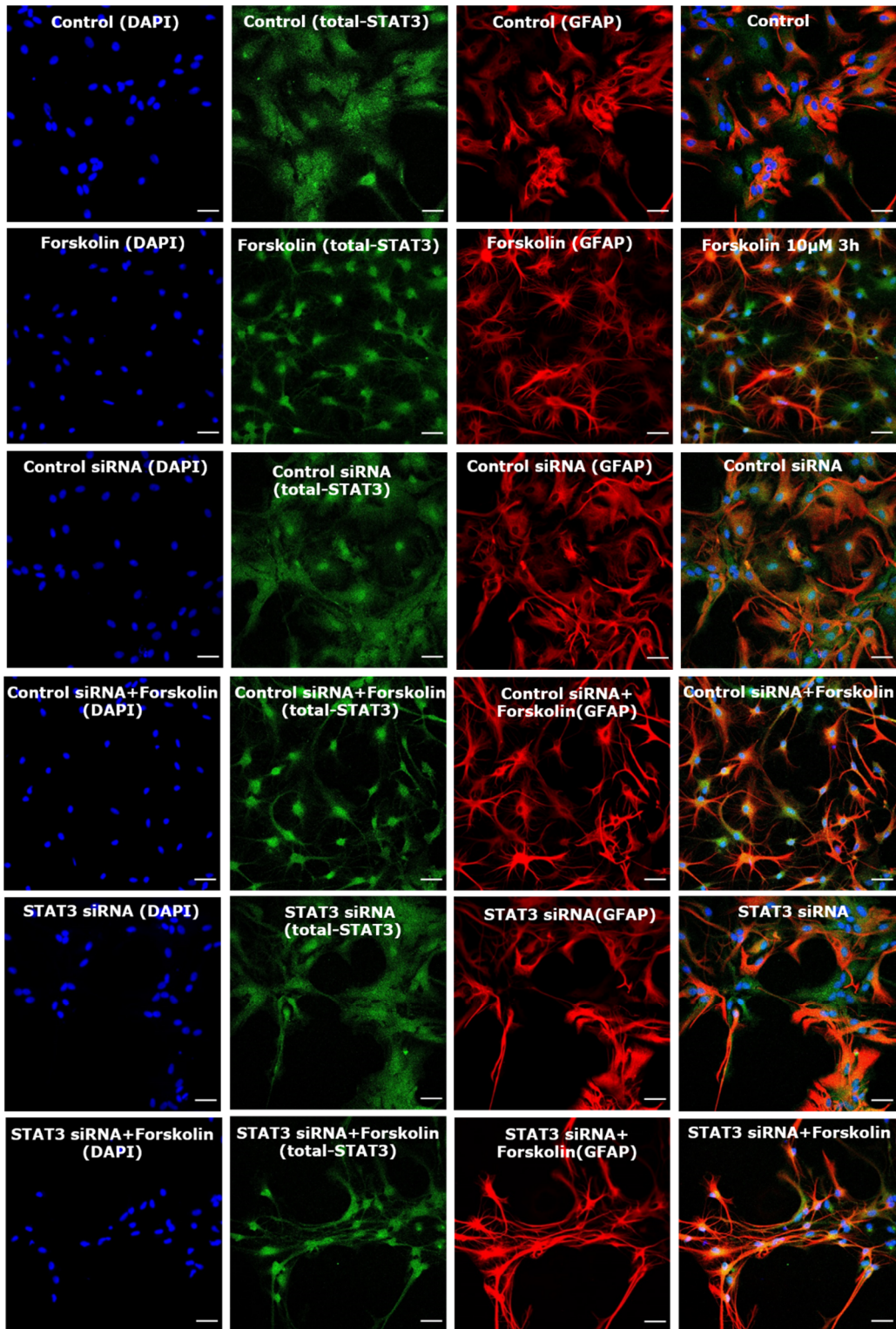
## **5.2.9 Effect of Accell siRNA STAT3 transfection in astrocytes stellation**

### **5.2.9.1 Accell siRNA STAT3 in 2% serum medium**

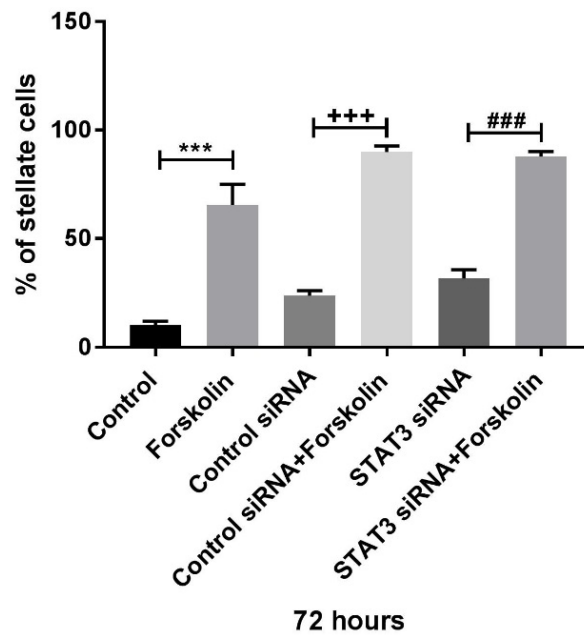
The next goals were to inhibit STAT3 phosphorylation by a non-pharmacological method. To knockdown STAT3 expression, Accell siRNA was used. The cells were incubated with Accell siRNA for 72 and 96 hours, and then treated with forskolin to induce stellation.

The intensity of STAT3 labelling was measured by confocal microscopy to check the effectiveness of the transfection and knockdown process. After 72 hours incubation, treat the cells with siRNA either control or STAT3 did not significantly increase stellation. In addition, the percentage of stellate cells after forskolin treatment in non-transfected cells, transfected cell with non-targeting siRNA and transfected cell with STAT3 siRNA were increased ( $P < 0.001$ ). However, no significantly decreased in the intensity of STAT3 was detected after transfection with STAT3 siRNA ( $P = 0.155$ ) (Figure 5.27).

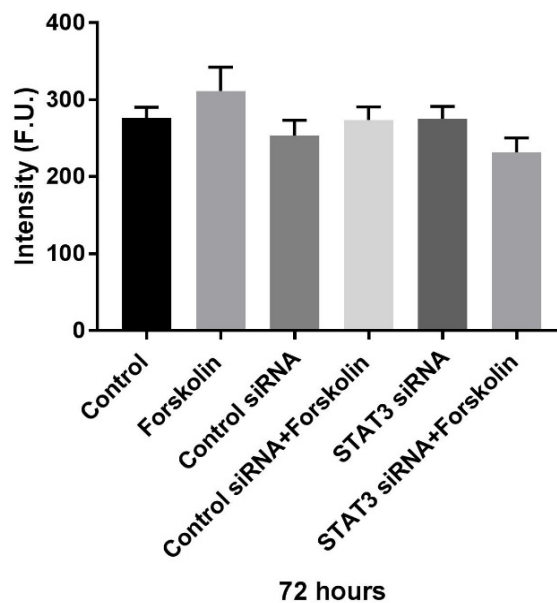
After extending the incubation time to 96 hours, the percentage of stellate cells significantly increased after forskolin treatment in all cases and even after treating the cells with non-targeting and STAT3 siRNA alone ( $P < 0.001$ ). The intensity of STAT3 after STAT3 siRNA knockdown was significantly decreased in untreated cells ( $P = 0.02$ ) and treated cells with forskolin ( $P = 0.0005$ ). Also, transfected cells with non-targeting siRNA treated with forskolin were significantly lower STAT3 intensity ( $P = 0.007$ ) (Figure 5.28). This result indicates that decreased the STAT3 intensity, not due to knockdown of STAT3 it's due to reducing the number of cells after transfection.



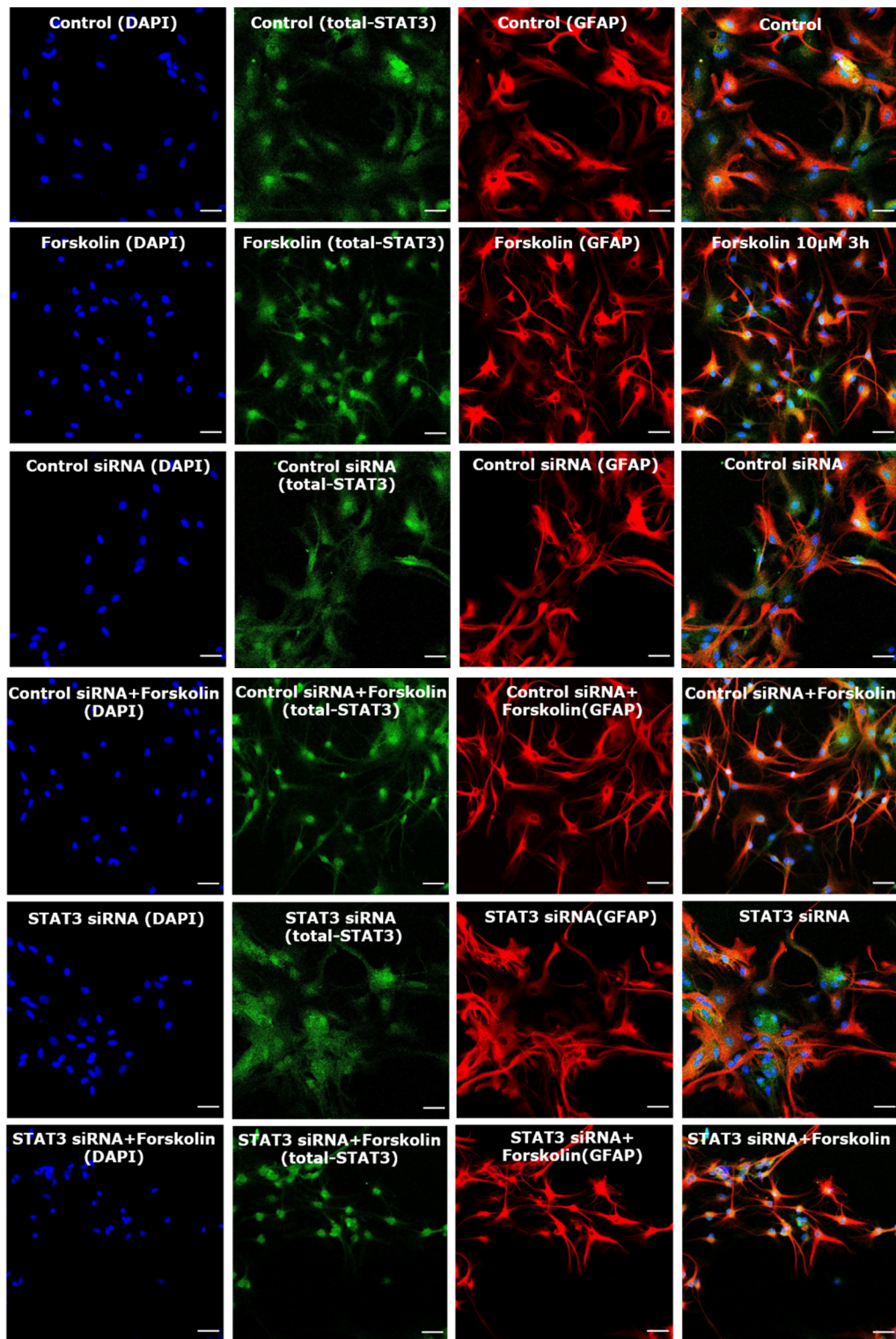
### Stellation assay of STAT3 siRNA in neonatal cortical astrocytes



### Intensity of total STAT3



**Figure 5.27 Stellation assay of astrocytes transfected with siRNA knockdown of STAT3 for 72 hours in 2% serum medium.** Neonatal cortical astrocytes were imaged with confocal microscopy; cells are stained with GFAP in red, total-STAT3 in green and DAPI in blue. Cells are transfected with 1 $\mu$ M Accell non-targeting control siRNA and Accell STAT3 siRNA following with forskolin 10 $\mu$ M treatment for 3 hours. The scale bar = 40 $\mu$ m. Aggregate data represent the mean of total-STAT3 intensity per pixel and the percentage of stellate cells. Data are presented as a mean  $\pm$  SEM. The statistical significance was determined using the one way ANOVA followed by Tukey's multiple comparisons test, where (\*\*\*) $P < 0.001$  was considered statistically significant



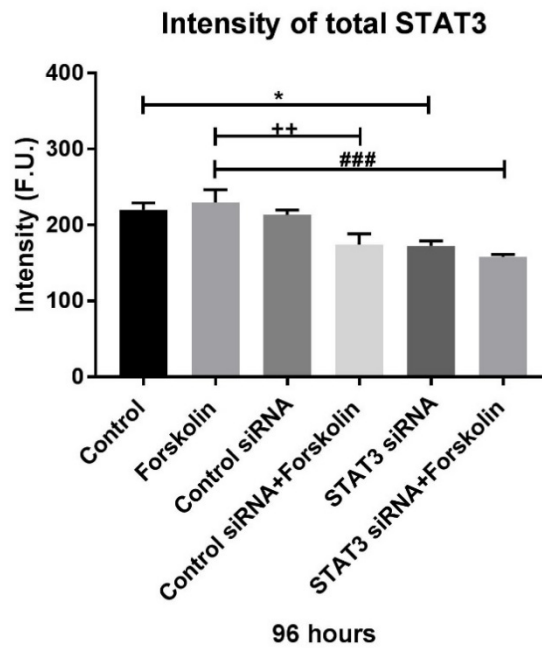
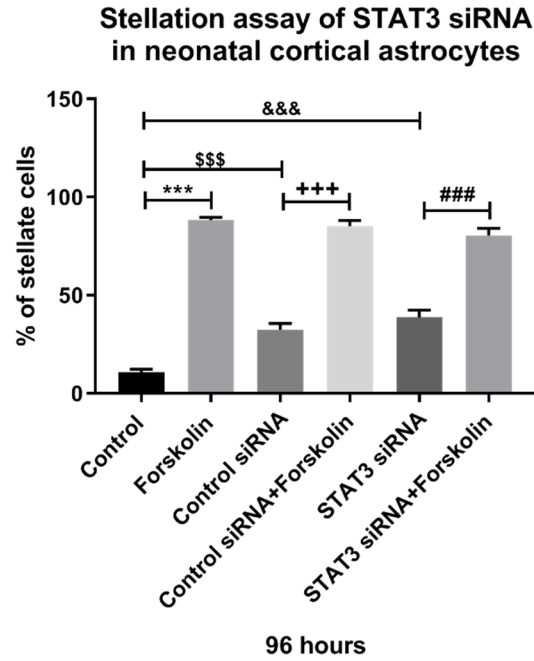
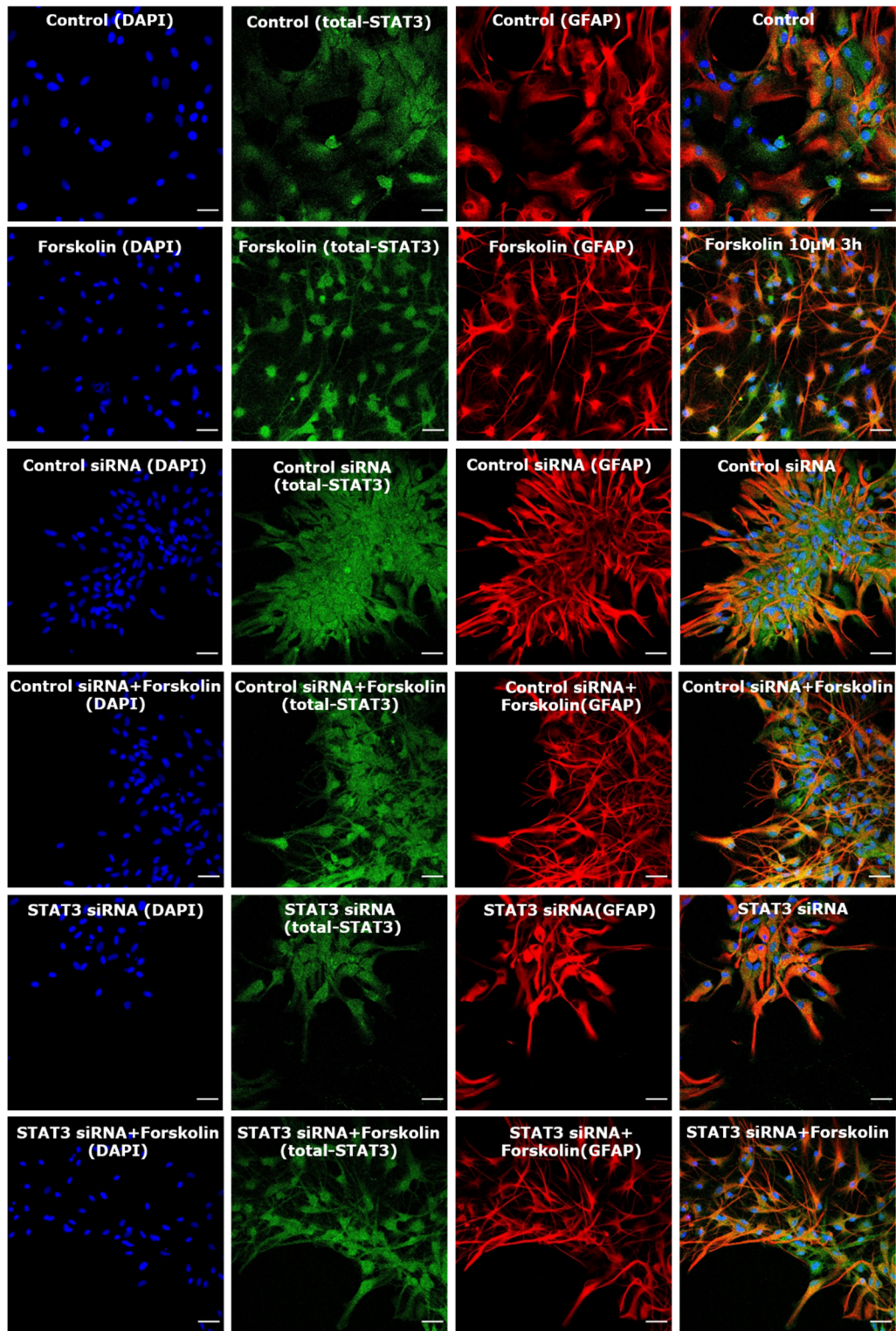


**Figure 5.28 Stellation assay of astrocytes transfected with siRNA knockdown of STAT3 for 96 hours in 2% serum medium.** Neonatal cortical astrocytes were imaged with confocal microscopy; cells are stained with GFAP in red, total-STAT3 in green and DAPI in blue. Cells are transfected with 1 $\mu$ M Accell non-targeting control siRNA and Accell STAT3 siRNA following with forskolin 10 $\mu$ M treatment for 3 hours. The scale bar = 40 $\mu$ m. Aggregate data represent the mean of total-STAT3 intensity per pixel and the percentage of stellate cells. Data are presented as a mean  $\pm$  SEM. The statistical significance was determined using the one way ANOVA followed by Tukey's multiple comparisons test, where (\* $P$ <0.05, \*\* $P$ <0.01 and \*\*\* $P$ <0.001) was considered statistically significant.

#### **5.2.9.2** Accell siRNA STAT3 in serum-free medium

The same experiment was done but using a serum-free medium to try and improve the knockdown of the STAT3. In the case of 72 hours, the percentage of stellate cells was significantly increased after forskolin treatment in non-transfected and transfected cells ( $P < 0.001$ ). There was a significant decrease of STAT3 intensity in control transfected STAT3 cells compared with control non-transfected cells ( $P = 0.012$ ) (Figure 5.29).

After 96 hours incubation, the number of stellate cells still higher after forskolin treatment compared with control in transfected and non-transfected cells. Transfect cells with STAT3 siRNA was unable to prevent stellation after forskolin treatment, which produces 85% of cell stellation ( $P = 0.003$ ) and it was induced stellation in both control siRNA and STAT3 siRNA of the untreated cell with forskolin. However, no significant change of STAT3 intensity was discovered before or after STAT3 knockdown ( $P = 0.295$ ) (Figure 5.30).



**Stellation assay of STAT3 siRNA  
in neonatal cortical astrocytes**

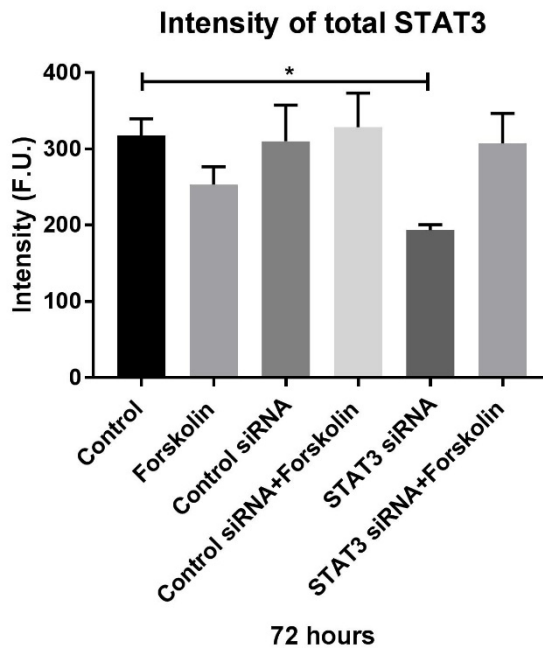
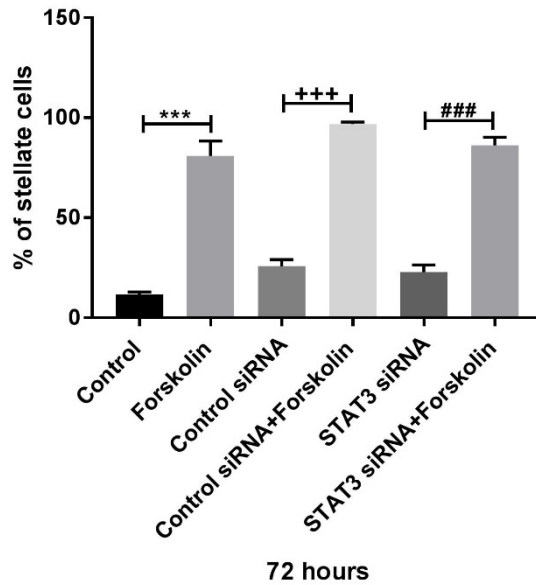
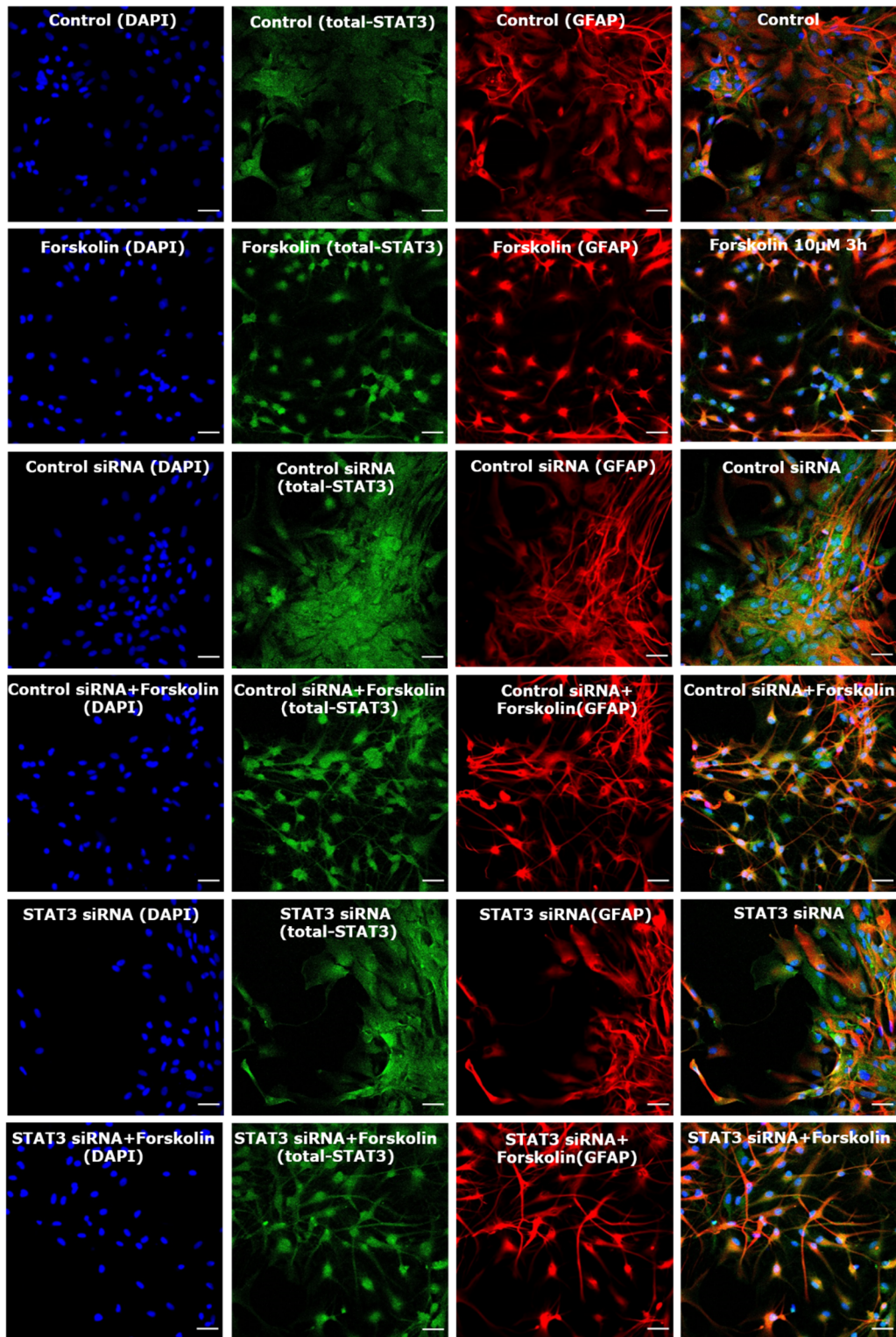
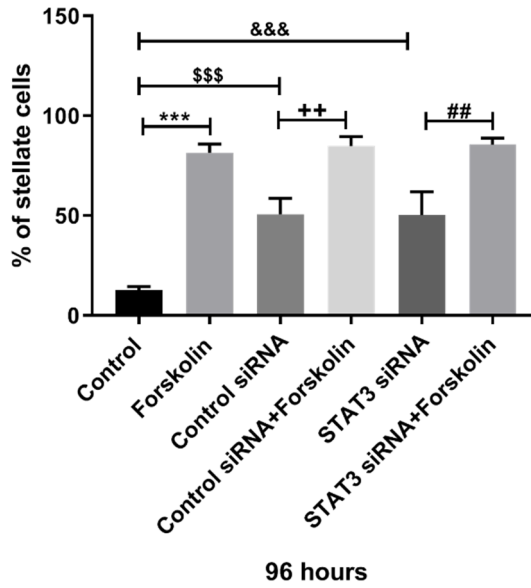


**Figure 5.29 Stellation assay of astrocytes transfected with siRNA knockdown of STAT3 for 72 hours in serum-free medium.** Neonatal cortical astrocytes were imaged with confocal microscopy; cells are stained with GFAP in red, total-STAT3 in green and DAPI in blue. Cells are transfected with 1 $\mu$ M Accell non-targeting control siRNA and Accell STAT3 siRNA following with forskolin 10 $\mu$ M treatment for 3 hours. The scale bar = 40 $\mu$ m. Aggregate data represent the mean of total-STAT3 intensity per pixel and the percentage of stellate cells. Data are presented as a mean  $\pm$  SEM. The statistical significance was determined using the one way ANOVA followed by Tukey's multiple comparisons test, where (\* $P$ <0.05 and \*\*\* $P$ <0.001) was considered statistically significant.



**Stellation assay of STAT3 siRNA  
in neonatal cortical astrocytes**



**Intensity of total STAT3**

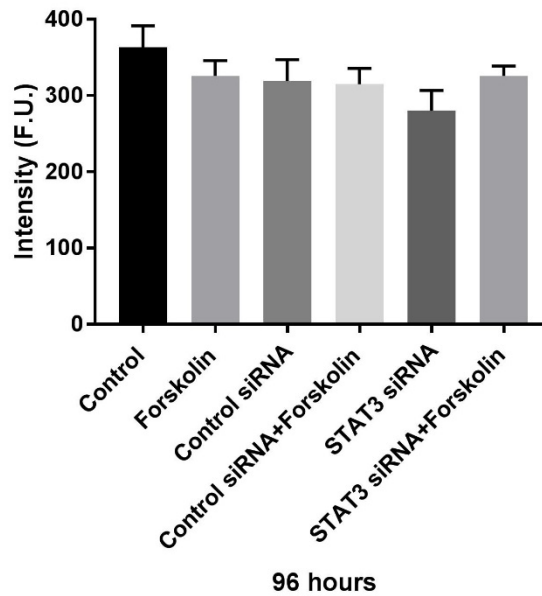


**Figure 5.30 Stellation assay of astrocytes transfected with siRNA knockdown of STAT3 for 96 hours in serum-free medium.** Neonatal cortical astrocytes were imaged with confocal microscopy; cells are stained with GFAP in red, total-STAT3 in green and DAPI in blue. Cells are transfected with 1 $\mu$ M Accell non-targeting control siRNA and Accell STAT3 siRNA following with forskolin 10 $\mu$ M treatment for 3 hours. The scale bar = 40 $\mu$ m. Aggregate data represent the mean of total-STAT3 intensity per pixel and the percentage of stellate cells. Data are presented as a mean  $\pm$  SEM. The statistical significance was determined using the one way ANOVA followed by Tukey's multiple comparisons test, where (\*\*P<0.01 and \*\*\*P<0.001) was considered statistically significant.

### 5.3 Discussion

STAT3 is a key signalling pathway in reactive gliosis and often described as the “master regulator” of gliosis. Several lines of evidence demonstrate the involvement of STAT3 in reactive gliosis in vivo (Herrmann et al., 2008; Sloan and Barres, 2015; Wanner et al., 2013; LeComte et al., 2015; Colombo and Farina, 2016; Kang and Hébert, 2011). Liu et al. (2013) demonstrated that stattic could block the phosphorylation of STAT3 and decreased reactive astrogliosis by reducing GFAP intensity in vivo. This could be due to the inhibition of the transcriptional activity of STAT3. However, in the current study, we found effects within a short time incubation of the inhibitors including both stattic (which is used to suppress STAT3 activation (Schust et al., 2006)) and WP1066 (that is used as a JAK inhibitor (Dimri, Sukanya and De, 2017)). These inhibitors very effectively blocked the stellation process triggered by forskolin and noradrenaline in vitro. This was not just due to compromised cell viability because calcium responses were normal.

The inhibitors gave mixed results for altering cAMP response – in some cases reducing cAMP levels (forskolin in cortical cells), but in other cases having no impact. Some lines of evidence propose that there is an interaction between STAT3 and cAMP or adenylyl cyclase. Increases in cAMP level lead to activation of the Epac-Rap1 pathway and up-regulation of SOCS3, which then down-regulates p-STAT3 (Sands et al., 2006). It was found that cAMP can activate STAT3 by up-regulating IL-1 $\beta$ -induced IL-6 synthesis through enhancement of the JAK2/STAT3 pathway (Tanabe, Kozawa and Iida, 2016). In addition, it was discovered that activation of the adenylyl cyclase/PKA pathway could lead to STAT3 Tyr705 and Ser727 phosphorylation as well as its transcriptional activation in HEK 293 cells via activating ERK, JNK, c-Src, and JAK2 (Liu et al., 2006). However, these processes are based on changes in gene expression due to STAT3 transcription regulation. This could not explain our result because we detected the changes in

1 hour treated with inhibitors and did not decrease the cAMP level in case of noradrenaline. Furthermore, the STAT3 and JAK inhibitors could also block stellation induced by a cAMP analog, suggesting they are operating independently of cAMP synthesis mechanisms. Collectively, these results suggest that cAMP and STAT3 are operating in parallel to bring about astrocyte stellation. Neither pathway alone is sufficient to cause stellation. Both are required.

Measuring changes in p-STAT3 levels in cells treated with forskolin and noradrenaline proved difficult, due to the challenge of quantification of confocal and western blot data. These challenges include the high intensity and expression of p-STAT3 in untreated cells due to the presence of the serum in the medium which contains growth factor that could activate STAT3, and the sensitivity of immunocytochemistry possibly not being enough to detect p-STAT3 levels quantitatively (Fu et al., 2004). These made the results equivocal, but there was some evidence for small changes in p-STAT3 due to forskolin treatment.

In contrast, the response to a positive control – IL-6 – was much clearer, and could be predictably blocked by the STAT3 inhibitors used earlier. However, direct activation of STAT3 by IL-6 did not in itself cause stellation. März et al. (1999) found that long term treatment with IL-6 and sIL-6 receptor over several days lead to changes in astrocytes morphology to a fibrous phenotype. Still, because IL-6 alone was unable to keep STAT3 signalling going for 7 days (as it will be degraded), it required treatment with a stabilised form. Here, IL-6 was added for a few hours, but we know that through 10 minutes the level of p-STAT3 can increase.

Interestingly, the level of p-STAT3 in neonatal cortical astrocytes was consistently higher than in spinal or embryonic astrocytes. Thus, STAT3 levels do correlate with the ability to undergo stellation. Consistent with these findings, Gautron, De Smedt-Peyrusse and Layé (2006) established that the STAT3 level was increased

by age (P3, P10, and P21). However, serine and tyrosine phosphorylation of STAT3 can be identified in the embryonic and postnatal brain (Fu et al., 2004), and expression of STAT3 in embryonic and postnatal stages is necessary to transit astrocytes from immature and nestin-containing cells to mature and GFAP-containing astrocytes (Kálmán and Ajtai, 2001).

Overall, our results suggest that cAMP and STAT3 are both necessary for stellation, but there is little evidence for a large increase in STAT3 phosphorylation in response to agents that can induce stellation. The signalling pathways, therefore, appear to work in parallel to facilitate stellation, but STAT3 may be playing a “permissive” role, where tonic levels (or the tonic activation observed in serum-containing media) is sufficient to cause stellation. The observation that WP1066 as an upstream JAK inhibitor has similar effects to static supports the idea of tonic signalling being required for stellation.

A previous study has shown that PI3K inhibition induces the depolymerisation of actin stress fibres and stellation of astrocytes (Perez et al., 2005). However, we found here that PI3K inhibitor alone did not cause stellation and co-treatment of the astrocytes with forskolin and PI3K inhibitor did not prevent cells stellation either. These suggest that PI3K inhibitor does not have a role in stellation. Inhibiting PKA, which is the known pathway to activate STAT3 through cAMP, did not significantly block stellation with forskolin. It was found that Rho kinase inhibitor, but not the protein kinase C inhibitor or the protein kinase A inhibitor produce stellation (Abe and Misawa, 2003). This finding is correlated with our results; we discovered that only RhoA inhibitor but not PKA or Akt inhibitors induce stellation. These indicate the role of RhoA inhibitor in modifying the astrocyte cytoskeleton and induce stellation (Zeug et al., 2018) effect by cAMP and this pathway could be a link to STAT3 cause stellation rather than PKA pathway.

Identifying the exact sequence of events for stellation will be challenging, given the range of known sites for crosstalk between the pathways (Figure 5.31).

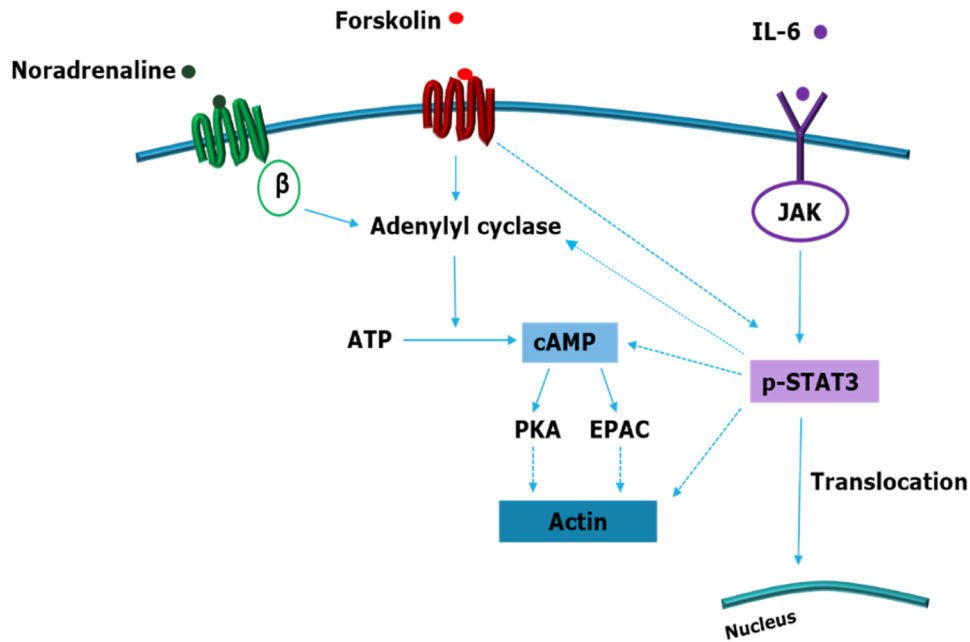


**Figure 5.31 Known pathways for potential crosstalk between cAMP and STAT3 signalling**

As a final result of note, the time scale of stellation seems inconsistent with a transcriptional role of STAT3. A 1 hour pre-incubation is sufficient to block stellation, and stellation is measurable within 2-3 hours of forskolin or noradrenaline treatment. This may indicate a non-genomic mechanism of action for STAT3.

Unfortunately, attempts to validate pharmacological results with siRNA were unsuccessful, leaving open the possibility that the inhibitors could be having off-target effects. siRNA is a synthetic RNA duplex designed to induce gene knockdown in a variety of cell. We used Accell siRNA because it has advantages which have a novel passive-entry mechanism through the cell membrane and can transfect cell types without any need for transfection reagents, lentiviral vectors, or electroporation/nucleofection instrument (Strezoska and Yamada, 2018). Moreover, using other methods could induce cells stress and change their morphology for untreated cells. However, we discovered the same problem with

this technique. Therefore, this experiment is not suitable for this study because we are interested in studying astrocytes morphology in vitro.

To conclude, the data in this chapter provides evidence for a novel non-genomic role of p-STAT3 in astrocytes stellation. Several experiments still need to be done to test this hypothesis, such as non-pharmacological STAT3 knockdown, and there is further need to find the link between p-STAT3 blockers and cytoskeletal rearrangements.

## **Chapter 6 General discussion**

## **6.1 Summary of findings**

The introduction of this thesis described how astrocytes are an essential cell in the CNS under physiological and pathological conditions. There is a significant level of uncertainty about how and when astrocytes become reactive during the onset of many diseases to form foci of reactive gliosis. Nevertheless, the mechanisms of reactive astrocytes are not well understood. In this work, the main goal was to investigate the mechanisms underlying reactive gliosis for astrocytes in different CNS regions and during development in vitro.

We first tested different assays of reactive gliosis. We found that stellation is the most reliable assay for neonatal cortical astrocytes, as it demonstrated time-dependent, reproducible effects in response to forskolin and noradrenaline. We tested the stellation assay in neonatal spinal and embryonic cortical astrocytes to investigate how the other astrocytes (spinal and embryonic cortical) induce stellation: is it the same level of stellation as the neonatal cortical astrocytes? Our results revealed significant differences in astrocyte stellation depending on the CNS region and during development. We aimed to identify the primary mechanism underlying these differences in stellation and discovered that stellation induced in astrocytes is controlled by the STAT3 and cAMP signalling pathway.

## **6.2 Overall significance of findings**

### **6.2.1 Quantitative assays of reactive gliosis**

In chapter 3, we tested different assays of reactive gliosis in response to various stimuli known to induce gliosis in vivo. These assays were: assessing the morphological change of astrocytes with GFAP immunocytochemistry, live imaging of cells loaded with calcein-AM, testing for up-regulation of P2Y<sub>14</sub>R GPCR by Ca<sup>2+</sup> imaging and measuring the intensity of p-STAT3 in the nucleus.

Through GFAP labelling, we found significant stellation in response to forskolin and noradrenaline, an outcome consistent with other studies (Tanabe, Kozawa and Iida, 2016; Donnell et al., 2013). In contrast, the other inflammatory stimuli

tested, LPS and TNF $\alpha$ , did not reliably induce stellation for any of the astrocyte types tested; however, it was found that these compounds are linked to gliosis in vivo (Morioka et al., 2015; Zamanian et al., 2012). A possible explanation for this observation is that the full gliosis response requires the presence of microglia as a second cell class that communicates with astrocytes (Liddelow et al., 2017; Vega-Avelaira, Moss and Fitzgerald, 2007; Norden et al., 2016). Moreover, the expression of TLR4 in astrocytes is controversial, and the presence of TLR4-positive microglia with astrocytes determines the astrocyte response to LPS (Holm, Draeby and Owens, 2012; Facci et al., 2014). Other investigators have also observed that LPS is unable to induce any morphological alterations in astrocytes (Norden et al., 2016).

As an alternative to the standard stellation method, we developed a live-cell morphological assay based on cytoplasmic loading of the astrocytes with calcein-AM. The advantage of this assay is that it allowed for real-time imaging of changes in cell shape. By monitoring cell perimeter and area after the addition of stellation-inducing agents, it was possible to observe changes in cell morphology within minutes of adding forskolin. The circularity of the astrocytes decreased during stellation. The disadvantage of this approach is that it is laborious when analysed manually and suffers due to subjectivity in identifying the edge of the cell reliably. In principle, it would be possible to automate the process. This would also solve the problem that only a small sample of the cell population can be measured. If automation could be developed, this method would be much more useful.

Moving to test the functional assays of reactive gliosis, a previous study by Hamby et al. (2012) showed that treating the astrocytes with inflammatory stimuli can change the level of the P2Y<sub>14</sub> receptor and increase Ca<sup>2+</sup> signalling, which is consistent with the role of this receptor in other inflammatory states (Abbracchio et al., 2003; Bianco et al., 2005; Moore et al., 2003; Lazarowski and Harden, 2015). However, our results demonstrate that the neonatal cortical astrocytes

treated with forskolin, but not with LPS and TNF $\alpha$ , individually have a small increase in mean Ca<sup>2+</sup> release due to up-regulation of the P2Y<sub>14</sub> receptor in reactive astrocytes, but this was not statistically significant due to a high degree of variation between groups. One explanation for this inconsistency is that the combinational treatment of inflammatory stimuli used by Hamby et al. may be essential to change the level of the P2Y<sub>14</sub> receptor and increase Ca<sup>2+</sup> signalling (Hamby et al., 2012), and individual stimuli were insufficient. Regardless, this did not seem to be a reliable assay, as any changes we observed were not nearly as dramatic and reproducible as those reported by Hamby et al.

The p-STAT3 intensity was also tested. We discovered that serine p-STAT3 intensity increased in the nucleus after exposure to forskolin, LPS and TNF $\alpha$  as measured by confocal imaging, but only TNF $\alpha$  could increase the localisation of tyrosine p-STAT3 in the nucleus. This result was partially consistent with other studies which highlighted the importance of STAT3 activation in reactive astrocytes (Liu et al., 2013; Sofroniew, 2009; Zhang et al., 2013). However, the observed changes were small in magnitude, and further attempts to investigate tyrosine STAT3 phosphorylation but not serine STAT3 phosphorylation by Western blots gave similarly small responses, which were on the limit of detection. In contrast, stimulation with a well-known activator of Y705 p-STAT3, IL-6, gave larger responses that could be easily measured; however, uridine-5'-triphosphate (UTP), a S727 p-STAT3 activator (Washburn and Neary, 2006), was not used. This makes it challenging to determine whether the treatment (forskolin) did not activate serine p-STAT3 or if there was a problem with the antibody, which is a shortcoming of this experiment. Together, these results suggest that stellation can occur without overt changes in the distribution of p-STAT3 in the nucleus.

To conclude the usefulness of these assays, we can say that the astrocytes continue to be heterogeneous in their behaviour. None of the assays gave predictable results, but the most useful, reliable and reproducible assay was

stellation; however, most of the inflammatory agents tested and known to trigger reactive gliosis *in vivo* did not induce stellation. Moreover, stellation did not appear to be associated with the accumulation of p-STAT3 in the nucleus. Therefore, it is probable that stellation is not related to the gene expression regulation of STAT3 the same as reactive gliosis. This makes the correlation between stellation and reactive gliosis less clear.

Culturing astrocytes in serum-free medium results in stellation of cells without treating them with any stimuli inducing reactive gliosis, whereas treating the astrocytes with microglial-conditioned medium activated with LPS or treating them with IL-1 $\alpha$ , TNF $\alpha$ , and C1q in combination can induce A1 phenotype astrocytes characterised with a non-stellate cell shape (Liddelow et al., 2017). These results show that the presence of serum in the culture medium can induce a flat, morphological shape without processes due to a reduction in Mob protein levels, which regulate cell morphogenesis through alteration of the actin cytoskeleton arrangement (Fang et al., 2012).

We are searching for a morphological change in astrocytes *in vitro*. This change does not correspond to astrocyte morphology *in vivo*. *In vivo*, GFAP labelling identifies dramatically star-shaped astrocytes that develop more defined processes and demonstrate up-regulation of GFAP in response to diseases. However, *in vitro*, the morphology is a flat shape that can change into a star shape in the presence of many stimuli. This may suggest that stellation is indeed a process which indicates cultured cells are becoming less reactive.

It is likely the reason why early investigations assumed that stellation *in vitro* was an indicator of reactive gliosis, as a look in the glial scar reveals strongly defined stellate astrocytes (Daginakatte et al., 2008; Fedoroff et al., 1984; Masaki et al., 2000; Tiryaki, Ayres, et al., 2015). Foo et al. (2011) demonstrated that polygonal astrocytes *in vitro* have different genetic profiles compared to astrocytes *in vivo*

and have similar genes compared to reactive astrocytes. Adding the serum to the astrocyte culture medium can induce flat-shaped astrocytes that express high levels of GFAP (Ben Haim et al., 2015a). Conversely, culturing astrocytes in a serum-free medium with heparin-binding EGF-like growth factor (Foo et al., 2011) or a 3D polymer matrix (Puschmann et al., 2013) induces star-shaped astrocytes with reduced reactivity and the same gene expression as resting astrocytes in vivo (Wolfes et al., 2017). Changing polygonal astrocytes into stellate astrocytes is a model used to identify the cellular architecture necessary to maintain the typical astrocyte morphology (Schiweck, Eickholt and Murk, 2018) but may not follow the gene expression profile of reactive astrocytes mentioned in the details of Ben Haim et al. (2015a) and Sofroniew (2009). Similarly, our results reveal that inflammatory mediators do not cause stellation, whereas neurotransmitters like noradrenaline can cause stellation very effectively. These results suggest that stellation may not relate to reactive gliosis but instead mimics the physiological morphology of astrocytes in vivo.

However, both stellation in vitro and reactive gliosis in vivo are regulated by the cytoskeletal organisation. These cytoskeletons include microtubules which are found in a dense network of mature astrocytes, intermediate filament proteins (GFAP and vimentin), the actin cytoskeleton, myosin and the ezrin/radixin/moesin (ERM) protein (Burgos et al., 2007; Schiweck, Eickholt and Murk, 2018). During reactive gliosis, intermediate filament proteins and microtubules bind together to increase and elongate the processes of astrocytes. The actin cytoskeleton has a role in the extension of the processes and induces hypertrophy of astrocytes located around the cell body (Schiweck, Eickholt and Murk, 2018). In the polygonal shape of astrocytes, the actin fibres interact with myosin-II, whereas stellate forms of astrocytes are characterised by the loss and depolymerisation of actin fibres and activation of the Arp2/3-dependent actin protein (Murk et al., 2013).

Altogether, regarding what we found here and in support of other evidence, it appears that the stellation phenomenon is not the early stage of reactive gliosis. It entails rearrangement of the cytoskeleton and does not link to the reactive astrocyte gene profiles.

### **6.2.2 Developmental variation in stellation**

A defining feature of astrocyte responses was their heterogeneity. This makes identifying trends difficult, as there is a lot of variation even within the same treatment group. However, in chapter 4, the results show that astrocyte morphology and function during development and between the cortex and spinal cord were significantly different. In stellation, cortical astrocytes produced a high number of stellate cells compared with spinal astrocytes, and the neonatal stage more readily induced the morphological change than the embryonic. This was correlated with cAMP concentration, which was higher in the brain than the spinal cord and higher during the neonatal stage than the embryonic. For the functional assay, measuring the Ca<sup>2+</sup> responses showed a slight variation between the brain and spinal cord region and developmental stages, but none of the stimuli could induce obvious reactive gliosis by altering the response to UDP-glucose.

This consistency with other studies demonstrated that the changing of astrocyte phenotype is dependent on the cells' region and developmental stages. Regarding morphology changes, here we detected that astrocytes from a different region of the CNS (brain and spinal cord) and during development have the distinct ability to undergo stellation. Similarly, differential astrocyte morphology changes have been observed between brain regions at different time points after injury (Hill, Barbarese and McIntosh, 1996) as well as between adolescent and adulthood astrocytes (Testen et al., 2019). Many factors can affect the change in astrocyte morphology in vivo such as the environment surrounding the astrocyte, status of neurons, neuronal subtypes and properties (Hill, Barbarese and McIntosh, 1996;

Ben Haim and Rowitch, 2016) and the distance of astrocytes from the site of injury (O'Callaghan et al., 2014).

In addition, this heterogeneity may be linked to the element or gene expressed in order to induce stellation, and the amount of this expression is linked to determining how the cell stellate differs according to region and development. Bachoo et al. (2004) determined that at certain ages, each brain region has a distinct molecular profile of genes. Many components such as, cytokines, chemokines and neurotransmitter, was detected to express differently in cortex, cerebellum, optic nerve and brainstem astrocytes (Doyle et al., 2008; Yeh et al., 2009). Regarding developmental changes, Cahoy et al. (2008) discovered that early astrocytes express genes which play a role in astrocyte development, and in a later stage, they demonstrate mature gene expression.

In this study, we are interested in the signalling pathways controlling stellation and what may be the origin of the difference in types of astrocytes. We found that a cAMP analog can induce stellation the same as forskolin, with a high percentage of stellation in neonatal cortical astrocytes and less in neonatal spinal and embryonic cortical astrocytes. Similarly, Won and Oh (2000) discovered neonatal brain astrocyte regional heterogeneity in morphological changes in response to cAMP stimulation in vitro. Moreover, we demonstrate that the level of cAMP is higher in neonatal cortical astrocytes than neonatal spinal and embryonic cortical astrocytes after forskolin and noradrenaline treatment. But the main weakness of these experiments remains repeating the samples from the same cell culture in each condition.

A previous report also described a difference in stellation between E18 and P2 astrocytes (Abe and Saito, 1997). In contrast to our results, they reported that cyclic AMP production was similar in E18 and P2 astrocytes, and only cAMP sensitivity was different. These findings suggest that regional and age-related

heterogeneity of astrocyte stellation may be linked to either differential cAMP synthesis activity or diversity in the sensitivity to cAMP.

Altogether, there were clear differences observed for morphological and functional changes relative to different ages and regions, suggesting a postnatal switch of some sort and regional differences with the capacity to undergo stellation and functional changes. Understanding these changes allows us to recognise the roles of these cells in normal and pathological conditions in the CNS at specific ages and sites.

### **6.2.3 STAT3 controlling astrocyte stellation**

STAT3 is a master regulator of reactive gliosis (Ceyzériat et al., 2018). Studies have demonstrated that STAT3 can regulate the induction of reactive astrogliosis features after spinal cord injury in vivo, such as cell hypertrophy, up-regulation of GFAP and scar formation (Herrmann et al., 2008; Sloan and Barres, 2015; Wanner et al., 2013). Another in vivo study found that blocking the phosphorylation of STAT3 by stattic can decrease reactive astrogliosis by reducing GFAP intensity (Liu et al., 2013). This evidence supports the importance of the transcriptional role of STAT3; however, our evidence suggests that STAT3 regulates the process of astrocyte stellation in vitro on a time-scale inconsistent with changes in transcription activity.

p-STAT3 and JAK inhibitors reduced tonic STAT3 levels and significantly blocked stellation in the presence of forskolin, noradrenaline and a cAMP analog. In addition, the level of p-STAT3 correlated with variation in stellation potential according to age and region. Although p-STAT3 and JAK inhibitors were able to reduce the p-STAT3 protein level as measured by Western blotting, stimuli that induced stellation did not consistently increase p-STAT3 levels or promote nuclear translocation of p-STAT3. Overall, these results suggest that STAT3 is necessary for stellation to proceed, but it can occur without translocation and transcription roles.

STAT3 is necessary but does not seem to directly affect cAMP signalling. We found that the p-STAT3 and JAK inhibitors were able to reduce the level of cAMP in response to forskolin but not with noradrenaline. Also, STAT3 activation by IL-6 (in the absence of AC activation) does not cause stellation. Moreover, forskolin and noradrenaline did not directly increase the level of p-STAT3 to the same extent as IL-6. These results suggest that there is not a linear interaction between STAT3 and cAMP. Instead, they work together in parallel to achieve stellation. However, some studies have demonstrated such a link between both signalling pathways, although it is transcription-based (Sands et al., 2006; Tanabe, Kozawa and Iida, 2016), which seems too slow for a 1 hour incubation of the inhibitors and also does not affect NA-induced cAMP increases.

We also found that the time course of stellation (especially from calcein-AM assays) indicates a rapid phenomenon that is complete within two hours and detectable within minutes following treatment with forskolin or noradrenaline. On the other hand, STAT3 is a transcription factor which requires a longer time (up to 72 hours) to achieve its genomic role (Tripathi et al., 2017). Many studies have found that STAT3 can have non-genomic functions which can occur in the cytoplasm. STAT3 can inhibit the stathmin protein in the cytoplasm (Ng et al., 2006), which regulates the microtubule cytoskeleton (Rubin and Atweh, 2004). Knockdown STAT3 in astrocytes reduced the amount of phosphorylated ezrin by an unknown mechanism that prevents the inhibition of RhoA and induces stellation (Renault-Mihara et al., 2017). STAT3 inhibits the negative role of the phosphatase and tensin homolog (PTEN) to form a glial scar (Renault-Mihara and Okano, 2018). Furthermore, activation of Rac1 can be regulated by cytoplasmic STAT3 in mouse embryonic fibroblasts (Teng et al., 2009). These ideas likely support the results of our work with astrocytes as well. Another mechanism of STAT3 that induces stellation could be the direct interaction with actin in the cytoplasm. It was found

that cucurbitacin I (STAT3 blocker) may play a role in the actin cytoskeleton and modulate cell morphology (Graness, Poli and Goppelt-Struebe, 2006).

Collectively, it is likely that STAT3 and cAMP play an important role in stellation; both are needed and are two parallel signalling pathways working together. The involvement of STAT3 could be through a direct action on the cytoskeleton or protein kinase in the cytoplasm, and the transcription activity of STAT3 does not appear to be necessary, which supports the notion that stellation is not the same phenomenon as reactive gliosis.

### **6.3 Future work**

In this work, there were many limitations that require improvement. For example, manually counting cells impacted reliability, was a time-consuming process and only allowed us to consider a portion of the total number of cells. Automating the analysis of astrocyte stellation would improve reliability, save time and include all cells in the analysis. Measuring the intensity of p-STAT3 by ultra-confocal microscope or Western blots had some flaws such as the variation of GAPDH, presence of serum in astrocyte cultures cause a high intensity and expression of p-STAT3 in untreated cells, and sensitivity of immunocytochemistry to detect p-STAT3 is low. To address them, ELISA can be used to measure the protein level. In addition, an increase in the sample number is needed to effectively measure cAMP levels. While many assays of reactive gliosis were done, measuring the level of cytokines and chemokines or screening the gene profiles is needed to investigate whether we are inducing reactive gliosis or just normal stellate astrocytes.

The results of this thesis suggest that STAT3 is involved in stellation, but further evidence is needed using a genetic STAT3 knockdown model to confirm the results we found with the pharmacological blocking of STAT3 by inhibitors. Future studies should focus on treating the astrocytes with translation and transcription inhibitors with forskolin and stattic to confirm that the stellation is related to the genomic

role of STAT3. Studies should also focus on investigation of the relation between p-STAT3 and cytoskeleton such as actin and measuring the expression of adenylyl cyclase and PKA after inhibition STAT3 to test the possibility of STAT3 may directly activate both or one of them, which can affect the cAMP level.

## List of References

- Abbracchio, J.M. et al. (2003) 'Characterization of the UDP-glucose receptor (re-named here the P2Y<sub>14</sub> receptor) adds diversity to the P2Y receptor family', *TRENDS in Pharmacological Sciences*, 24(2), pp. 52–55. doi: 10.1038/nm0402-338.
- Abe, K and Saito, H. (1997) 'Developmental Changes of Cultured in Cyclic Rat AMP-Stimulated Astrocytes Stellation Cortical', *Jpn J Pharmacology*, 75, pp. 433–438.
- Abe, K. and Misawa, M. (2003) 'Astrocyte stellation induced by Rho kinase inhibitors in culture', *Developmental Brain Research*, 143, pp. 99–104.
- Acarin, L., González, B. and Castellano, B. (2000) 'STAT3 and NFκB activation precedes glial reactivity in the excitotoxically injured young cortex but not in the corresponding distal thalamic nuclei', *Journal of Neuropathology and Experimental Neurology*, 59(2), pp. 151–163. doi: 10.1093/jnen/59.2.151.
- Allen, N. J. and Eroglu, C. (2017) 'Cell Biology of Astrocyte-Synapse Interactions', *Neuron*. Elsevier Inc., 96(3), pp. 697–708. doi: 10.1016/j.neuron.2017.09.056.
- Anderson, M. A. et al. (2016) 'Astrocyte scar formation aids CNS axon regeneration', *Nature*, 532(7598), pp. 195–200. doi: 10.1038/nature17623.Astrocyte.
- Anderson, M. A., Ao, Y. and Sofroniew, M. V. (2014) 'Heterogeneity of reactive astrocytes', *Neuroscience Letters*. Elsevier Ireland Ltd, 565, pp. 23–29. doi: 10.1016/j.neulet.2013.12.030.
- Araque, A. et al. (2002) 'Synaptically released acetylcholine evokes Ca<sup>2+</sup> elevations in astrocytes in hippocampal slices.', *The Journal of neuroscience: the official journal of the Society for Neuroscience*, 22(7), pp. 2443–50. doi: 20026212.
- Araújo, G. et al. (2014) 'Sonic hedgehog signaling regulates mode of cell division of early cerebral cortex progenitors and increases astrogliogenesis', *Frontiers in Cellular Neuroscience*, 8(March), pp. 1–11. doi: 10.3389/fncel.2014.00077.
- Bachoo, R. M. et al. (2004) 'Molecular diversity of astrocytes with implications for neurological disorders', *Proceedings of the National Academy of Sciences*, 101(22), pp. 8384–8389. doi: 10.1073/pnas.0402140101.
- Baorto, D., Mellado, W. and Shelanski, M. L. (1992) 'Astrocyte process growth induction by actin breakdown', *Journal of Cell Biology*, 117(2), pp. 357–367. doi: 10.1083/jcb.117.2.357.
- Barbin, G. et al. (1988) 'Brain astrocytes express region-specific surface glycoproteins in culture', *Glia*, 1(1), pp. 96–103. doi: 10.1002/glia.440010111.
- Barres, B.A., Chun, L.L.Y. and Corey, D.P. (1989) 'Calcium Current in Cortical Astrocytes: Induction by CAMP and Neurotransmitters and Permissive Effect of Serum Factors'. *The Journal of Neuroscience*, 9(9), pp. 3189-3175.

- Bayraktar, O. A. et al. (2015) 'Astrocyte development and heterogeneity', *Cold Spring Harbor Perspectives in Biology*, 7(1). doi: 10.1101/cshperspect.a020362.
- Beckerman, S. et al. (2015) 'Phenotypic Assays to Identify Agents That Induce Reactive Gliosis: A Counter-Screen to Prioritize Compounds for Preclinical Animal Studies'. *Assay and Drug Development Technologies*, 13(7), pp.377-388.
- Bekar, L. K., He, W. and Nedergaard, M. (2008) 'Locus coeruleus  $\alpha$ -adrenergic-mediated activation of cortical astrocytes in vivo', *Cerebral Cortex*, 18(12), pp. 2789–2795. doi: 10.1093/cercor/bhn040.
- Ben Haim, L. and Rowitch, D. H. (2016) 'Functional diversity of astrocytes in neural circuit regulation', *Nature Reviews Neuroscience*. Nature Publishing Group, 18(1), pp. 31–41. doi: 10.1038/nrn.2016.159.
- Ben Haim, L. et al. (2015a) 'Elusive roles for reactive astrocytes in neurodegenerative diseases', *Frontiers in Cellular Neuroscience*, 9(August), pp. 1–27. doi: 10.3389/fncel.2015.00278.
- Ben Haim, L. et al. (2015b) 'The JAK/STAT3 Pathway Is a Common Inducer of Astrocyte Reactivity in Alzheimer's and Huntington's Diseases', *Journal of Neuroscience*, 35(6), pp. 2817–2829. doi: 10.1523/JNEUROSCI.3516-14.2015.
- Benarroch, E. (2005). 'Neuron-Astrocyte Interactions: Partnership for Normal Function and Disease in the Central Nervous System'. *Mayo Clinic Proceedings*, 80(10), pp.1326-1338.
- Benito-Muñoz, M., Matute, C. and Cavaliere, F. (2016) 'Adenosine A1 receptor inhibits postnatal neurogenesis and sustains astrogliogenesis from the subventricular zone', *Glia*, 64(9), pp. 1465–1478. doi: 10.1002/glia.23010.
- Bernal, G. M. and Peterson, D. A. (2011) 'Phenotypic and Gene Expression Modification with Normal Brain Aging in GFAP-Positive Astrocytes and Neural Stem Cells', *Aging Cell*, 466–482(3), pp. 466–482. doi: 10.1111/j.1474-9726.2011.00694.x.Phenotypic.
- Bianco, F. et al. (2005) 'Pathophysiological roles of extracellular nucleotides in glial cells: Differential expression of purinergic receptors in resting and activated microglia', *Brain Research Reviews*, 48(2), pp. 144–156. doi: 10.1016/j.brainresrev.2004.12.004.
- Birck, C. et al. (2016) 'Transcriptomic analyses of primary astrocytes under TNF $\alpha$  treatment', *Genomics Data*. The Authors, 7, pp. 7–11. doi: 10.1016/j.gdata.2015.11.005.
- Black, J. A., Sontheimer, H. and Waxman, S. G. (1993) 'Spinal cord astrocytes in vitro: Phenotypic diversity and sodium channel immunoreactivity', *Glia*, 7(4), pp. 272–285. doi: 10.1002/glia.440070403.
- Boisvert, M. M. et al. (2018) 'The Aging Astrocyte Transcriptome from Multiple Regions of the Mouse Brain', *Cell Reports*. ElsevierCompany., 22(1), pp. 269–285. doi: 10.1016/j.celrep.2017.12.039.

- Bosworth, A. P. and Allen, N. J. (2017) 'The diverse actions of astrocytes during synaptic development', *Current Opinion in Neurobiology*. Elsevier Ltd, 47, pp. 38–43. doi: 10.1016/j.conb.2017.08.017.
- Brambilla, R. et al. (2009) 'Transgenic inhibition of astroglial NF- $\kappa$ B leads to increased axonal sparing and sprouting following spinal cord injury', *Journal of Neurochemistry*, 110(2), pp.765-778.
- Brozzi, F. et al. (2009) 'S100B protein regulates astrocyte shape and migration via interaction with Src kinase: Implications for astrocyte development, activation, and tumor growth', *Journal of Biological Chemistry*, 284(13), pp. 8797–8811. doi: 10.1074/jbc.M805897200.
- Buffo, A., Rolando, C. and Ceruti, S. (2010) 'Astrocytes in the damaged brain: Molecular and cellular insights into their reactive response and healing potential', *Biochemical Pharmacology*, 79(2), pp. 77–89. doi: 10.1016/j.bcp.2009.09.014.
- Buosi, A. S. et al. (2017) 'Heterogeneity in Synaptogenic Profile of Astrocytes from Different Brain Regions', *Molecular Neurobiology*. *Molecular Neurobiology*, pp. 1–12. doi: 10.1007/s12035-016-0343-z.
- Burda, J. E. and Sofroniew, M. V. (2014) 'Reactive gliosis and the multicellular response to CNS damage and disease', *Neuron*. Elsevier Inc., 81(2), pp. 229–248. doi: 10.1016/j.neuron.2013.12.034.
- Burgos, M. et al. (2007) 'PKC $\epsilon$  induces astrocyte stellation by modulating multiple cytoskeletal proteins and interacting with Rho a signalling pathways: Implications for neuroinflammation', *European Journal of Neuroscience*, 25(4), pp. 1069–1078. doi: 10.1111/j.1460-9568.2007.05364.x.
- Cahoy, J. D. et al. (2008) 'A transcriptome database for astrocytes, neurons, and oligodendrocytes: a new resource for understanding brain development and function', *The Journal of neuroscience: the official journal of the Society for Neuroscience*, 28(1), pp. 264–78. doi: 10.1523/JNEUROSCI.4178-07.2008.
- Cai, Z., Schools, G. P. and Kimelberg, H. K. (2000) 'Metabotropic Glutamate Receptors in Acutely Isolated Hippocampal Astrocytes: Developmental Changes of mGluR5 mRNA and Functional Expression', *GLIA*, 29, pp. 70–80.
- Cao, F. et al. (2010) 'Conditional deletion of Stat3 promotes neurogenesis and inhibits astrogliogenesis in neural stem cells', *Biochemical and Biophysical Research Communications*. Elsevier Inc., 394(3), pp. 843–847. doi: 10.1016/j.bbrc.2010.03.092.
- Cao, P. et al. (2019) 'The age-related changes and differences in energy metabolism and glutamate-glutamine recycling in the D-gal-induced and naturally occurring senescent astrocytes in vitro', *Experimental Gerontology*. Elsevier, 118(December 2018), pp. 9–18. doi: 10.1016/j.exger.2018.12.018.
- Ceyzériat, K. et al. (2016) 'The complex STATES of astrocyte reactivity: How are they controlled by the JAK-STAT3 pathway?', *Neuroscience*, 330, pp. 205–218. doi: 10.1016/j.neuroscience.2016.05.043.

- Ceyzériat, K. et al. (2018) 'Modulation of astrocyte reactivity improves functional deficits in mouse models of Alzheimer's disease', *Acta neuropathologica communications*. *Acta Neuropathologica Communications*, 6(1), p. 104. doi: 10.1186/s40478-018-0606-1.
- Chaboub, L. S. and Deneen, B. (2012) 'Developmental origins of astrocyte heterogeneity: The final frontier of CNS development', *Developmental Neuroscience*, 34(5), pp. 379–388. doi: 10.1159/000343723.
- Chaboub, L. S. and Deneen, B. (2013) 'Astrocyte form and function in the developing central nervous system', *Seminars in Pediatric Neurology*. Elsevier, 20(4), pp. 230–235. doi: 10.1016/j.spen.2013.10.003.
- Chai, H. et al. (2017) 'Neural circuit-specialized astrocytes: transcriptomic, proteomic, morphological and functional evidence', *Neuron*, 95(3), pp. 531–549. doi: 10.1126/science.aar3799.Tropism.
- Chang, Y., et al. (2010) 'Unilateral Focal Burn Injury Is Followed by Long-Lasting Bilateral Allodynia and Neuronal Hyperexcitability in Spinal Cord Dorsal Horn', *The Journal of Pain*, 11(2), pp.119-130.
- Chiang, C., Sessle, B. and Dostrovsky, J. (2012). 'Role of Astrocytes in Pain'. *Neurochem Res*, 37(11), pp.2419-2431.
- Christiansen, S. H. et al. (2011) 'Combined anti-inflammatory effects of  $\beta$ 2-adrenergic agonists and PDE4 inhibitors on astrocytes by up-regulation of intracellular cAMP', *Neurochemistry International*. Elsevier B.V., 59(6), pp. 837–846. doi: 10.1016/j.neuint.2011.08.012.
- Clarke, L. E. et al. (2018) 'Normal aging induces A1-like astrocyte reactivity', *Proceedings of the National Academy of Sciences*, 115(8), pp. E1896–E1905. doi: 10.1073/pnas.1800165115.
- Coco, S. et al. (2003) 'Storage and Release of ATP from Astrocytes in Culture', *Journal of Biological Chemistry*, 278(2), pp.1354-1362.
- Colombo, E. and Farina, C. (2016) 'Astrocytes: Key Regulators of Neuroinflammation', *Trends in Immunology*, 37(9), pp. 608–620. doi: 10.1016/j.it.2016.06.006.
- Coulombe, P. et al. (2003) 'Rho Family GTPases Are Required for Activation of Jak/STAT Signaling by G Protein-Coupled Receptors', *Molecular and Cellular Biology*, 23(4), pp. 1316–1333. doi: 10.1128/MCB.23.4.1316.
- Daginakatte, G. C. et al. (2008) 'Expression profiling identifies a molecular signature of reactive astrocytes stimulated by cyclic AMP or proinflammatory cytokines', *Experimental Neurology*. Elsevier Inc., 210(1), pp. 261–267. doi: 10.1016/j.expneurol.2007.10.016.
- Debidda, M. et al. (2005) 'A role of STAT3 in Rho GTPase-regulated cell migration and proliferation', *Journal of Biological Chemistry*, 280(17), pp. 17275–17285. doi: 10.1074/jbc.M413187200.

- Deneen, B. et al. (2006) 'The Transcription Factor NFIA Controls the Onset of Gliogenesis in the Developing Spinal Cord', *Neuron*, 52(6), pp. 953–968. doi: 10.1016/j.neuron.2006.11.019.
- Dimri, S., Sukanya and De, A. (2017) 'Approaching non-canonical STAT3 signaling to redefine cancer therapeutic strategy', *Integrative Molecular Medicine*, 4(1), pp. 1–10. doi: 10.15761/IMM.1000268.
- Donnell, J. O. et al. (2013) 'Norepinephrine: A Neuromodulator That Boosts the Function of Multiple Cell Types to Optimize CNS Performance', *Neurochem Res*, 37(11), pp. 2496–2512. doi: 10.1007/s11064-012-0818-x.Norepinephrine.
- Dorf, M. E. et al. (2000) 'Astrocytes express functional chemokine receptors', *Journal of Neuroimmunology*, 111(1–2), pp. 109–121. doi: 10.1016/S0165-5728(00)00371-4.
- Doyle, J. P. et al. (2008) 'Application of BACarray for comparative analysis of CNS cell types', *Cell*, 135(4), pp. 749–762. doi: 10.1016/j.cell.2008.10.029.Application.
- Doyle, K. P. et al. (2010) 'TGF $\beta$  signaling in the brain increases with aging and signals to astrocytes and innate immune cells in the weeks after stroke', *Journal of Neuroinflammation*, 7, pp. 1–13. doi: 10.1186/1742-2094-7-62.
- Dusaban, S. S. et al. (2017) 'Sphingosine 1-phosphate receptor 3 and RhoA signaling mediate inflammatory gene expression in astrocytes', *Journal of Neuroinflammation*. *Journal of Neuroinflammation*, 14(1), pp. 1–10. doi: 10.1186/s12974-017-0882-x.
- East, E., Golding, J. and Phillips, J. (2009) 'A versatile 3D culture model facilitates monitoring of astrocytes undergoing reactive gliosis'. *J Tissue Eng Regen Med*, 3(8), pp.634-646.
- Emsley, J. and Macklis, J. (2006). 'Astroglial heterogeneity closely reflects the neuronal-defined anatomy of the adult murine CNS'. *Neuron Glia Biol*, 2(03), p.175.
- Eriksson, J. E. et al. (2002) 'Intermediate Filament Protein Partnership in Astrocytes', *Journal of Biological Chemistry*, 274(34), pp. 23996–24006. doi: 10.1074/jbc.274.34.23996.
- Facci, L. et al. (2014) 'Toll-like receptors 2, -3 and -4 prime microglia but not astrocytes across central nervous system regions for ATP-dependent interleukin-1 $\beta$  release', *Scientific Reports*, 4, pp. 1–9. doi: 10.1038/srep06824.
- Fahrig, T. and Sommermeyer, H. (1993) 'Dibutyryl cyclic AMP-induced morphological differentiation of rat brain astrocytes increases  $\alpha$ 1-adrenoceptor induced phosphoinositide breakdown by a mechanism involving protein synthesis', *Brain Research*, 602(2), pp. 318–324. doi: 10.1016/0006-8993(93)90696-K.
- Fang, K. M. et al. (2012) 'Mps one binder 2 gene up-regulation in the stellation of astrocytes induced by cAMP-dependent pathway', *Journal of Cellular Biochemistry*, 113(9), pp. 3019–3028. doi: 10.1002/jcb.24180.

- Fang, K. M. et al. (2012) 'Mps one binder 2 gene up-regulation in the stellation of astrocytes induced by cAMP-dependent pathway', *Journal of Cellular Biochemistry*, 113(9), pp. 3019–3028. doi: 10.1002/jcb.24180.
- Faulkner, J. R. (2004) 'Reactive Astrocytes Protect Tissue and Preserve Function after Spinal Cord Injury', *Journal of Neuroscience*, 24(9), pp. 2143–2155. doi: 10.1523/jneurosci.3547-03.2004.
- Favero, C. B. and Mandell, J. W. (2007) 'A pharmacological activator of AMP-activated protein kinase (AMPK) induces astrocyte stellation', *Brain Research*, 7(1168), pp. 1–10. doi: 10.1038/jid.2014.371.
- Fedoroff, S. et al. (1984) 'Astrocyte cell lineage. V. Similarity of astrocytes that form in the presence of dBcAMP in cultures to reactive astrocytes in vivo', *Journal of Neuroscience Research*, 12(1), pp. 15–27. doi: 10.1002/jnr.490120103.
- Fellner, L. et al. (2013) 'Toll-like receptor 4 is required for  $\alpha$ -synuclein dependent activation of microglia and astroglia', *Glia*, 61(3), pp. 349–360. doi: 10.1002/glia.22437.
- Fields, R.D. (2009) 'Purinergic Signaling in Astrocyte Function and Interactions with Neurons', In: Parpura, V. & Haydon, P.G. ed. *Astrocytes in (Patho) Physiology of the Nervous System*. Springer Science + Business Media: LLC, pp. 443-460
- Fitting, S. et al. (2010) 'Regional heterogeneity and diversity in cytokine and chemokine production by astroglia: Differential responses to HIV-1 tat, gp120, and morphine revealed by multiplex analysis', *Journal of Proteome Research*, 9(4), pp. 1795–1804. doi: 10.1021/pr900926n.
- Foo, L. C. et al. (2011) 'Development of a Novel Method for the Purification and Culture of Rodent Astrocytes', *Neuron*, 71(5), pp. 799–811. doi: 10.1016/j.neuron.2011.07.022.Development.
- Formichella, C. et al. (2014) 'Astrocyte Reactivity: A Biomarker for Retinal Ganglion Cell Health in Retinal Neurodegeneration'. *J Clin Cell Immunol*, 05(01), pp1-37.
- Franke, H. and Illes, P. (2014) 'Nucleotide signaling in astrogliosis', *Neuroscience Letters*. Elsevier Ireland Ltd, 565, pp. 14–22. doi: 10.1016/j.neulet.2013.09.056.
- Fu, A. K. Y. et al. (2004) 'Cyclin-dependent kinase 5 phosphorylates signal transducer and activator of transcription 3 and regulates its transcriptional activity', *Proceedings of the National Academy of Sciences*, 101(17), pp. 6728–6733. doi: 10.1073/pnas.0307606100.
- Fukuda, S. et al. (2007) 'Potentiation of Astrogliogenesis by STAT3-Mediated Activation of Bone Morphogenetic Protein-Smad Signaling in Neural Stem Cells', *Molecular and Cellular Biology*, 27(13), pp. 4931–4937. doi: 10.1128/MCB.02435-06.
- Fumagalli, M. et al. (2003) 'Nucleotide-mediated calcium signaling in rat cortical astrocytes: Role of P2X and P2Y receptors', *Glia*, 43(3), pp. 218–230. doi: 10.1002/glia.10248.

- Gao, Y. J. and Ji, R. R. (2010) 'Targeting Astrocyte Signaling for Chronic Pain', *Neurotherapeutics*, 7(4), pp. 482–493. doi: 10.1016/j.nurt.2010.05.016.
- Gautron, L., De Smedt-Peyrusse, V. and Layé, S. (2006) 'Characterization of STAT3-expressing cells in the postnatal rat brain', *Brain Research*, 1098(1), pp. 26–32. doi: 10.1016/j.brainres.2006.04.115.
- Gavin Norris, J. and Benveniste, E. N. (1993) 'Interleukin-6 production by astrocytes: Induction by the neurotransmitter norepinephrine', *Journal of Neuroimmunology*, 45(1–2), pp. 137–145. doi: 10.1016/0165-5728(93)90174-W
- Gavrilyuk, V. et al. (2002) 'Norepinephrine Increases I $\kappa$ B $\alpha$  Expression in Astrocytes', *Journal of Biological Chemistry*, 277(33), pp. 29662–29668. doi: 10.1074/jbc.m203256200.
- Ge, W. P. et al. (2012) 'Local generation of glia is a major astrocyte source in postnatal cortex', *Nature*. Nature Publishing Group, 484(7394), pp. 376–380. doi: 10.1038/nature10959.
- Ge, W.P. and Jia, J.M. (2016) 'Local production of astrocytes in the cerebral cortex', *Neuroscience*, 323, pp. 3–9. doi: 10.1002/cnrc.27633.Percutaneous.
- Gingras, M. et al. (2007) 'Optimized protocols for isolation of primary motor neurons, astrocytes and microglia from embryonic mouse spinal cord', *Journal of Neuroscience Methods*, 163(1), pp. 111–118. doi: 10.1016/j.jneumeth.2007.02.024.
- Gonçalves, C., Concli Leite, M. and Nardin, P. (2008) 'Biological and methodological features of the measurement of S100B, a putative marker of brain injury', *Clinical Biochemistry*, 41(10-11), pp.755-763.
- Gorina, R. et al. (2011) 'Astrocyte TLR4 activation induces a proinflammatory environment through the interplay between MyD88-dependent NF $\kappa$ B signaling, MAPK, and Jak1/Stat1 pathways', *Glia*, 59(2), pp. 242–255. doi: 10.1002/glia.21094.
- Gosselin, R., et al. (2010) 'Glial Cells and Chronic Pain', *The Neuroscientist*, 16(5), pp.519-531.
- Graness, A., Poli, V. and Goppelt-Struebe, M. (2006) 'STAT3-independent inhibition of lysophosphatidic acid-mediated up-regulation of connective tissue growth factor (CTGF) by cucurbitacin I', *Biochemical Pharmacology*, 72(1), pp. 32–41. doi: 10.1016/j.bcp.2006.04.001.
- Guedes, R. P. et al. (2014) 'A20 deficiency causes spontaneous neuroinflammation in mice', *Journal of Neuroinflammation*, 11(1), pp. 1–16. doi: 10.1186/1742-2094-11-122.
- Guillamón-Vivancos, T., Gómez-Pinedo, U. and Matías-Guiu, J. (2015) 'Astrocytes in neurodegenerative diseases (I): function and molecular description', *Neurología (English Edition)*. SEGO, 30(2), pp. 119–129. doi: 10.1016/j.nrleng.2014.12.005.
- Haas, B. et al. (2006) 'Activity-dependent ATP-waves in the mouse neocortex are independent from astrocytic calcium waves'. *Cereb. Cortex* 16, pp. 237–246.

- Hamby, M. E. et al. (2006) 'Characterization of an improved procedure for the removal of microglia from confluent monolayers of primary astrocytes', *Journal of Neuroscience Methods*, 150(1), pp. 128–137. doi: 10.1016/j.jneumeth.2005.06.016.
- Hamby, M. et al. (2012). 'Inflammatory Mediators Alter the Astrocyte Transcriptome and Calcium Signaling Elicited by Multiple G-Protein-Coupled Receptors', *Journal of Neuroscience*, 32(42), pp.14489-14510.
- Han, Z. et al. (2014) 'Inhibition of STAT3 signaling targets both tumor-initiating and differentiated cell populations in prostate cancer', *Oncotarget*, 5(18), pp. 8416–8428. doi: 10.18632/oncotarget.2314.
- Hansen, R. and Malcangio, M. (2013) 'Astrocytes—Multitaskers in chronic pain', *European Journal of Pharmacology*, 716(1-3), pp.120-128.
- Hazan-halevy, I., Harris, D. and Chen, X. (2010) 'STAT3 is constitutively phosphorylated on serine 727 residues, binds DNA and activates transcription in CLL cells Copyright © 2010 American Society of Hematology', 115(14), pp. 2852–2864. doi: 10.1182/blood-2009-10-230060.
- He, F. et al. (2005) 'A positive autoregulatory loop of Jak-STAT signaling controls the onset of astroglialogenesis', *Nat Neurosci*, 8(5), pp. 616–625. doi: 10.1038/mp.2011.182.doi.
- Herrmann, J. E. et al. (2008) 'STAT3 is a Critical Regulator of Astroglialosis and Scar Formation after Spinal Cord Injury', *Journal of Neuroscience*, 28(28), pp. 7231–7243. doi: 10.1523/JNEUROSCI.1709-08.2008.
- Hertz, L. and Zielke, H. (2004) 'Astrocytic control of glutamatergic activity: astrocytes as stars of the show', *Trends in Neurosciences*, 27(12), pp.735-743.
- Hertz, L. et al. (2010) 'Adrenoceptors in brain: Cellular gene expression and effects on astrocytic metabolism and [Ca<sup>2+</sup>]', *Neurochemistry International*, 57(4), pp.411-420.
- Hibino, H. et al. (2004) 'Differential assembly of inwardly rectifying K<sup>+</sup> channel subunits, Kir4.1 and Kir5.1, in brain astrocytes', *Journal of Biological Chemistry*, 279(42), pp. 44065–44073. doi: 10.1074/jbc.M405985200.
- Hill, S. J., Barbarese, E. and McIntosh, T. K. (1996) 'Regional heterogeneity in the response of astrocytes following traumatic brain injury in the adult rat. *Exp. Neurol.*', *J. Neuropathol.*, 55, pp. 1221–1229.
- Hol, E. M. and Pekny, M. (2015) 'Glial fibrillary acidic protein (GFAP) and the astrocyte intermediate filament system in diseases of the central nervous system', *Current Opinion in Cell Biology*. Elsevier Ltd, 32, pp. 121–130. doi: 10.1016/j.ceb.2015.02.004.
- Holm, T. H., Draeby, D. and Owens, T. (2012) 'Microglia are required for astroglial toll-like receptor 4 response and for optimal TLR2 and TLR3 response', *Glia*, 60(4), pp. 630–638. doi: 10.1002/glia.22296.

- Holst, C. B. et al. (2019) 'Astroglialogenesis in human fetal brain: complex spatiotemporal immunoreactivity patterns of GFAP, S100, AQP4 and YKL-40', *Journal of Anatomy*, (January). doi: 10.1111/joa.12948.
- Hu, C. et al. (2012) 'Opposite regulation by PI3K/Akt and MAPK/ERK pathways of tissue factor expression, cell-associated procoagulant activity and invasiveness in MDA-MB-231 cells', *Journal of Hematology and Oncology*, 5(Ea 3829), pp. 1–10. doi: 10.1186/1756-8722-5-16.
- Hu, X. et al. (2019) 'Region-Restrict Astrocytes Exhibit Heterogeneous Susceptibility to Neuronal Reprogramming', *Stem Cell Reports*. Elsevier Company., 12(2), pp. 290–304. doi: 10.1016/j.stemcr.2018.12.017.
- Huang, L. et al. (2015) 'STAT3 Phosphorylation at Tyrosine 705 and Serine 727 Differentially Regulates Mouse ESC Fates', 85(0 1), pp. 1–27. doi: 10.1016/j.neuroimage.2013.08.045.The.
- Huang, L. et al. (2019) 'Astrocyte Signaling in the Neurovascular Unit After Central Nervous System Injury', *International Journal of Molecular Sciences*, 20(2), p. 282. doi: 10.3390/ijms20020282.
- Hucho, T. and Levine, J. D. (2007) 'Signaling Pathways in Sensitization: Toward a Nociceptor Cell Biology', *Neuron*, 55(3), pp. 365–376. doi: 10.1016/j.neuron.2007.07.008.
- Hung, C.C. et al. (2016) 'Astrocytic GAP43 Induced by the TLR4/NF- B/STAT3 Axis Attenuates Astroglial-Mediated Microglial Activation and Neurotoxicity', *Journal of Neuroscience*, 36(6), pp. 2027–2043. doi: 10.1523/jneurosci.3457-15.2016.
- Israel, J. M. et al. (2003) 'GABA<sub>A</sub> Receptor-Expressing Astrocytes in the Supraoptic Nucleus Lack Glutamate Uptake and Receptor Currents', *Glia*, 44(2), pp. 102–110. doi: 10.1002/glia.10272.
- Ito, D. et al. (2001) 'Enhanced Expression of Iba1, Ionized Calcium-Binding Adapter Molecule 1, After Transient Focal Cerebral Ischemia In Rat Brain', *Stroke*, 32(5), pp.1208-1215.
- Jabs, R. et al. (2007) 'Lack of P2X Receptor Mediated Currents in Astrocytes and GluR Type Glial Cells of the Hippocampal CA1 Region', *GLIA*, 55, pp. 1648–1655. doi: 10.1002/glia.
- Jennings, A. and Rusakov, D. (2016) 'Do Astrocytes Respond To Dopamine?', *Opera Medica Et Physiologica*, 2(1 (2)), pp. 47–56.
- Ji, R., Berta, T. and Nedergaard, M. (2013) 'Glia and pain: Is chronic pain a gliopathy? '. *Pain*, 154, pp.S10-S28.
- John, G. R. et al. (2004) 'Interleukin-1 $\beta$  Induces A Reactive Astroglial Phenotype via Deactivation of the Rho GTPase-Rock Axis', *Journal of Neuroscience*, 24(11), pp. 2837–2845. doi: 10.1523/JNEUROSCI.4789-03.2004.
- John, G. R. et al. (2005) 'IL-1-regulated responses in astrocytes: Relevance to injury and recovery', *Glia*, 49(2), pp. 161–176. doi: 10.1002/glia.20109.

- Junker, V. et al. (2002) 'Stimulation of  $\beta$ -adrenoceptors activates astrocytes and provides neuroprotection', *European Journal of Pharmacology*, 446(1–3), pp. 25–36. doi: 10.1016/S0014-2999(02)01814-9.
- Kálmán, M. and Ajtai, B. M. (2001) 'A comparison of intermediate filament markers for presumptive astroglia in the developing rat neocortex: Immunostaining against nestin reveals more detail, than GFAP or vimentin', *International Journal of Developmental Neuroscience*, 19(1), pp. 101–108. doi: 10.1016/S0736-5748(00)00058-7.
- Kang, J., et al. (2008) 'Connexin 43 Hemichannels Are Permeable to ATP', *Journal of Neuroscience*, 28(18), pp.4702-4711.
- Kang, W. and Hébert, J. M. (2011) 'Signaling pathways in reactive astrocytes, a genetic perspective', *Molecular Neurobiology*, 43(3), pp. 147–154. doi: 10.1007/s12035-011-8163-7.
- Kang, W. et al. (2014) 'Astrocyte activation is suppressed in both normal and injured brain by FGF signaling'. *Proceedings of the National Academy of Sciences*, 111(29), pp.E2987-E2995.
- Karavanova, I. et al. (2007) 'Novel regional and developmental NMDA receptor expression patterns uncovered in NR2C subunit- $\beta$ -galactosidase knock-in mice', *Molecular and Cellular Neuroscience*, 34(3), pp. 468–480. doi: 10.1016/j.mcn.2006.12.001.
- Kerstetter, A.E. and Miller, R.H. (2012). 'Isolation and Culture of Spinal Cord Astrocytes'. In: Milner, R. ed. *Astrocytes: Methods and Protocols*, *Methods in Molecular Biology*. Springer Science+Business Media: LLC, pp.93-104
- Khakh, B. S. and Sofroniew, M. V. (2015) 'Diversity of astrocyte functions and phenotypes in neural circuits', *Nature Neuroscience*. Nature Publishing Group, 18(7), pp. 942–952. doi: 10.1038/nn.4043.
- Kim, Y. H. et al. (2010) 'Differential regulation of proliferation and differentiation in neural precursor cells by the Jak pathway', *Stem Cells*, 28(10), pp. 1816–1828. doi: 10.1002/stem.511.
- Kimelberg, H. K. (2010) 'Functions of mature mammalian astrocytes: A current view', *Neuroscientist*, 16(1), pp. 79–106. doi: 10.1177/1073858409342593.
- Kinoshita, M. et al. (2013) 'Secretion of matrix metalloproteinase-9 from astrocytes by inhibition of tonic P2Y<sub>14</sub>-receptor-mediated signal(s)', *Cellular and Molecular Neurobiology*, 33(1), pp. 47–58. doi: 10.1007/s10571-012-9869-4.
- Klein, R. S. and Fricker, L. D. (1992) 'Heterogeneous expression of carboxypeptidase E and proenkephalin mRNAs by cultured astrocytes', *Brain Research*, 569(2), pp. 300–310. doi: 10.1016/0006-8993(92)90643-N.
- Kubo, A. et al. (1991) 'Histamine-induced cyclic AMP accumulation in type-1 and type-2 astrocytes in primary culture', *European Journal of Pharmacology: Molecular Pharmacology*, 208(3), pp. 249–253. doi: 10.1016/0922-

4106(91)90102-N.

Lalo, U. et al. (2008) 'P2X1 and P2X5 Subunits Form the Functional P2X Receptor in Mouse Cortical Astrocytes', *Journal of Neuroscience*, 28(21), pp. 5473–5480. doi: 10.1523/jneurosci.1149-08.2008.

Laureys, G. et al. (2014) 'β2-adrenergic agonists modulate TNF-α induced astrocytic inflammatory gene expression and brain inflammatory cell populations', *Journal of Neuroinflammation*, 11, pp. 1–10. doi: 10.1186/1742-2094-11-21.

Lazarowski, E. R. and Harden, T. K. (2015) 'UDP-sugars as extracellular signaling molecules: Cellular and physiologic consequences of P2Y14 receptor activation', *Molecular Pharmacology*, 88(1), pp. 151–160. doi: 10.1124/mol.115.098756.

LeComte, M. D. et al. (2015) 'Notch1–STAT3–ETB R signaling axis controls reactive astrocyte proliferation after brain injury ', *Proceedings of the National Academy of Sciences*, 112(28), pp. 8726–8731. doi: 10.1073/pnas.1501029112.

Lee, C. et al. (2017) 'Selective induction of alternatively spliced FynT isoform by TNF facilitates persistent inflammatory responses in astrocytes'. *Scientific Reports*, 7, p.43651.

Lehre, K.P. et al. (1995) 'Differential expression of two glial glutamate transporters in the rat brain: quantitative and immunocytochemical observations'. *J. Neurosci.* 15, 1835–1853.

Li, T. et al. (2019) 'update on reactive astrocyte in CCI'. *Journal of Neuroinflammation*, pp. 1–13. Available at: <https://jneuroinflammation.biomedcentral.com/track/pdf/10.1186/s12974-019-1524-2>.

Liddel, S. A. and Barres, B. A. (2017) 'Reactive Astrocytes: Production, Function, and Therapeutic Potential', *Immunity*. Elsevier Inc., 46(6), pp. 957–967. doi: 10.1016/j.immuni.2017.06.006.

Liddel, S. A. et al. (2017) 'Neurotoxic reactive astrocytes are induced by activated microglia', *Nature*. Nature Publishing Group, 541(7638), pp. 481–487. doi: 10.1038/nature21029.

Lin, G. S. et al. (2014) 'STAT3 serine 727 phosphorylation influences clinical outcome in glioblastoma', *International Journal of Clinical and Experimental Pathology*, 7(6), pp. 3141–3149.

Lin, S. et al. (2008) 'Tetrahydrocannabinol suppresses LPS-induced astrocyte activation via modulating IKKs-IκBα-NF-κB signaling pathway'. *Molecular and Cellular Biochemistry*, 315(1-2), pp.41-49.

Liu, A. M. F. et al. (2006) 'Activation of STAT3 by Gas distinctively requires protein kinase A, JNK, and phosphatidylinositol 3-kinase', *Journal of Biological Chemistry*, 281(47), pp. 35812–35825. doi: 10.1074/jbc.M605288200.

- Liu, X. et al. (2013) 'Stat3 Inhibition Attenuates Mechanical Allodynia through Transcriptional Regulation of Chemokine Expression in Spinal Astrocytes', *PLoS ONE*, 8(10). doi: 10.1371/journal.pone.0075804.
- Lukin, J. et al. (2017) 'Toll-Like Receptor 4 (TLR4) and Triggering Receptor Expressed on Myeloid Cells-2 (TREM-2) Activation Balance Astrocyte Polarization into a Proinflammatory Phenotype', *Molecular Neurobiology*. *Molecular Neurobiology*, 4. doi: 10.1007/s12035-017-0618-z.
- Luo, X., et al. (2016) 'Crosstalk between astrocytic CXCL12 and microglial CXCR4 contributes to the development of neuropathic pain', *Molecular Pain*, 12(0), pp.1-15
- Lynch, A. M. et al. (2010) 'The impact of glial activation in the aging brain', *Aging and disease*, 1(3), pp. 262–78. Available at: <http://www.ncbi.nlm.nih.gov/pubmed/22396865>  
<http://www.pubmedcentral.nih.gov/articlerender.fcgi?artid=PMC3295033>.
- Magavi, S. et al. (2012) 'Coincident generation of pyramidal neurons and protoplasmic astrocytes in neocortical columns', *Journal of Neuroscience*, 32(14), pp. 4762–4772. doi: 10.1523/JNEUROSCI.3560-11.2012.
- Malatesta, P., Appolloni, I. and Calzolari, F. (2008) 'Radial glia and neural stem cells'. *Cell Tissue Res*, 331(1), pp.165-178.
- Martini, S. et al. (2013) 'A critical role for Sox9 in Notch-induced astrogliogenesis and stem cell maintenance', *Stem Cells*, 31(4), pp. 741–751. doi: 10.1002/stem.1320.
- März, P. et al. (1999) 'Role of interleukin-6 and soluble IL-6 receptor in region-specific induction of astrocytic differentiation and neurotrophin expression', *Glia*, 26(3), pp. 191–200. doi: 10.1002/(SICI)1098-1136(199905)26:3<191::AID-GLIA1>3.0.CO;2-#.
- Masaki, R. et al. (2000) '7 $\beta$ -Hydroxysterol is cytotoxic to neonatal rat astrocytes in primary culture when cAMP levels are increased', *Journal of Neuroscience Research*, 62(1), pp. 99–111. doi: 10.1002/1097-4547(20001001)62:1<99::AID-JNR11>3.0.CO;2-2.
- Masliantsev, K. et al. (2018) 'Impact of STAT3 phosphorylation in glioblastoma stem cells radiosensitization and patient outcome', *Oncotarget*, 9(3), pp. 3968–3979. doi: 10.18632/oncotarget.23374.
- Matias, I., Morgado, J. and Gomes, F. C. A. (2019) 'Astrocyte Heterogeneity: Impact to Brain Aging and Disease', *Frontiers in Aging Neuroscience*, 11(March), pp. 1–18. doi: 10.3389/fnagi.2019.00059.
- Matyash, V. and Kettenmann, H. (2010) 'Heterogeneity in astrocyte morphology and physiology'. *Brain Research Reviews*, 63(1-2), pp.2-10.
- McNamee, E. N. et al. (2010) 'Noradrenaline induces IL-1ra and IL-1 type II receptor expression in primary glial cells and protects against IL-1 $\beta$ -induced neurotoxicity', *European Journal of Pharmacology*. Elsevier B.V., 626(2–3), pp. 219–228. doi: 10.1016/j.ejphar.2009.09.054.

- Meeuwssen, S. et al. (2003) 'Cytokine, chemokine and growth factor gene profiling of cultured human astrocytes after exposure to proinflammatory stimuli', *Glia*, 43(3), pp. 243–253. doi: 10.1002/glia.10259.
- Middeldorp, J. and Hol, E. (2011) 'GFAP in health and disease'. *Progress in Neurobiology*, 93(3), pp.421-443.
- Milligan, E. and Watkins, L. (2009). 'Pathological and protective roles of glia in chronic pain'. *Nature Reviews Neuroscience*, 10(1), pp.23-36.
- Miyano, K. et al. (2010) 'Activation of the neurokinin-1 receptor in rat spinal astrocytes induces Ca<sup>2+</sup> release from IP<sub>3</sub>-sensitive Ca<sup>2+</sup> stores and extracellular Ca<sup>2+</sup> influx through TRPC3', *Neurochemistry International*. Elsevier Ltd, 57(8), pp. 923–934. doi: 10.1016/j.neuint.2010.09.012.
- Miyazaki, I. and Asanuma, M. (2016) 'Serotonin 1A Receptors on Astrocytes as a Potential Target for the Treatment of Parkinson's Disease', *Current Medicinal Chemistry*, 23(7), pp. 686–700. doi: 10.2174/0929867323666160122115057.
- Moldrich, R. et al. (2002). 'Astrocyte mGlu2/3-mediated c-AMP potentiation is calcium sensitive: studies in murine neuronal and astrocyte cultures'. *Neuropharmacology*, 43(2), pp.189-203.
- Molofsky, A. V et al. (2012) 'Astrocytes and disease: a neurodevelopmental perspective', *Genes & Development*, 26, pp. 891–907. doi: 10.1101/gad.188326.112.tal.
- Molofsky, A. V et al. (2014) 'Astrocyte-encoded positional cues maintain sensorimotor circuit integrity', *Nature*, 509(7499), pp. 189–194. doi: 10.1038/nature13161.Astrocyte-encoded.
- Molofsky, A. V. and Deneen, B. (2015) 'Astrocyte development: A Guide for the Perplexed', *Glia*, 63(8), pp. 1320–1329. doi: 10.1002/glia.22836.
- Moore, D. J. et al. (2003) 'GPR105, a novel Gi/o-coupled UDP-glucose receptor expressed on brain glia and peripheral immune cells, is regulated by immunologic challenge: Possible role in neuroimmune function', *Molecular Brain Research*, 118(1–2), pp. 10–23. doi: 10.1016/S0169-328X(03)00330-9.
- Morga, E., Faber, C. and Heuschling, P. (1999) 'Regional heterogeneity of the astroglial immunoreactive phenotype: Effect of lipopolysaccharide', *Journal of Neuroscience Research*, 57(6), pp. 941–952. doi: 10.1002/(SICI)1097-4547(19990915)57:6<941::AID-JNR20>3.0.CO;2-Z.
- Morioka, N. et al. (2015) 'Tumor necrosis factor-mediated down-regulation of spinal astrocytic connexin43 leads to increased glutamatergic neurotransmission and neuropathic pain in mice', *Brain, Behavior, and Immunity*. Elsevier Inc., 49, pp. 293–310. doi: 10.1016/j.bbi.2015.06.015.
- Mothet, J., et al. (2005) 'Glutamate receptor activation triggers a calcium-dependent and SNARE protein-dependent release of the gliotransmitter D-serine', *Proceedings of the National Academy of Sciences*, 102(15), pp.5606-5611

- Murk, K. et al. (2013) 'The antagonistic modulation of Arp2/3 activity by N-WASP, WAVE2 and PICK1 defines dynamic changes in astrocyte morphology', *Journal of Cell Science*, 126(17), pp. 3873–3883. doi: 10.1242/jcs.125146.
- Muyderman, H. et al. (2001) ' $\alpha$ 1-Adrenergic Modulation of Metabotropic Glutamate Receptor-induced Calcium Oscillations and Glutamate Release in Astrocytes', *Journal of Biological Chemistry*, 276(49), pp. 46504–46514. doi: 10.1074/jbc.M103849200.
- Nagy, J. I. et al. (1999) 'Connexin30 in rodent, cat and human brain: Selective expression in gray matter astrocytes, co-localization with connexin43 at gap junction and late developmental appearance', *Neuroscience*, 88(2), pp. 447–468.
- Nakano, Y. et al. (2015) 'Astrocytic TLR4 expression and LPS-induced nuclear translocation of STAT3 in the sensory circumventricular organs of adult mouse brain', *Journal of Neuroimmunology*. Elsevier B.V., 278, pp. 144–158. doi: 10.1016/j.jneuroim.2014.12.013.
- Nam, M. H. et al. (2018) 'Expression of  $\mu$ -opioid receptor in CA1 hippocampal astrocytes', *Experimental Neurobiology*, 27(2), pp. 120–128. doi: 10.5607/en.2018.27.2.120.
- Neal, M. and Richardson, J. R. (2018) 'Epigenetic regulation of astrocyte function in neuroinflammation and neurodegeneration', *Biochimica et Biophysica Acta - Molecular Basis of Disease*. Elsevier, 1864(2), pp. 432–443. doi: 10.1016/j.bbadis.2017.11.004.
- Nedergaard, M., Rodríguez, J. and Verkhratsky, A. (2010) 'Glial calcium and diseases of the nervous system', *Cell Calcium*, 47(2), pp.140-149.
- New, D. C. and Wong, Y. H. (2007) 'Molecular mechanisms mediating the G protein-coupled receptor regulation of cell cycle progression', *Journal of Molecular Signaling*, 2, pp. 1–15. doi: 10.1186/1750-2187-2-2.
- Ng, D. C. H. et al. (2006) 'Stat3 regulates microtubules by antagonizing the depolymerization activity of stathmin', *Journal of Cell Biology*, 172(2), pp. 245–257. doi: 10.1083/jcb.200503021.
- Nimmerjahn, A., Mukamel, E. A. and Schnitzer, M. J. (2010) 'Motor Behavior Activates Bergmann Glial Networks', *Neuron*, 46(2), pp. 220–231. doi: 10.1016/j.freeradbiomed.2008.10.025.The.
- Nobuta, H. et al. (2012) 'STAT3-Mediated astrogliosis protects myelin development in neonatal brain injury', *Annals of Neurology*, 72(5), pp. 750–765. doi: 10.1002/ana.23670.
- Norden, D. M. et al. (2016) 'Sequential activation of microglia and astrocyte cytokine expression precedes increased iba-1 or GFAP immunoreactivity following systemic immune challenge', *Glia*, 64(2), pp. 300–316. doi: 10.1002/glia.22930.
- O'Callaghan, J. P. et al. (2014) 'Early activation of STAT3 regulates reactive astrogliosis induced by diverse forms of neurotoxicity', *PLoS ONE*, 9(7). doi: 10.1371/journal.pone.0102003.

- Oberheim, N.A., Goldman, S.A. and Nedergaard, M. (2012) 'Heterogeneity of Astrocytic Form and Function'. In: Milner, R. ed. *Astrocytes: Methods and Protocols*, Methods in Molecular Biology. Springer Science+Business Media: LLC, pp.23-45
- Okada, S. et al. (2006) 'Conditional ablation of Stat3 or Socs3 discloses a dual role for reactive astrocytes after spinal cord injury', *Nature Medicine*, 12(7), pp. 829–834. doi: 10.1038/nm1425.
- Okada, S. et al. (2018) 'Astrocyte reactivity and astrogliosis after spinal cord injury', *Neuroscience Research*. Elsevier Ireland Ltd and Japan Neuroscience Society, 126, pp. 39–43. doi: 10.1016/j.neures.2017.10.004.
- Old, E.A., Clark, A.K. and Malcangio, M. (2015) 'The Role of Glia in the Spinal Cord in Neuropathic and Inflammatory Pain', In: Schaible, H.G. ed. *Pain Control, Handbook of Experimental Pharmacology* 277. Springer: Berlin, pp. 145-170.
- Olsen, M.L., Campbell, S.L. and Sontheimer, H. (2007) 'Differential distribution of Kir4.1 in spinal cord astrocytes suggests regional differences in K<sup>+</sup> homeostasis', *J. Neurophysiol.* 98, pp.786–793.
- Orre, M. et al. (2014) 'Isolation of glia from Alzheimer's mice reveals inflammation and dysfunction', *Neurobiology of Aging*, 35(12), pp. 2746–2760. doi: 10.1016/j.neurobiolaging.2014.06.004.
- Orthmann-Murphy, J., Abrams, C. and Scherer, S. (2008) 'Gap Junctions Couple Astrocytes and Oligodendrocytes', *Journal of Molecular Neuroscience*, 35(1), pp.101-116.
- Paco, S. et al. (2016) 'Cyclic AMP signaling restricts activation and promotes maturation and antioxidant defenses in astrocytes', *BMC Genomics*. BMC Genomics, 17(1), pp. 1–11. doi: 10.1186/s12864-016-2623-4.
- Paixão, S. & Klein, R. (2010) 'Neuron–astrocyte communication and synaptic plasticity', *Current Opinion in Neurobiology*, 20(4), pp.466-473.
- Pang, Y., Cai, Z. and Rhodes, P. G. (2001) 'Analysis of genes differentially expressed in astrocytes stimulated with lipopolysaccharide using cDNA arrays', *Brain Research*, 914(1–2), pp. 15–22. doi: 10.1016/S0006-8993(01)02766-4.
- Pekny, M. & Nilsson, M. (2005) 'Astrocyte activation and reactive gliosis', *Glia*, 50(4), pp.427-434.
- Pekny, M. and Pekna, M. (2004) 'Astrocyte intermediate filaments in CNS pathologies and regeneration', *Journal of Pathology*, 204(4), pp. 428–437. doi: 10.1002/path.1645.
- Pekny, M. et al. (2019) 'Astrocyte activation and reactive gliosis—A new target in stroke?', *Neuroscience Letters*. Elsevier, 689(May 2018), pp. 45–55. doi: 10.1016/j.neulet.2018.07.021.
- Perez, V. et al. (2005) 'Dynamic reorganization of the astrocyte actin cytoskeleton elicited by cAMP and PACAP: A role for phosphatidylinositol 3-kinase inhibition', *European Journal of Neuroscience*, 21(1), pp. 26–32. doi: 10.1111/j.1460-9568.2004.03845.x.

Petrelli, F. et al. (2018) 'Dysfunction of homeostatic control of dopamine by astrocytes in the developing prefrontal cortex leads to cognitive impairments', *Molecular Psychiatry*. Springer US. doi: 10.1038/s41380-018-0226-y.

Poopalasundaram, S. et al. (2000) 'Glial heterogeneity in expression of the inwardly rectifying K<sup>+</sup> channel, Kir4.1, in adult rat CNS', *Glia*, 30(4), pp. 362–372. doi: 10.1002/(SICI)1098-1136(200006)30:4<362::AID-GLIA50>3.0.CO;2-4.

Porter, J. T. and McCarthy, K. D. (1996) 'Hippocampal Astrocytes In Situ Respond to Glutamate Released from Synaptic Terminals', *The Journal of Neuroscience*, 16(16), pp. 5073–5081.

Potokar, M. et al. (2007) 'Cytoskeleton and vesicle mobility in astrocytes', *Traffic*, 8(1), pp. 12–20. doi: 10.1111/j.1600-0854.2006.00509.x.

Puschmann, T. B. et al. (2013) 'Bioactive 3D cell culture system minimizes cellular stress and maintains the in vivo-like morphological complexity of astroglial cells', *Glia*, 61(3), pp. 432–440. doi: 10.1002/glia.22446.

Racchetti, G., D'Alessandro, R. and Meldolesi, J. (2012) 'Astrocyte stellation, a process dependent on Rac1 is sustained by the regulated exocytosis of enlargeosomes', *Glia*, 60(3), pp. 465–475. doi: 10.1002/glia.22280.

Ramakers, G. J. A. and Moolenaar, W. H. (1998) 'Regulation of astrocyte morphology by RhoA and lysophosphatidic acid', *Experimental Cell Research*, 245(2), pp. 252–262. doi: 10.1006/excr.1998.4224.

Regan, M. R. et al. (2007) 'Variations in Promoter Activity Reveal a Differential Expression and Physiology of Glutamate Transporters by Glia in the Developing and Mature CNS', *Journal of Neuroscience*, 27(25), pp. 6607–6619. doi: 10.1523/JNEUROSCI.0790-07.2007.

Renault-Mihara, F. and Okano, H. (2018) 'STAT3: Down the R(h)oAd', *Cytokine*, 102(August 2017), pp. 149–150. doi: 10.1016/j.cyto.2017.08.003.

Renault-Mihara, F. et al. (2017) 'Regulation of RhoA by STAT3 coordinates glial scar formation', *Journal of Cell Biology*, 216(8), pp. 2533–2550. doi: 10.1083/jcb.201610102.

Rodríguez-Arellano, J. J. et al. (2016) 'Astrocytes in physiological aging and Alzheimer's disease', *Neuroscience*, 323, pp. 170–182. doi: 10.1016/j.neuroscience.2015.01.007.

Rossi, D. (2015) 'Astrocyte physiopathology: At the crossroads of intercellular networking, inflammation and cell death', *Progress in Neurobiology*. Elsevier Ltd, 130, pp. 86–120. doi: 10.1016/j.pneurobio.2015.04.003.

Rowitch, D. H. and Kriegstein, A. R. (2010) 'Developmental genetics of vertebrate glial-cell specification', *Nature*, 468(7321), pp. 214–222. doi: 10.1038/nature09611.

- Rubin, C. I. and Atweh, G. F. (2004) 'The role of stathmin in the regulation of the cell cycle', *Journal of Cellular Biochemistry*, 93(2), pp. 242–250. doi: 10.1002/jcb.20187.
- Rusnakova, V. et al. (2013) 'Heterogeneity of Astrocytes: From Development to Injury – Single Cell Gene Expression', *PLoS ONE*, 8(8), p. e69734. doi: 10.1371/journal.pone.0069734.
- Sadana, R. and Dessauer, C. W. (2009) 'Physiological roles for G protein-regulated adenylyl cyclase isoforms: Insights from knockout and overexpression studies', *NeuroSignals*, 17(1), pp. 5–22. doi: 10.1159/000166277.
- Sands, W. A. et al. (2006) 'Exchange Protein Activated by Cyclic AMP (Epac)-Mediated Induction of Suppressor of Cytokine Signaling 3 (SOCS-3) in Vascular Endothelial Cells', *Molecular and Cellular Biology*, 26(17), pp. 6333–6346. doi: 10.1128/MCB.00207-06.
- Sarafian, T. et al. (2010). 'Disruption of Astrocyte STAT3 Signaling Decreases Mitochondrial Function and Increases Oxidative Stress In Vitro'. *PLoS ONE*, 5(3), p.e9532.
- Schiweck, J., Eickholt, B. J. and Murk, K. (2018) 'Important Shapeshifter: Mechanisms Allowing Astrocytes to Respond to the Changing Nervous System During Development, Injury and Disease', *Frontiers in Cellular Neuroscience*, 12(August), pp. 1–17. doi: 10.3389/fncel.2018.00261.
- Schust, J. et al. (2006) 'Stattic: A Small-Molecule Inhibitor of STAT3 Activation and Dimerization', *Chemistry and Biology*, 13(11), pp. 1235–1242. doi: 10.1016/j.chembiol.2006.09.018.
- Schweinhuber, S. K. et al. (2015) 'Profilin isoforms modulate astrocytic morphology and the motility of astrocytic processes', *PLoS ONE*, 10(1), pp. 1–23. doi: 10.1371/journal.pone.0117244.
- Scimemi, A. (2019) 'The Role of Astrocytes in Neurotransmitter Uptake and Brain Metabolism', Switzerland: Springer International Publishing. doi: 10.1007/978-3-030-00817-8.
- Seifert, G. et al. (2009) 'Analysis of Astroglial K<sup>+</sup> Channel Expression in the Developing Hippocampus Reveals a Predominant Role of the Kir4.1 Subunit', *Journal of Neuroscience*, 29(23), pp. 7474–7488. doi: 10.1523/JNEUROSCI.3790-08.2009.
- Silva et al. (1998) 'A novel and rapid method for culturing pure rat spinal cord astrocytes on untreated glass'. *Journal of Neuroscience Methods*, 80(1), pp.75-79.
- Sloan, S. A. and Barres, B. (2015) 'Mechanisms of astrocyte development and their contributions to neurodevelopmental disorders', *Curr Opin Neurobiology*, 34(6224), pp. 882–886. doi: 10.1126/science.aaa1823.Using.
- Sofroniew, M. V (2015) 'Astrogliosis', *Cold Spring Harbor perspectives in biology*, 7(2), pp. 1–16. doi: 10.1101/cshperspect.a020420.

- Sofroniew, M. V (2017) 'Astrocyte barriers to neurotoxic inflammation', *Nat Rev Neurosci*, 16(5), pp. 249–263. doi: 10.1038/nrn3898.Astrocyte.
- Sofroniew, M. V. (2009) 'Molecular dissection of reactive astrogliosis and glial scar formation', *Trends in Neurosciences*, 32(12), pp. 638–647. doi: 10.1016/j.tins.2009.08.002.
- Sofroniew, M. V. and Vinters, H. V. (2010) 'Astrocytes: Biology and pathology', *Acta Neuropathologica*, 119(1), pp. 7–35. doi: 10.1007/s00401-009-0619-8.
- Sohn, J. et al. (2015) 'The Subventricular Zone Continues to Generate Corpus Callosum and Rostral Migratory Stream Astroglia in Normal Adult Mice', *Journal of Neuroscience*, 35(9), pp. 3756–3763. doi: 10.1523/JNEUROSCI.3454-14.2015.
- Sriram, K. et al. (2004) 'Induction of gp130-related cytokines and activation of JAK2/STAT3 pathway in astrocytes precedes up-regulation of glial fibrillary acidic protein in the 1-methyl-4-phenyl-1,2,3,6-tetrahydropyridine model of neurodegeneration: Key signaling pathway for ast', *Journal of Biological Chemistry*, 279(19), pp. 19936–19947. doi: 10.1074/jbc.M309304200.
- Strezoska, Z. and Yamada, C. (2018) 'Accell siRNA Reagents: Achieving Long-term Gene Silencing', *Horizon Discovery Group Company*, p. 2. Available at: <http://dharmacn.gelifesciences.com/uploadedFiles/Resources/accell-app-note.pdf>.
- Sullivan, S. M. et al. (2010) 'Structural remodeling of gray matter astrocytes in the neonatal pig brain after hypoxia/ischemia', *Glia*, 58(2), pp. 181–194. doi: 10.1002/glia.20911.
- Sun, D. and Jakobs, T. C. (2012) 'Structural Remodeling of Astrocytes in the Injured CNS', *Neuroscientist*, 18(6), pp. 567–588. doi: 10.1038/mp.2011.182.doi.
- Sun, D. et al. (2010) 'Structural Remodeling of Fibrous Astrocytes after Axonal Injury', *Journal of Neuroscience*, 30(42), pp. 14008–14019. doi: 10.1523/jneurosci.3605-10.2010.
- Sun, Y. E., Martinowich, K. and Ge, W. (2003) 'Making and repairing the mammalian brain - Signaling toward neurogenesis and gliogenesis', *Seminars in Cell and Developmental Biology*, 14(3), pp. 161–168. doi: 10.1016/S1084-9521(03)00007-7.
- Tabata, H. (2015) 'Diverse subtypes of astrocytes and their development during corticogenesis', *Frontiers in Neuroscience*, 9(APR), pp. 1–7. doi: 10.3389/fnins.2015.00114.
- Taft, J. R., Vertes, R. P. and Perry, G. W. (2005) 'Distribution of GFAP+ astrocytes in adult and neonatal rat brain', *International Journal of Neuroscience*, 115(9), pp. 1333–1343. doi: 10.1080/00207450590934570.
- Takata, N. and Hirase, H. (2008) 'Cortical layer 1 and layer 2/3 astrocytes exhibit distinct calcium dynamics in vivo', *PLoS ONE*, 3(6). doi: 10.1371/journal.pone.0002525.

- Tamashiro, T. T., Dalgard, C. L. and Byrnes, K. R. (2012) 'Primary Microglia Isolation from Mixed Glial Cell Cultures of Neonatal Rat Brain Tissue', *Journal of Visualized Experiments*, (66), pp. 1–5. doi: 10.3791/3814.
- Tanabe, K., Kozawa, O. and Iida, H. (2016) 'cAMP/PKA enhances interleukin-1 $\beta$ -induced interleukin-6 synthesis through STAT3 in glial cells', *Cellular Signalling*. Elsevier Inc., 28(1), pp. 19–24. doi: 10.1016/j.cellsig.2015.10.009.
- Tanaka, K. et al. (2016) 'Epilepsy and exacerbation of brain injury in mice lacking the glutamate transporter GLT-1'. *Science*. 1997;276:1699–1702.
- Tang, X., Taniguchi, K. and Kofuji, P. (2009) 'Heterogeneity of Kir4.1 channel expression in glia revealed by mouse transgenesis', *Glia*, 57(16), pp. 1706–1715. doi: 10.1002/glia.20882.
- Teng, T. S. et al. (2009) 'Stat3 promotes directional cell migration by regulating Rac1 activity via its activator PIX', *Journal of Cell Science*, 122(22), pp. 4150–4159. doi: 10.1242/jcs.057109.
- Testen, A. et al. (2019) 'Region-Specific Differences in Morphometric Features and Synaptic Colocalization of Astrocytes During Development', *Neuroscience*. IBRO, 400, pp. 98–109. doi: 10.1016/j.neuroscience.2018.12.044.
- Thompson, R. & Macvicar, B. (2008) 'Connexin and pannexin hemichannels of neurons and astrocytes', *Channels*, 2(2), pp.81-86.
- Tian, G. et al. (2017) 'Astrocyte contributes to pain development via MMP2-JNK1/2 signaling in a mouse model of complex regional pain syndrome', *Life Sciences*. Elsevier Inc., 170, pp. 64–71. doi: 10.1016/j.lfs.2016.11.030.
- Tiryaki, V. M., Ayres, V. M., et al. (2015) 'Differentiation of reactive-like astrocytes cultured on nanofibrillar and comparative culture surfaces', *Nanomedicine*, 10(4), pp. 529–545. doi: 10.2217/nnm.14.33.
- Tiwari, N. et al. (2018) 'Stage-Specific Transcription Factors Drive Astrogliogenesis by Remodeling Gene Regulatory Landscapes', *Cell Stem Cell*, 23(4), pp. 557-571.e8. doi: 10.1016/j.stem.2018.09.008.
- Tripathi, S. K. et al. (2017) 'Genome-wide Analysis of STAT3-Mediated Transcription during Early Human Th17 Cell Differentiation', *Cell Reports*, 19(9), pp. 1888–1901. doi: 10.1016/j.celrep.2017.05.013.
- Tsai, H. et al. (2014) 'Regional astrocyte allocation regulates CNS synaptogenesis', *Science*, 337(6092), pp. 358–362. doi: 10.1126/science.1222381.Regional.
- Tsuda, M. et al. (2011) 'JAK-STAT3 pathway regulates spinal astrocyte proliferation and neuropathic pain maintenance in rats', *Brain*, 134(4), pp. 1127–1139. doi: 10.1093/brain/awr025.
- Tyzack, G. E. et al. (2014) 'Astrocyte response to motor neuron injury promotes structural synaptic plasticity via STAT3-regulated TSP-1 expression', *Nature Communications*, 5. doi: 10.1038/ncomms5294.
- Vallejo, M. (2009) 'PACAP signaling to DREAM: A cAMP-dependent pathway that regulates cortical astrogliogenesis', *Molecular Neurobiology*, 39(2), pp. 90–100. doi: 10.1007/s12035-009-8055-2.

- Vallejo, R., et al. (2010) 'The Role of Glia and the Immune System in the Development and Maintenance of Neuropathic Pain', *Pain Practice*, 10(3), pp.167-184.
- Vardjan, N., Kreft, M. and Zorec, R. (2014) 'Dynamics of  $\beta$ -adrenergic/cAMP signaling and morphological changes in cultured astrocytes', *Glia*, 62(4), pp. 566–579. doi: 10.1002/glia.22626.
- Vega-Avelaira, D. et al. (2012) 'The emergence of adolescent onset pain hypersensitivity following neonatal nerve injury', *Molecular Pain*, 8, pp. 1–12. doi: 10.1186/1744-8069-8-30.
- Vega-Avelaira, D., Moss, A. and Fitzgerald, M. (2007) 'Age-related changes in the spinal cord microglial and astrocytic response profile to nerve injury', *Brain, Behavior, and Immunity*, 21(5), pp. 617–623. doi: 10.1016/j.bbi.2006.10.007.
- Verkhatsky, A. et al. (2014) 'Glia in the pathogenesis of neurodegenerative diseases'. *Biochim. Soc. Trans.*, 42(5), pp.1291-1301.
- Voet, S. et al. (2018) 'A20 critically controls microglia activation and inhibits inflammasome-dependent neuroinflammation', *Nature Communications*, 9(1). doi: 10.1038/s41467-018-04376-5.
- Volterra, A., Liadet, N. & Savtchouk, I. (2014) 'Astrocyte Ca<sup>2+</sup> signalling: an unexpected complexity', *Nature Reviews Neuroscience*, 15(5), pp.327-335.
- Voskuhl, R. et al. (2009) 'Reactive Astrocytes Form Scar-Like Perivascular Barriers to Leukocytes during Adaptive Immune Inflammation of the CNS', *Journal of Neuroscience*, 29(37), pp.11511-11522.
- Wandosell, F., Bovolenta, P. and Nieto-Sampedro, M. (1993) 'Differences between reactive astrocytes and cultured astrocytes treated with di-butryl-cyclic AMP', *J Neuropathol Exp Neurol*, 52(3), pp. 205–15.
- Wang, Z., et al. (2009) 'Cell-type specific activation of p38 and ERK mediates calcitonin gene-related peptide involvement in tolerance to morphine-induced analgesia', *The FASEB Journal*, 23(8), pp.2576-2586.
- Wanner, I. B. et al. (2013) 'Glial Scar Borders Are Formed by Newly Proliferated, Elongated Astrocytes That Interact to Corral Inflammatory and Fibrotic Cells via STAT3-Dependent Mechanisms after Spinal Cord Injury', *Journal of Neuroscience*, 33(31), pp. 12870–12886. doi: 10.1523/JNEUROSCI.2121-13.2013.
- Washburn, K. B. and Neary, J. T. (2006) 'P2 purinergic receptors signal to STAT3 in astrocytes: Difference in STAT3 responses to P2Y and P2X receptor activation', *Neuroscience*, 142(2), pp. 411–423. doi: 10.1016/j.neuroscience.2006.06.034.
- Watkins, L. and Maier, S. (2003) 'GLIA: A novel drug discovery target for clinical pain', *Nature Reviews Drug Discovery*, 2(12), pp.973-985.
- Wen, Y., et al. (2009) 'Activation of p38 Mitogen-activated Protein Kinase in Spinal Microglia Contributes to Incision-induced Mechanical Allodynia', *Anesthesiology*, 110(1), pp.155-165.

- Wilhelmsson, U. et al. (2006) 'Redefining the concept of reactive astrocytes as cells that remain within their unique domains upon reaction to injury', *Proceedings of the National Academy of Sciences*, 103(46), pp. 17513–17518. doi: 10.1073/pnas.0602841103.
- Wolfes, A. C. et al. (2017) 'A novel method for culturing stellate astrocytes reveals spatially distinct Ca<sup>2+</sup> signaling and vesicle recycling in astrocytic processes', *The Journal of General Physiology*, 149(1), pp. 149–170. doi: 10.1085/jgp.201611607.
- Won, C. K. and Oh, Y. S. (2000) 'cAMP-induced stellation in primary astrocyte cultures with regional heterogeneity', *Brain Research*, 887(2), pp. 250–258. doi: 10.1016/S0006-8993(00)02922-X.
- Xi, Q. et al. (2011) 'Glutamate-induced calcium signals stimulate CO production in piglet astrocytes', *American Journal of Physiology - Heart and Circulatory Physiology*, 301(2). doi: 10.1152/ajpheart.01277.2010.
- Xia, X. G. et al. (2002) 'Induction of STAT3 signaling in activated astrocytes and sprouting septal neurons following entorhinal cortex lesion in adult rats', *Molecular and Cellular Neuroscience*, 21(3), pp. 379–392. doi: 10.1006/mcne.2002.1180.
- Xu, J. et al. (2018) 'Histamine up-regulates the expression of histamine receptors and increases the neuroprotective effect of astrocytes', *Journal of Neuroinflammation*. *Journal of Neuroinflammation*, 15(1), pp. 1–10. doi: 10.1186/s12974-018-1068-x.
- Yang, H. et al. (2007) 'Optimized and efficient preparation of astrocyte cultures from rat spinal cord', *Cytotechnology*, 52(2), pp. 87–97. doi: 10.1007/s10616-006-9033-4.
- Yang, J. et al. (2016) 'Astrocytes contribute to synapse elimination via type 2 inositol 1,4,5-trisphosphate receptor-dependent release of ATP', *eLife*, 5(APRIL2016), pp. 1–17. doi: 10.7554/eLife.15043.
- Yang, Y., Higashimori, H. and Morel, L. (2013) 'Developmental maturation of astrocytes and pathogenesis of neurodevelopmental disorders', *Journal of Neurodevelopmental Disorders*. *Journal of Neurodevelopmental Disorders*, 5(1), p. 1. doi: 10.1186/1866-1955-5-22.
- Yeh, T. H. et al. (2009) 'Microarray analyses reveal regional astrocyte heterogeneity with implications for neurofibromatosis type 1 (NF1)-regulated glial proliferation', *Glia*, 57(11), pp. 1239–1249. doi: 10.1002/glia.20845.
- Yoon, H. et al. (2017) 'Astrocyte heterogeneity across the brain and spinal cord occurs developmentally, in adulthood and in response to demyelination', *PLoS ONE*, 12(7), pp. 1–19. doi: 10.1371/journal.pone.0180697.
- You, L. et al. (2015) 'The role of STAT3 in autophagy', *Autophagy*, 11(5), pp. 729–739. doi: 10.1080/15548627.2015.1017192.
- Yu, H. et al. (2014) 'Revisiting STAT3 signalling in cancer: New and unexpected biological functions', *Nature Reviews Cancer*. *Nature Publishing Group*, 14(11), pp. 736–746. doi: 10.1016/j.ijgo.2015.09.021.

- Zamanian, J. L. et al. (2012) 'Genomic Analysis of Reactive Astrogliosis', *Journal of Neuroscience*, 32(18), pp. 6391–6410. doi: 10.1523/JNEUROSCI.6221-11.2012.
- Zeug, A. et al. (2018) 'Control of astrocyte morphology by Rho GTPases', *Brain Research Bulletin*. Elsevier, 136(May 2017), pp. 44–53. doi: 10.1016/j.brainresbull.2017.05.003.
- Zhang, S. et al. (2013) 'Expression and Activation of STAT3 in the Astrocytes of Optic Nerve in a Rat Model of Transient Intraocular Hypertension', *PLoS ONE*, 8(1). doi: 10.1371/journal.pone.0055683.
- Zhang, Y. and Barres, B. A. (2010) 'Astrocyte heterogeneity: An underappreciated topic in neurobiology', *Current Opinion in Neurobiology*. Elsevier Ltd, 20(5), pp. 588–594. doi: 10.1016/j.conb.2010.06.005.
- Zhou, Z., Ikegaya, Y. and Koyama, R. (2019) 'The Astrocytic cAMP Pathway in Health and Disease', *International Journal of Molecular Sciences*, 20(3), p. 779. doi: 10.3390/ijms20030779.
- Zhu, Y. and Kimelberg, H. K. (2004) 'Cellular expression of P2Y and  $\beta$ -AR receptor mRNAs and proteins in freshly isolated astrocytes and tissue sections from the CA1 region of P8-12 rat hippocampus', *Developmental Brain Research*, 148(1), pp. 77–87. doi: 10.1016/j.devbrainres.2003.10.014.
- Zhuang, Z., et al. (2006) 'A Peptide c-Jun N-Terminal Kinase (JNK) Inhibitor Blocks Mechanical Allodynia after Spinal Nerve Ligation: Respective Roles of JNK Activation in Primary Sensory Neurons and Spinal Astrocytes for Neuropathic Pain Development and Maintenance', *Journal of Neuroscience*, 26(13), pp.3551-3560.